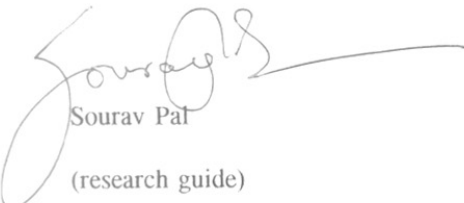
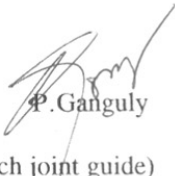


CERTIFICATE

Certified that the work incorporated in this thesis entitled "*STRUCTURE-PROPERTY CORRELATIONS IN LAYERED PEROVSKITES AND RELATED OXIDES; IMPORTANCE OF ATOMIC SIZES*", was carried by Ms. Neepa Shah, under our supervision. Such material as has been obtained by the other sources has been duly acknowledged in the thesis.


Sourav Pal
(research guide)


P. Ganguly
(research joint guide)

Date: 29-12-95

Place: Pune



COMPUTERISED

**STRUCTURE-PROPERTY CORRELATIONS IN
LAYERED PEROVSKITES AND RELATED OXIDES:
IMPORTANCE OF ATOMIC SIZES**

**Thesis submitted to
University of Pune
For the degree of**

DOCTOR OF PHILOSOPHY

IN

CHEMISTRY

RR

BY

TH-1041

541.61:541.451(043)

SHA

**Ms. NEEPA SHAH
PHYSICAL CHEMISTRY DIVISION
NATIONAL CHEMICAL LABORATORY
PUNE 411 008
INDIA**

DECEMBER 1995

ACKNOWLEDGEMENT

It gives me a great pleasure to express my deep sense of gratitude to my research supervisor, Prof. P. Ganguly for introducing me to a wide variety of topics and for his excellent guidance, help and incessant encouragement during the course of this investigation. I am indebted to him for his deep interest in the subject and in contributing to the format and content of this thesis.

It also gives me a great pleasure in extending my sincere thanks to Dr. Sourav pal for his support, advice and encouragement throughout the course of this investigation.

I am deeply indebted to Dr. P.A. Joy for his inspiring guidance, helpful suggestions and neverfailing deep interest throughout the progress of this work. Frequent discussions with him have much enriched my awareness and helped directly in the work reported in the thesis. Without his constant help it would have been difficult to bring the thesis in this form.

I am thankful to Dr. Sreedhar for his suggestions and occasional comments. I am thankful to Drs. Mulla, M.Sastri, K.Vijaymohanan for their duly help in various ways during the course of my research work.

I thank Drs. Kuber, Mrs.Mitra, Ms.Pavaskar, Kshirsagar, Shinde, Bakre, Prabhat singh and Date for their technical help in obtaining XRD, Raman, ESR, Electron diffraction spectra respectively. I also thank Dr. Hegde and Dr.Belekar for their in recording the IR spectra. I am thankful to Drs.Ganapathy, Rajamohanan and Mr. Prakash for their help in obtaining NMR spectra.

Slow step-scan XRD measurements were carried out in TIFR, Bombay with the help of Drs. Elankumaran and Sundaresan. I am thankful to them. Low temperature susceptibility measurement were carried out at the SSCU Unit of IISc, Bangalore in collaboration with Dr. Vasantacharya, I am grateful to him. I thank Dr.F.C. Matacotta, ICTP, Trieste, Italy for his for his interest in part of my work.

I thank Drs. A.V. Ramaswamy, Veda Ramaswamy, Sathaye, Soni, Awate, Pathak , Waghmare, Pradhan and Mr. Borker for their duly help. I am thankful to all the office staff of Physical Chemistry Division for their prompt assistance and cooperation.

I thank my colleagues and friends, Nayana, Anjali, Priya, Anil, Prakash, Santhosh, Sipra, Keshavraja, Reni, Vinod, Krisanu, Shruti for their cheerful company and warm friendship.

I sincerely appreciate the moral support of my parents and other family members for their patience and inspiration.

I am thankful to authority of, NCL, for giving me the opportunity of working in NCL. Finally I am thankful to CSIR for financial assistance.

Neepa

(Neepa Shah)

PREFACE

Relating the structure to the properties of oxides has been of much interest after discovery of high T_c superconductivity. In order to test theoretical predictions based on model systems, synthesis of new classes of solids as well as novel members of the known types of the solids are practiced traditionally and their properties are correlated with the structures. Such an approach based on structure-property correlations is more successful than approaches based on microscopic theory.

Perovskite structure occupies a prominent place under all the known ternary systems of composition ABO_3 . Layered perovskite oxides of composition A_2BO_4 are derived from the perovskite structure and are defined as alternation of perovskite layers with rock salt type (ΔO) layers.

There are few attempts to examine the structure-property correlation of the K_2NiF_4 related layered perovskites and most of the studies are based on the nature of the bonding in oxides. The main objective of the present work is to find a relationship between crystallographic structure and the physicochemical properties of the various layered perovskite oxides and related structures, based on the cationic size.

Chapter 1 gives a brief introduction, wherein existing literature of the K_2NiF_4 type of layered perovskite compounds is reviewed. The scope and the nature of the present work are defined at end of the chapter. Chapter 2 gives a brief description of the synthesis and various characterization techniques used for the present study.

In chapter 3, a formulation is proposed based on a model of the AX_3 close-packing for various layered cuprate perovskites for understanding the role of various A ions. The layered perovskite systems have been modelled on the basis of two types of AX_3 close-packing based on Cu_3Au and Ni_3Ti structures. The AX_3 close-packing in the former is similar to that in the ABX_3 perovskite structure. The latter gives rock-salt structure upon the loss of X_2 . An admixture of two kinds of packing yields the layered perovskite structure. The AX_3 close-packing have been modelled in terms of pseudo-spins in the ANNNI model. Three sites for the A ions may then be distinguished in this model. In this description the role of A ions in influencing the structure and thence the properties, become more transparent.

The phenomenon of high-temperature superconductivity in layered perovskites multinary copper oxide systems have revealed important aspects which are yet to be satisfactorily understood. One of the most fascinating of these behavior of $La_{2-x}Sr_xCuO_4$ is that the superconducting transition temperature, T_c , goes through a maximum when x is between 0.15 - 0.20 and then decreases with increasing hole concentration, and becoming zero at $x = 0.33$. At this value of x , the system still remains metallic and the basic crystal structure remains the same. In chapter 4, the application of Vegard's law to the changes in c parameter of the solid solutions $La_{2-x}A'_xCuO_{4-d}$ ($A' = Ba, Sr, Ca$) is examined in terms of the rigidity of the CuO_2 layers, especially for the $A' = Sr$ series with $d = 0$ and for $0 < x < 1.2$. The significance of the results in terms of insulator-superconductor-metal transition in $La_{2-x}Sr_xCuO_4$, $0 < x < 0.3$ is briefly discussed. From these dependences a general expression for c -axis expansion is obtained and the changes in the c parameter obtained with other A' ions such as Pb^{12} , Ln^{13} ($Ln = \text{rare earth ion}$) are compared.

Early exploratory studies have shown that the structures of A_2BO_4 phases can be predicted by the perovskite tolerance factor (t). In contrast, there are other non-copper oxide systems that fall within the K_2NiF_4 limit ($0.86 < t < 1.02$), but adopt different structures like Sr_2PbO_4 and Ca_2IrO_4 . The mutual solubility of these structures i.e. how Sr_2PbO_4 structure transforms into Ba_2PbO_4 and into Sr_2SnO_4 structure, is discussed in chapter 5. The hexagonal phases in Sr-Pb-M-O ($M = Cu, Zn, Cd$) system which is related to the Ca_2IrO_4 structure are also examined. Crystal structure determination is done by using Reitveld refinement analysis. The conclusion drawn from above studies are examined by infra-red transmission and Raman studies.

The structure and properties of oxycarbonates of transition metal compounds are discussed in chapter 6 and 7. In chapter 6, the close-packing description of the carbonate structure and its relation to the perovskite structure is discussed. Further, the cuprocarbonate $Ba_3SrCu_2O_6 \cdot 2CO_2$ is discussed with special emphasis on the changes in the ESR spectra of copper atoms in the carbonate plane when the carbonate groups are partially replaced by salts of weak base and strong acid. In chapter 8 the preparation of $Ba_{2-x}Sr_xLi_{0.5}Cu_{0.5}O_{2.5}(CO_3)$ and $Ba_{2-x}Sr_xLi_{0.5}Ni_{0.5}O_{2.5}(CO_3)$ is discussed. These compounds have been characterised by 7Li solid state NMR, IR, and ESR spectra. Anomalous 7Li NMR behavior is analysed in terms of the creation of holes on Oxygen.

CONTENTS

Certificate

Acknowledgements

Preface

Chapter 1. Introduction to Layered Perovskites and Related Metal Oxides

1.1. Introduction	2
1.2. Stability of the perovskite structure	6
1.3. Cationic radius ratio and formation of K_2NiF_4 type compounds	8
1.4. Compounds related to K_2NiF_4 structure	9
1.5. Role of tolerance factor in two- and three-dimensional perovskite systems	11
1.6. Non-stoichiometry in layered perovskites	15
1.7. Background of atomic sizes (ionic radii)	19
1.8. Scope and nature of the thesis work	22
References	25

Chapter 2. Experimental Methods: Synthesis and Characterisation

2.1. Chemical methods	32
2.1.1. Solid state Synthesis	32
2.1.2. Estimation of oxygen content	33

2.2.	Instrumental Methods	34
2.2.1.	X-ray diffraction	34
2.2.2.	Electron spin resonance	34
2.2.3.	Resistivity measurements	35
2.2.4.	Magnetic susceptibility measurements	36
2.2.5.	Infrared spectra	36
2.2.6.	Raman Spectra	36
2.2.7.	Nuclear magnetic resonance	37
2.3.	Computational Methods	38
2.3.1.	The PDP11 programme	38
2.3.2.	The LAZY-PULVERIX programme	38
2.3.3.	Rietveld refinement method	39
	References	41

Chapter 3. AX₃ Close-Packing Description of the Layered Perovskites

3.1.	Introduction	43
3.2.1.	Two kinds of AX ₃ close-packing	45
3.2.	Generation of layered perovskites	49
3.3.	Consequences of close-packing description	58
3.3.1.	Effects of anion, X, vacancies	58
3.3.2.	Choice of A cations for various sites	59
3.3.3.	Similarity between inter-metallic compounds and layered perovskites	60
3.3.4.	Role of various A ions	63

3.3.5.	Influence of tolerance factor	65
3.4.	Conclusions	71
	References	74

Chapter 4. Vegard's Law Behaviour in $\text{La}_{2-x}\text{A}'_x\text{CuO}_{4-d}$ ($\text{A}'=\text{Ba, Sr, Ca}$)

4.1.	Introduction	78
4.2.	Experimental	82
4.3.	Results	84
4.4.	Discussions	89
4.4.1.	Effect of size of A ion	89
4.4.2.	Effect of holes	91
4.4.3.	Effect of tolerance factor	91
4.4.4.	Effect of loss of oxygen	94
4.4.5.	Influence of tolerance factor	98
4.4.6.	Applications to other systems	100
4.5.	General remarks	101
	References	103

Chapter 5. Structure and Properties of A_2BO_4 Type Compounds with Different Structures

5.1.	Introduction	107
5.2.	Experimental	111
5.3.	Description of various structures	112
5.4.	Results and discussions	114

5.4.1	X ray diffraction studies	115
5.4.1.1.	The $Ba_{2-x}Sr_xPbO_4$ system	115
5.4.1.2.	The $Sr_2Sn_{1-x}Pb_xO_4$ system	117
5.4.1.3.	The $Sr_{1.5}M_xPbO_{3.5+1x}$ system (M=Cu, Zn, Cd; $0.05 < x < 0.5$)	119
5.4.2.	Vibrational Spectra	135
5.4.2.1.	Classification of normal modes	135
5.4.2.2.	Compounds with K_2NiF_4 system	136
5.4.2.2a.	Infrared spectra	140
5.4.2.2b.	Raman spectra	144
5.4.2.3.	Compounds with Sr_2PbO_4 and Ca_2IrO_4 structures	149
5.4.3.	Electron Spin Resonance studies	155
5.5.	Description of various A_2BX_4 structures on the basis of hexagonal packing of A atoms	155
	References	161
Chapter 6.	The Layered Cuprocarbonate, $Ba_3SrCu_2O_6 \cdot 2CO_2$: Characterization and Properties	
6.1.	Introduction	165
6.2.	Close packing description of carbonates	167
6.2.1.	Close packing in perovskites	169
6.2.2.	Carbonates: Aragonite and Calcite	169
6.2.3.	Relation between close-packing of cuprocarbonates and perovskites	173
6.3.	Experimental	178

6.4.	Results and discussions	180
6.4.1.	X-ray diffraction studies	180
6.4.2.	Infrared spectra	180
6.4.3.	Electron Spin Resonance studies	186
6.5.	Conclusions	190
	References	193

Chapter 7. Synthesis and Characterisation of New Cupro- carbonate Containing Li and Transition Metal Ions

7.1.	Introduction	196
7.2.	Experimental	196
7.3.	Results and discussions	198
7.3.1.	X-ray diffraction studies	198
7.3.2.	Magnetic susceptibility	207
7.3.3.	Electron Spin Resonance studies	207
7.3.4.	IR and Raman spectra	209
7.3.5.	⁷ Li Nuclear Magnetic Resonance	214
7.3.6.	Reactivity with NH ₄ F	217
	References	221
	List of Publications	222

CHAPTER 1

INTRODUCTION TO LAYERED PEROVSKITES

AND

RELATED METAL OXIDES

1.1. Introduction

There has been an increasing interest in the recent past in the synthesis and properties of many new oxide systems mainly due to exciting new development which has taken place in various fields. Amongst the various oxides, those related to the perovskite family display a wide spectrum of important physical properties such as superconductivity, giant magnetoresistance, catalysis etc. The layered perovskites exhibit many interesting properties and thus much attention is focussed on the study of their structural chemistry and physico-chemical properties. The prototype compounds are the A_2BO_4 oxides with the K_2NiF_4 or related structures. A variety of oxides are known to crystallize in structures related to K_2NiF_4 [1-15]. Intense interest in these layered oxides was generated with the discovery of high superconducting transition temperatures (T_c) in compounds derived from La_2CuO_4 [16-18]. Such a discovery focused attention on the perovskite family as a whole especially since the highest T_c in an oxide was found in the 3D perovskite system, $BaPb_{1-x}Bi_xO_3$ and the layered oxides derived from the perovskite structure [19].

Perovskite is a rare mineral ($CaTiO_3$) named after a Russian mineralogist. The ideal perovskite (ABX_3) structure possesses a simple cubic structure with space group $Pm\bar{3}m$. It is usually depicted schematically as in fig. 1.1a, where A is the larger cation in twelve-fold coordination and B is a smaller cation in six-fold coordination and X is the anion. The perovskite structure is conventionally described as consisting of a BO_3 array formed by corner-sharing of BO_6 octahedra. The perovskite structure can be related directly to that of ReO_3 . The BX_3 framework of the ABX_3 perovskite is similar to that in ReO_3 structure consisting of corner shared BX_6 octahedra and after incorporation of larger A cation in the center of the cube, the ABX_3 perovskite structure is formed [20].

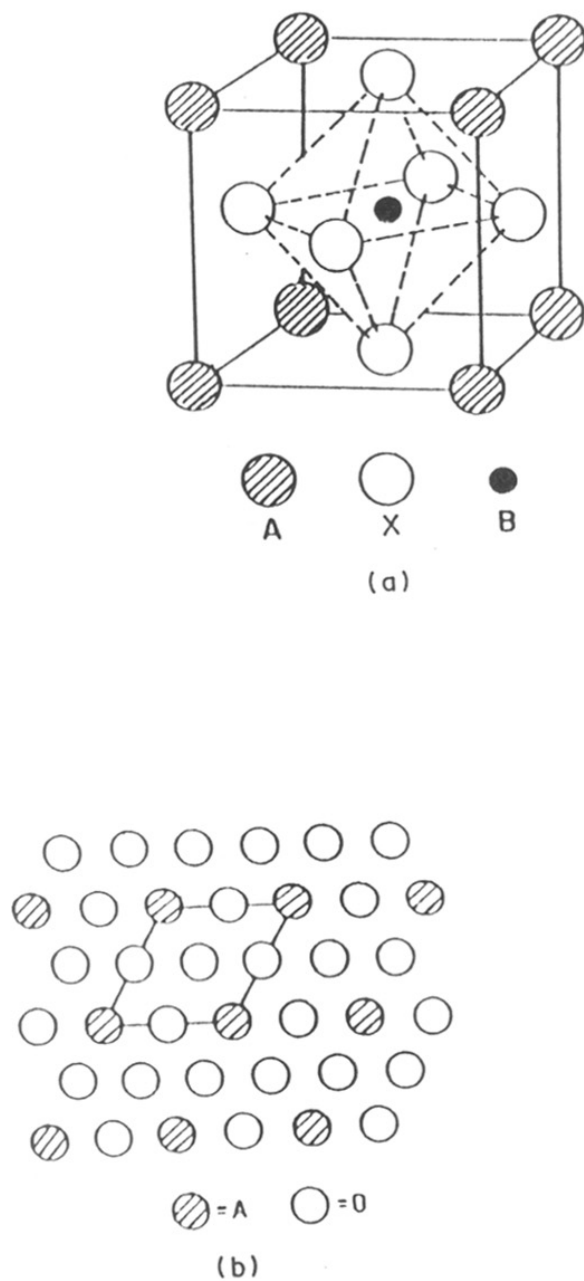


Fig. 1.1. (a) The ideal perovskite structure. (b) Close-packed AO_3 layers in perovskites.

Katz and Ward [21] have given an alternative description of the ABX_3 perovskite structure in terms of close-packing of A and X atoms. In this model there is a cubic close-packing of close-packed AX_3 layers made up of AX and XX rows (fig. 1.1b). Hexagonal close-packing or cubic close-packing of these layers may be effected such that one X_6 octahedra is generated per AX_3 unit. The B cations occupy these octahedral sites to generate the ABX_3 structure. The description is more general and helps to understand the occurrence of hexagonal polytypes of perovskites. A more detailed general packing scheme is discussed in chapter 3.

The perovskite structure is a versatile structure and is able to accommodate a wide range of valence states and atomic sizes of elements. The composition can be changed widely and the oxidation state of the cation and the oxygen non-stoichiometry can be controlled to a significant extent. This flexibility makes the perovskite family very useful in engineering oxides for practical applications such as piezoelectric, dielectric and pyroelectric devices, catalysts, sensors, solid electrolytes, magnetic devices and other devices that exploits the recently discovered high T_c superconductivity and giant magnetoresistance.

The basic composition of the perovskite family including the layered perovskite structures may be written as $(A'X)_m(ABX_3)_n$ with m rock-salt-like $A'X$ layers stacked alternately with n perovskite-like ABX_3 layers. In this notation, when $m = 0$ and $n = 1$, the 3D perovskite is obtained. When $m = 1$ and $n = 1$, K_2NiF_4 type layered perovskite structure is obtained. Thus K_2NiF_4 structure can be described by an alternation of perovskite layers with rock salt layers [22]. The structure is illustrated in fig. 1.2. The NiF_6 octahedra share corners with each other to form a two-dimensional perovskite like $(KNiF_3)$ array and these perovskite layers are interleaved with KF rocksalt layers

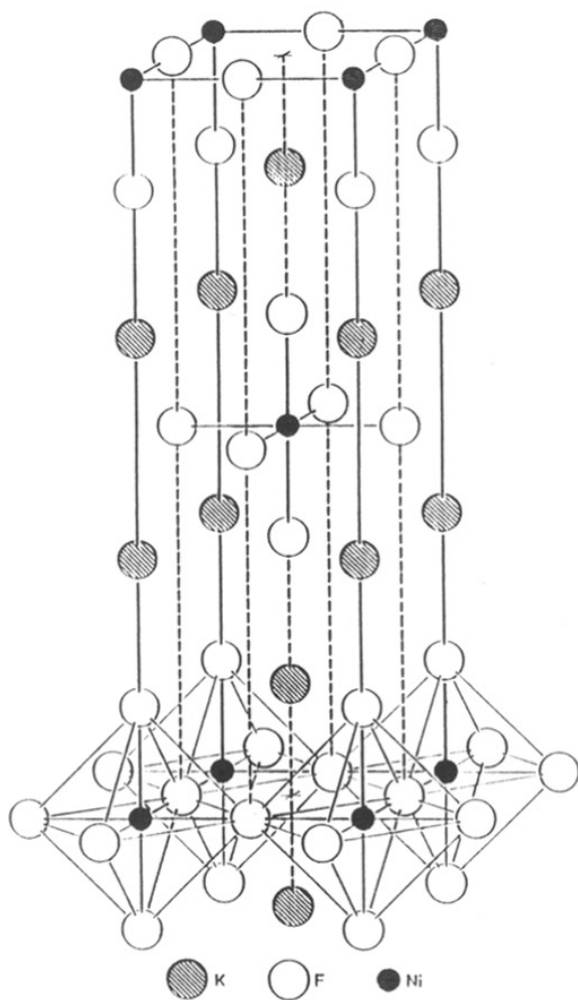


Fig. 1.2. The K_2NiF_4 structure. The perovskite octahedral layer is shown at the bottom part of drawing.

in the *c*-direction. This gives the K^+ ions a coordination number of 9. This structure is adopted by number of A_2BX_4 oxides, fluorides, chlorides, sulphides, hydrides and oxycarbonates.

Before the discovery of high-temperature superconductivity in these layered perovskite oxides, $m = 1$, was only observed in the Ruddlesdon-Popper phases with n being as large as 3 in the pure phases such as $Sr_4Ti_3O_{10}$ or $La_4Ni_3O_{10}$, etc. [23]. Ganguly and Rao [4] had discussed the possibility of $m = 2$ and $n = 2$ to account for the diffraction pattern of $LaNaTiO_4$ as given by Blasse [24].

1.2. Stability of the perovskite structure

The early discussions on the stability of perovskite structure were primarily based on the electrostatic Madelung energy stabilization that is achieved when cations occupy corner-shared octahedra [25]. In this approach the first prerequisite for a stable perovskite structure is the existence of the stable, polar octahedral site building blocks. This in turn requires that the B cation should have the preference for octahedral coordination of X anions for the effective charge on the B cation. In this approach the role of the A cation is primarily for charge neutralization purposes. Since any A cation must occupy the relatively large interstice created by corner-shared octahedra, a second prerequisite is an appropriate size for the A cation. When the size of A is too large, the B-X bond length cannot be optimized and the hexagonal stacking with the face-shared octahedra becomes competitive. As an example, it may be noted that $SrTiO_3$ has the perovskite structure while $BaTiO_3$ takes up the hexagonal perovskite structure [3]. On the other hand $BaPbO_3$ has cubic perovskite structure while $SrPbO_3$ or $CaPbO_3$ have orthorhombic (distorted perovskite) structures [3,20]. When the size of the A cation is

too small, the A-X bonding stabilizes structures having smaller anionic coordination around the A cation. The above discussion stresses the importance of octahedral site preference energy with the nature of the A cation having only a secondary role.

The relative sizes of the A and B cations are crucial in stabilizing the perovskite structure. In the ideal perovskite structure (fig. 1.1a) the B-X distance is equal to $a/2$ whereas the A-X distance is $a/\sqrt{2}$ (a = cubic unit cell length). The following relation between the ionic radii must hold in the ideal perovskite structure:

$$(r_A + r_X) = \sqrt{2} (r_B + r_X) \quad (1.1)$$

where r_A , r_B and r_X are the ionic radii of A, B and X ions respectively. It was found that the cubic perovskite structure or its slightly distorted variants are still retained in ABX_3 compounds even though the above relation is not exactly obeyed. As a measure of deviation from ideality Goldschmidt [26] introduced a tolerance factor t , which is defined as,

$$t = (r_A + r_X) / \sqrt{2} (r_B + r_X) \quad (1.2)$$

For an ideal perovskite, t is unity. However the perovskite structure is also found for lower values of t in the perovskite limit ($0.75 < t < 1.0$). In such cases, where t is less than 1, the structure distorts to tetragonal, rhombohedral or other lower symmetries. In general, distortions from the ideal structure involve cation displacement or tilting of the BO_6 octahedra or to a combination of both. Different kinds of octahedral tiltings have been reported [27,28]. Many perovskite oxides are polymorphs since the A cation must be stable in twelve-fold (12 or (8+4) or (6+6)) and the B cation in sixfold coordination.

The tolerance factor condition sets lower limits for the cationic radii. In oxide systems these limits have been claimed to be $r_A > 0.90 \text{ \AA}$ and $r_B > 0.51 \text{ \AA}$ using coordination number dependent ionic radii tabulated by Shannon and Prewitt [29]. It has to be noted that the choice of atomic sizes for a given atom is not unique. In general effective ionic radii compiled by Shannon and Prewitt [29,30] are to be preferred.

1.3. Cationic radius ratio and formation of K_2NiF_4 type of compounds

Effective ionic radius values of Shannon were used for computing $r_A[IX]/r_B[VI]$ ratio in A_2BO_4 compounds with K_2NiF_4 structure by Ganguli [31]. The term effective ionic radii is used to emphasize that these radii are empirical and include effects of covalence in specific M-O bonds (M = cation). These radii take into account electronic state, coordination numbers of both cations and anions, repulsive forces and polyhedral distortion. It was found that the cationic radius ratio assume the values around 2.00 varying with narrow range of 1.7 to 2.40. This spread (~0.7) is relatively narrow compared to other A_2BX_4 structural families (like β - K_2SO_4 - 9.5 Spinel - 4.00, thenardite - 5.00, Phenacite - 1.8, Olivine - 4.00 [26,32]). There are very few exceptions for compounds with K_2NiF_4 structure having r_A/r_B ratio lying outside the prescribed range. La_2CuO_4 , La_2CoO_4 and Nd_2NiO_4 have a tetragonal structure only at elevated temperatures [33,34]. They have their cationic radius ratio below the minimum value i.e. around 1.6 - 1.7. Also, for $CaLnCrO_4$, where Ln = Pr, Nd, Sm, Gd, r_A/r_B ratios are below the minimum value [35]. Compounds yielding values less than 1.7 are mostly distorted form of K_2NiF_4 or isotopes of Sr_2PbO_4 structure [31]. Those having higher values are mostly β - K_2SO_4 type. The $r_A[IX]/r_B[VI]$ values for hypothetical K_2NiF_4 type polymorphs for compounds belonging to other structural groups largely fall outside the range because of their inability to crystallize in a K_2NiF_4 structure. Ganguli [31] claims

that this relatively narrow spread makes $r_A[\text{IX}]/r_B[\text{VI}]$ ratio a characteristic parameter for ascertaining whether a certain A_2BX_4 compound can under some pressure and temperature conditions crystallize with a K_2NiF_4 type structure or not.

Although the criterion used by Ganguli [31] is somewhat successful, there is little useful insight that can be obtained from these conclusions because it completely ignores the role of the X anionic species. The tolerance factor derived from the perovskite may also be used to rationalize the wide occurrence of tetragonal lattice amongst mixed metal oxides of A_2BO_4 stoichiometry. The tolerance factor calculated using the Shannon-Prewitt radius for a number of ternary metal oxides exhibiting the K_2NiF_4 and related structure are listed in table 1.1. From the table, it can be concluded that K_2NiF_4 structure is stable for $0.87 < t < 1.02$. A justification can be given for this empirical observation which is discussed in chapter 3.

1.4. Compounds related to K_2NiF_4 structure

A number of compounds are apparently related to the K_2NiF_4 structure. Compounds of the type A_2CuF_4 ($\text{A} = \text{K}, \text{Rb}, \text{Tl}$) have a superstructure with $a' = a\sqrt{2}$, is closely due to Jahn-Teller effect acting on divalent copper [36]. Similar superstructures have been described for the orthorhombic La_2CoO_4 or La_2CuO_4 [37,2].

Compounds of the type NaN_mTiO_4 ($\text{Ln} = \text{La-Lu}$) have an ordered K_2NiF_4 structure with the rare-earth and sodium ions occupying different sites in (0 0 1) layers [24]. More strongly distorted type of K_2NiF_4 type variants have been reported for the orthorhombic $\beta\text{-Na}_2\text{UO}_4$ and $\alpha\text{-Li}_2\text{UO}_4$ [38].

Table 1.1. Tolerance factors (t) for oxides with the T , T' and T^* phases.

Compound	t	Compound	t
T phase			
La ₂ NiO ₄	0.885	LaSrGaO ₄	0.932
Ba ₂ PbO ₄	0.933	LaSrCrO ₄	0.935
GdSrNiO ₄	0.941	Sr ₂ IrO ₄	0.921
Ca ₂ MnO ₄	0.945	Sr ₂ TiO ₄	0.950
LaSrCoO ₄	0.960	LaSrCuO ₄	0.971
Ba ₂ SnO ₄	0.971	LaSrAlO ₄	0.973
LaSrMnO ₄	0.976	Sr ₂ MnO ₄	0.993
NdSrCrO ₄	0.925	K ₂ UO ₄	1.014
LaSrGaO ₄	0.932	GdSrAlO ₄	0.953
GdSrFeO ₄	0.902	SrDyCrO ₄	0.91
GdSrFeO ₄	0.914	GdSrCrO ₄	0.915
Sr ₂ MoO ₄	0.917		
T' -phase			
La _{1.5} Nd _{0.5} CuO ₄	0.864	Eu ₂ CuO ₄	0.837
Pr ₂ CuO ₄	0.856	Gd ₂ CuO ₄	0.832
Nd ₂ CuO ₄	0.851	LaNdCuO ₄	0.860
Sm ₂ CuO ₄	0.841	LaSmCuO ₄	0.855
LaEuCuO ₄	0.853	Nd _{1.85} Ce _{0.15} CuO ₄	0.847
T^* -phase			
La _{0.9} Y _{0.8} Sr _{0.3} CuO ₄	0.855	LaDy _{0.8} Sr _{0.2} CuO ₄	0.854
LaGd _{0.8} Sr _{0.2} CuO ₄	0.857	La _{0.8} EuSr _{0.2} CuO ₄	0.856
La _{1.3} Tb _{0.7} CuO ₄	0.855	La _{0.8} SmSr _{0.2} CuO ₄	0.858

Sr_2CuO_3 and Sr_2PdO_3 [39,40] can both be described as orthorhombically deformed K_2NiF_4 types with one quarter of the anions removed. This reduced oxygen content leaves Cu and Pd as "square planar" coordinated, and Sr ions are surrounded by only seven nearest oxygen neighbors.

1.5. Role of tolerance factor in two- and three-dimensional perovskite systems.

When the tolerance factor $t = 1$, there is perfect matching of A-O-A and B-O-B distances in perovskites and A_2BO_4 oxides. But when $t < 1$, the situation in A_2BO_4 is different from that of perovskites. In the 3D perovskite structure there is buckling of three-dimensional corner-shared octahedral network tending to make B-O-B angle less than 180° so that the effective B-O-B distance is reduced. In A_2BO_4 oxides the situation is somewhat different as pointed out by Ganguly and coworkers [4]. In these structures the intervening rock salt layers imparts rigidity to the two dimensional octahedral network and prevents it from buckling. Instead there is pressure effect on B-O_I-B bond tending to reduce its distance while A-O_I-A distance is stretched in order that the two distances match in the tetragonal structure. (where O_I and O_{II} are basal and axial oxygens respectively). In most A_2BO_4 oxides including Sr_2TiO_4 , $t < 1$, and as a consequence of the internal pressure effect the in-plane B-O_I-B distance reduces and the axial B-O_{II} distance increases. There is also a compression of the axial A-O_{II} distance.

In LaSrFeO_4 and LaSrCrO_4 the values of the a lattice parameter (3.86 Å and 3.84 Å respectively) are considerably smaller than that of corresponding perovskites ($a = 3.93$ Å, LaFeO_3 and $a = 3.883$ Å, LaCrO_3) [4]. Similarly a parameter of Sr_2TiO_4 is 3.88 Å and that of SrTiO_3 is 3.90 Å [4]. Thus in general pressure effect on B-O_I-B bond increases as t decreases from unity or as the size of B ion decreases (or the formal

charge decreases). Accordingly, Ni-O_t distance in La₂NiO₄ is 1.93 Å [37] compared to that of 2.09 Å in NiO [41].

Elongation of the BO₆ octahedra along axial direction can lead to stabilization of unusual electronic configurations. Thus intermediate spin Co³⁺ ions (t_{2g}^5, e_g^1) are found to exist at low temperatures in La₄LiCoO₈ and LaSrCoO₄ [42,44]. At high temperature they are transformed to high spin configuration (t_{2g}^4, e_g^2). High spin Fe⁴⁺ ions are found in La₃SrLiFeO₈ [45]. In Sr₂FeO₃F, the Fe³⁺ ions are found in the low spin configuration due to apical positioning of the Fluorine atom [46].

Variation of *c/a* ratio in LaSrBO₄ (B = Al, Cr, Fe, Ni) type compounds shows linear dependence on the size of the rare earth ion. The Al-O_t distance in LaSrAlO₄ (2.01 Å) is larger than that in GdSrAlO₄ (1.95 Å), compared to Al-O distance computed from the ionic radii (1.935 Å) [4]. In LaSrNiO₄ there is an abrupt change in the *c/a* ratio [47]. Since the size of low spin Ni³⁺ is comparable to that of Al³⁺, the marked different behaviour cannot be alone due to ionic size effects, electronic effects seems to be much important. A similar behaviour can be seen for LnSrCrO₄ and LnSrFeO₄ [48].

Another feature of A₂BO₄ oxides with the K₂NiF₄ structure is that the average B-O distance is less than that computed from ionic radii tables of Shannon especially when *t* is considerably less than unity. Thus in La₂NiO₄ and La₂CuO₄ the average Ni-O and Cu-O distances are 2.03 Å and 2.07 Å respectively compared to the computed values using ionic radii 2.09 Å and 2.13 Å respectively [30,37]. Ganguly and Rao [1984] [4] have proposed the possibility of charge disproportionation of B ion when B-O distance is too small. Thus Cu²⁺ can disproportionate into Cu⁺ and Cu³⁺. The average (Cu⁺, Cu³⁺)-O distance is coincidentally 2.07 Å.

The tolerance factors derived for perovskite structure has been used to rationalize the wide occurrence of a tetragonal (T) lattice among the mixed metal oxides of A_2BO_4 stoichiometry. The rare earth copper oxides of stoichiometry $(RE)_2CuO_4$, possess a richness of structural and physical properties as a consequence of the wide range in rare earth ionic sizes, and the fact that some deviation in the oxygen stoichiometry from its ideal value can be tolerated. There are three closely related structure types with stoichiometry $(RE)_2CuO_4$, each containing isolated sheets of four-fold (T' -structure), five fold (T'' - structure) and six-fold (T -structure) Cu-O coordination. Crystal chemistry and doping preferences affect phase stability of different T , T' and T'' phases in $La_{2-x}(RE)_xCuO_4$, ($RE = Nd, Sm, Eu, Gd, Dy, Ho, Er, Yb$ and Y). These studies have been discussed within a framework of simple ionic model [49,50] in which a perovskite like tolerance factor t is found to be remarkable predictor of T , T' and T'' stability limits.

For the largest rare earth cation, (La), $(RE)_2CuO_4$ crystallizes in an orthorhombically distorted K_2NiF_4 [T] structure. It contains perovskite like sheets of elongated CuO_6 octahedra, sharing corners in the (001) planes and separated by rock-salt like La-O layers in which La^{13} is nine-fold coordinated by oxide ions [51].

The rare earth ions of intermediate size (Pr - Gd) assume the T' structure of Nd_2CuO_4 [52,53]. In this structure two dimensional square-planar CuO_2 sheets share corners in the (0 0 1) plane and are separated by NdO_2 fluorite layer. The RE ion is eight fold coordinated by oxygen ions. A third RE_2CuO_4 structure denoted T'' , is observed with certain A' site rare earth and alkaline earth cation (e.g. $LaGd_{0.8}Sr_{0.2}CuO_4$ [52,54]), the T'' structure consists of a hybrid of the T and T' structure.

A study of the mutual solubility of La_2CuO_4 (T) and Nd_2CuO_4 (T') shows that the T structure occurs up to $x = 0.4$ in $\text{La}_{2-x}\text{Nd}_x\text{CuO}_4$ system and the average rare-earth cation radius at this composition is 1.205 \AA . In other $\text{La}_{2-x}\text{RE}_x\text{CuO}_4$ systems, T -phase solid solution limits and average rare-earth cation sizes at these extrema are similar, Sm, $x = 0.2$, 1.208 \AA ; Eu, $x = 0.3$, 1.202 \AA and Gd, $x = 0.3$, 1.200 \AA [55,49]. From these values, it may be concluded that the T to T' transitions takes place sharply at an average RE cation radius of 1.204 \AA . This corresponds to a tolerance factor $t = 0.865$, defining the lower limit of stability of the K_2NiF_4 structure. Tolerance factors calculated for number of cuprates with T and T'_i * structures are also listed in table 1.1. It can be seen that K_2NiF_4 structure is stable for $0.865 \leq t \leq 1.01$.

The T structure is orthorhombically distorted at the lower limit of the tolerance factor, $0.865 \leq t \leq 0.88$. Thus La_2CuO_4 ($t = 0.868$) has an orthorhombic structure because the structure must "pucker" to accommodate La^{+3} in the nine-fold site, i.e. La^{+3} itself is of border line stability in the nine-fold coordinated structure. When smaller rare earth cations replace La in $\text{La}_{2-x}\text{RE}_x\text{CuO}_4$, the degree of orthorhombicity increases with increase in x until a transformation to the T' (tetragonal Nd_2CuO_4) structure, occurs at $t = 0.865$. The orthorhombic transition can therefore be thought of as distortion originating in the RE-O layers, signalling the onset of the instability which eventually leads to the T' phase.

Electronic Factors may also be involved in the structural transition since the energy of the Cu^{+2} like x^2-y^2 antibonding states can be lowered by such a distortion [56], the La-O bond strength may increase as well. Band structure calculations by Whangbo *et al* showed [57] that the driving force for the tetragonal to orthorhombic transition

originates from strength of La-O interactions. When the RE radius become too small corresponding to $t = 0.865$ a major transformation to the T' structure occurs.

The T' structure itself exists only in the narrow range $0.83 \leq t \leq 0.86$. Rare earth-copper oxide systems with $t < 0.83$ do not form RE_2CuO_4 phase at ambient pressures. Only $\text{RE}_2\text{Cu}_2\text{O}_7$ compounds with t less than 0.83 and RE = HO ... Ly, Y, in six-fold coordinated RE sites are known [58].

Ganguly and Rao [4] have interpreted the T to T' transition in terms of competition between RE and Cu ions for bonding with the apical oxygens of La_2CuO_4 asserting that the smaller rare earths destabilise the structure by elongating the Cu-O bond in this competition.

The structural deformation on traversing the T to T' transition may be understood in terms of the different RE-O arrangements (rock-salt-like Vs fluorite-like) in the T and T' phases. For eight-fold coordination the ideal radius ratio of the A and X ions should be 0.73. For oxides we may assume the anion radius to be 1.40 \AA so that the radius of the A atom should be $\sim 1.03 \text{ \AA}$. This value is smaller than the size of, say, Nd ions. The transformation from rock-salt to fluorite like RE-O layers must then be governed by the value of the tolerance factor such that the size of the B ions play an important role.

1.6. Non-Stoichiometry in layered perovskites

The perovskite oxides are known to accommodate different kinds of stoichiometry [14,59,60]. Defects in these oxides can arise from cation deficiency (in A or B site), oxygen deficiency or oxygen excess.

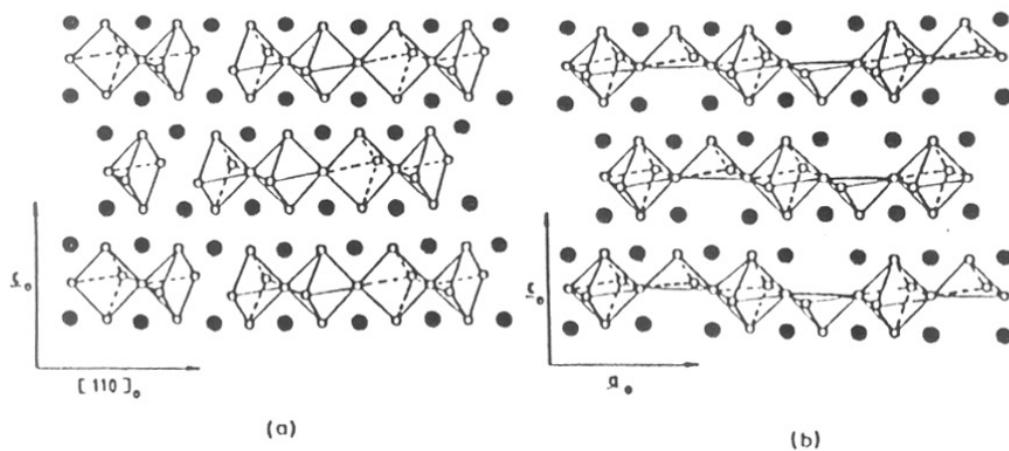


Fig. 1.3. Vacancy ordering in (a) $\text{Ca}_2\text{MnO}_{3.5}$, (b) $\text{Ca}_2\text{FeO}_{3.5}$.

Physical and chemical properties of oxygen deficient compounds of the $ABX_{3,\delta}$ and $A_2BO_{4,\delta}$ are strongly affected by some preferred coordination of B cations adjacent to oxygen vacancies. [61] Oxygen deficient non-stoichiometry is found in Ca_2MnO_4 which can be reduced topotactically to $Ca_2MnO_{3.5}$ [62]. Oxygen deficient $Ca_2MnO_{3.5}$ shows MnO_6 distortion due to oxygen vacancies generated by Mn^{+4} to Mn^{+3} transition. Oxygen sites in two dimensional corner shared network of Mn^{+4} octahedra are defected in planes, thus producing a layer structure of interconnected distorted square-pyramidal Mn^{+3} coordination polyhedron. The unit cell dimensions are $a = 5.30 \text{ \AA}$, $b = 10.05 \text{ \AA}$, $c = 12.24 \text{ \AA}$, the relationship with the tetragonal K_2NiF_4 stoichiometry being $a \approx \sqrt{a_T}$, $b \approx 2\sqrt{2a_T}$ and $c \approx c_T$. Fig. 1.3a. shows the defect structure of $Ca_2MnO_{3.5}$.

The structure of oxygen deficient $Ca_2FeO_{3.5}$ characterized by Vidyasagar *et al* [63] is different from ($a = 14.79 \text{ \AA}$, $b = 13.71 \text{ \AA}$, $c = 12.19 \text{ \AA}$) that of $Ca_2MnO_{3.5}$. They reported that the ordering of anion vacancies in $Ca_2FeO_{3.5}$ is similar to that in the brown-millerite stoichiometry consisting of alternating rows of tetrahedra and octahedra in the perovskite like layers of the K_2NiF_4 stoichiometry. (fig. 1.3b). Such vacancies often give rise to ordered superstructure.

The oxide $La_4Li_2O_7$ is the first reported defect K_2NiF_4 type oxide to have purely monovalent cations in the Ni positions [64]. One quarter of the O sites are empty which reduces the mean La^{+3} and Li^{+1} co-ordination numbers to 8 and 5 respectively. The Li environment is irregular. The randomly arranged oxygen vacancies account for large B factors and c/a ratio 3.616 which is extremely high for a K_2NiF_4 type of oxide [64]. It is possible that there may be a superstructure or lowering of symmetry.

RR
541.61:541.451(043)
SHA

COMPUTERISED

TH-1041

After the discovery of superconductivity in $\text{La}_{2-x}(\text{BaSr})_x\text{CuO}_4$ system, evidence for superconductivity at 40 K in oxygen excess undoped $\text{La}_2\text{CuO}_{4+\delta}$ was first reported by Grant *et al* [65]. Later on it was confirmed that superconductivity results from excess bulk oxygen ($\delta \approx 0.05$) incorporated as an O^{2-} interstitial defect [66].

Oxygen excess non-stoichiometry is found in La_2NiO_4 where intergrowth phases containing $\text{La}_3\text{NiO}_2\text{O}_7$, $\text{La}_4\text{Ni}_3\text{O}_{10}$ etc. are found when the deviation in the oxygen stoichiometry is large [67]. Excess oxygen in $\text{La}_2\text{NiO}_{4+\delta}$ is incorporated as an interstitial oxygen defect as first predicted by Ganguly [4]. $\text{La}_2\text{NiO}_{4+\delta}$ exhibits behaviour remarkably similar to superconducting $\text{La}_2\text{CuO}_{4+\delta}$, suggesting oxygen defect structures are same in both the systems. In the earlier literature this non-stoichiometry in $\text{La}_2\text{NiO}_{4+\delta}$ was attributed to the presence of Ruddelsden-Popper intergrowth phases or deviation in the metal ion ratio (i.e. metal site vacancies). However, more recent studies including neutron diffraction studies [68] have conclusively shown that the observed stoichiometry cannot be attributed to the presence of intergrowth phases or deviation in the metal atom ratio [69] but is due to the presence of oxygen interstitials. The system can accommodate large concentration of the oxygens interstitials with δ as large as 0.2.

Nonstoichiometric K_2NiF_4 phases in the La-Co-O system has been studied by Ganguly and Ramsesha [70] and vacancy formation on both the La and O sublattices has been observed. A range of stoichiometries have been suggested in the literature which is represented by the formula $\text{La}_2\text{CoO}_{4+\delta}$ which is explained by the presence of excess oxygen or Ruddelsden-Popper phase intergrowths. However, Lewandowskii *et al* [71] reported that the material is La deficient and not rich in oxygen. The data reported by them were consistent with $\text{La}_{1.83}\text{CoO}_{4+\delta}$, $0 < \delta < 0.13$.

1.7. Background of atomic sizes (ionic radii)

Transferable interatomic length scales such as atomic radii have been used for the understanding of the organization of matter in several important problems such as the crystal structure of solids, the coordination number of metal atoms in various environments, structures of biologically important molecules etc. By far the most important parameter by which an ion can be described is its size, hence the "ionic radii" assumes a critical role in crystal chemistry. Such radii have been obtained from geometrical data related to interatomic distances provided by diffraction analyses of crystal structures. Traditionally a set of radii was judged solely by the accuracy with which the relation

$$R_{\text{anion}} + R_{\text{cation (from ionic radii table)}} = \textit{Interatomic distance}_{\text{(measured)}}$$

was satisfied.

Traditionally, ionic radii have been determined by treating the atoms and ions as hard spheres. The first attempt to obtain a systematic set of atomic length scales was by W.L. Bragg [72] who showed that many crystal structures could be approximated by tightly packed assemblies of spherical atoms, each of which was assigned a radius characteristic of that particular element. To first order those interatomic distances within the crystals could be approximated by sums of radii of spherical model atoms.

Goldschmidt *et al* derived a set of radii which could be used only for ionic crystals [73]. Goldschmidt was the first to note that ionic radii vary with

co-ordination number [26]. Wyckoff and Huggins subsequently showed that, whereas many interatomic distances could be approximated closely by Bragg's additive radii, others could not.

Pauling [74] recognized the effect of coordination number on ionic radius. He has concluded from these studies that the transferable radii, especially in solids, depend on whether the bonding in a compound is covalent, ionic or metallic. Each cation tends to increase the size with increasing coordination number. It has been shown that the high spin and low spin electronic configurations for some transition metal ions give rise to different ionic radii. When determining radii for bonded atoms the assignment of an electric charge on the ions is critical. Radii for negative ions are larger than those of corresponding free atoms because of increased electron-electron repulsion. Conversely the radii for electro-positive ions are reduced.

Subsequently, many revised sets of radii were tabulated by various authors (Zachariasen [75], Ahrens [76], Slater [77]) based on Pauling's or Bragg's ionic radii. Ahren's or Paulings radii were preferred because of simplicity of extracting radii directly from a table rather than calculations from univalent radii with corrections from valence and coordination.

Shannon and Prewitt tabulated an empirical set of "effective ionic radii" based on techniques similar to those of Goldschmidt [29,30]. These radii are calculated by considering electronic spin state, co-ordination number of both cation and anion, electronic repulsion and polyhedral distortion. In the present work these radii are utilized to study ionic radii effect on bonding. The precision of any relationship involving ionic radii can only be good if care has been taken to use the most

precisely defined appropriate radii. In evaluating utility, a criteria that the ionic radii should allow the better prediction of coordination changes, charge etc., is applied. These radii are environment-dependent, depending on the coordination number, charge, valence, etc. and are more closely reproduced interatomic distances in solids than the previous sets of radii.

The emphasis on environment-independent transferable atomic length scales that is useful in classifying crystal structures has been obtained from the pseudopotential approximation. The angular momentum dependent "pseudo-potential orbital radii" (r_p) is defined as the radius at which the potential $V_l(r)$ of the outermost electron crosses over from negative to positive values ($V_l = 0$ at $r = r_p$). Zunger, using *ab initio* atomic methods [78], calculated these radii which were correlated with length scales such as covalent radii or Pauling's tetrahedral or univalent radii. Such core radii are invariance with respect to chemical environment.

Recently the efforts have been made to define radii such as a mean valence radius, obtained from atomic valence electron charge density [79]. In these method, interatomic distances are calculated with the help of electronegativity and system dependent functions of the number of valence electrons.

More recently Ganguly [80] proposed a universal method based on r_i , obtained from the classical turning point of the valence electron wave function of angular momentum, l , to obtain interatomic distances for all bonding situations without requiring a prior knowledge of the electronegativity scale. Single bond interatomic distances has been expressed in terms of a universal multiplicative constant of a core s

orbital radius and another universal additive term which is close to the interatomic distance in the hydrogen molecule. The relationships are obtained from the dependence of the radii of positive or negative singly charged ionic species, CR^+ , CR^- , on r_i in homopolar compounds without considering bonding situations. Further, the relationship of the core orbital radii to the interatomic distances is shown for all bonding situations including that between transition metal elements, multiple bonds, heteropolar bonds as well as nonbonding situations [81].

1.8. Scope and nature of the thesis work

The perovskite structure and related layered structures affords a diversity in structure that is not matched in any other system so far. Such a diversity of structure leads to the accommodation of various kinds of metal ions with various valence states. This in turn leads to the vast diversity of properties ranging from insulating ferroelectrics to superconductors.

Critical to the delineation of the structures is the role of the tolerance factor, t , which takes into account the role of atomic sizes which is a single atom property. One requires therefore an appreciation of the meaning of the tolerance factor so that we may understand the limits, $0.86 < t < 1$, of the perovskite-related structures. In this thesis, the major attempt has been to understand the role of geometric factors such as atomic sizes, coordination number etc. on the nature of the structures that can be obtained and the possible influence of such structural constraints could have on the physical properties. In the present research work, effective ionic radii compiled by Shannon are used to study effect of size on bonding.

An AX_3 close-packing model, for describing the general family of the perovskite and perovskite-related structures is proposed. These structures has been discussed in terms of a new intralayer polytypism which depends on a competition between the relative orientation of neighboring AX rows in describing the structure. The close-packing model helps in defining the lower limits of the tolerance factor t . It also helps in understanding the role of the A ions such as Tl, Bi, Pb, etc in enhancing the superconducting transition temperatures.

Further, the non-Vegard's law behaviour of the c parameter in $La_{2-x}Sr_xCuO_{4-\delta}$ as a function of x is examined. The onset of the non-vegard's law behaviour coincides with the maximum in superconducting transition temperature. It has been found that two factors are responsible for the increase in c parameter. There are difference in size between La and Sr ions as well as the changes in tolerance factor. As t is increased the internal pressure is decreased which causes expansion of the lattice. The non-Vegard's law behaviour is due to the saturation of effects due to the tolerance factor at large Sr concentrations because of the competition with the effect of holes which tend to decrease atomic sizes. A general expression for the changes in the c parameter as a function of change in size of A ions, tolerance factor and the oxygen ion deficiency, *is given*.

Certain A_2BX_4 compounds, in spite of having tolerance factor, t , in the perovskite stability limit do not adopt K_2NiF_4 structure but adopt various distorted structures. These compounds are Sr_2PbO_4 , Ca_2IrO_4 etc. In this context the chemistry of Sr-Pb-Cu-O systems is studied. The motivation was to understand why Sr_2PbO_4 does not take up the K_2NiF_4 structure eventhough the tolerance factor of this compound is greater than 0.86. Therefore the solid solution of Ba_2PbO_4 and Sr_2PbO_4 and that of Sr_2SnO_4 and Sr_2PbO_4 is studied. The lower limit of the tolerance factor in obtaining the K_2NiF_4 structure is found

to be $t \approx 0.90$ instead of $t \approx 0.86$. In other compounds such as La_2CuO_4 the orthorhombically distorted phase is stabilized at low tolerance factors. Just as the conversion of the T structure of La_2CuO_4 to the T' structure of Nd_2CuO_4 is accompanied by an increase in the unit cell volume despite a decrease in the size of the A atom, the conversion of the K_2NiF_4 structure to the orthorhombic Sr_2PbO_4 structure is accompanied by a relative increase in the unit cell volume. Such an increase in the unit cell volume seems to allow space for the incorporation of several atoms which in turn leads to the transformation to an hexagonal structure derived from Ca_2IrO_4 structure type. We have studied the incorporation of atoms such as Cu, Zn and Cd in Sr-Pb-Cu-O system and have characterized the compounds by Rietveld X-ray diffraction analysis and by IR and Raman spectra.

The recent discovery of layered perovskite oxycarbonates and their high temperature superconducting behaviour has spurred interest in the synthesis of several layered multinary oxides of transition metal elements. The new layered Oxycarbonates which have got K_2NiF_4 related structures are studied. The similarity between the aragonite and calcite structures of the alkaline-earth carbonates, ACO_3 , and their relationship to the hexagonal and cubic ABX_3 perovskites is discussed. The importance of atomic sizes is brought out. The possible configurations of the carbonate group in the oxycarbonates is examined. Further, the cuprocarbonates derived from $\text{Sr}_{2-x}\text{Ba}_x\text{CuO}_2 \cdot \text{CO}_3$ is discussed with special emphasis on the changes in ESR spectra of the copper atoms in the CO_3 plane. The chemical and physical properties of the recently discovered compounds, $(\text{Sr},\text{Ba})_2\text{Li}_{0.5}\text{Cu}_{0.5}\text{O}_2 \cdot \text{CO}_3$ and $\text{Sr}_2\text{Li}_{0.5}\text{Ni}_{0.5}\text{O}_2\text{CO}_3$ are studied.

References

1. F.S. Galasso, 'Structure, Properties and preparation of perovskite type compounds', Pergamon Press, Oxford, (1969).
2. J.B. Goodenough and J.M. Longo, Landolt-Bornstein Tabellen, New Series, Gr. III/vol.4a (Part a), p.126, Springer-Verlag, Berlin (1970).
3. O. Müller and R. Roy, 'The Major Ternary structural families', Springer Verlag, Berlin-HeidelBerg, New York, (1974).
4. P. Ganguly and C.N.R. Rao, J. Solid state Chem., **53**, 193 (1984).
5. R. Roth, J. Res. Natl. Bur. Stand., **58**, 75 (1957); A. Rabeneau and P. Eckerlin, Acta Cryst., **11**, 30 (1958).
6. P. Poix, C.R. Acad. Sci.(Paris), **C 268**, 1139 (1969).
7. O. Fukanaga and T. Fryita, J. Solid State Chem., **8**, 331 (1973); P. Ganguly and C.N.R. Rao, Mater. Res. Bull., **8**, 405 (1973).
8. O. Fukanaga and T. Fryita, J. Solid State Chem., **8**, 331 (1973); J. M. Longo and P. Racciah, J. Solid State Chem., **6**, 526 (1973); B. Grande, H. R. Mullerbuschbaum and M. Schweizer, Z. Anorg. Allg. Chem., **428**, 120 (1977).
9. N. Ramdass, Mater. Sci. Eng., **36**, 231 (1978).
10. P. Poix, J. Solid State Chem., **31**, 95 (1980).
11. V.V. Lehmann and H.R. Mullerbuschbaum, Z. Anorg. Allg. Chem., **470**, 59 (1980).
12. C.N.R. Rao, D. Buttrey, N. Otsuka, P. Ganguly, H.R. Harrison, C.J. Sandberg and J.M. Honig, J. Solid State Chem., **51**, 266 (1984).
13. R. Berjoan, J.P. Coutures, G. Le Flem and S. Saux, J. Solid State Chem., **42**, 75 (1982).

14. C.N.R. Rao and B. Raveau, *Acc. Chem. Res.*, **22**, 106 (1989); Q. Yitai and Wu Yichang, *J. Crystal Growth*, **94**, 273 (1989).
15. R.J. Cava, *Science*, **247**, 656 (1990); J.P. Attfield and G. Ferey, *J. Solid State Chem.*, **80**, 112 (1990).
16. J.G. Bednorz and K.A. Muller, *Z. Phys.*, **B64**, 189 (1986).
17. S. Ochida, H. Takagi, K. Kitazawa and S. Tanaka, *Jpn. J. Appl. Phys.*, **26**, L1 (1987).
18. C.W. Chu, P.H. Hor, R.L. Mong, L. Guo, Z.J. Huang and Y. Q. Wang, *Phys. Rev. Lett.* **58**, 405, (1987).
19. A.W. Sleight, J.L. Gillson and P.E. Bierstedt, *Solid State Commun.*, **17**, 27 (1975).
20. A.F. Wells, 'Structural Inorganic Chemistry', 5th Edition, Clarendon Press, Oxford, (1984).
21. L. Katz and R. Ward, *Inorg. Chem.*, **3**, 205 (1964).
22. D. Balz and K. Plieth, *Z. Elektrochem.*, **59**, 545 (1955).
23. S.N. Ruddelsden and P. Popper, *Acta Cryst.*, **11**, 54 (1958).
24. G. Blasse, *J. Inorg. Nucl. Chem.*, **30**, 656 (1958).
25. H.D. Megaw, *Proc. Phys. Soc.*, **58**, 326 (1946).
26. V.M. Goldschmidt, *Skeifter Norske Videnskaps-Akad. Oslo. I. Matemat. Naturwiss.*, Klasse No. **8**, (1926).
27. A.M. Glazer and H.D. Megaw, *Phil. Mag.*, **25**, 1119 (1972).
28. A.M. Glazer, *Acta. Cryst.*, **B28**, 3384 (1972).
29. R.D. Shannon and C.T. Prewitt, *Acta Cryst.*, **B25**, 925 (1969).
30. R.D. Shannon, *Acta Cryst.*, **A32**, 751 (1976).
31. D. Ganguli, *J. Solid State Chem.*, **30**, 353 (1979).

32. D. Ganguli, *Neues Jahrb. Mineral. Abh.*, **123**, 313 (1975); D. Ganguli, *Neues Jahrb. Mineral. Abh.*, **130**, 303 (1977).
33. P. Lehuede and M. Daire, *C. R. Akad. Sci. Ser.*, **C276**, 1011 (1973).
34. P. Lehuede and M. Daire, *C. R. Akad. Sci. Ser.*, **C276**, 1783 (1973).
35. S. Tamura, *J. Phys. Soc. Jpn.*, **33**, 574 (1972).
36. D. Babel, 'Structure and Bonding', **3**, 1 Berlin-Heidelberg, Springer, New York, (1967).
37. A. Rabeneau and P. Eckerlin, *Acta Cryst.*, **11**, 304 (1958).
38. L.M. Kovba, E.A. Ippolitova, I.P. Simanov and V.I. Spittsyn, *Dokl. Akad. Nauk. SSSR*, **120**, 1042 (1958).
39. T.L. Teske and H.K. Mullerbuschbaum, *Z. Anorg. Allg. Chem.*, **371**, 325 (1969).
40. H.D. Wasel-Nielsen and R.Hoppe, *Z. Anorg. Allg. Chem.*, **375**, 209 (1970).
41. H.P. Roosky, *Acta Cryst.*, **1**, 266 (1948).
42. G. Demazeau, M. Pouchard, M. Thomas, J.F. Colombet, J.C. Grenier, L. Fournes, J.L. Soubeyroux and P. Hagenmuller, *Mater. Res. Bull.*, **15**, 451 (1980).
43. G. Demazeau, P. Courbin, G. Le Flem, M. Pouchard, P. Hagenmuller, J.L. Soubeyroux, I.G. Main and G.A. Robins, *Nouv. J. Chim.*, **3**, 171 (1979).
44. G.A. Robins, M.F. Thomas, J.D. Rush, G. Demazeau and I.G. Main, *J. Phys.*, **C 15**, 233 (1982).
45. G. Demazeau, M. Pouchard, N. Chevreau, M. Thomas, F. Menil, and P. Hagenmuller, *Mater. Res. Bull.*, **16**, 689 (1981).
46. L. Fournes, N. Kinomura and F. Menil, *C.R. Acad. Sci.*, (Paris) **C 291**, 235 (1980).

47. G. Demazeau, M. Pouchard and P. Hagemuller, *J. Solid State Chem.*, **18**, 159 (1976).
48. J.C. Joubert, A. Collomb, D. Elmaleh, G. Le Flem, A. Daoudi and G. Olliver, *J. Solid State Chem.*, **2**, 343 (1970).
49. A. Manthiram and J.B. Goodenough, *J. Solid State Chem.*, **87**, 402 (1990).
50. J.F. Bringley, S.S. Trail and B.A. Scott, *J. Solid State Chem.*, **86**, 310 (1990).
51. V.B. Grandle, H. Muller-Buschbaum and M. Schweizer, *Z. Anorg. Allg. Chem.*, **428**, 120 (1977).
52. H. Muller-Buschbaum, *Angew. Chem. Int. Ed. Engl.*, **16**, 674 (1977).
53. Von H. Muller-Buschbaum and W. Wollschlager, *Z. Anorg. Allg. Chem.* **414**, 76 (1975).
54. S.W. Cheong, Z. Fisk, J.D. Thompson and R.B. Schwarz, *Physica C* **159**, 407 (1989).
55. J.M. Tarascon, L.H. Greene, W.R. Mckinnon and G.W. Hull, *Solid State Commun.*, **63**, 499 (1987).
56. J.K. Burdett and K. Kulkarni, *Chem. Phys. Lett.*, **160**, 350 (1989).
57. M.-H. Whangbo, M. Evain, M.A. Beno and J. M. Williams, *Inorg. Chem.*, **26**, 1829 (1987).
58. N. Kimizuka, E. Takayama and S. Horiuchi, *J. Solid State Chem.*, **42**, 322 (1982).
59. C. Michel and B. Raveau, *Revue de Chimie minerale*, t. **21**, p.407 (1984).
60. C.N.R. Rao and J.Gopalkrishnan, in 'New directions in Solid State Chemistry', Cambridge University Press, Cambridge, (1986).
61. M.E. Leonowicz, *J. Solid State Chem.* **59**, 71 (1965); L. ER. Rakho, C. Michael, *J. Solid State Chem.*, **37**, 151 (1981).

62. K.R. Poeppemeier, H.E. Leonowicz and J.M. Longo, *J. Solid State Chem.*, **44**, 89 (1982).
63. K. Vidyasagar, J. Gopalakrishnan and C.N.R. Rao, *Inorg. Chem.*, **25**, (1984).
64. J.P. Attfield. and G. Ferey, *J. Solid State Chem.*, **80**, 112 (1989); F. Galasso and W. Darby, *J. Phys.Chem.*, **68**, 1318 (1962).
65. P.M. Grant, SSP Parkin, V.Y. Lee, E.M. Engler, M.L. Ramirej, G. Lim, and R.D. Jacowitz, *Phys. Rev. Lett.*, **58**, 2482 (1987).
66. J.D. Jorgensen, B. Dabrowski, S. Pei, D.G. Hinks and L. Solderholm, *Phys. Rev.* **B38**, 11337 (1988); J. Zhou, S. Sinha, J.B.Goodenough, *Phys. Rev.*, **B39**, 12331 (1988).
67. J. Drennan, C.P. Traveres and B.C.H. Steele, *Mater. Res. Bull.*, **17**, 621 (1982).
68. J.D. Jorgensen, B. Dabrowski, S. Pei, D.R. Richards, D.G. Hinks, *Phys. Rev.* **B40**, 2187 (1989).
69. D.J. Buttrey, P. Ganguly, J.M. Honig, C.N.R. Rao., R.R. Schartman and G.N. Subbanna, *J. Solid State Chem.*, **74**, 233 (1988); D.J. Buttrey, H.R. Harrison, J.M. Honig and R.R. Schartman *J. Solid State Chem.*, **54**, 407 (1984).
70. P. Ganguly and S. Ramasesha, *Magn. Lett.*, **1**, 131 (1980).
71. J.T. Lewandowski, R.A. Beyerlein, J.M. Longo, R.A. McCauley, *J. Am. Cer. Soc.*, **69**, 699 (1986).
72. W.L. Bragg, *Philo. Mag.*, **40**, 169 (1920).
73. V.M. Goldschmidt, T. Barth, G. Lunde and W.H. Zachariasen, *Skr. Norske vidensk, Akad*, **1**, Mat. kl. No.2, (1926).
74. L. Pauling, 'The Nature of the Chemical Bond', Cornell Univ. Press, Ithaca, New York, Chapter 7, **11** and **13**, (1960); L. Pauling, *J. Amer. Chem. Soc.*, **49**, 765 (1927).
75. W.H. Zachariasen, *Z. Kristallogr.*, **80**, 137 (1931).

76. L.H. Ahrens, *Geochem. cosmotrum Acta*, **2**, 155 (1952).
77. J.C. Slater, *J. Chem. Phys.*, **41**, 3199 (1964).
78. A. Zunger, *Phys. Rev.*, **B22**, 5839 (1980).
79. S.B. Zhang, M.L. Cohen, *Phys. Rev.*, **B39**, 1077 (1989); A. Garcia, M.L. Cohen, *Phys. Rev.*, **B47**, 4221 (1993).
80. P. Ganguly, *J. Am. Chem. Soc.*, **115**, 9287 (1993).
81. P. Ganguly, *J. Am. Chem. Soc.*, **117**, 1777 (1995).

CHAPTER 2

EXPERIMENTAL METHODS: SYNTHESIS AND CHARACTERISATION

This chapter describes the various instrumental techniques employed for the general synthesis methods for oxides and the physicochemical characterisation of different oxide systems.

2.1. Chemical methods

A variety of synthetic strategies have been employed to prepare pure monophasic oxides of different families with good physical properties. The most common method of synthesis of oxide material is the traditional ceramic method [1]. Although the ceramic method has yielded many of the cuprates with satisfactory results, different synthetic strategies have become necessary in order to control factors such as cation composition, oxygen stoichiometry, cation oxidation states and carrier concentration. Amongst these, chemical or solution routes are noteworthy which permit better mixing of constituent cations in order to reduce diffusion distances in the solid state [2,3].

2.1.1. Solid State synthesis

This is the most common method of synthesizing inorganic oxides by the reaction of the component materials at elevated temperatures. If all the components are solids, the method is called ceramic method [4]. If one of the component is volatile or sensitive to atmosphere, the reaction is carried out in sealed evacuated capsules. Platinum, silica or alumina containers are generally used for the synthesis of metal oxides. The starting materials are metal oxides, carbonates, or other salts, which are mixed, homogenised and

heated at a given temperature sufficiently long for the reaction to be completed. A knowledge of the phase diagram is useful in fixing the the composition and conditions in such a synthesis. A successful synthesis by the ceramic method depends on several factors which include the nature of the starting materials, homogeneity of the mixture of powders, the rate of heating and the reaction temperature and duration.

In the present study, the ceramic method is employed which involves mixing and grinding of the component oxides, carbonates, nitrates or other salts, in the appropriate metal ratio and heating the mixture, generally in pellet form, at the desired temperature. A common variation of the method is to heat the mixture of nitrates obtained by digesting the molar oxides or carbonates in concentrated nitric acid and evaporating the solution to dryness. Heating is carried out in air or in appropriate atmosphere to get the oxide, controlling the partial pressure of oxygen, wherever necessary.

2.1.2. Estimation of oxygen content

Oxygen stoichiometry of the materials is determined by iodometric titrations. Iodometry deals with the titration of liberated iodine in chemical reactions [5]. Weighed quantity of the material (after dissolving in dilute HCl solution) is titrated against Standard (0.02 N) $\text{Na}_2\text{S}_2\text{O}_8$ solution using fresh starch solution as an indicator. Saturated KI solution was used as an oxidizing agent for liberation of free iodine. Amount of iodine liberated could be determined from titre reading. Total content of the oxygen is then calculated from number of moles of iodine liberated.

2.2. Instrumental Methods

2.2.1. X-ray Diffraction

Powder X-ray diffraction technique was used to identify the structure and phases of the samples prepared under various conditions. X-ray powder diffraction patterns were obtained with a **Philips-Norelco diffractometer model PW 1730** using monochromatic high intensity $\text{CuK}\alpha$ radiation ($\lambda = 1.54056 \text{ \AA}$). A Nickel filter was used to eliminate the $\text{K}\beta$ lines. For qualitative identification of the phases present, the patterns were taken from $8 < 2\theta < 80$ at a scan rate of the $2^\circ 2\theta/\text{min}$. The scan rate used to obtain X-ray patterns for precision cell constant determinations was $0.25^\circ 2\theta/\text{min}$ with a chart speed of 30 inches/hr. For structural refinement purpose, XRD pattern was recorded on a **JEOL JAD-8030** Cell parameters were determined by the least-squares refinement of the reflection using a computer program which corrects for the systematic errors of the measurement. Lattice parameters were obtained for the material using internal standard for the calibration.

2.2.2. Electron Spin Resonance

The use of electron paramagnetic resonance technique for the macro- and micro-structural investigation of the paramagnetic substances is based on the equation $h\nu = g\beta H$. This law emphasizes the exact matching of the photon radiation energy and the energy separation between the two energy levels. A **BRUKER X-band EPR spectrometer, model ER 200D-SRC** was used in the present studies. The spectrometer mainly consists of a magnet, a magnetic power supply unit, a microwave bridge and a

console consisting of a time base unit, a signal channel and a field controller. In addition to these, three prestanding assemblies are provided. These are chart recorder, a microwave cavity and a safety box. The chart recorder is mounted in the console. The cavity is supported between the poles of the magnet by a wave-guide which connects it to the microwave bridge. The safety box is mounted in the magnet power supply unit. It isolates all power to the system. The output of the spectrometer is in the form of spectrograph covering selected portion of the microwave region of the electromagnetic spectrum. The spectrograph can be displayed on a cathod ray tube or can also be plotted on a paper. The ESR signals were recorded in the derivative mode at a resonance frequency of 9.71 GHz, magnetic field modulation of 100 KHz and microwave radiation power of 2mW. In the present work the ESR spectrum is used to detect the paramagnetic centres in various perovskite systems. Spectra were recorded at room temperature (300K) and at 77 K wherever necessary.

2.2.3. Resistivity Measurements

Four probe d.c. resistivity measurements were performed by van der Pauw method [6] in the temperature range 12-300 K using an APD close-cycle helium cryostat. Electrical contacts were made by using silver paste. Resistance measurements has been done using a **Keithley 220 constant current source** and a **Keithley 196 DMM** which are connected to an IBM PC through IEEE 488 interface. The temperature controller of the cryostat (**Scientific Instrument 9650**) was also controlled by the computer which allowed for continuous data collection at several fixed temperatures in the range 12-300 K.

2.2.4. Magnetic Susceptibility measurements

Magnetic susceptibility measurements on powder samples were done by the Faraday method in the temperature range 10-300 K (using an APD close-cycle helium cryostat). Magnetic field strength of 5000 gauss was used for the measurement.

2.2.5. Infra-red spectra

The IR spectra of the samples were recorded in a **Nicolet 60-SXB Fourier Transform Infra-red spectrometer** having a resolution ± 2 cm^{-1} . The IR spectra were taken in a standard manner with the samples being ground in KBr (0.3% w/w) and then pelletised to form transparent discs. 100 scans were taken for recording each spectrum in the region 4000-400 cm^{-1} .

2.2.6. Raman spectra

The Raman scattering measurements were performed in the region 20 - 800 cm^{-1} in the back scattering mode using a **spex 1403** reflection grating type double spectrometer. The **spex 1442** third monochromator slaved in tandem to the double monochromator was used to reduce the Rayleigh light and other background effects. The data were collected in the photon counting mode using **RCA C31034** GaAs photomultiplier detector system and **SPEX DMI DATAMATE** spectrometer controller and data processor. The radiation of wave length 514.5 nm from the Argon ion laser, filtered through the spex lasermate, was allowed to fall on the sample (sample was taken in a pellet form) in a line focus geometry with the help of the cylindrical lense. The

intensity of the radiation incident on the sample was less than 150 mW. The scattered radiation was collected and focused on to the spectrometer slit using a Minolta camera lens. The polarisation of the incident radiation was kept fixed in the horizontal plane. The actual positions, intensities and widths of the various Raman bands were measured after a light smoothing of the raw data by using the in built software of the DM1 data processor. The ultimate resolution at the 250- μm - wide exit slit was better than $\pm 2 \text{ cm}^{-1}$.

2.2.7. Nuclear magnetic resonance

^7Li NMR experiments were carried out on a **Bruker MSL 300 FT-NMR spectrometer** operating at a magnetic field of 7T. For ^7Li NMR observation at 116.64 MHz. the probe had to be retuned with additional circuitry. In the present work experiments were carried out in the single pulse (SP) sequence (a single non-selective pulse with a preacquisition delay of 4 microseconds was employed). Free induction decays were collected in a quadrature channels of a **Bruker BC-131** digitizer and standard phase cycling into the pulse sequence was incorporated to minimize artifacts in the receiver. Pulse sequences such as quadrupolar echo pulse (QEP) [7]., $(\pi/2)_x - \tau - (\pi/2)_y - \tau - \text{echo}$ and Spin - echo (SE) [8] $(\pi/2)_x - \tau - (\pi)_y - \tau - \text{echo}$ sequences were used. All the experimental parameters are indicated in the respective figure captions. Temperature was varied using **BVT-1000** temperature controller unit .

2.3. Computational methods

Various computer programmes are used for the calculation and refinement of a powder x- ray diffraction patterns. The values of atomic scattering factor for various elements for various 2θ values are taken from International table for X-ray crystallography [9]. This analysis is useful in studying the effects of substitution of various elements and also the effect of partial occupation of various sites by other atoms in off-stoichiometric composition.

2.3.1. The PDP11 programm

The PDP11 (Powder diffraction package version 1.1) Program is written by M. Calligaris [10] was used for indexing and simulation of XRD patterns. This programme allows indexing of XRD pattern and refining of cell parameters for different crystal systems. The programme also allows calculation of the X-ray powder diffraction patterns of a pure phase from the known crystal data (cell parameters, space groups and atomic coordinates) as well as the calculation of patterns for mixture of phases.

2.3.2. The LAZY-PULVERIX programme

This computer program [11] is also used for calculation of powder XRD patterns. The powder diffraction patterns are calculated using information such as lattice parameters, space groups symbols and the atomic positions and atomic symbols of the atoms in asymmetric unit cell. The main advantage of this programme is that it automatically derives the required crystallographic parameters such as equivalent point

position, scattering factors etc., from the space group and element symbols so that only a minimum amount of input data is necessary for the intensity calculation. The output of the programme consists of a tabular listing of hkl, d spacing, 2θ values and intensities.

2.3.3. Rietveld Refinement method

Structure refinement from the X-ray powder diffraction data has been carried out using the Rietveld refinement method of structure refinement [12]. The PC version of the programme DBW 3.2S- PC-9011 [13] was used for the calculation. This program refines powder diffraction data collected with a $\theta - 2\theta$ diffractometer operated in a step-scan mode (equal steps in 2θ) and with either one or two wavelengths. The program uses the Newton-Raphson algorithm to minimize the quantity;

$$\sum W_i(y_i - y_{ci})^2$$

where the sum is over all data points, N, and

$$W_i = 1/Y_i,$$

Y_i = observed intensity at the i^{th} step,

Y_{ci} = calculated intensity at the i^{th} step.

The output file contains R pattern-factors, S (goodness of fit), corrected data list, observed and calculated intensities, reflection list at each step after the last cycle. At the end of each cycle, the parameters shifts, and standard deviations are given. The standard deviation is estimated from the formula:

$$\sigma = \sqrt{M_{ii}^{-1} \sum (y_i - y_{ic})^2 / N - P + C}$$

where, M_{ii}^{-1} is the corresponding diagonal element in the inverted matrix,

N is the number of observations, P is the number of parameters that are refined and C is the total number of constraints.

The 'R-factors' used to judge the quality of the refinement are given as,

The pattern R-factor

$$R_p = 100 \frac{\sum |Y_i - Y_{ci}|}{\sum |Y_i|}$$

The weighted pattern R-factor

$$R_{wp} = 100 \sqrt{\frac{\sum W_i (Y_i - Y_{ci})^2}{\sum W_i Y_i^2}}$$

The expected R-factor

$$R_{exp} = 100 \sqrt{N - P + C / \sum W_i Y_i^2}$$

S is the 'goodness of fit', the ratio R_{wp} / R_{exp} .

Crystal structure projection pictures are obtained using SCHAKAL-88 software package.

References

1. C.N.R. Rao, *Phil. Trans. R. Soc.*, **A336**, 595 (1991).
2. C.N.R. Rao, (ed.) . *Chem. High Temp. Super.* (Singapore: World Scientific) (1991).
3. C.N.R. Rao and J. Gopalakrishnan, 'New directions in solid state chemistry', Cambridge University press, (1989).
4. C.N.R. Rao, *Mater. Sci. Eng.*, **167**, 34 (1992).
5. A.I. Vogel, a 'A Textbook of Quantitative Inorganic Analysis Including Elementary Instrumental Analysis', Third Edⁿ., Longman, London, (1961).
6. L.J. Van der Pauw, *Philips Research Reports*, **13**, 1 (1958).
7. J.H. Davis, K.R. Jeffrey, M. Bloom, M. Valic and T.P. Higgs, *Chem. Phys. Lett.*, **42**, 390 (1976).
8. H.Y. Carr and E.M. Purcell, *Phys. Rev.*, **B94**, 630 (1954).
9. 'International tables For X-ray Crystallography, ' 2, edited by N.F.M. Henry and K. Landscale, The Kynnoch Press, Birhimgham (1952).
10. M. Calligaris, *Dipartominto di scinze chimiche, Universita di Trieste, Italy* (1989).
11. K. Yvon, W. Jeitschko and E. Parthe, *J. Appl. Cryst.*, **10**, 73 (1977).
12. H.M. Rietveld, *J. Appl. Cryst.*, **2**, 65, (1966); H.M. Rietveld, *Acta. Cryst.* **20**, 508 (1969).
13. D.B. Wiles, A. Sakhivel and R.A. young, School of Physics, Georgia Institute of Technology, Atlanta, G. A. 30332, (1990).

CHAPTER 3

AX₃ CLOSE-PACKING DESCRIPTION OF THE LAYERED PEROVSKITES

3.1. Introduction

Ever since high-temperature superconductivity was first seen [1-3] in compounds derived from La_2CuO_4 the emphasis has been on examining the properties of the CuO_2 planes in the La_2CuO_4 structure. Little attention has been paid to the role of the A ions in the rock-salt layers. The structural principles leading to the formation or stabilization of these layered perovskite compounds has not been properly enunciated. In the absence of such a formalism the physico-chemical insights based on structure-property correlations, perhaps first put on a sound physical footing by Goodenough [4], are likely to be flawed.

Besides the novel phenomenon of high-temperature superconductivity, the cuprate perovskite oxides have in addition a chemical component which is entirely new. The layered perovskite oxides studied earlier [5] were mainly those with the K_2NiF_4 structure or the Ruddlesdon-Popper structure belonging to the series $[\text{AO}]_n (\text{ABO}_3)_m$ with $n' = 1$. The layered perovskite cuprate oxides such as the 2212 compound, $\text{Bi}_2\text{Sr}_2\text{CaCu}_2\text{O}_8$, have the additional feature that $n' > 1$ [2]. The so-called rock-salt $(\text{AO})_n$ layers are considered to play a crucial role as charge reservoirs [6] for doping in the CuO_2 planes. The possible mechanism of charge-transfer is believed to be entirely electronic in origin. The role of structural constraints in effecting such a charge transfer has not been considered. That n' can be greater than 1, was discussed earlier by Ganguly and Rao [5] but was not satisfactorily demonstrated. In the description of layered perovskites in terms of stacking of rock-salt and perovskite building blocks, no special insight is obtained regarding the nature of the A ions that may be incorporated in the rock-salt or perovskite layers or at the boundaries of these domains. This is a serious limitation as so far there has been no rationale for the fact that the octahedrally coordinated A ions in the rock-salt

layer do not occupy the octahedral B sites in the perovskite layer. In addition, the formulation $(AO)_n \cdot (ABO_3)_m$ for the layered perovskites does not easily account for the incorporation of excess oxygen in (or its loss from) the rock-salt layer.

One may obtain a better understanding of the role of the A ions when a close-packed description of these structures involving the A and oxygen ions are considered. The copper ions occupy the interstitial octahedral sites arising from the close-packing. Such a close-packed description is equally applicable to some of the intermetallic compounds. In this description the role of the A ions in influencing the structure becomes more transparent. One may also obtain the number and chemical nature of the A ions in the rock-salt and the perovskite layers. The A ions in the rock-salt layer are too large to occupy O_6 octahedral interstices. The rock-salt structures in compounds such as BaO, KF etc., are instead shown to be derived from an AX_3 close-packed description with the loss of X_2 . The close-packed description also yields an understanding of the peculiar oxygen chemistry of the layered cuprate oxides.

In this chapter, the structural similarity between the layered perovskite compounds (when only the A and oxygen ions are considered) and the incommensurate phases in intermetallic compounds [7,8] that has been associated with the existence of antiphase domain boundaries (APB) are considered. Instead of rock-salt and perovskite layers as the building blocks of the perovskite structure, a formulation of the structure of the layered perovskites in terms of a two AX_3 close-packing scheme is presented. It has been proposed that the layered perovskite structures are obtained due to an admixture of the two types of AX_3 close-packing. This happens when the ratio of the number of A ions to that of the B ions is greater than 1. The justification for a close-packing description of intermetallic compounds lies in the

non-directional character of metallic bonding [9]. This is not the case for the oxides that are described below as they can be both good insulators and good metals.

The close-packing model is useful in obtaining some chemical insights on the mechanism of charge transfer reservoir in the rock-salt layers to the CuO_2 planes. From this analysis it has found below that there are constraints imposed by such a close-packing which helps in understanding several factors such as the selectivity of various A ions for various sites, the lower limits of the tolerance factor, an additional role of the "charge-reservoir" layers etc., which are not available from the earlier analysis of the structure in terms of rock-salt and perovskite building blocks.

3.2. Close-packed model for layered perovskites

3.2.1. Two kinds of AX_3 close-packing

In this section, the AX_3 close-packing model is applied to the layered perovskites. Such a description is based on the two types of AX_3 close-packing exemplified [7,8,10] in compounds such as Cu_3Au and Ni_3Ti . The two AX_3 close-packing schemes of figs. 3.1a and b, are responsible for the L1_2 (fig. 3.2a) and DO_{22} (fig. 3.2b) structures of Cu_3Au and Ni_3Ti , respectively. The DO_{22} structure is an antiphase boundary (APB) structure derived from the basic building block with L1_2 structure. The (001) plane is the antiphase plane with the displacement vector $[\frac{1}{2}, 0, \frac{1}{2}]$.

The AX_3 close-packing generates different a,b or c sites as illustrated, for

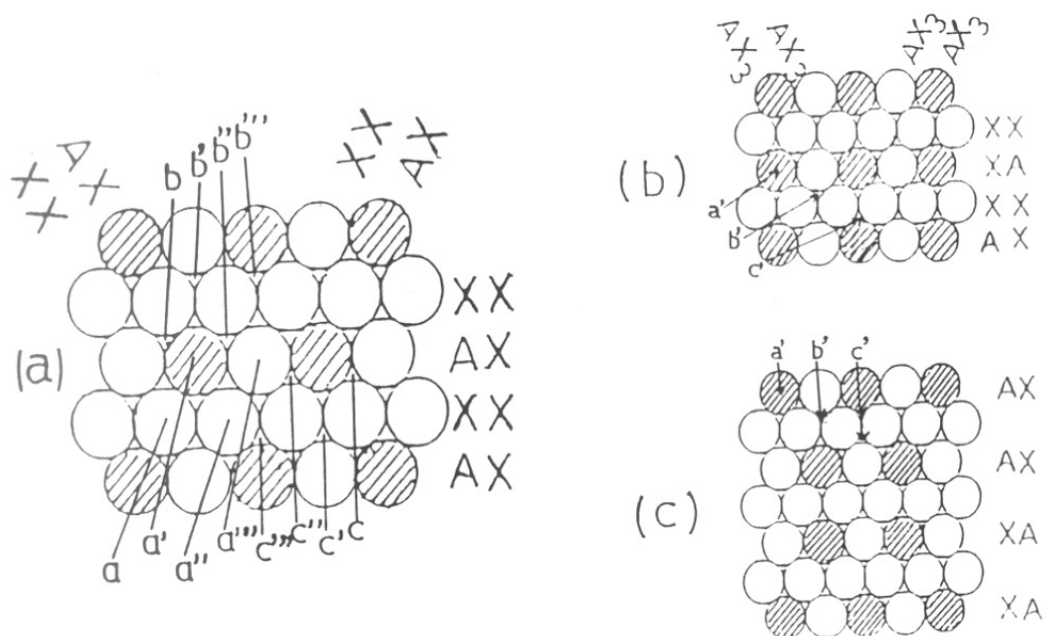


Fig. 3.1. (a) AX_3 close-packing leading to perovskite structures. The four possible b(or c or a) sites are shown. (b) AX_3 close-packing leading to DO_{22} structure (c) the $\langle 2 \rangle A_2X_6$ close-packing scheme that gives rise to DO_{23} structure. \odot : A ions \circ : X ions. These closed packed layers are to be considered as A layers in the *ccp* ...ABCABC... sequence. The a', b' and c' sites employed in the *ccp* scheme are shown in (b) and (c).

example, in fig. 3.1a. These sites may in turn be occupied by different A or X ions. Four inequivalent sites are thus generated as shown in fig. 3.1a. A constraint is imposed that the a' (or b' or c') sites involve only A ions. This minimizes the Coulomb repulsion between the A cations in the ionic limit. (In the homopolar or non-ionic limit in which there is not much charge separation as in the intermetallic compounds all the four sites may be occupied and this gives rise to the complexity of structures that are observed). The packing of these layers is always "cubic-close-packed" (ccp) in the sense that the A ions in each layer are stacked such that the ...a'b'c'a'b'c'a'b'c'... sequence is maintained (as illustrated in figs. 3.1b and 3.1c, for example). A cubic ...ABCABCABCABC... close-packing of the AX₃ layers with the above constraints is shown in fig. 3.1a. The close-packed layer is along one of the {111} planes. The structure in fig. 3.2a has the L1₂ structure involving noble metals such as Cu₃Pd, Cu₃Au, Ag₃Mg, Au₃Cd, Au₃Zn etc.[7,8,11]. The packing in fig. 3.1b yields the structure in fig. 3.2b. The close-packed layer is now parallel to the {112} planes. The structure in fig. 3.2b corresponds to the DO₂₂ structure as in TiAl₃ or Ni₃Ti. In such a description the four translational variants of the APB structure arising from the four atomic coordinates of the AX₃ unit [7,8] may now be related by the occupancy of the A ion of the four a (or b or c) sites in fig. 3.1a.

The AX₃ close-packing scheme in L1₂ as well as DO₂₂ structures may be considered to arise from an alternation of AX and XX rows in at least one direction. In the L1₂ sequence, the packing of the rows are considered to be in the sequence, ..AX.XX.AX.XX.AX.XX.AX..XX... (fig. 3.1a). In fig. 3.2a, these AX and XX rows are along the <110> direction. The close-packed AX₃ layers are along the {111} planes. In the DO₂₂ close-packing (along the {112} planes, fig. 3.2b) the sequence is ...AX.XX.XA.XX.XA.XX.AX.XX... (see fig. 3.1b). The rows are along <101> directions and the close-packing is in the {114} planes for the unit cell of fig. 3.2c (in

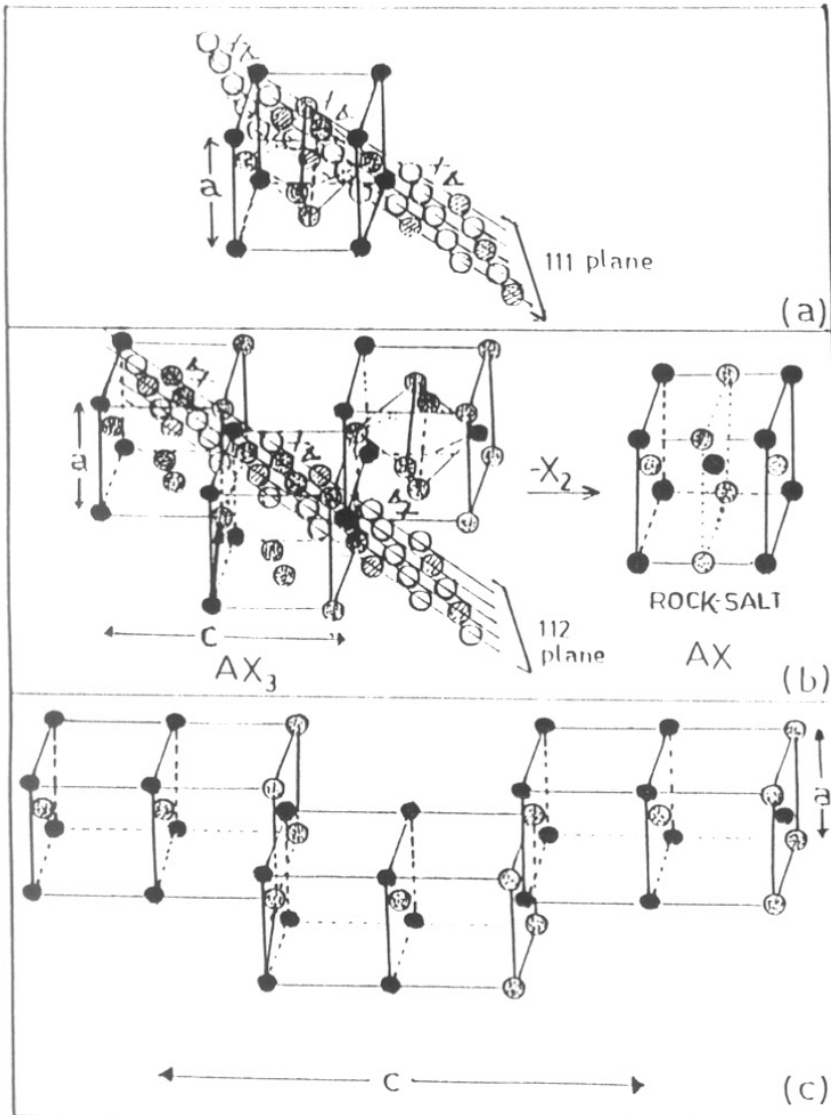


Fig. 3.2. (a) The close-packing in the L₁₂ structure of Cu₃Au. The close-packed 111 plane is shown. The AX and XX rows are parallel to the $\langle 110 \rangle$ direction. The relative positions of the A ions in adjacent AX rows correspond to that in fig.3.1a. (b) The DO₂₂ structure with an antiferromagnetic AX₃ close-packing along the 112 plane; the relative positions of the A ions in adjacent AX rows correspond to that in fig.3.1b. Removal of X₂ rows yields the rock-salt structure as shown. (c) The DO₂₃ structure from ref.(8). ●, ⊗ : A ions, ○, ⊙ : X ions. The filled and dotted circles are part of the cell drawn.

which the X_2 rows have been omitted). The two kinds of close-packed layers are differentiated by the locations of the A ions (figures 3.1 a and b) relative to each other. It is known that the AO_3 close-packing scheme corresponding to the Li_2 structure leads [10,12] to the perovskite ABO_3 when there are B ions to occupy the O_6 octahedral sites. The other AX_3 packing responsible for the DO_{22} structure would lead to the rock-salt structure in oxides by the loss of an oxygen molecule. This latter packing is stabilized when there are no B ions.

The above description may also be applied to systems in which there are cation or anion vacancies. These vacancies are represented by A' and X' . Thus $A'BX_3$ corresponds to perovskite structures such as WO_3 , ReO_3 etc. The AX_3 packing in fig. 3.2b is important for describing the structure of layered perovskites. *The removal of the X_2 rows from the packing scheme in fig. 3.2b yields the rock-salt structure as indicated.* This in turn yields a new criterion for distinguishing between two kinds of rock-salt structure. These are the AX rock-salt compounds such as KF, BaO etc. in which $r_A/r_X > 0.73$, which are derived from a close-packing description of A and X ions, and BX rock-salt compounds such as MgO, NiO, LiF, etc for which $0.41 < r_B/r_X < 0.73$ which are derived from a close-packed description of only the X ions with the B ions occupying the X_6 octahedral interstices.

3.2. Generation of layered perovskites

The stability of competing close-packed phases in intermetallic compounds began to be understood after it was recognized that the main contributions come from changes in next-nearest-neighbor bonding [9,13]. In itinerant electron systems, the phase stabilities were sought to be ultimately rationalized in terms of the

Hume-Rothery/Mott/Jones criterion of alloy phase instability [9,14]. However, the band structure calculations of the anisotropic systems gave details of the Fermi surface which were not amenable to simple Hume-Rothery interpretations [9]. The importance of next-nearest-neighbor interactions (instead of k space in band picture) in the axial next-nearest-neighbor Ising (ANNNI) model [15] as first demonstrated experimentally by Loiseau *et al* [8].

As mentioned earlier, the intermetallic compounds are usually described in terms of APB structures which are ordered and periodically distributed along a modulation direction perpendicular to the boundary planes. The APB structures are then described by the length of domains in units of one Ll_2 unit length. The DO_{22} structure is the simplest structure where the antiphase boundary occurs at every unit cell. In the Zhdanov notation [16] the DO_{22} structure is represented as 11. The AX_3 structures in fig. 3.1b or 3.2b, have been described in the pseudo-spin language of the ANNNI model [8,10] as a one-dimensional antiferromagnet which corresponds to $\langle 1 \rangle$ in the Fisher-Selke notation [17], while that in fig. 3.1a or 3.2a corresponds to the ferromagnetic ground state $\langle \rangle$. When there are m spins in ferromagnetic domains and n spins in antiferromagnetic domains, the Fisher-Selke notation would be $\langle m, 1^n \rangle$ (which can be written simply as $\langle m, n \rangle$). The Ising Pseudo-spins can be identified by \langle or \rangle . Thus a $\langle 3, 1^2 \rangle$ notation would be written as $\dots \underline{\langle \langle \langle \rangle} \underline{\langle \langle \langle \rangle} \underline{\langle \langle \langle \rangle} \underline{\langle \langle \langle \rangle} \dots$ with the underlined spins corresponding to the ferromagnetic domains. It can be seen that there is a maximum of three distinguishable spin sites in this model when m and n are both not equal to zero. These correspond to the two sites with nearest-neighbor ferro- or antiferromagnetic interactions and the sites at the domain boundaries. Such sites are characterized by one nearest-neighbor alignment of the spins.

In the model of the layered perovskites, the two types of AX₃ close-packing are admixed within a close-packed layer by changing the relative orientations of the AX rows, as for example ...AX.XX.XA.XX.XA.XX.AX.XX.XA.XX.XA.XX... (fig.3.1c). The AX row is distinguished from the XA row simply by the relative disposition of the A ions. It is seen from fig. 3.1a that in adjacent AX (or XA) rows in a plane the A ions are disposed diagonally to each other; in AX (XA) rows adjacent to XA (AX) rows the A ions are on top of each other (fig. 3.1b). The nature of the A ion in each AX row is physico-chemically similar (say in terms of ionic radii, charge, polarisability, etc.). There are only two possible orientations of the AX rows so that they may be represented by Ising pseudospins. The layered perovskites may then be considered to be polytypes arising from different spin orientations *within* a close-packed AX₃ layer which are cubic-close-packed with the constraint that the A ions occupy the a' or b' or c' sites. It is important to note that when the constraint of a "*ccp*" packing of the layers with the A ions occupying only a' (or b' or c') sites of fig. 3.1, is imposed, a unique structure is obtained. Although these structures are derived from a stacking of planes with different orientations of the AX rows in a close-packed plane, it is the "*ccp*" packing that ensures the layered perovskite structure with its characteristic unit cell. The conventional description of the structure in terms of rock-salt or perovskite layers is now possible for these unit cells obtained from *diffraction studies*. However, the close-packed description gives some new insights that are not accessible to a description of the structure which employs purely rock-salt and perovskite building blocks.

The present model is similar in spirit to that used by Katz and Ward [10] to explain polytypism in hexagonal perovskites [18]. The polytypism in this case arose from an admixture of hcp and ccp sequences of the same kind of close-packed AX₃ layers as in Cu₃Au. This is the classical kind of polytypism found, for example, in SiC, and has

been studied in terms of the axial next-nearest-neighbor-Ising (ANNNI) model [12]. The anticyclic hcp ...ABABABAB... stacking and cyclic ccp ...ABCABCABCABC... stacking of the close-packed layers have been represented by the two state Ising notation by Zhdanov and Minervina [16]. The two-state notations used by us to describe the layered perovskites is unique and novel concerning itself as it does with different structural types arising from the relative *intraplanar* orientations of the rows and not the stacking of the planes.

The conditions for stabilizing either of the AX_3 close-packing schemes leading to the $L1_2$ or DO_{22} structure are discussed below. The structure in fig. 3.2a arising from the packing in fig. 3.1a yields three A_2X_4 and one X_6 octahedra for each AX_3 unit (as shown in fig. 3.3a). On the other hand, the structure in fig. 3.2b arising from the packing in fig. 3.1b yields two A_2X_4 and two AX_3 octahedra (as shown in fig. 3.3b). The Coulomb repulsion between the A ions at the vertices of the octahedron is therefore reduced. The occupation of the X_6 octahedra in fig.3.3a yields the ABX_3 perovskite. The electrostatic attractive B-X interactions in BX_6 octahedra stabilize the perovskite structure of ionic compounds so that the AX_3 close-packing of fig. 3.1a is preferred. In the absence of the B ions the packing in fig. 3.2b is preferred. The layered perovskite structures are thus obtained in the AX_3 close-packing model when the ratio of A:B ions is greater than 1.

The $\langle 2, 1^\circ \rangle$ or $\langle 2 \rangle$ notation corresponds to the composition A_2BX_6 with the spin sequence ... $\langle \rangle \langle \rangle \langle \rangle \langle \rangle \langle \rangle \langle \rangle \dots$. In intermetallic compounds the $\langle 2 \rangle$ phase (figs. 3.1c, 3.2c) corresponds to $ZrAl_3$. In the $\langle 2 \rangle$ case all spins are at the domain boundaries. There is thus only one kind of A ion, which is termed as the A_p ions. The $\langle 2 \rangle$ structure (fig. 3.2c) is topologically similar to that of the Aurivillius

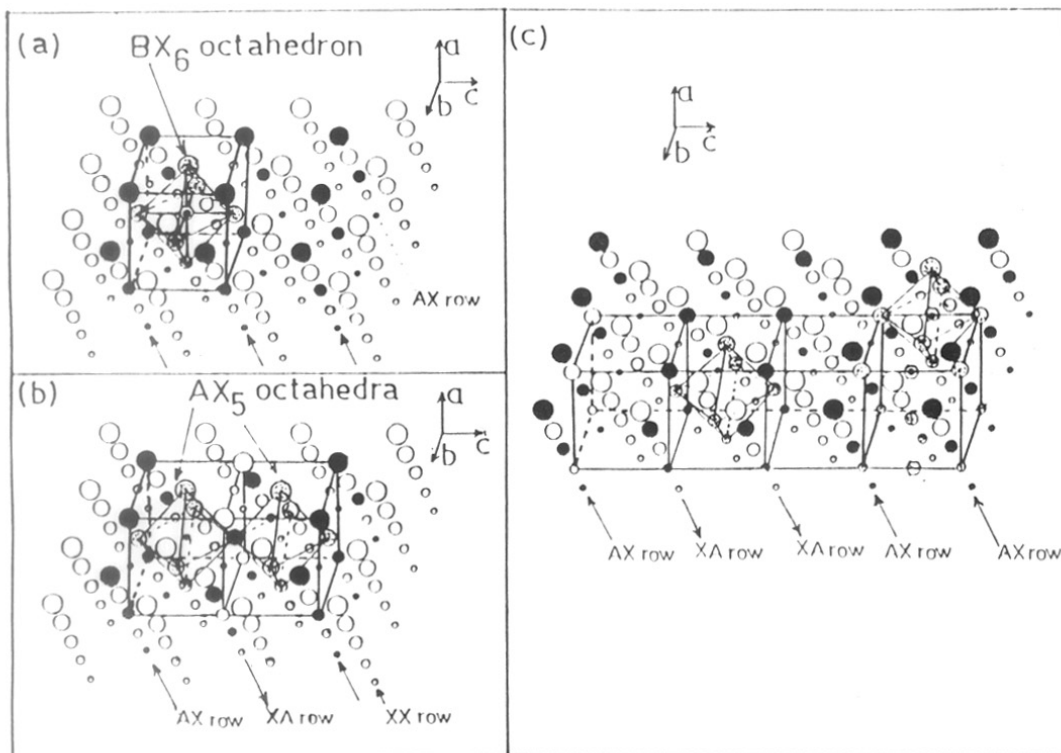


Fig. 3.3. The formation of X_6 and AX_5 octahedra in *ccp* structure. The pseudo-spins associated with the AX rows are indicated. \bullet : A ions, \circ : X ions. \oplus : X ions at the vertices of octahedra. A decreasing size of the circles indicates different decreasing levels of species.

phase compounds [19,20] Bi_2MO_6 ($M = \text{MO}^{6+}$, W^{6+}) or to compounds such as Ba_2CuF_6 or Sr_2CuF_6 . The simplest layered perovskite with K_2NiF_4 structure in which the ratio of the number of A and B atoms is 2:1, is thus an equal admixture of the two types of AX_3 close-packing. This structure is usually described as one with an alternation of the rock-salt (KF), and perovskite (KNiF_3) layers. The ratio of the ionic radii $r_{\text{K}^{+}}/r_{\text{F}^{-}}$ is greater than 0.73 [23] so that the rock-salt layer is not obtained by the occupation of anionic octahedral interstices by A ions. The KF rock-salt structure is instead derived from the AX_3 close-packing of figs. 3.1b and 3.2b. The K_2NiF_4 structure is obtained from the $\langle 2 \rangle$ packing of fig. 3.2c when vacancies are included. The $\langle 2 \rangle$ packing scheme $(\text{ABX}_3)(\text{AXX}^*\text{X}^*)$ or



gives the K_2NiF_4 structure. When the structure is written as derived from,



the Nd_2CuO_4 structure is obtained [22].

In the $\langle 3 \rangle$ notation, the A_p sites at the domain boundaries and the A_r sites with only ferromagnetic alignment of the nearest-neighbor pseudo-spins can now be distinguished. The $\langle 4 \rangle$ notation corresponds to an $\text{A}_4\text{B}_3\text{O}_{12}$ (for example $\text{Bi}_4\text{Ti}_3\text{O}_{12}$ in ref. [23]) with a spin sequence $\dots \rangle \rangle \rangle \langle \langle \langle \rangle \rangle \rangle \langle \langle \langle \rangle \rangle \rangle \dots$. Similarly the Ruddlesdon-Popper structures [24] $\text{AX}(\text{ABX}_3)_p$ such as $\text{Sr}_3\text{Ti}_2\text{O}_7$, $\text{Sr}_4\text{Ti}_3\text{O}_{10}$ are to be written as $\langle m \rangle$ structures with $p = m-1$. There is a loss of X_2 rows at the domain boundaries in the $\langle m \rangle$ notation. There is an additional feature in $\text{La}_2\text{CaCu}_2\text{O}_6$ which corresponds to the $\langle 3 \rangle$ structure with the sequence,



In such oxides, besides the loss of X_2 rows at the domain boundaries, there is also a loss of X from the A_rX rows.

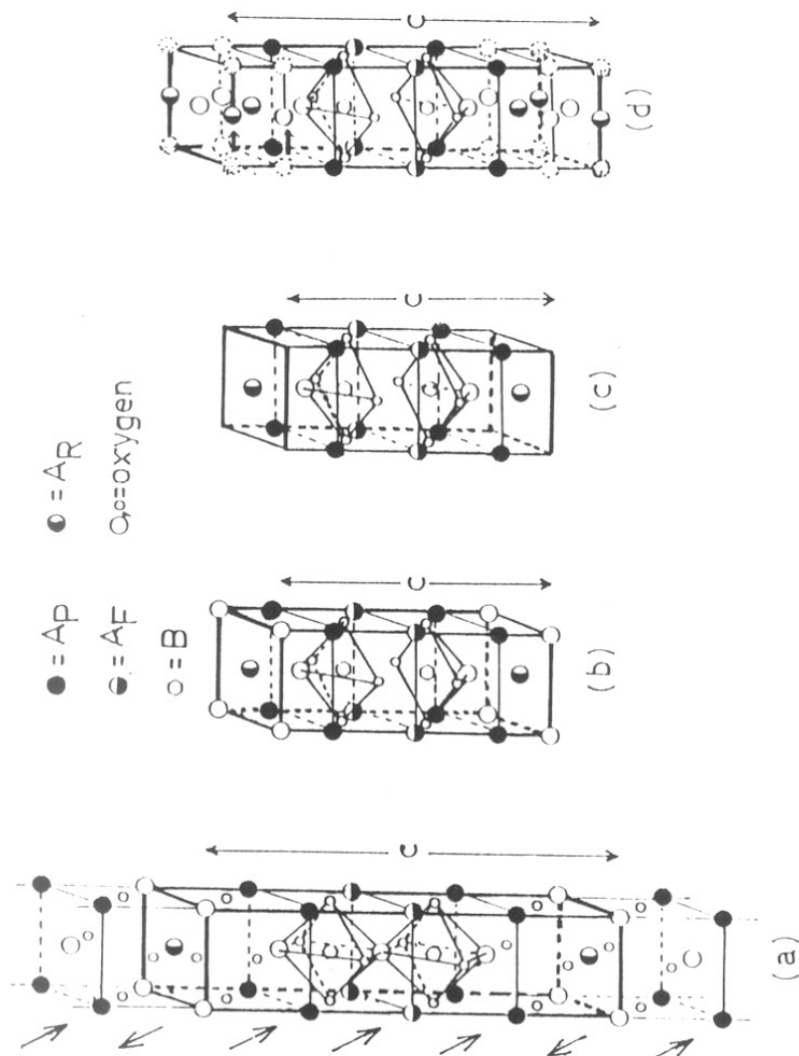


Fig. 3.4. The idealized $\langle 3,1 \rangle AX_3$ structure distinguishing between X ions in AX rows (\circ) and XX rows (\bullet). The different A ions are shown. (b) idealized structure of $YBa_2Cu_3O_6$, derived from fig. 3.4a. (c) idealized structure of $YBa_2Cu_3O_{6.5}$ derived from the $\langle 3,1 \rangle$ notation. The displacement of Cu and O sites from their idealized positions in the A_p O layers (shown as \bullet) are shown in (c) and (d).

Table. 3.1. Fisher-selke notation $\langle m, l^n \rangle$ and tolerance factor for the layered cuprate perovskite oxides.

Compound	$\langle m, l^n \rangle$		t
	m	n	
$\text{La}_{1.85}\text{Sr}_{0.15}\text{CuO}_4$	2	0	0.87
$\text{Tl}_2\text{Ba}_2\text{CuO}_6$	2	2	0.89
$\text{Tl}_2\text{Ba}_2\text{CaCu}_2\text{O}_6$	3	2	0.88
$\text{Bi}_2\text{Sr}_2\text{CaCu}_2\text{O}_6$	3	2	0.87
$(\text{CuPb}_2)\text{Sr}_2\text{CaCu}_2\text{O}_8$	3	3	0.86
$\text{TlBa}_2\text{CaCu}_2\text{O}_7$	3	1	0.89
$\text{CuBa}_2\text{YCu}_2\text{O}_7$	3	1	0.87
$\text{Tl}_2\text{Ba}_2\text{Ca}_2\text{Cu}_3\text{O}_{10}$	4	2	0.89
$\text{Bi}_2\text{Sr}_2\text{Ca}_2\text{Cu}_3\text{O}_{10}$	4	2	0.89
$(\text{Tl, Pb})\text{Sr}_2\text{Ca}_2\text{Cu}_3\text{O}_{10}^{\oplus}$	4	1	0.89

may be associated with the $\langle 311 \rangle$ or $\langle 3, 1^2 \rangle$ notation with two Cu atoms at the A_R sites with one of these Cu atoms displaced by $[0, \frac{1}{2}, 0]$ from their idealized positions. This is shown schematically in fig. 3.4d. $Y_2Ba_4Cu_7O_{15}$ is then to be written as $\langle 31311 \rangle$ in the Fisher-Selke notation. The 2222 compound $Bi_2Sr_2RE_2Cu_2O_{10}$ [26] can be considered as $\langle 2211 \rangle$ or $\langle 2^2, 1^2 \rangle$ in the Fisher-Selke notation. The Fisher-Selke notations for most of the important superconductors are given in table 3.1.

3.3. Consequences of the close-packing description

In this section some of the consequences of the close-packing scheme that are not anticipated in the conventional description is described.

3.3.1. Effects of anion, X, vacancies

An advantage in the close-packed AX_3 description is that the location of the oxygen vacancies and excess oxygen can be easily understood. The excess oxygen may be accommodated either as XX rows as in the $Bi_2Sr_2CaCu_2O_{8+\delta}$ compositions giving rise to incommensurations, or as isolated interstitial oxygens as in $La_2CuO_{4+\delta}$ or $La_2NiO_{4+\delta}$.

The stabilization of various $\langle m, n \rangle$ with $n \neq 0$ using AX_3 close-packing without anion vacancies, is not possible in oxides when the valence state of the B ion is less than three, as this would require A ions with valence greater than three and a large enough radius for r_A/r_X to be greater than 0.73. There are no A cations which satisfy such a constraint. The creation of anion vacancies, X' , is solely due to charge neutrality constraints for the given valence of the A, X and B ions. The maximum oxygen

vacancies would be in the antiferromagnetic domains which requires an AO_3 composition in the ideal case. The oxygen stoichiometry may be preserved in the ferromagnetic domains with ABO_3 compositions where both the A and B cations are in the trivalent state, for instance, as in $BiFeO_3$ or $LaNiO_3$.

3.3.2. Choice of A cations for various sites

When the AX_3 composition is maintained all the A ions would have twelve-fold coordination as in the ABO_3 perovskite oxides. On the creation of anion vacancies the coordination number of A ion (and B ion) would change. This in turn imposes size constraints on the A cations. When $B = Cu^{2+}$, the preference for square-planar geometry of such ions imposes an eight-fold coordination for the A_r ions as in the fluorite structure. Ca and Y ions have ionic radii [21] of 1.04 and 1.12 Å, respectively, in eight-fold coordination. The observed ratio r_A/r_o is then between 0.73 and 0.80. Such a ratio is close to the minimum radius for an A ion in eight-fold coordination in the fluorite, CaF_2 . The A_p ions would have nine-fold coordination in the layered cuprate perovskite oxides, and they have relatively the largest size. The coordination number is expected to be lowest for the A_r ions. In the layered cuprate perovskite oxides the A_r ions are Tl, Bi, Pb etc. The peculiarity of these ions is that in the higher oxidation states such as Tl^{3+} , Bi^{5+} , Pb^{4+} , the $r_A/r_o < 0.73$ so that these ions are stable in octahedral coordination (the radius of the oxygen ion is taken to be 1.40 Å). These ions, however, have stable lower oxidation states with larger size so that they are not stable in octahedral coordination. It is the admixture of these valence states that satisfies the size constraints for the A_r ions discussed above.

For the $\langle m, 1^n \rangle$ layered cuprate perovskite oxides to be stable, the A_R ions should have a radius ratio, r_A/r_O close to 0.73. If it is much less than 0.73 (as when $A = Mg^{2+}, Cd^{2+}$ etc.), they are not amenable to the close-packing description. The A_R ions would either substitute at the B site or separate out as another oxide phase with the rock-salt structure. If the ratio is more than 0.73, these ions would occupy the A_F or A_P sites. There is thus a severe size constraint on the A_R ions. It seems that it is *the possibility of mixed valence* in the A_R ions that allows the *average* size of these ions to be close to the required value of 1.02 \AA (assuming an oxygen ion radius of 1.40 \AA). The radii of the A_R ions in various oxidation states are given in table 3.1. The ratio of $M^{q+}:M^{(q+2)+}$ for the average size of the A_R ion to be 1.02 \AA is then 0.76 for Tl ($q = 1$), 0.68 for Pb ($q = 2$). The size of Bi^{3+} in octahedral sites (0.96 \AA) is too small to require an admixture with Bi^{5+} states in order to satisfy the size constraint. Instead, when $A_R = Bi$, there would be a tendency for the Bi^{3+} ion to increase its size by the incorporation of excess oxygen which increases its coordination number and thence its size. This it does by incorporating a few additional oxygens at the X' sites. When a vacant $X'X'$ row is filled completely by oxygen, it would lead to the well-known incommensurations [27].

3.3.3. Similarity between intermetallic compounds and layered perovskites

The application of the ANNNI model [15,28] to the $\langle m, 1^n \rangle$ ($m, n \neq 0$) layered cuprate perovskite oxides is unusual in the sense that there are both ferro- and antiferromagnetic domains. The classical ANNNI model is a thermodynamic model based on competing nearest- and next-nearest-neighbor interactions. This happens, for

example, when the next-nearest-neighbor exchange integral J_2 is negative (antiferromagnetic) and comparable in magnitude to the nearest-neighbour exchange integral, J_1 , which is also negative. In the theoretical simulations involving such a model there can be no co-existence of ferro- and antiferromagnetic domains. The $\langle m, 1^n \rangle$ situations in which there is such a coexistence are, however, quite common. They are observed, for example, in the classical experimental paper [8] of Loiseau *et al*, in which the appearance of several incommensurate phases of TiAl_3 as a function of temperature was described in terms of the ANNNI model. The incommensurate phases found in the Ti-Al system have a formal similarity with the conclusions of the close-packing model discussed above. Next-next-next-nearest-neighbour interactions, J_4 , have been proposed [29] for the Cu-Au system, for example, in order to account for the seeming co-existence of ferro- and antiferromagnetic domains.

The layered perovskite oxides are to be considered as molecularly epitaxial semiconductor systems. This is particularly so in the sense that there is a very small interlayer diffusion coefficient even at high temperatures. In semiconductors, the studies on epitaxial growth methods have shown that ternary compounds [30] which are unstable in the bulk form may become stable in layered phases. There has been an element of surprise in the fact that compounds such as $(\text{GaAs})_1/(\text{AlAs})_1$ can grow [31] spontaneously without resort to artificial growth conditions. It is recognized that in layered phases the phase diagram is modified from that of the bulk because of strains introduced as a consequence of epitaxial lattice matching. Wood *et al* [30] have suggested that a charge transfer can contribute to a decrease in the strain energy at the interface. There would be a stabilization due to the extra electrostatic attractive interaction due to charge transfer between neutral layers. Perhaps the more

important condition for stability is that the epitaxial layer is pseudo-morphic or has registry with the substrate layer. This may also be brought about by charge transfer.

The existence of $\langle m, 1^n \rangle$ systems is equivalent to the problem of the stability of ordered ternary $A_m B_n C$ compounds with respect to phase separation to the pure binary AC or BC compounds under epitaxial growth conditions [32]. Under these conditions the cell dimensions parallel to the substrate are fixed. The epitaxy-induced strain energies may be lowered by using some other internal degrees of freedom such as a tetragonal degree of freedom. Such degrees of freedom may control, for example, the A-C or B-C bond lengths but nevertheless introduce "frozen in" strains. The tetragonal degree of freedom results in elongation or compression of c -axis bond lengths. For example, the axial Cu-O distance in La_2CuO_4 is lengthened while the axial La-O distance is shortened [22]. In the layered perovskite $\langle m, 1^n \rangle$ systems the "substrate" is not defined. Now it is proposed that in these layered systems the "substrate" lattice parameter that is required to be fixed is the basal plane, ab , parameter of the crystallographic unit cell. Mbaye *et al* [32] have pointed out that in the solid solutions of AC with BC the epitaxial constraints could destabilize the individual AC and BC layers relative to that of the ordered $A_m B_n C$ epitaxial compound. It is because of this constraint on the basal parameters that the conventional description of the structure in terms of rock-salt and perovskite building blocks gives rise to an adequate description of the structure. As discussed in next section (3.4) the actual structural parameters and the individual valence states are a cumulative effect of *all* the A ions.

The size constraints discussed in section 3.3.2, may also be present in the intermetallic compounds. In itinerant electron systems such constraints are satisfied by the nesting of Fermi surfaces for given electron/atom ratios. It is important to note that

the chemical potential oscillations envisaged in the model of Blandin *et al* [9,13] are a function of the valence state of the metal ion so that the variable valency of the system is important for the phenomenon. It is the itinerancy of the electron or the possibility of *homogeneous* mixed valence that stabilizes the $\langle m, 1^n \rangle$ systems in the intermetallic compounds.

3.3.4. Role of various A ions

The role of A ions in bringing about superconductivity in the layered cuprate perovskite oxides may now be examined. It has been pointed out earlier [33] that in $\text{YBa}_2\text{Cu}_3\text{O}_7$, the large sizes of the Ba^{2+} ions have an important role to play in enforcing the eight-fold coordination of the Y ions. The Ba ions ($r_{\text{Ba}} = 1.52 \text{ \AA}$) in ten-fold coordination are too big for the site they occupy. As a result the Ba ions lean on the chain O_1 oxygens and push the Cu_2O_2 planes so that they are pushed away from their ideal perovskite sites. This in turn ensures that the axial $\text{Cu}_2\text{-Cu}_2$ distance is too small for an oxygen atom to be incorporated between the planes, thereby ensuring the eight-fold coordination of the A_p ions. Similarly the Ba ions push the O_4 oxygens towards the Cu_1 ions thereby resulting in a short axial distance. Despite this, the Ba-O_4 distance is only 2.74 \AA , being considerably smaller than the ionic radii value of 2.92 \AA . It has been proposed [33] that the pressure due to the large Ba ions on the chain oxygens leads to a facile creation of holes on the axial O_4 oxygens. The substitution of Ba by smaller ions such as Sr^{2+} or Ca^{2+} in $\text{YBa}_2\text{Cu}_3\text{O}_7$ reduces the steric pressure on the O_4 oxygens. This in turn reduces the number of holes created so that the doping in the CuO_2 planes is reduced.

The Coulomb repulsion between the A_F ions and the Cu ions in the CuO_2 planes, is decreased when the charge on the A_F ion is less. It is likely that in this case the holes are more easily introduced when $A_F = \text{Ca}^{2+}$ than when $A_F = \text{Y}^{3+}$. At the same time an increase in the Coulomb repulsion increases the separation between the CuO_2 planes. This would decrease the transfer integral, t , between the CuO_2 planes and could lower [34] T_c .

The A_R ions seem to have the most important role in the superconductivity mechanism. It has been recognized quite early that the rock-salt like layers (A_R -O layers) act [5] as charge reservoir for doping in the CuO_2 planes. Thus the Cu ions would be formally in the divalent state in compounds such as $\text{Tl}_2\text{Ba}_2\text{CaCu}_2\text{O}_8$, when the Tl ions are formally in the trivalent state. In order that holes are introduced in the CuO_2 planes, the Tl ions should go to a lower valent state. The constraint of 1.02 \AA on the ionic radius of the A_R ion ensures an admixture of the lower valent state of Tl^{1+} so that holes are introduced in the CuO_2 planes in order to conserve charge. As mentioned earlier, a Bi^{3+} ion is slightly small for the A_R site. The average size may be increased to 1.02 \AA by an admixture with Pb^{2+} ions. The ratio of Bi:Pb has to be close to 7:3 for the average size of the A_R site ions to be close to 1.02 \AA . This is close to the value that is experimentally required [35] for the T_c to be maximum in $(\text{Bi,Pb})\text{Sr}_7\text{Ca}_2\text{Cu}_3\text{O}_{10}$. Similarly the radius of the Tl^{3+} ion (table 3.2) is too small to occupy the A_R site. In $(\text{Tl,Pb})\text{Sr}_2\text{CaCu}_2\text{O}_7$, the T_c is a maximum for a Tl:Pb ratio of 1:1. For this ratio the average size of Tl^{3+} and Pb^{2+} in six-fold coordination is close to 1.02 \AA (table 3.2). Since the size of the Bi^{3+} ion is less than the required value of 1.02 \AA , and the Bi^{1+} state is inaccessible, the Bi ions are not likely to be involved as charge reservoirs.

3.3.5. Influence of tolerance factor

The close-packing description is important because it gives an insight into the domain of stability of the perovskite structures. It has been stressed [5, 36-38] in the literature that the tolerance factor is one of the important geometrical constraints relevant to the understanding of the properties of layered perovskite oxides. The tolerance factor, t , of ABX_3 perovskites has been defined by Goldschmidt [36-38] in 1926 from simple geometrical constraints as,

$$t = d_{A-X}/\sqrt{2}d_{B-X} \quad (3.1)$$

where d_{A-X} and d_{B-X} are the A-X and B-X distances, respectively, calculated from the sum of the corresponding ionic radii, r_i . Since the ionic radii are empirical (and as yet not uniquely defined) quantities, the limits of the tolerance factor t for defining the stability of perovskite structures would depend on the actual ionic radii tables used. In this article the coordination-number-dependent ionic radii as tabulated by Shannon are used [21]. It will be seen that these radii give results which are consistent with the general features. The lower limit of the tolerance factor, t_{\min} , below which the perovskite structures are unstable depends on the nature of the X anion when eqn. (3.1) is used. For three-dimensional perovskites [34], $t_{\min} \approx 0.88$ for ionic fluorides, while for the more covalent oxides or chlorides, t_{\min} may be as low as 0.77. It also seems to depend on the dimensionality. In the layered perovskites with the tetragonal (T phase) K_2NiF_4 structure [5], $t_{\min} \approx 0.86$. These differences in the tolerance factor have obscured any attempts at rationalization of structure and structural distortions based on the semi-empirical ionic radii.

The value of t_{\min} may be rationalized on the basis of the simple AX_3 close-packed model in which there is close-packing of AX and XX rows [39]. The tolerance factor is then given by

$$t = d_{A-X}/d_{X-X} \quad (3.2a)$$

$$= 0.5 [(r_A/r_X) + 1] \quad (3.2b)$$

where $d_{X-X} = \sqrt{2}d_{B-X}$. Equation (3.1) may be used instead of eq. (3.2a) when r_X is modified by B-X hybridization. In ionic compounds, on the other hand, eqn. (3.2a) may be used with d_{A-X} and d_{X-X} being obtained from the corresponding ionic radii [21]. When this is done it is found that $t_{\min} \geq 0.86$ even in the more covalent compounds such as the oxides and chlorides. The value of t_{\min} is obtained immediately from eq. (3.2b) once a lower limit of $r_A/r_X \geq 0.73$ is placed for the close-packed AX_3 model for perovskite structures to be valid. From simple geometrical considerations it is well known that when $0.41 \leq r_A/r_X \leq 0.73$ the A ions would occupy octahedral X_6 sites.

A second factor that could be responsible for the charge transfer is the internal pressure that arises when the tolerance factor, t (eqns. (3.1) and (3.2)), is small. In table 3.2 the tolerance factor for the various compounds using eqn. (3.2) is given. In calculating the tolerance factor, the average coordination-number-dependent size [24] of all the A ions is used. The size of the O ion is more difficult to obtain. In the close-packing model that is employed here it is appropriate to consider the average size of *all* the oxygens instead of those in the CuO_2 planes. In the close-packing model, the oxygen-oxygen separation is less than 2.80 \AA . The copper-oxygen hybridization is an important ingredient in determining the size. It has assumed that $r_O \sim d_{Cu-O} / \sqrt{2}$ with r_{Cu} , the average value of the *divalent* copper ions in the appropriate coordination state. It is

Table. 3.2. The coordination number-dependent ionic radii as tabulated Shannon [21].

Ion(a)	Ionic radii (Å)			
	Co-ordination number			
	6	8	10	12
La ⁺³ (A _P)	1.03	1.16	1.27	1.36
Ba ⁺² (A _P)	1.35	1.42	1.52	1.61
Sr ⁺² (A _P)	1.18	1.26	1.36	1.44
Pr ⁺⁴	0.99	1.126		
Pr ⁺⁴	0.85	0.96		
Ca ⁺² (A _F)	1.00	1.12	1.23	1.34
Y ⁺³ (A _F)	0.90	1.02		
Tl ⁺¹ (A _R)	1.45	1.50	1.59	1.72
Tl ⁺³ (A _R)	0.89			
Bi ⁺³ (A _R)	0.96	1.03		
Bi ⁺⁵ (A _R)	0.76			
Pb ⁺² (A _R)	1.19	1.29		
Pb ⁺⁴ (A _R)	0.94			

(a) The type of the A ion (A_P or A_F or A_R) is given in brackets.

rather striking that, when the tolerance factor is calculated in this way, most of the superconductors have a tolerance factor close to the lower limit of 0.866.

A low tolerance factor leads to an internal strain and thereby an internal pressure. This leads, for example, to a shortening [5] of the basal Cu-O distances. An examination of equations (3.1) or (3.2) suggests that the tolerance factor may be increased by an increase in the A-O distance or a decrease in the O-O distance. The latter is equivalent to a decrease in the Cu-O distance when the holes are created in the CuO₂ planes. The holes are indicated on [CuO] as [CuO]⁺. A low tolerance factor would shift to the right the equilibria shown in eqns. (3.3) and (3.4) :



or



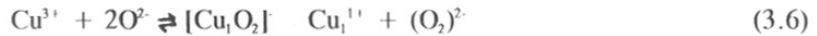
The A_F or A_p ions such as Ba, Ca or Y cannot change their valence states. The A_R ions such as Tl, Bi, Pb etc., have valence skipping states so that they change their valence states by two. Equation (3.4) is applicable in this case. When spin-conservation constraints are imposed, and since it is well recognized [40] that [CuO]⁺ has no spin, it is apparent that the following relation holds,



Equation (3.5) has been expressed usually as a Zhang-Rice singlet. Equation (3.5) is written to emphasize the possibility of a pairing of spins on Cu²⁺ ions in an

antiferromagnetic state with dimerization of holes on oxygen. It has to be emphasised that the dimerized hole on oxygen is only "peroxide"-like and not a static peroxide ion in the sense that the dimerization is a part of a dynamic (homogeneous) double valence fluctuation [41]. Since A_R ions such as Tl, Pb etc. are $S = 0$ ions in their usual valence states, it is apparent that an equilibrium such as that shown in eqn. (3.4) would favour a pairing of spins on the copper or oxygen ions. Such a pairing of charge carriers is considered to be favourable for superconductivity. Equation (3.4) may be therefore visualized (coupled perhaps with eq. (3.5)) as a mechanism by which the A_R ion enhances T_c by enhancing the pairing fluctuations.

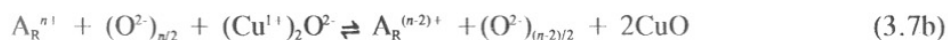
The chains in $YBa_2Cu_3O_7$ have a similar role to play. As discussed earlier the O_1 or O_4 chain oxygens have holes created on them due to a pressure exerted on them because of the Ba ions. The double valence fluctuation of the A_R ions in eqn. (3.4) may now be visualized as,



when the double valence fluctuation in eqn. (3.6) is dynamic the chains could contribute to the enhancement of the superconducting transition temperature. Thus, the existence [42] of two superconducting regions in the $YBa_2Cu_3O_{7-\delta}$ plateau comes about.

A low tolerance factor may also be interpreted in terms of eqn. (3.1). Thus both an increase in the radius of the A ion as well as a decrease in the radius of the Cu ion could increase the tolerance factor. A disproportionation of two Cu^{2+} and Cu^{3+} would reduce the average size of the copper ion. The coupling between the $A_R O$ layer and the CuO_2 planes could involve either of the Cu^{1+} or Cu^{3+} ions. Thus one may have Tl^{3+}

being reduced by Cu^{1+} or Pb^{2+} being oxidized by Cu^{3+} . Thus it can be written as,2



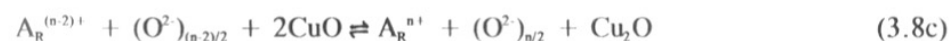
from which we obtain,



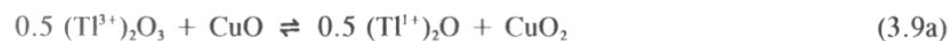
Alternatively it can be,



so that



As an example of eqn. (3.7c) it may be written as,



and as an example of eqn. (3.8c) it may be written as,



Equations (3.7)-(3.9) involve double valence fluctuations and require an oxygen atom or ion to be actively involved in the charge fluctuation. In such cases the bridging oxygens between the $A_R O$ layers and the CuO_2 planes are expected to play an important role [43]. The above equations also give the impression that a "neutral oxygen" is changing its valency by two and is reminiscent of the mechanism first proposed by Khomskii and Zvezdin [44]. In the present mechanism as proposed here it is a pair of charged oxygens which has the double valence fluctuation as in eqns. (3.6)-(3.8). In terms ^{of above} A discussion in section 3.3.3, the important interface is that involving the $A_R O$ layers and both the size and the charge of the A_R ions have an important role to play. The layers to which such a charge transfer can take place are the CuO_2 layers as the other A ions have stable valencies.

3.4. Conclusions

A novel description of the layered perovskite structures is proposed on the basis of an admixture of $L1_2$ and DO_{22} types of cubic AX_3 close-packing found in intermetallic compounds such as Cu_3Au and Al_3Ti , respectively. These two schemes are determined by the relative orientations of the AX rows in a given plane. The similarity between the layered perovskite compounds and the incommensurate phases in intermetallic compounds [7,8] that has been associated with the existence of anti-phase domain boundaries (APB) has been pointed out. The $L1_2$ structure is well known to yield the perovskite ABX_3 structure by the incorporation of B cations in the X_6 octahedral sites. It has pointed out that the DO_{22} structure is stable in the absence of B ions and is the precursor to the rock-salt structure in compounds such as KF , BaO etc. in which the radius ratio of the cation to anion is greater than 0.73. The ratio of the A to B cations determines

the structure of the layered perovskite. The advantages of this description over the conventional one using perovskite and rock-salt building blocks are pointed out.

The ANNNI model and the Fisher-Selke notation for the description of the structure have been used here. The use of the pseudo-spin notation gives rise to the coexistence of "antiferromagnetic" (DO_{22}) and "ferromagnetic" ($L1_2$) domains which is unusual in the conventional ANNNI model but is similar to that found in intermetallic compounds which are described in the language of antiphase domain boundaries. The sign of the interactions is determined by whether there are B ions to occupy the interstitial sites ("ferromagnetic") or not ("antiferromagnetic"). The layered perovskite structures are described by the Fisher-Selke notation $\langle m, 1^n \rangle$ where m is the number of A ions in the "ferromagnetic" $L1_2$ domains and n is the number of corresponding A ions in "antiferromagnetic" DO_{22} domains. The $\langle m, 1^n \rangle$ notation gives rise to three distinguishable spin sites which may be associated with three A ions. In the layered cuprate oxides there are thus A_p (Ba, Sr, La, etc.) ions at domain boundaries, A_f (Ca, Y, etc.) ions in "ferromagnetic" domains between CuO_2 planes and A_r (Tl, Bi, Pb, etc.) in the "antiferromagnetic" or rock-salt domains. It is proposed that the co-existence of the two structural domains arises when the constraint is fulfilled that the ratio r_A/r_x for the A_r ions is therefore necessary in order to adjust the ionic radii to stabilize such structures.

The close-packing description is also useful in rationalizing the empirically observed limits for the tolerance factor that determines the limits of stability of perovskite structures. It is proposed that the close-packing model may be considered to be applicable when the a parameter is greater than $\sqrt{2} \times 2.80 \text{ \AA}$. A new way of defining the tolerance factor is introduced which emphasizes the role of *all* the A ions. In such a definition of

the tolerance factor the valence coupling of the A_R ions (charge reservoir) and the B ions is more readily understood. The possible role of the A_R ions in enhancing the superconducting transition temperature is discussed as a natural consequence when these arguments are extended further.

The novel description of the structures has thus several distinct advantages in the understanding of the structure-property correlation that are not apparent in the conventional description of the structures in terms of perovskite and rock-salt layers. The X^* species in the AX_3^* close-packing description includes anion vacancies. The charge neutrality constraints for given oxidation states of the A and B ions determine the number of vacancies, and the preferred coordination number of the A or B ions determines the location of such vacancies.

References

1. J.G. Bednorz and K.A. Muller, *Z. Phys.*, **B64**, 189 (1986).
2. C.N.R. Rao and B. Raveau, *Acts. Chem. Res.*, **22**, 106 (1989).
3. (a) J.B. Goodenough, *Supercond. Sci. Technol.*, **3**, 26 (1990); (b) K. Yvon and M. Francois, *Z. Phys.*, **B76**, 413 (1989).
4. J.B. Goodenough, *Progr. Solid State Chem.*, **5**, (1974).
5. P. Ganguly and C.N.R. Rao, *J. Solid State Chem.*, **53**, 193 (1984).
6. M.S. Hybertsen and L.F. Mattheiss, *Phys. Rev. Lett.*, **60**, 1661 (1988); R.J. Cava, *Science*, **247**, 656 (1990).
7. G. van Tendeloo and S. Amelinckx, *Phys. Status Solidi*, **A43**, 563 (1977) and references therein.
8. A. Loiseau, F. Ducastelle, R. Portier and G. Van Tendeloo, *J. Phys. (Paris)*, **46**, 595 (1985).
9. See A. Zangwill and R. Bruinsma, *Comments Cond. Mat. Phys.*, **13**, 1 (1987)
10. For a discussion on AX_3 close-packing in inorganic compounds, see A.F. Wells, 'Structural Inorganic Chemistry' 5th ed. (Clarendon, Oxford, 1984) chapter 4.
11. D. Broddin, G. Van Tendeloo, J. Van Landuyt, S. Amelinckx, R. Portier, M. Guymont and A. Loisequ, *Philos. Mag.*, **A54**, 395 (1986).
12. L. Katz and R. Ward, *Inorg. Chem.*, **3**, 205 (1964).
13. A. Blandin, J. Friedel and G. Saada, *J. Phys. (Paris)*, **27**, C3-128 (1966).
14. R. Evans, P. Lloyd and S.M. Mujibur Rahman, *J. Phys.* **F9** (1979) 1939.
15. For a recent review see J.M. Yeomans, *Solid State Phys.*, **41**, 151 (1988) 151.
16. G.S. Zhdanov and Z. Minervani, *Zh. Fiz.*, **9**, 151 (1945).

17. M.E. Fisher and W. Selke, *Phys. Rev. Lett.* **44**, 402 (1980); *idem*, *Philos. Trans. R. Soc., London* **302**, (1981) 1.
18. J.B. Goodenough and J.M. Longo, 'Landolt Bornstein Tabellen', Neue Series, III/4a, (Springer, Berlin, 1970).
19. B. Aurivillius, *Ark. Kemi.*, **2**, 519 (1950).
20. E.C. Subba Rao, *J. Phys. Chem. Solids*, **23**, 665 (1962).
21. R.D. Shannon, *Acta Crystallogr.*, **A32**, 751 (1976).
22. Hk. Muller Buschbaum, *Angew. Chem. Int. Ed. Engl.*, **28**, 1472 (1989).
23. J.F. Dorrian, R.E. Newnham, D.K. Smith and M.I. Kay, *Ferroelectrics*, **3**, 17 (1971).
24. S.N. Ruddlesdon and P. Popper, *ActaCrystallogr.*, **10**, 538 (1957);
S.N. Ruddlesdon and P. Popper, *ActaCrystallogr.*, **11**, 54 (1958).
25. S.S.P. Parkin, V.Y. Lee, A.I. Nazzal, R. Savoy, T.C. Huang, G. Gormann and R. Beyers, *Phys. Rev.*, **B38**, 6531 (1988).
26. A. Schilling, F. hulliger, S. Samarappuli and H.R. Ott, *Physica*, **C185-189**, 659 (1991).
27. See H.W. Zandbergen, W.A. Groen, F.C. Mijlhoff, G. van Tendeloo and S. Amelinckx, *Physica*, **C 156**, 325 (1988) and references therein.
28. P. Bak, *Rep. Prog. Phys.*, **45** 587.
29. D. De Fontaine and J. Kulik, *Acta Metall.*, **33**, 145 (1985).
30. D.M. Wood. S.-H. Wei and A. Zunger, *Phys. Rev.*, **B37**, 1342 (1988).
31. T.S. Kuan T.F. Kuech, W.I. Wang and E.L. Wilkie, *Phys. Rev. Lett.*, **54**, 201 (1985).
32. See A.A. Mbaye, D.M. Wood and A. Zunger, *Phys. Rev.*, **B37**, 3003 (1988) and references therein.

33. C. Infante, M.K. El Mously, R. Dayal, M. Husain, S.A. Siddiqui and P. Ganguly, *Physica*, **C167**, 640 (1990).
34. J.M. Wheatley, T.C. Hsu and P.W. Anderson, *Nature (London)*, **333**, 121 (1988); J.M. Wheatley, T.C. Hsu and P.W. Anderson, *Phys. Rev.* **B37**, 5897 (1988); P.W. Anderson, *Physica*, **C185-189**, 11 (1991).
35. (a) U. Endo, S. Koyama and T. Kawajj. *J. Appl. Phys.*, **27**, L1476 (1988); J. Jianyi, S. Yuping, Z. Fanchun, Y. Huaqing and D. Jaiju, *Z. Phys.*, **B77**, 641 (1989); (b) see R.S. Liu and P.P. Edwards, *Physica*, **C185-189**, 655 (1991) and references therein.
36. O. Muller and R. Roy, 'The Major Ternary Structural Families' Springer-Verlag, Berlin-Heidelberg-New York, (1974).
37. K.K. Singh, P. Ganguly and J.B. Goodenough, *J. Solid State Chem.*, **52**, 254.
38. P. Ganguly, in: 'Adv. in Solid State Chemistry', ed. C.N.R. Rao (Indian National Science Academy, New Delhi, 1986) p.135.
39. P. Ganguly, unpublished results.
40. F.C. Zhang and T.M. Rice, *Phys. Rev.*, **B37**, 3759 (1988).
41. P. Ganguly and M.S. Hegde, *Phys. Rev.* **B37**, 5107 (1988).
42. R.J. Cava, A.W. Hewat, E.A. Hewat, B. Batlogg, M. Marezio, K.M. Rabe, J.J. Krajewski, F. Peckir and L.W. Ruppel, *Physica*, **C165**, 419 (1990); J.D. Jorgensen, D.G. Hinks P.G. Radaelli, S. Pei, P. Lightfoot, B. Dabrowski, C.V. Segre and B.A. Hunter, *Physica*, **C185-189**, 185 (1991).
43. A.R. Bishop, R.L. Martin, K.A. Muller and Z. Tesanovic, *Z. Phys.*, **B76**, 17 (1989).
44. D.I. Khomskii and A.K. Zvezdin, *Solid State Commun.*, **66**, 651 (1988).

CHAPTER 4

VEGARD'S LAW BEHAVIOR IN $\text{La}_{2-x}\text{A}'_x\text{CuO}_{4-d}$ ($\text{A}' = \text{Ba}, \text{Sr}, \text{Ca}$)

4.1. Introduction

The phenomenon of high-temperature superconductivity in layered perovskite multinary copper oxide systems [1-3] has revealed several important aspects which are yet to be satisfactorily understood. One of the most fascinating of these is the behavior of $\text{La}_{2-x}\text{Sr}_x\text{CuO}_4$ in which the superconducting transition temperature, T_c , goes through a maximum at $x \approx 0.15 - 0.20$ and then decreases with increasing hole concentration [4-6], becoming zero at $x \approx 0.30$. At this value of x , the system still remains metallic and the basic crystal structure remains the same. Little is understood about the origin of this behavior. Systematics of the changes in the structural parameters could be of importance in obtaining an insight. Extraction of such chemical insights depend strongly on structure-property correlations and the most basic of these is the changes in lattice parameters.

Traditionally, the quality of a solid solution has been examined from the composition-dependent lattice parameter changes in terms of the empirical Vegard's law [7]. This law states that in the absence of strong electronic effects, the variation of lattice parameters is linear with composition in a true three-dimensional solid solution. The Vegard's law is a consequence of the way a solid solution reduces strain (by an expansion or compression) when species of different sizes are involved. In two-dimensional systems, the non-Vegard's law behavior (non-linear changes in lattice parameter with composition) has been well documented [8-11] especially in $\text{A}_{1-x}\text{A}'_x\text{L}$ systems where the solid solution involves the A or A' ions of different size intercalated between L layers. The non-Vegard's law behavior of the lattice c parameter in these compounds, has been explained [11] in terms of an one-parameter model which examines the layer rigidity with respect to out of plane distortions when there is a random

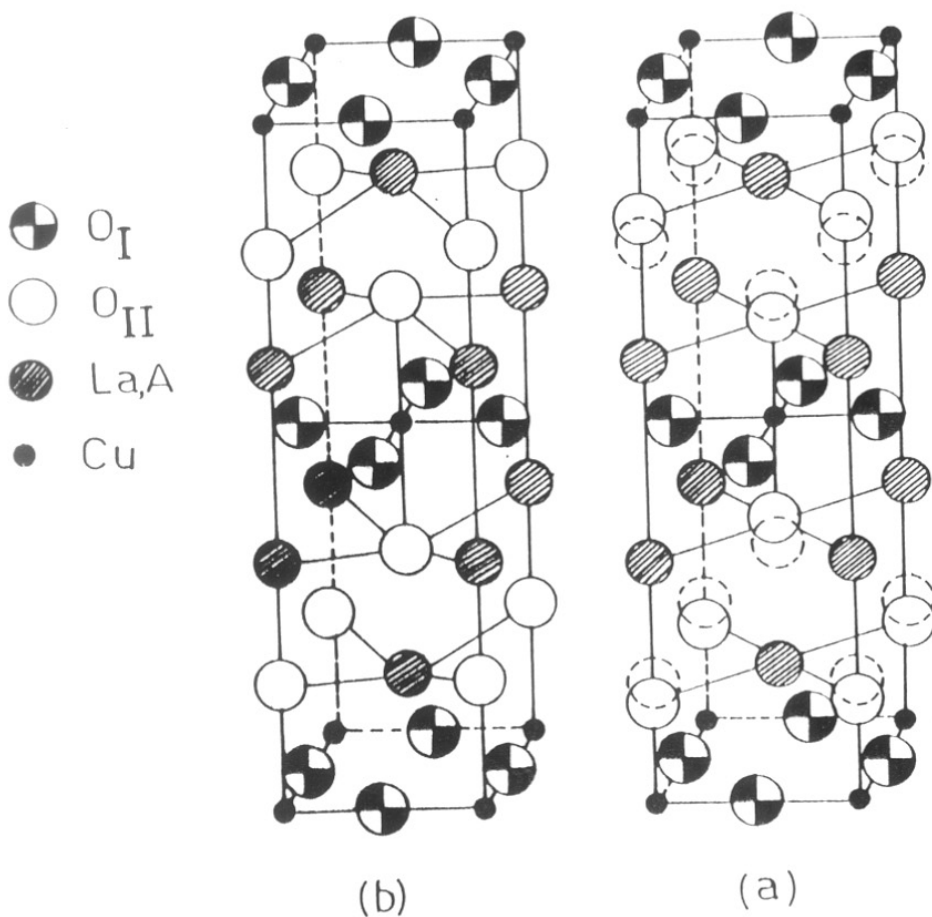


Fig. 4.1. The K_2NiF_4 structure in $La_{2-x}A_xCuO_4$ compounds showing different axial (O_{II}) and basal (O_I) oxygens. (a) The idealized structure with regular BO_6 octahedra and the $A-O_{II}$ distance being $\sqrt{2}B-O_I$ distance. (b) the actual structure in La_2CuO_4 . The a parameter is same in both (a) and (b). The distortion in (b) is mainly achieved by the displacement of the O_{II} ions.

distribution of A and A' ions. Earlier models [11-13] had used several parameters. The findings of Lee *et al* [11] is expressed simply by the statement that the more rigid the layer the more the deviations from Vegard's law on intercalation.

The general applicability of Vegard's law in the layered perovskite superconductors obtained by doping is therefore important. There are, however, certain constraints. Since the model considers the A or A' ions to be rigid one must consider only incompressible or non-polarizable ions with stable valence states such as La^{3+} , Ba^{2+} , Sr^{2+} , Y^{3+} etc. The application of the model to most of the high-temperature superconductors which contain Tl or Bi, or Pb or even $\text{YBa}_2\text{Cu}_3\text{O}_7$, is complicated by the fact that one must take into account the compressibility of the intercalated A or A' ion. In addition, there are several different kinds of layers, such as the TlO or BiO or PbO layers, or Cu-O chains, which also contribute to the dimensions of the c parameter. The simplest system to examine, therefore, is the K_2NiF_4 structure (see fig. 4.1), since there is only one CuO_2 layer and the La and A' ions may be considered as rigid incompressible ions.

The lattice c parameter of $\text{La}_{2-x}\text{Sr}_x\text{CuO}_4$ changes in a markedly non-linear fashion [4,6,14] with x . Two typical cases reported in the literature [4,14], for which changes in the lattice c parameter as a function of x , are given in figure 4.2. A marked deviation from Vegard's law in the two cases can be noted. The deviation becoming prominent around $x = 0.15 - 0.20$. It is at this value of x that T_c is a maximum for $\text{La}_{2-x}\text{Sr}_x\text{CuO}_4$ system. Such a deviation is also seen in the low-temperature limit [15]. The question arises whether the non-Vegard's law behavior arises from the intercalation of larger [16] Sr^{2+} ions in place of La^{3+} ions between rigid CuO_2 layers or whether it is a

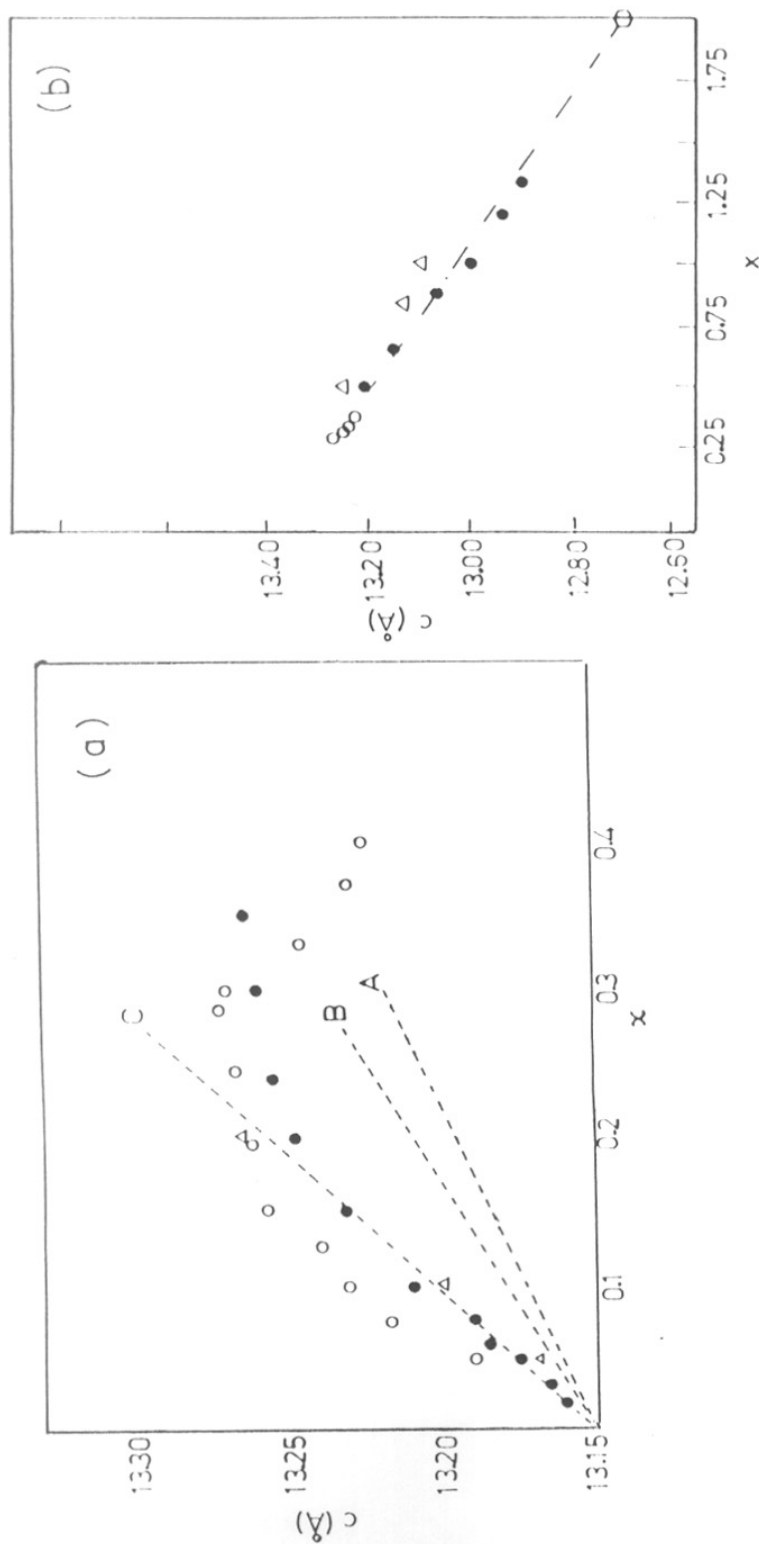


Fig. 4.2. Variation in the c parameter in $\text{La}_{2-x}\text{Sr}_x\text{CuO}_{4-d}$ for (a) $x < 0.3$ (\circ : ref.4; \bullet : $d=0$; ref.15) Δ s are obtained from this study. The dashed lines correspond respectively, to the expected value of c parameter from Eqn.(4.2) for different sizes and from Eqn.(4.4) for increasing hole concentration; the line C is the sum of the lines A and B. (b) for $x > 0.3$ (\circ : ref.4, Δ : ref.6, \bullet : ref.21). The value for $x = 2.0$, is obtained from ref.35. (\odot)

reflection of new electronic effects being introduced with increasing x . The latter may be important in understanding the superconductor-metal transition with increasing x .

The changes in lattice parameters have been examined as the average size of the A' ions, hole concentration as well as deviations from oxygen stoichiometry are varied in a controlled manner. The results of the investigation are reported in this chapter. The main findings are that for small values of x , the changes in the c parameter arises from effects due to the introduction of holes as well as that due the difference in size between the A' ion and the La ion. The changes in the c -axis parameter obeys the Vegard's law when the size of the A' ion is changed for a fixed hole concentration or when the hole concentration is changed for a fixed average size of the A' ion. For large values of x only the size effect is operative. The increase of the c parameter by the introduction of holes for small values of x , is discussed in the context of the creation of holes on Cu. A general expression for the c parameter, $c_{x,d}$, as a function of x and d in $\text{La}_{2-x}\text{A}'_x\text{CuO}_{4-d}$ is obtained and the changes in the c parameter obtained with other A ions such as Pb^{2+} , Ln^{3+} (Ln = rare earth ion) are compared to those reported in the literature [17,18].

4.2. Experimental

The compounds were prepared by standard ceramic methods using La_2O_3 (pre-fired at 1000°C just before use), BaCO_3 , SrCO_3 , CaCO_3 , and CuO as starting material. Required stoichiometric amounts of the starting material were weighed out and ground under alcohol for several hours. The dried mixture was then pre-fired in air at 900°C for 24 hours. The partially decomposed product was then pelletized and fired in air at temperatures ranging between 950° to 1100°C for 48 hours with intermittent

Table 4.1. Lattice parameters and oxygen content of various $\text{La}_{2-x}\text{A}_x\text{CuO}_{4-d}$
(A = Ba, Sr, Ca)

A	x	Lattice parameters (\AA)		$d(\pm 0.005)$
		a	c	
Sr	0.00	3.807*	13.158	-0.012
	0.05	3.799*	13.166	-0.012
	0.10	3.793	13.201	-0.050
	0.20	3.77	13.267	-0.085
Ca	0.05	3.811*	13.150	0.043
	0.10	3.799	13.156	0.068
	0.15	3.796	13.166	0.076
	0.20	3.793	13.161	0.080
$\text{Ca}_{0.66}\text{Sr}_{0.33}$	0.05	3.799*	13.178	0.001
	0.10	3.790	13.180	0.008
	0.15	3.789	13.191	0.016
	0.20	3.786	13.208	0.020
$\text{Ca}_{0.5}\text{Ba}_{0.5}$	0.1	3.796	13.184	0.014
$\text{Ca}_{0.15}\text{Ba}_{0.85}$	0.1	3.790	13.168	0.010
$\text{Ca}_{0.5}\text{Sr}_{0.5}$	0.1	3.790	13.180	0.011
$\text{Ba}_{0.5}\text{Sr}_{0.5}$	0.1	3.794	13.210	0.016

* pseudo-tetragonal values from an orthorhombic cell.

grinding and repelletising. After single phase product was obtained the samples were given various treatments in oxygen so as to obtain various values of d . Low temperatures of firing were required to obtain $d = 0$ compositions when $A' = \text{Ca}$.

The oxygen stoichiometry has been determined by iodometric titration methods using saturated KI solutions. XRD patterns were recorded on a powder diffractometer. The lattice parameters were calculated by least-squares method using PDP package and by using an internal standard for calibration.

4.3. Results

All the compounds in the $\text{La}_{2-x}\text{A}'_x\text{CuO}_4$ ($A' = \text{Ba, Sr, Ca}$; $x = 0.0 - 0.20$) series could be indexed on a tetragonal unit cell. The a and c lattice parameters and the value of d for all the compounds studied in this investigation are given in table 4.1. The changes in the lattice c parameter as a function of x in the system $\text{La}_{2-x}\text{Sr}_x\text{CuO}_{4-d}$ as obtained in this investigation ($d \approx 0$) and as reported in the literature [4,14] for $x < 0.3$ is shown in fig. 4.2a. We note in fig. 4.2a that Torrance *et al* [4] report a larger oxygen content ($d < 0$) while Takagi *et al* [14] report nearly exact stoichiometry ($d \approx 0$). This indicates that the excess oxygen itself or the excess holes that are created, increase the lattice c parameter.

The changes in the c parameter as a function of x in the system $\text{La}_{2-x}\text{Sr}_x\text{CuO}_{4-d}$ for $x < 0.3$ with $d = 0$ as well as for $x > 0.3$ with $d \approx x/2$, shown in figures 4.2 (a and b) are compared with the literature value [4,6]. The non-Vegard's law behavior of the c parameter with x , for $x \leq 0.3$ and Vegard's law behavior in the $0.3 \leq x \leq 1.2$ (extrapolated to the value of Sr_2CuO_3) is apparent from figs. 4.2 (a and b).

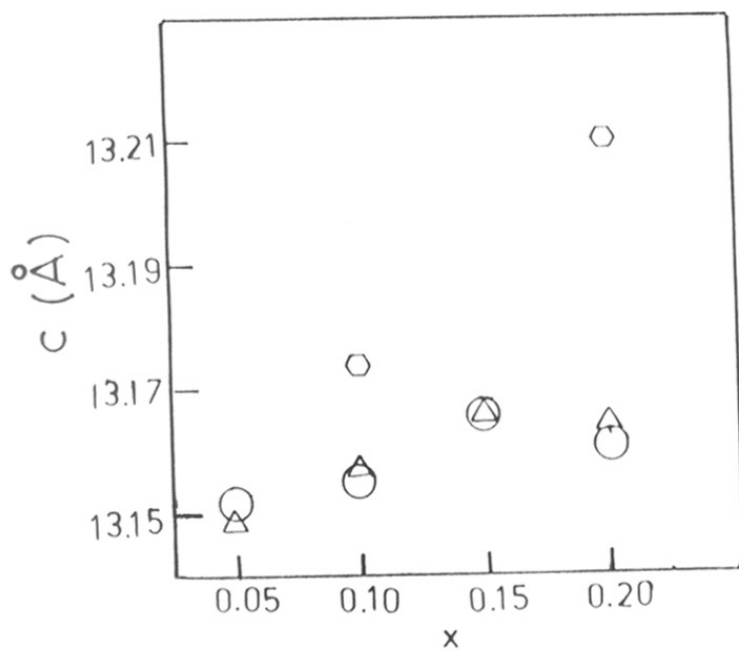


Fig. 4.3. Variation in the c lattice parameter for the $\text{La}_{1-x}\text{Ca}_x\text{CuO}_{4-\delta}$; Δ : this work, \circ : ref.21, \circ : ref.23.

The changes in the c parameter as a function of x in the system $\text{La}_{2-x}\text{A}'_x\text{CuO}_{4-d}$ when $\text{A}' = \text{Ca}$ and when $d \approx x/2$ as well as for the situation when $d \approx 0$ are shown in fig. 4.3. Results are compared with some data available in the literature [20,21,22].

The changes in the c parameter for $d = 0$ and $x = 0.1$, for various proportions of different A' ions are given in fig. 4.4. The changes are plotted as a function of the average difference in radius $\delta r_{\text{A}',\text{La}} = x(r_{\text{A}'} - r_{\text{La}})$. There is a linear dependence of the c parameter on $\delta r_{\text{A}',\text{La}}$. The extrapolated value when $\delta r_{\text{A}',\text{La}} = 0$ is nearly 13.18 \AA which is larger than that for, $x = 0$ composition, La_2CuO_4 ($c = 13.158 \text{ \AA}$) [20-22]. The important point is that the effect of introducing holes is to increase the c parameter.

The changes in the c parameter reported by Kishio *et al* [21] for $\text{La}_{1.8}\text{A}'_{0.2}\text{CuO}_4$ ($\text{A}' =$ various ratios of Ba, Sr and Ca) have been replotted in fig. 4.4, as a function of $\delta r_{\text{A}',\text{La}}$. A linear dependence of the c parameter on $\delta r_{\text{A}',\text{La}}$ is found again. The extrapolated value of the c parameter when $x = 0.2$ and $\delta r_{\text{A}',\text{La}} = 0$ is 13.21 \AA compared to 13.158 \AA when $x = 0$. The role of the holes thus seems to be to increase the c parameter.

The average ionic radius of Ca^{2+} and Sr^{2+} ions taken in the ratio of 2:1 is the same as that of La^{3+} using the ionic radii tables of Shannon [16]. The lattice parameters of the solid solutions $\text{La}_{2-x}(\text{Ca}_{0.66}\text{Sr}_{0.33})_x\text{CuO}_4$ as a function of the hole concentration, x , shows a linear Vegard's law behavior (fig. 4.5). The extrapolated values for the c parameter when $\delta r_{\text{A}',\text{La}} = 0$ from fig. 4.4 also falls on the same line.

Thus two linear relationships are obtained for the dependence of the c parameter; on the size-difference, $\delta r_{\text{A}',\text{La}}$, for a fixed hole concentration and hole concentration x for a fixed $\delta r_{\text{A}',\text{La}}$. Interestingly, the rate of increase in the c axis

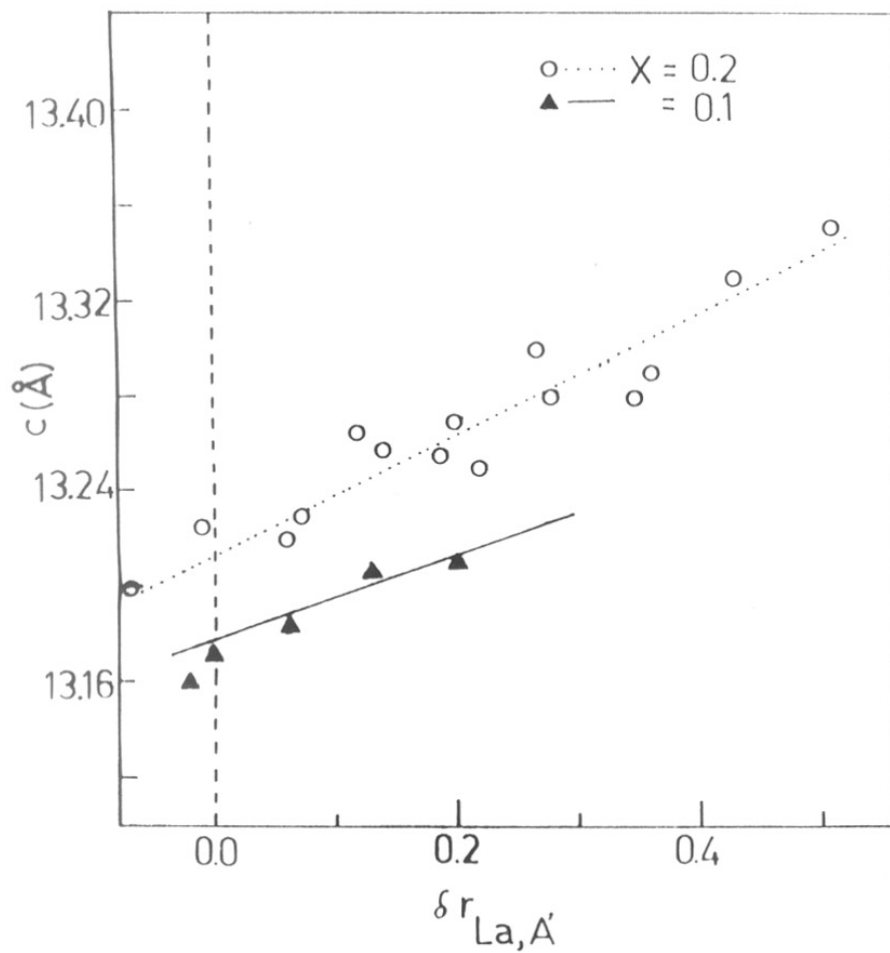


Fig. 4.4. Changes in the c parameter in $\text{La}_{1-x}(\text{Ba}_{1-x}\text{Sr}_x\text{Ca}_x)_{0.1}\text{CuO}_4$ as obtained in this work (▲). The results of Kishio *et al* replotted for the $\text{La}_{1-x}\text{A}_{0.2}\text{CuO}_4$ compounds (○).

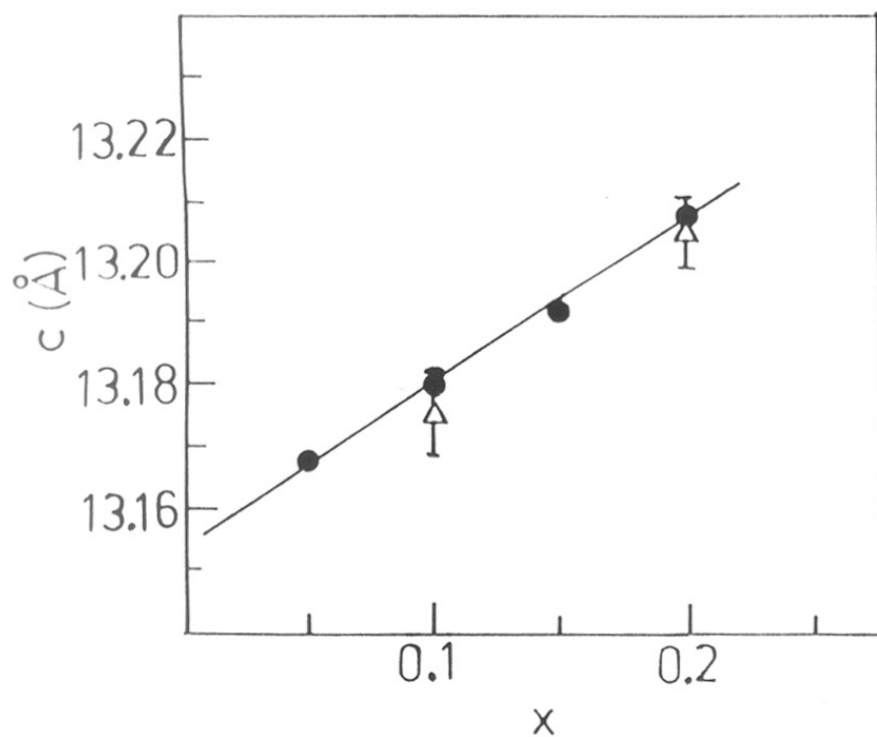


Fig. 4.5. Changes in the c parameter in the $\text{La}_{7-x}(\text{Ca}_{.66}\text{Sr}_{.34})_x\text{CuO}_4$ compounds as a function of the x (•). The extrapolated value of the c parameter when $\delta r_{A',A} = 0$ as obtained in fig.4.4 is also shown (Δ).

follows the same eqn.(4.4) when holes are introduced by intercalated oxygen [23,24] in $\text{La}_2\text{CuO}_{4+d}$ (for $x = 0$).

4.4. Discussions

4.4.1. Effect of size of A ion

In the model of Lee *et al* [11], which is characterized by a rigidity parameter, P , the incremental spacing, λ_x between the layers as a function of x is given by

$$\lambda_x = 1 - (1 - r_A)^P \quad (4.1)$$

When $P = 1$, the incremental spacing λ_x is proportional to r_A . When there are several kinds of A' ions as in the solid solution $\text{La}_{2-x}(\text{Ba}_{1-y_2}\text{Sr}_y\text{Ca}_x)\text{CuO}_4$, eqn. (4.1) would be strictly valid when we consider each value of x to correspond to a different compound. The linear dependence of the c parameter on $\delta r_{A'La}$ as seen in fig. 4.4, shows experimentally that $P = 1$ for a fixed value of x . From the slope of the plots of c vs $\delta r_{A'La}$ for fixed value of x , the dependence of c on $\delta r_{A'La}$ alone to be obtained as,

$$c = c_0 + S \cdot \delta r_{A'La} = c_0 + S \cdot \delta x_A \quad (4.2)$$

with the proportionality constant $S = 2.5 \pm 0.25$ and c_0 is the lattice c parameter of La_2CuO_4 . From fig. 4.1a, c parameter is given by the relation,

$$c = 4d_{\text{Cu-O}(m)} + 2d_{\text{A-O}(m)} \quad (4.3a)$$

where $d_{\text{Cu-O(II)}}$ and $d_{\text{A-O(II)}}$ are the axial Cu-O(II) and A-O(II) distances, respectively. In the ideal perovskite structure,

$$d_{\text{A-O(II)}} = \sqrt{2}d_{\text{Cu-O(II)}},$$

therefore,

$$4d_{\text{Cu-O(II)}} = 4 \times 1/\sqrt{2} d_{\text{A-O(II)}} = 2.82d_{\text{A-O(II)}}$$

Thus,

$$c = 4.82d_{\text{A-O(II)}} = 4.82(r_{\text{A}} + r_{\text{O}}) \quad (4.3b)$$

In the AX_3 close-packing model for the perovskites (see section 3.2 of chapter 3), the A and O ions, which are of similar size, form a close-packed array with the B ions occupying the octahedral O_6 sites. The size of the A ions determines the packing of the B ions and hence could determine indirectly the size of the octahedral sites and hence the B-O distances especially when the size of the A ion is less than that of the oxygen ion. We obtain eqn. (4.3b) from eqn. (4.3a) with r_{A} and r_{O} being the radius of the A and O ions, respectively. The change, δc , in the c parameter from eqn. (4.2) is thus due to changes, $\delta r_{\text{A,La}} = [r_{\text{A}} - r_{\text{La}}]$ and δr_{O} in the average radius of the A and O ions. It is shown below that the changes in the c parameter may be understood as arising due to the two contributions by the A and O ions as in eqn. (4.3b). Writing the formula of $\text{La}_{2-x}\text{A}'_x\text{CuO}_{4-d}$ with $x = 2y$, the change δc , in the c parameter as a function of size of the A ion should then be $\approx 4.82y\delta r_{\text{A}} = 2.41x\delta r_{\text{A}}$. This is what is experimentally

observed in eqn. (4.2). This implies that for a fixed hole concentration the solid solution involving various A' ions obey the Vegard's law.

4.4.2. Effect of holes

The most interesting aspect of this investigation is the observation that there is a linear relation between the hole concentration and the increase in the c parameter for small values of x , shown in fig. 4.5. The dependence of c parameter on the hole concentration, x , is experimentally found to be

$$c = c_0 + Hx \quad (4.4)$$

with $H \approx 0.3$. As can be seen in fig. 4.2, the experimentally observed increase in the c parameter with x , is just that expected from combined effect of holes and size of the A' ions on the c parameter.

4.4.3. Effect of Tolerance Factor

The average Cu-O distances in La_2CuO_4 [25, 26] of $\sim 2.07 \text{ \AA}$ is about 0.06 \AA smaller per Cu-O linkage, using the ionic radii of Shannon for Cu^{2+} ions in six-fold coordination. The mechanism which suppresses the average Cu-O distance in La_2CuO_4 is likely to be due to constraints imposed by the lattice compatibility condition on the intercalated species. This aspect has not been addressed to, in the model of Lee *et al* [11]. For perovskites this compatibility constraint is expressed in terms of a tolerance factor [27,28] which is discussed below.

When a "compatibility constraint" is imposed on the intercalation in the $A_xA'_yL$ compounds, the matching of the lattice vectors in L as well as the (A, A') plane is important. Such lattice vector matching in real systems are difficult since the sizes of the different chemical species are usually quite different. The strain imposed by the lattice mismatch has become an important aspect in the area of strained superlattices [29]. The properties of such strained superlattices could be measured for example in terms of a "constituent strain" [30] which is the energy of the epitaxial strained superlattice relative to the energy of the bulk states. These strains could affect the valence forces. Thus, Hybertesen [31] has shown from first-principles total energy minimum calculations that in the nominally lattice-matched $\text{In}_{0.53}\text{Ga}_{0.47}\text{As}/\text{InP}$ (001) heterostructures interface strain is reduced by anion mixing.

In the ABO_3 perovskite or layered A_2BO_4 perovskites a matching of A-O and B-O distances is expressed in terms of the classical tolerance factor [27,28] (as discussed in chapters 1 and 3) $t = d_{A-O}/\sqrt{2d_{B-O}}$, where d_{A-O} and d_{B-O} are the A-O and the B-O distances obtained from the sum of the ionic radii. The layered perovskite structure is stable only in the limit $0.86 \leq t \leq 1.02$ [27]. When t is close to the lower limit there is a buckling distortion of the CuO_2 planes giving rise to a distorted structure which tends to reduce the basal a, b parameters and increasing the c parameter.

The increase in the c parameter as the number of holes is increased could be understood from lattice compatibility or tolerance factor arguments. For La_2CuO_4 , the tolerance factor is close to 0.86 [26]. This indicates that the basal Cu-O distance is too large and has to be compressed. The compression is mainly in the ab plane and leads to an elongation of the CuO_6 octahedra which is an additional factor for the elongation of the c axis in La_2CuO_4 and accounts for its substantially larger c/a value (≈ 1.25)

compared to that [32] of K_2NiF_4 itself ($c/a \approx 1$, $t \approx 1$). Despite the elongations, it is such a compression or pressure effect that could be the reason that the average Cu-O distance (2.07 \AA) in La_2CuO_4 is less than that calculated from ionic radii (2.13 \AA).

In these $\text{La}_{2-x}\text{A}'_x\text{CuO}_{4-d}$ compounds, t is increased when the radius of the A' ion is larger than that of the La^{3+} ion (as when $\text{A}' = \text{Sr}$ or Ba) as well as when a hole is introduced on the Cu ion instead of on the oxide ion. Since the tolerance factor increases as x is increased, lattice compatibility constraints elongating the c parameter need no longer be present. Thus, as the tolerance factor increases with higher levels of doping, the pressure on the Cu-O bonds in the basal plane is reduced. The creation of itinerant holes could also affect the expansion of the c axis due to static Jahn-Teller effects [27,28]. The increase in the tolerance factor and the reduction in the static Jahn-Teller effects due to creation of itinerant electron charge carriers as x is increased could therefore be important in accounting for the observed non-Vegard's law behavior at high hole concentration in the $\text{La}_{2-x}\text{Sr}_x\text{CuO}_4$ series for $0.15 \leq x$.

The deviation from the Vegard's law at $x = 0.15$, may be understood as well if the changes are attributed to the changes in the c parameter to the changes in the axial Cu-O_{||} distances. We examine the empirical constraint obtained from ionic radii [16] for the average $\text{Cu}^{2+}\text{-O}^{2-}$ ([Cu-O]) distance of 2.13 \AA , the ionic radius of O^{2-} ion being assumed to be the same (1.40 \AA) in all cases. For such an average ionic Cu-O distance, the axial [Cu-O_{||}] distance should be $2.61\text{-}2.59 \text{ \AA}$, for the basal [Cu-O_⊥] distance in La_2CuO_4 of $1.89\text{-}1.90 \text{ \AA}$. The experimentally observed [Cu-O_{||}] distance of $\sim 2.43 \text{ \AA}$ is then due to a low t . The increase in t due to the introduction of holes reduces the internal pressure and is thus expected to increase the Cu-O_{||} distance. On the other hand, on the introduction of holes, the axial [Cu-O_{||}]' distance is expected to be reduced

to $\sim 2.04 \text{ \AA}$ only for an ab plane distance of $\sim 1.89 \text{ \AA}$ assuming an average [Cu-O] $_n$ distance of 1.94 \AA . The changes in the Cu-O $_n$ distance is thus a combined effect of the above factors which act in opposite directions. The changes are expected to be proportional to $[(2.59 - 2.43)(1-x) - (2.43 - 2.04) x] x$. The maximum increase is thus expected when $x = 0.15$. The increase in the tolerance factor could therefore be important in accounting for the observed non-Vegard's law behavior at high hole concentration in La $_{2-x}$ Sr $_x$ CuO $_4$ series for $0.3 \geq x \geq 0.15$.

This non-Vegard's law behavior is concomitant with the disappearance of superconductivity [4-6, 14] in La $_{2-x}$ Sr $_x$ CuO $_4$ compounds when $x \geq 0.3$. When elongation of the c axis is not favored the degeneracy of the e_g ($d_{x^2-y^2}$, and d_{z^2}) orbital is reintroduced. When the two orbital are degenerate there is no ferrodistortive ordering of $d_{x^2-y^2}$ orbital that renders the system two-dimensional as far as exchange interactions are concerned. The system thus becomes effectively three-dimensional.

4.4.4. Effect of loss of Oxygen ($2d > x$)

The linear decrease in the c parameter as a function of increasing x in the region $0.3 < x < 1.2$ is to be associated with loss of oxygen from this system. In terms of the model of Lee *et al* [11] this would indicate that the loss of oxygen is associated with healing lengths which are of unit cell dimensions or low rigidity of the layers. The loss of oxygen from the CuO $_2$ planes could affect greatly the rigidity of the layers.

The model of Lee *et al* [11] for layered systems does not take into account staging [9]. Thus it seems that when the intercalation process is a staged one, i.e. the

intercalation in a second layer takes place only after all the sites in the first layer is completed, the c axis will then increase step by step as a function of concentration. Within the limits of the available experimental control the changes in the c axis will show an effective Vegard's law behavior. If this interpretation is correct then the linear variation in the c parameter would indicate that the oxygen is lost layer by layer.

The rapid decrease in the c parameter for high values of x may be attributed to changes in the nature of the Cu-O_n linkage along the c axis. In La₂CuO₄ the Cu-O_n linkage [23,24] is elongated (2.40 Å). The changes in the c parameter as a consequence of the changes in the Cu-O_n distances alone is then expected to follow the relation.

$$c_d = c_0 - B \cdot d \cdot \Delta r_c \quad (4.5)$$

where B is a constant to be determined and Δr_c is the change in the Cu-O_n distance. Δr_c arises essentially from a change in coordination around the copper ion as a result of the loss of oxygen ($d \neq 0$).

The Cu-O_n distances may be calculated from the assumption that the average Cu-O distance is the sum of the ionic radii and that the oxygen is lost only from the basal plane. The ionic radius of O²⁻ ion is assumed to be the same (1.40 Å) in all cases. Given the ionic radii [16] of Cu²⁺ of 0.73 Å, 0.57 Å and 0.65 Å (extrapolated) for six-, four- and five-fold coordination, respectively, with four, two or three in-plane Cu-O_i distances of 1.90 Å, respectively, one obtains Cu-O_n distances of 2.59 Å, 2.04 Å and 2.28 Å, respectively. These values are high compared to the experimental value of 2.40 Å and 1.96 Å for six-fold (La₂CuO₄) and four-fold (Sr₂CuO₃, Ca₂CuO₃, Refs. [33,34]) coordination.

For small values of d , a change from six- to five-fold coordination is expected. In this case every oxygen lost is expected to change four Cu-O_n distance in the two neighboring copper ions. Since there are four Cu-O_n linkages parallel to the c axis in the unitcell and every oxygen vacancy brings about a change in four Cu-O_n bonds, the factor B for five-fold coordinated coppers should be close to four. For four-fold coordination each oxygen vacancy changes two Cu-O_n distances so that B is close to two.

For a change from six-fold to four-fold coordination Δr_c in eqn. (4.5) is then expected to close to be $\approx 0.55 \text{ \AA}$ in the ionic limit. For a change to five-fold coordination on the loss of oxygen, the expected value Δr_c is 0.31 \AA . If the initial Cu-O_n distance is taken to be 2.40 \AA as in La_2CuO_4 , then the values of Δr_c is expected to be 0.36 \AA and 0.12 \AA for the change to four- and five-fold coordination, respectively.

The value of 12.68 \AA for the c parameter in Sr_2CuO_3 [33] then consistent with the expected value of c from a combination of equations (4.2) and (4.6) if we assume $\delta r_{(\text{Sr},\text{La})} \approx 0.094 \text{ \AA}$ and $\delta r_c \approx 0.47 \text{ \AA}$. In the case of Ca_2CuO_3 ($c = 12.26 \text{ \AA}$), $\delta r_{(\text{Ca},\text{La})} = -0.036 \text{ \AA}$ and $\delta r_c = 0.36 \text{ \AA}$. These values are within the limits discussed above.

Equations (4.2), (4.4) and (4.5) may be combined to give a general expression for the c parameter which takes into account all the changes expected due to the incorporation of holes, change in size of A' ion as well as that due to the loss of oxygen, d , in the series of compounds $\text{La}_{2-x}\text{A}'_x\text{CuO}_{4-d}$. The resultant equation is,

$$c(\text{\AA}) = 13.158 + H(x - 2d) + S.x.r_{A',La} - B.d.\Delta r_c \quad (4.6)$$

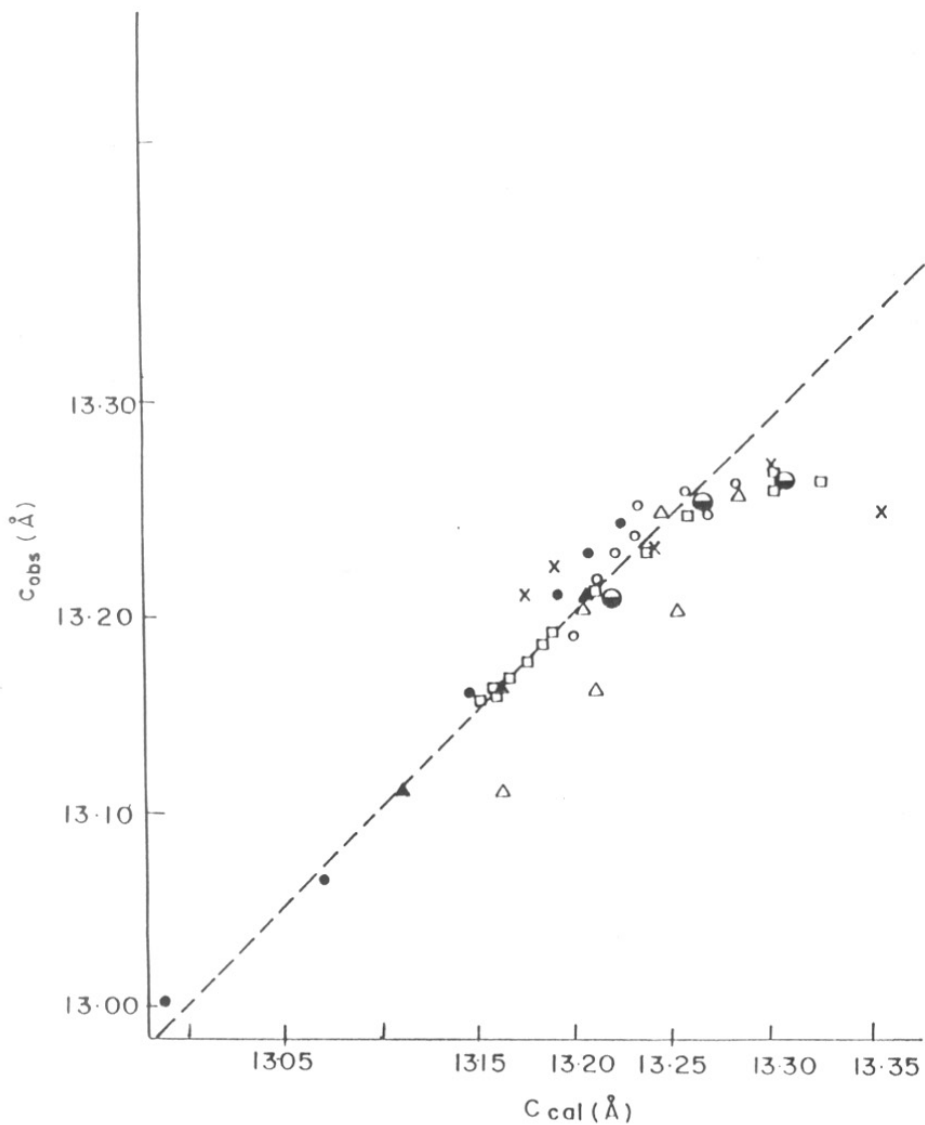


Fig. 4.6. Changes in the c parameter of $La_{2-x}Sr_xCuO_{4-d}$ calculated from eqn. (4.6). • : from [20], Δ ($x < 0.5$) and \blacktriangle ($x > 0.5$) : from [6], \square : from [14], \circ : from [4], \times : from [22a], \bullet : this work.

H , S and B have the values as discussed above and Δr_c is expected to vary most from system to system. We have assumed a fixed $\Delta r_c = 0.12 \text{ \AA}$ with $B = 4$, for small values of d (five-fold coordination) and $\Delta r_c = 0.40 \text{ \AA}$ with $B = 2$ (four-fold coordination) and have calculated the c parameters expected from our samples as well as those reported in the literature [4-6, 21-22]. The results are shown in fig. 4.7. We find a fairly good agreement only when we take $B = 0$ for $x < 0.3$ and $H = 0$ for $x > 0.5$. The reason for this behavior requires more accurate diffraction work. It has been reported that when $d \neq 0$ the oxygen could be accommodated at special oxygen interstitials [35] that exist in compounds such as $\text{La}_2\text{CuO}_{4+d}$ or $\text{La}_2\text{NiO}_{4+d}$ [36-38].

4.4.5. Influence of tolerance factor

Since the negatively charged oxygen anion is the more compressible, the decrease in the average Cu-O distance as a result of low tolerance factor is expected to be predominantly due to the compression of the oxygen ion. It is in this sense that the radius, r_o of the oxygen ion in eqn.(4.3b) plays a role in determining the changes in the c parameter. The value of the parameter H in eqn. (4.4) is obtained from,

$$H = 4.82x(\delta t/\delta x)(\delta r_o/\delta t) \quad (4.7)$$

The rate of change of tolerance factor (calculated from the tabulated ionic radii of Shannon) with x , $\delta t/\delta x \approx 0.1$. When $H \approx 0.3$, we should obtain $\delta r_o/\delta t \approx 0.7 \text{ \AA}$. The decrease of the average Cu-O distance to 2.078 \AA in La_2CuO_4 ($t = 0.868$) from the ionic radii value of 2.13 \AA implies that $\delta d_{\text{Cu-O}}/\delta t \approx \delta r_o/\delta t \approx 0.40 \text{ \AA}$. The discrepancy in the observed and estimated values could be attributed to the anisotropic nature of the internal compression.

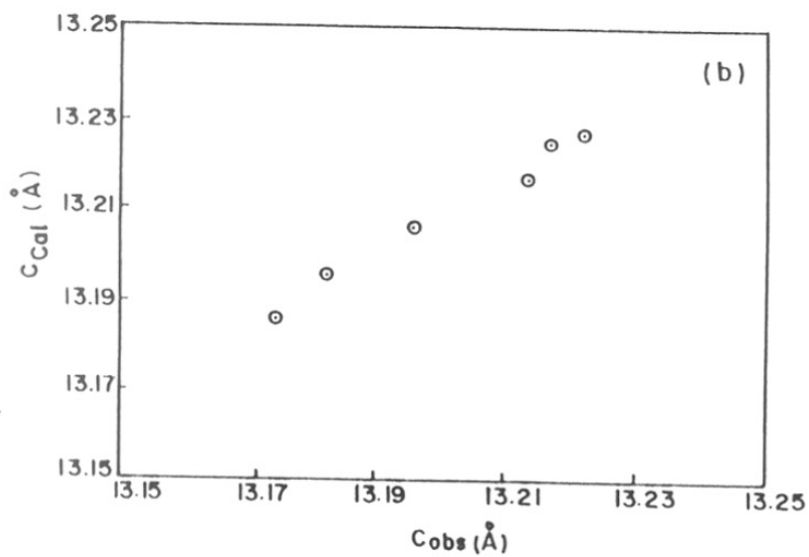
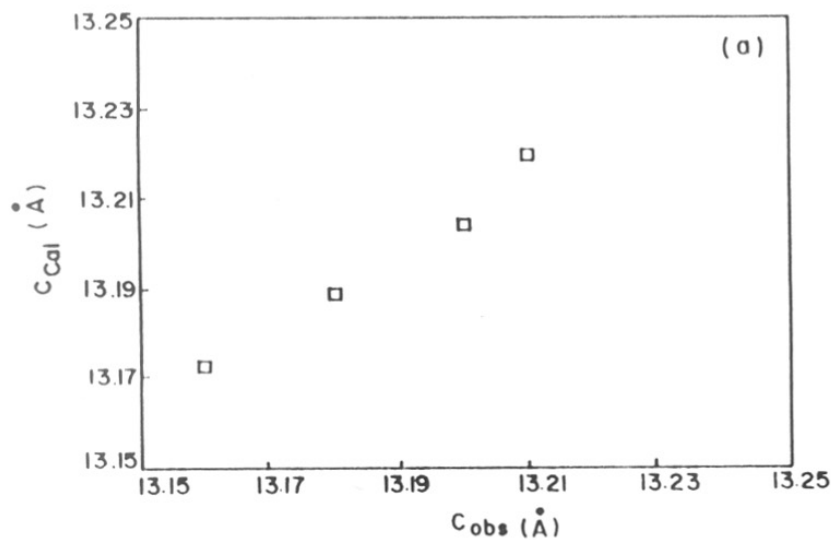


Fig. 4.7. Changes in c parameter in (a) $La_{2-x}Pb_xCuO_4$
(b) $La_{1.85-y}Nd_{0.15}Sr_{0.13}CuO_4$ series.

4.4.6. Applications to other systems

Eqn. (4.7) may be used to examine the lattice parameters of solid solutions of the same family, $\text{La}_{2-x}\text{A}'_x\text{CuO}_4$, in which the A' ions are polarisable ions such as Pb^{2+} or trivalent rare earth ion Nd^{3+} [17,18] (see fig. 4.8). In $\text{La}_{2-x}\text{Pb}_x\text{CuO}_4$ system, it is difficult to assess the reported lattice parameters as in all cases the oxygen stoichiometry is not given. The reported lattice parameters, [17] for $\text{A}' = \text{Pb}^{2+}$, are consistent with Eqn.(4.7) only if we assume that there is little contribution from holes ($H \rightarrow 0$). Thus the eqn. (4.6) can be modified as,

$$c(\text{\AA}) = 13.158 + S.x.r_{\text{A}'},\text{La} + 4.82 (0.6) \delta t \quad (4.8)$$

The plot of c_{cal} Vs c_{obs} shows linear behavior, (fig. 4.7a) if ionic radii of Pb^{2+} ions are considered in 8-fold coordination.

In $(\text{La}_{1-y}\text{Nd}_y)_{1.85}\text{Sr}_{0.15}\text{CuO}_4$ system, substitution of La site by trivalent Nd^{3+} ions does not change hole concentration. In this system, the rate of change of the c parameter with y can be calculated by using following equation,

$$c(\text{\AA}) = 13.158 + S [0.15 (r_{\text{Sr},\text{La}}) + y (r_{\text{Nd},\text{La}})] + H (0.15) + 4.82 (0.6) \delta t \quad (4.9)$$

where $H (0.15)$ gives hole concentration due to divalent Sr^{2+} ions. It can be seen from fig. 4.7b that the observed c parameter is consistent with calculated c for small values of y . At higher values of y the rate of change of the c parameter with y is much faster which would indicate that the actual coordination number for the Cu ions should be

decreased to four, with the Nd ions in eight-fold coordination. The local crystal structure when $A = \text{Nd}$, is similar to that in Nd_2CuO_4 (T' -phase) even though the bulk crystal structure remains the same as that of the K_2NiF_4 (T -phase). Such a behavior of local T' phases in a bulk T phase has been postulated from infra-red evidence in the solid solutions $\text{La}_{2-x}\text{Pr}_x\text{CuO}_4$ by Singh and Ganguly [39].

4.5. General Remarks

The use of single atom parameters such as ionic radii in understanding many body effects including simple interatomic distances is a purely empirical approach awaiting theoretical sanction. There has been very few *ab initio* attempts to predict interatomic distances in oxide systems. It may be interesting to note that the average Cu-O distance calculated from the *ab initio* potential-induced breathing ionic model by Cohen *et al* [40] is 2.113 Å which is close to the value of 2.13 Å used in the present calculation from the ionic radii tables of Shannon. The calculations of Cohen *et al* showed that the CuO_6 octahedra were actually elongated and they suggested that in the case of these oxides the simple ionic description is sufficient to describe structural features and that many body effects are not important.

Tolerance factor arguments give the general trend expected in the sense that low tolerance factors should elongate the octahedra [27,28]. The drawback in the calculation of Cohen *et al*, is that they overestimate the average Cu-O distance in La_2CuO_4 by a sizeable amount. This difference is attributed to an internal pressure brought about by lattice compatibility or tolerance factor arguments. This study shows that the effects due to low tolerance factors are important in reducing the Cu-O distance below that obtained from ionic radii considerations. In this case the lattice matching

constraints or the "constituent strain" [30,31] is the important many body effect obtaining the stability of valence states. A dynamic double valence situation [41,42] between the disproportionated Cu^{1+} and Cu^{3+} states could favor superconductivity provided there is a pre-existing antiferromagnetic coupling between the precursor Cu^{2+} ions. Only in this case would the $S = 0$ constraint be imposed on the spin states of the Cu^{1+} and Cu^{3+} states.

The tolerance factor arguments emphasizes "elastic factors" since it takes into account the mismatch between ionic radii or steric factors. Ferreira *et al* [43] have emphasized that the inclusion of such elastic terms along with the chemical interaction energy terms give much better results in describing alloy stability. It is suggested that such elastic factors could be related to the existence of superconductivity in the sense that valence changes due to the "constituent strain" could be important.

References

1. J.G. Bednorz and K.A. Muller, *Z. Phys.*, **B64**, 189 (1986).
2. C.N.R. Rao and B. Raveau, *Accts. Chem. Res.*, **22**, 106 (1989).
3. W.E. Pickett, *Revs. Mod. Phys.*, **61**, 433 (1986).
4. J.B. Torrance, Y. Tokura, A. Nazzal, A. Bezinge, T. Huang and S.S.P. Parkin, *Phys. Rev. Letts.*, **61**, 1127 (1988).
5. J.B. Torrance, A. Bezinge, A. Nazzal and S.S.P. Parkin, *Physica C*, **162-164**, 291 (1989).
6. K. Sreedhar and P. Ganguly, *Phys Rev.*, **B41**, 381 (1990).
7. L. Vegard *Z. Phys.*, **5**, 17 (1921).
8. M.S. Whittingham and F.R. Gamble, *Mat. Res. Bull.*, **10**, 363 (1975).
9. S.A. Safran, *Solid State Physics*, **40**, 183 (1987).
10. J. R. Dhan and R.R. Haering, *Solid State Commun.*, **40**, 245 (1981); J.R. Dhan and R.R. Haering, *Solid State Commun.*, **42**, 179 (1982).
11. S. Lee, H. Miyazaki, S.D. Mohanti and S.A. Solin, *Phys. Rev.*, **B62**, 3066 (1989).
12. A. Matsuda, M. Sugi, T. Fukui and S. Iizima, *J. Appl. Phys.*, **48**, 771 (1977).
13. H. Kim, W. Jin, S. Lee, P. Zhou, T.J. Pinnavaia, S.D. Mahanti and S.A. Solin, *Phys. Rev. Lett.*, **60**, 2168 (1988).
14. H. Takagi, T. Ido, S. Ishibashi, M. Uota and S. Uchida, *Phys. Rev.*, **B40**, 2254 (1990).
15. B. Buchner, M. Bruer, A. Freimuth and A.P. Kampf, *Phys. Rev. Lett.*, **73**, 1841 (1994); Y. Nakamura and S. Uchida, *Phys. Rev.*, **B46**, 5841 (1992).
16. R.D. Shannon, *Acta Cryst.*, **A32**, 751 (1976).

17. J. Gopalakrishnan, M.A. Subramanian and A.W. Sleight, *Mater. Res. Bull.*, **24**, 321 (1989).
18. M.A. Subramanian, J. Gopalakrishnan and A.W. Sleight, *J. Solid State Chem.*, **84**, 413 (1990); L. Solderholm, S. Mini, B. Dabrowski, G.W. Crabtree, D.G. Hinks and E.E. Alp, *J. Less Common Metals*, **153**, 207 (1989).
19. P. Ganguly and C.N.R. Rao, *Mater Res. Bull.*, **8**, 405 (1973).
20. C. Michel and B. Raveau, *Rev. Chim. Miner.*, **21**, 407 (1984).
21. K. Kishio, K. Kitazawa, S. Kanbe, I. Yasuda, N. Sugii, H. Tagaki, S. Uchida, K. Fueki and S. Tanaka, *Chem. Letts.*, **429**, 1987; K. Kishio, K. Kitazawa, N. Sugii, S. Kanbe, K. Fueki, H. Tagaki and S. Tanaka, *Chem. Letts.*, **635**, (1987).
22. K. OH-Ishi, M. Kikuchi, Y. Syono, K. Hiraga and Y. Moruda, *Jpn. J. Appl. Phys.*, **26**, L484, 1987; K. OH-Ishi, M. Kikuchi, Y. Syono, N. Kobayashi, T. Sasaoka, T. Matsuhira, Y. Muto and H. Yamauchi, *Jpn. J. Appl. Phys.*, **27**, L1449-L1452 (1988).
23. J. Zhou, S. Sinha and J.B. Goodenough, *Phys. Rev.*, **B39**, 12331 (1989).
24. J.B. Goodenough, *Superconductivity Sci.Tech.* **3**, 26 (1990).
25. Von B. Grande, HK. Muller-Buschbaum and M. Schweizer, *Z. Anorg. Allg. Chem.*, **428**, 120 (1977).
26. J.M. Longo and P.M. Raccach, *J. Solid State Chem.* **6**, 526 (1973).
27. P. Ganguly and C.N.R. Rao, *J. Solid State Chem.*, **53**, 193 (1984).
28. K.K. Singh, P. Ganguly and J.B. Goodenough, *J. Solid State Chem.*, **52**, 254 (1984).
29. P.B. Littlewood, *Phys. Rev.*, **B34**, 1363 (1986).
30. R.G. Dandrea, J.E. Bernard, S-H. Wei and A. Zunger, *Phys. Rev. Letts.*, **64**, 36 (1990).

31. M. S. Hybertsen Phys. Rev. Letts. **64**, 36 (1990).
32. J.B. Goodenough and J.M. Longo, in 'Landolt-Bornstein Tabellen', Neue Series, **III/4a**, Springer-Verlag, Berlin (1970).
33. H.K. Muller-Buschbaum and W. Wollschlager, Z. Anorg. Allg. Chem., **414**, 76 (1975); CHR. L. Teske and HK. Muller-Buschbaum. Z. Anorg. Allg. Chem., **371**, 325 (1969).
34. C.L. Teske and HK. Muller-Bushbaum, Z. Inorg. Chem., **379**, 234 (1970).
35. Z. Tan, M.E. Filipkowski, J.I. Budnick, E.K. Heller, D.L. Brewes, B.L. Chamberland, C.E. Bouldin, J.L. Woicik and D. Shi, Phys. Rev. Letts., **64**, 2715 (1990).
36. P. Ganguly, Proc. Ind. Sci. Acad., **A 52**, 135 (1986).
37. J.D. Jorgensen, B. Dabrowski, S. Pei, D.R. Richards and D.G. Hinks, Phys. Rev., **B40**, 2187 (1990); B. Dabrowski, J.D. Jorgensen, D.G. Hinks, S. Pei, D.R. Richards, H.B. Vanfleet and D.L. Decker, Physica C, **162-164**, 99 (1989).
38. C. Chailout, J. Chenavas, S.W. Cheong Z. Fisk, M. Marezio, B. Morosin and J.E. Shirber, Physica C, **170**, 87 (1990).
39. K.K. Singh and P. Ganguly, Spectrochimica Acta **A40**, 539 (1984).
40. R.E. Cohen, W.E. Pickett, L.L. Boyer and H. Krakauer, Phys. Rev. Letts., **60**, 817 (1989).
41. P. Ganguly and M.S. Hegde, Phys. Rev., **B37**, 5107 (1988).
42. K. Sreedhar, P. Ganguly and S. Ramasesha, J. Phys. C Solid State Phys., **21**, 1129 (1988).
43. L.B. Ferreira, A.A. Mbaye and A. Zunger, Phys. Rev., **B37**, 10547 (1988).

CHAPTER 5

STRUCTURE AND PROPERTIES OF A_2BO_4 TYPE COMPOUNDS
WITH DIFFERENT STRUCTURES

5.1. Introduction

Some aspects of the crystal chemistry of the oxides with particular reference to stability of the layered perovskites (A_2BO_4 compounds) with K_2NiF_4 structure in terms of the tolerance factor, t , has been discussed in chapters 1 and 3. It is observed that for the K_2NiF_4 structure to be stable, the value of the t should be within the limits, $0.86 < t < 1.01$.

On the basis of AX_3 close-packing model (as discussed in Chapter 3, Section 3.2) in which the A-X distance has to be matched with X-X distance, the lower limit of the tolerance factor can be justified and the tolerance factor may be defined as,

$$t = d_{A-X}/\sqrt{2}d_{B-X} \quad (5.1a)$$

$$= d_{A-X}/d_{X-X} = 1/2 (r_A/r_X + 1) \quad (5.1b)$$

The radius ratio r_A/r_X , should be greater than 0.732 in order to consider a model involving a close-packing of A and X ions. By the same criterion the condition $r_B/r_X < 0.732$ for the B ion to be occupied in the octahedral sites. Eqn. (5.1) then automatically defines the lower limit ($t \sim 0.865$) for the tolerance factor t in the AX_3 close-packing model.

The inter-relationship between various structures adopted by different A_2BX_4 type compounds have been discussed in terms of cationic radius ratio by various authors [1-3]. Fig. 5.1 shows the structure-field map for the domain of existence of various A_2BO_4 structures.

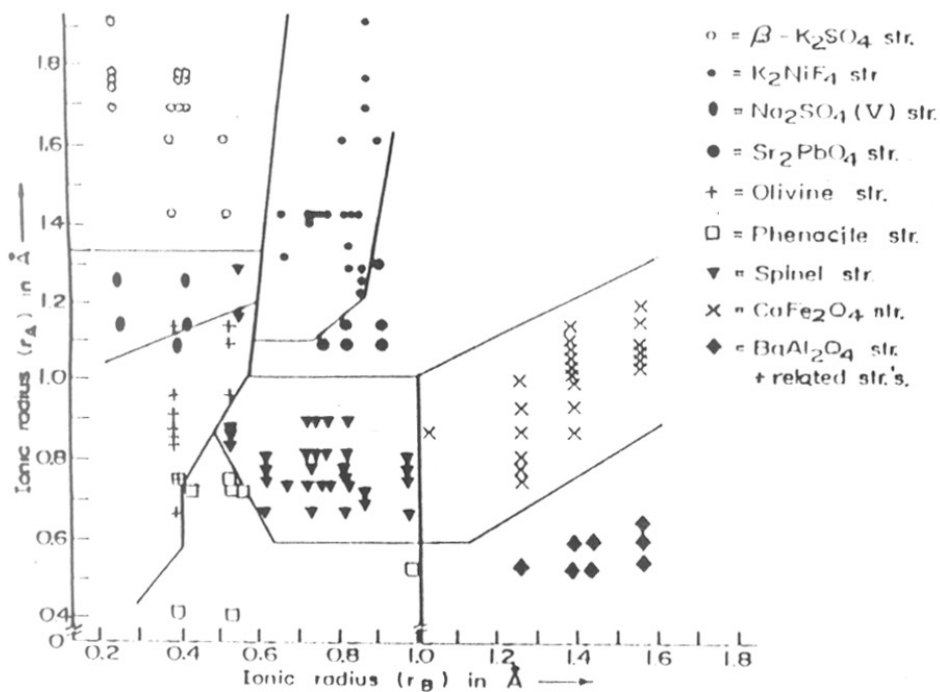


Fig. 5.1. Structure field map showing inter-relationship of various A_2BX_4 structures [1].

The tolerance factors calculated using eqn. (5.1a), for various A_2BO_4 compounds are given in table 5.1. From the table, it can be concluded that for the compounds having K_2NiF_4 type or related structure, the tolerance factor is within the limit $0.86 < t < 1.01$. It may be noted that many of the A_2BO_4 layered perovskite oxides with K_2NiF_4 related structure have tolerance factor close to lower limit, e.g. La_2CuO_4 (0.868), La_2CoO_4 (0.863), Nd_2NiO_4 (0.867), Pr_2NiO_4 (0.870), $YCaCrO_4$ (0.889). These A_2BO_4 compounds are known to show orthorhombic distortion [1,4,5]. On increasing the tolerance factor either by introduction of holes on B ion as in $La_{2-x}Sr_xCuO_4$ (as discussed in Chapter 4), or increasing the size of the A ion as in $(Y_{1-x}La_x)CaCrO_4$, the tetragonal structure is obtained. The orthorhombic distortion is known to disappear at $x > 0.08$ in $La_{2-x}Sr_xCuO_4$ system [4] and at $x > 0.7$ in $(Y_{1-x}La_x)CaCrO_4$ system [5].

The origin of orthorhombic distortion at low temperatures in K_2NiF_4 structures has been analyzed in terms of the Landau theory by Axe and co-workers [6]. There is not, however, any chemical reason for the existence of an orthorhombic strain in compounds with low t . It may be seen from table 5.1. that there are compounds such as Sr_2PbO_4 , Ca_2SnO_4 , Ca_2PtO_4 etc. which possess the required tolerance factor but do not adopt the K_2NiF_4 or related structure. The calculated tolerance factor for these compounds fall in the range $0.86 < t < 0.90$, which is just the range in which the orthorhombic distortion is seen in some compounds containing transition metal ions as discussed earlier. Thus while Ba_2PbO_4 ($t = 0.933$) and Sr_2SnO_4 ($t = 0.917$) have the K_2NiF_4 type tetragonal structure, orthorhombic Sr_2PbO_4 ($t = 0.881$) and Ca_2SnO_4 ($t = 0.873$) and hexagonal Ca_2IrO_4 ($t = 0.91$) have structures which have no relationship to the K_2NiF_4 structure [1]. In order to understand various aspects of this structural incompatibility among these compounds, a programme has been undertaken to study crystal chemistry and mutual solubility of these A_2BO_4 systems by substituting the A-site

Table.5.1. Tolerance factor for various A_2BO_4 structures.

K ₂ NiF ₄ type (tetragonal)					
La ₂ NiO ₄	0.885	La ₂ Li _{0.5} Cu _{0.5} O ₄	0.890	La ₂ Li _{0.5} Co _{0.5} O ₄	0.901
GdSrFeO ₄	0.902	SrDyCrO ₄	0.911	PrSrFeO ₄	0.914
GdSrCrO ₄	0.915	Sr ₂ MoO ₄	0.917	Sr ₂ ZrO ₄	0.917
Sr ₂ SnO ₄	0.917	Sr ₂ RuO ₄	0.921	Sr ₂ IrO ₄	0.921
LaSr ₃ RuO ₄	0.921	Sr ₂ IrO ₄	0.921	LaSrVO ₄	0.923
NdSrCrO ₄	0.925	LaSrGaO ₄	0.932	Ba ₂ PbO ₄	0.933
LaSrCrO ₄	0.935	GdSrNiO ₄	0.941	Ca ₂ MnO ₄	0.945
GdSrAlO ₄	0.953	Sr ₂ TiO ₄	0.956	Ba ₂ ZrO ₄	0.957
LaSrCoO ₄	0.968	LaSrCuO ₄	0.971	Ba ₂ SnO ₄	0.971
LaSrAlO ₄	0.973	LaSrMnO ₄	0.976	Sr ₂ MnO ₄	0.993
NdSrCrO ₄	0.925	K ₂ UO ₄	1.014	LaSrGaO ₄	0.932
K ₂ NiF ₄ related (orthorhombic)					
La ₂ CuO ₄	0.868	La ₂ CoO ₄	0.863	Nd ₂ NiO ₄	0.867
Pr ₂ NiO ₄	0.873	β-Na ₂ UO ₄	0.877	Ba ₂ TiO ₄	0.898
Sr ₂ PbO ₄ type (orthorhombic)					
Sr ₂ PbO ₄	0.881	Ca ₂ SnO ₄	0.873	Cd ₂ PtO ₄	0.873
Ca ₂ PbO ₄	0.839	Cd ₂ SnO ₄	0.846		
Sr ₂ PbO ₄ related					
Ca ₂ IrO ₄	0.910 (hex.)	Na ₂ CuO ₄	0.841 (monoclinic)		
β-K ₂ SO ₄ type					
NaLaSiO ₄	1.119	Eu ₂ SiO ₄	1.150	KBaVO ₄	1.173
Sr ₂ CrO ₄	1.116	K ₂ MnO ₄	1.260	Ca ₂ SiO ₄	1.099
Na ₂ SO ₄ type					
Na ₂ SO ₄	1.129	K ₂ SO ₄	1.293		

or B-site of compounds having a common ion in the respective sites. Thus we have studied the $\text{Ba}_{2-x}\text{Sr}_x\text{PbO}_4$ and $\text{Sr}_{2-x}\text{Sn}_x\text{Pb}_x\text{O}_4$ system in detail. Particular attention has been focused on compounds which approached edge instability in order to find out the value of t at which the K_2NiF_4 structure is destabilised.

Another interesting system is obtained when Sr site in Sr_2PbO_4 is replaced by another smaller cation like Cu by which the crystal symmetry changed from orthorhombic to hexagonal which has Ca_2IrO_4 related structure. Kim *et al* [7] have reported a hexagonal phase Sr-Pb-Cu-O with Ca_2IrO_4 structure. This new system has been re-investigated with respect to the limiting range of solubility of copper in the $\text{Sr}_{2-x}\text{Cu}_x\text{PbO}_4$ system as well as that of other divalent cations having almost the same ionic size (Zn^{+2}) as that of Cu^{+2} or with a larger size (Cd^{+2}) size compared to that of Cu^{+2} . These new phases are prepared with a nominal composition $\text{Sr}_{1.5}\text{PbM}_x\text{O}_{3.5+x}$ and it has been found that Cu, Zn and Cd can be incorporated to stabilize the Ca_2IrO_4 structure at high values of x . The compounds containing Zn and Cd are reported here for the first time.

All the compounds are examined by Powder X-ray diffraction to study the crystal chemistry in detail and also examined by IR, Raman and ESR studies to gain more information on the structural characteristics.

5.2. Experimental

All the compounds were prepared by conventional solid state reaction technique. Appropriate molar ratios of alkaline-earth carbonates and metal oxides (SrCO_3 , BaCO_3 , PbO_2 , CuO , ZnO , CdO) were well mixed and ground in an

agate mortar and fired at 800 °C for 24 hours. The resulting powders were reground and progressively refired according to following schedules:

$Ba_{2-x}Sr_xPbO_4$ ($0 \leq x \leq 2$) ---- 900 °C for 24 hrs.

$Sr_2Sn_{1-x}Pb_xO_4$ ----- 950 °C for 48 hrs.

Sr_2SnO_4 ----- 1300 °C for 24-30 hrs.

Intermediate regrindings and refirings were necessary for the formation of single-phase compounds. In $Ba_{2-x}Sr_xPbO_4$ and $Sr_2Sn_{1-x}Pb_xO_4$ compounds large amount of Sr_2PbO_4 phase was found initially.

For the $Sr_{1.5}PbM_xO_{3.5+x}$ compositions where $M = Cu, Zn$ and Cd $0 < x < 0.5$, the starting mixtures were decomposed at 800 °C, ground, pelletized and reheated at 860 °C for two to three days with intermediate regrinding and pelletizing. Observed and calculated weight losses were in fairly good agreement. Phase purity was checked by powder X-ray Diffraction.

For structural refinement purpose the data were collected on JEOL-JAD- 8030 diffractometer, digitally in steps of 0.05 ° 2 θ and 10 sec. counting time in the range 8 ° < 2 θ < 80 °. Structure refinement was performed by Rietveld method [8]. Shannon radii were used for the calculation of tolerance factor [9].

5.3. Description of various structures

Ba_2PbO_4 ($t = 0.933$) and Sr_2SnO_4 ($t = 0.917$) crystallize in K_2NiF_4 type tetragonal structure with I4/mmm space group [10,11]. (fig. 5.2a). Structure contains

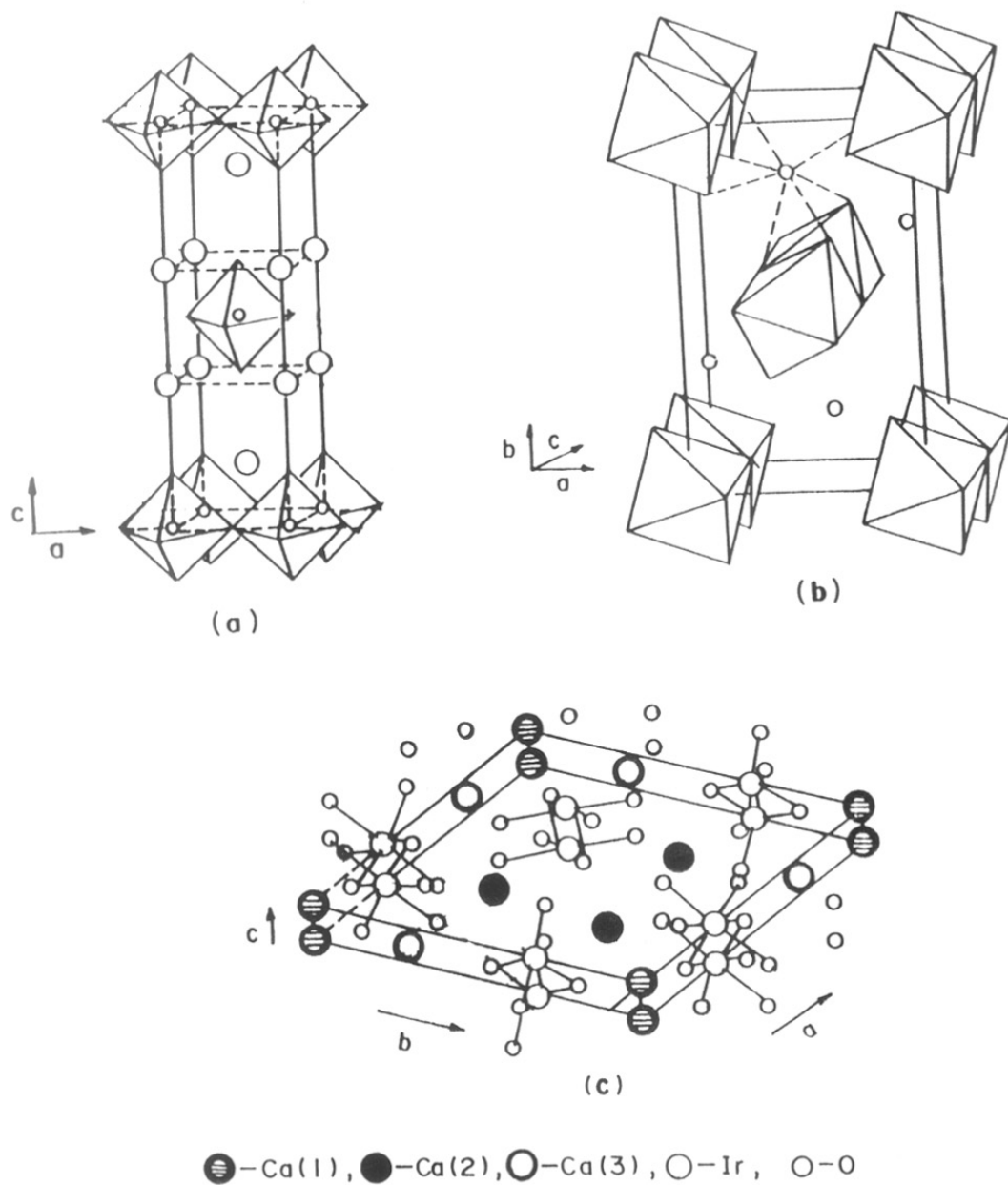


Fig. 5.2. Crystal structure of (a) Ba_2PbO_4 , (b) Sr_2PbO_4 , (c) Ca_2IrO_4 .

perovskite like sheets of elongated PbO_6 or SnO_6 octahedra sharing corners in the (001) planes and separated by Ba-O or Sr-O rock-salt type layers, in which Ba^{+2} or Sr^{+2} is nine-fold coordinated by oxide ions.

Sr_2PbO_4 ($t = 0.881$) has an orthorhombic structure which crystallizes in Pbam (or $\text{Pba}2$) space group [12,13]. (fig. 5.2b). The structure may be viewed as chains of PbO_6 octahedra sharing edges along the c -direction which are held together by SrO_7 polyhedra. The Sr^{+2} atoms are surrounded by seven oxygen atoms in an arrangement of lower symmetry.

Ca_2IrO_4 ($t = 0.91$) crystallizes in a hexagonal structure with space group $\text{P}\bar{6}2\text{m}$ [14]. Crystal structure of Ca_2IrO_4 (fig. 5.2c) consists of rows of edge sharing IrO_6 octahedra lying parallel to the c -axis direction with Ir at $1/3, 0, 0$. There are three different sites for calcium in the Ca_2IrO_4 structure. The Ca atoms are arranged in between rows of IrO_6 octahedra with a nine-fold coordination for Ca(1), seven-fold coordination for Ca(2) and five-fold coordination for Ca(3). A single Ca(1) atom occupies corner (1a) site at $0, 0, 0$ position. The (2d) and (3g) sites are occupied by Ca(2) and Ca(3) respectively.

5.4. Results and discussions

In this section, the results obtained by various characterization techniques, including Powder X-ray diffraction, Infra-red, Raman spectroscopy and Electron spin resonance are discussed.

5.4.1. X-Ray Diffraction Studies

5.4.1.1. The $\text{Ba}_{2-x}\text{Sr}_x\text{PbO}_4$ system

The Powder X-ray Diffraction pattern of Ba_2PbO_4 ($x = 0$) shows single-phase. Indexing and refinement shows a tetragonal K_2NiF_4 type structure with space group $14/mmm$ and refined lattice parameters are $a = 4.302 \text{ \AA}$ and $c = 13.303 \text{ \AA}$ which are comparable to those of reported in the literature, $a = 4.296 \text{ \AA}$, $c = 13.30 \text{ \AA}$ [10].

Sr_2PbO_4 ($x = 2$) shows an orthorhombic structure which crystallizes in Pbam space group. The refined lattice parameters are $a = 6.156 \text{ \AA}$, $b = 10.09 \text{ \AA}$ and $c = 3.498 \text{ \AA}$, which are close to literature values, $a = 6.152 \text{ \AA}$, $b = 10.08 \text{ \AA}$, $c = 3.502 \text{ \AA}$ [12,13].

In $\text{Ba}_{2-x}\text{Sr}_x\text{PbO}_4$ system, tetragonal phase is observed as Sr concentration increases in $0 < x < 1$ region. But as Sr concentration increases beyond $x > 1$, biphasic mixtures due to Sr_2PbO_4 (orthorhombic) and $\text{Ba}_{2-x}\text{Sr}_x\text{PbO}_4$ (tetragonal) are observed. Fig. 5.3. shows X-ray Diffraction pattern of BaSrPbO_4 which has lattice parameters $a = 4.265 \text{ \AA}$ and $c = 12.795 \text{ \AA}$ which are comparable to those reported in the literature [15,16]. Thus in the tetragonal phase region i.e., in the $0 < x < 1$ composition, both tolerance factor and lattice parameter decrease due to smaller size of Sr than that of Ba. The relative decrease in the c parameter is considerably large compared to the decrease in a parameter. The c/a ratio approaches 3.00, at the tetragonal phase limiting composition, $x = 1$, so that the positions of the (103) and (110) reflections overlap. BaSrPbO_4 has a tolerance factor, $t = 0.907$ defining the lower limit of the tolerance factor for the K_2NiF_4 type structure in these compounds.

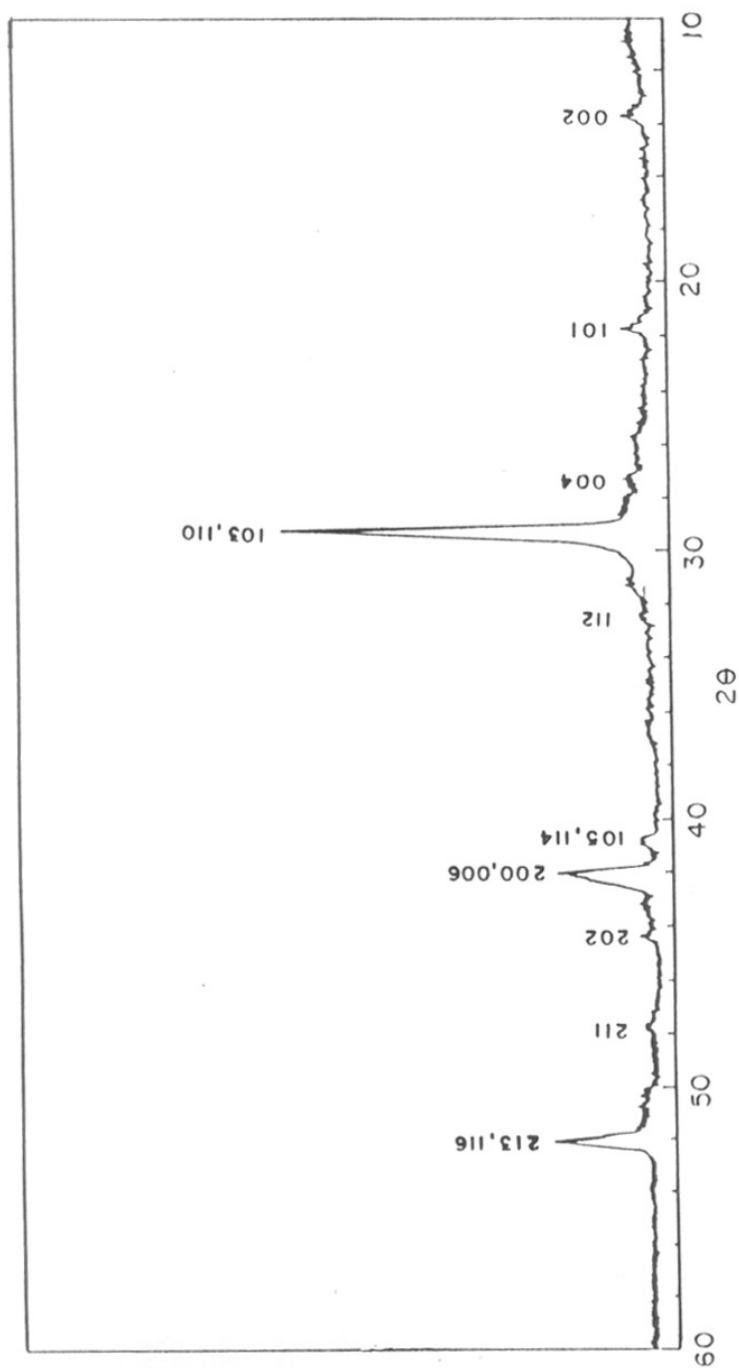


Fig. 5.3. Powder XRD pattern of tetragonal BaSrPbO, with lattice parameters $a = 4.265 \text{ \AA}$, $c = 12.795 \text{ \AA}$.

5.4.1.2. The $\text{Sr}_2\text{Sn}_{1-x}\text{Pb}_x\text{O}_4$ system

For $x = 0$ composition i.e. Sr_2SnO_4 , the XRD pattern shows single-phase behavior with tetragonal structure and the pattern could be indexed on I4/mmm symmetry. Refinement of XRD patterns gives lattice parameters, $a = 4.04 \text{ \AA}$ and $c = 12.51 \text{ \AA}$ which are comparable to the reported values, $a = 4.037 \text{ \AA}$, $c = 12.52 \text{ \AA}$ [10].

In $\text{Sr}_2\text{Sn}_{1-x}\text{Pb}_x\text{O}_4$ system, as concentration of Pb increases in $0.0 < x < 0.75$ region, tetragonal phases are observed. For higher Pb concentrations ($x > 0.75$), biphasic mixtures due to both orthorhombic (Sr_2PbO_4 related structure) and tetragonal (K_2NiF_4 related structure) structures are observed. In the $0.55 \geq x \geq 0.25$ composition range, X-ray Diffraction patterns showed some additional reflections apart from those arising due to the I4/mmm symmetry of Sr_2SnO_4 . These reflections could be indexed on the basis of a primitive lattice. Fig. 5.4. shows X-ray Diffraction pattern of $\text{Sr}_2\text{Sn}_{0.45}\text{Pb}_{0.55}\text{O}_4$ additional reflections (marked by arrows) are due to P4/mmm symmetry. This phase seems to represent a new modification of K_2NiF_4 structure as first noted by Chen and Eichhorn [16]. These authors have suggested that the P4/mmm structure arises from a preferential segregation of Sn and Pb into different layers. In the tetragonal-phase region, $0.0 < x < 0.75$, the tolerance factor decreases and the a parameter increases when the Pb atoms substitute for Sn. There is little change in the c parameter while the a parameter increases slowly as a function of x . The tolerance factor, $t \geq 0.89$ in the region, in which the tetragonal K_2NiF_4 structure is obtained.

From both the systems studied above and comparison with other known tetragonal phases [17], it is clear that in A_2BO_4 compounds with K_2NiF_4

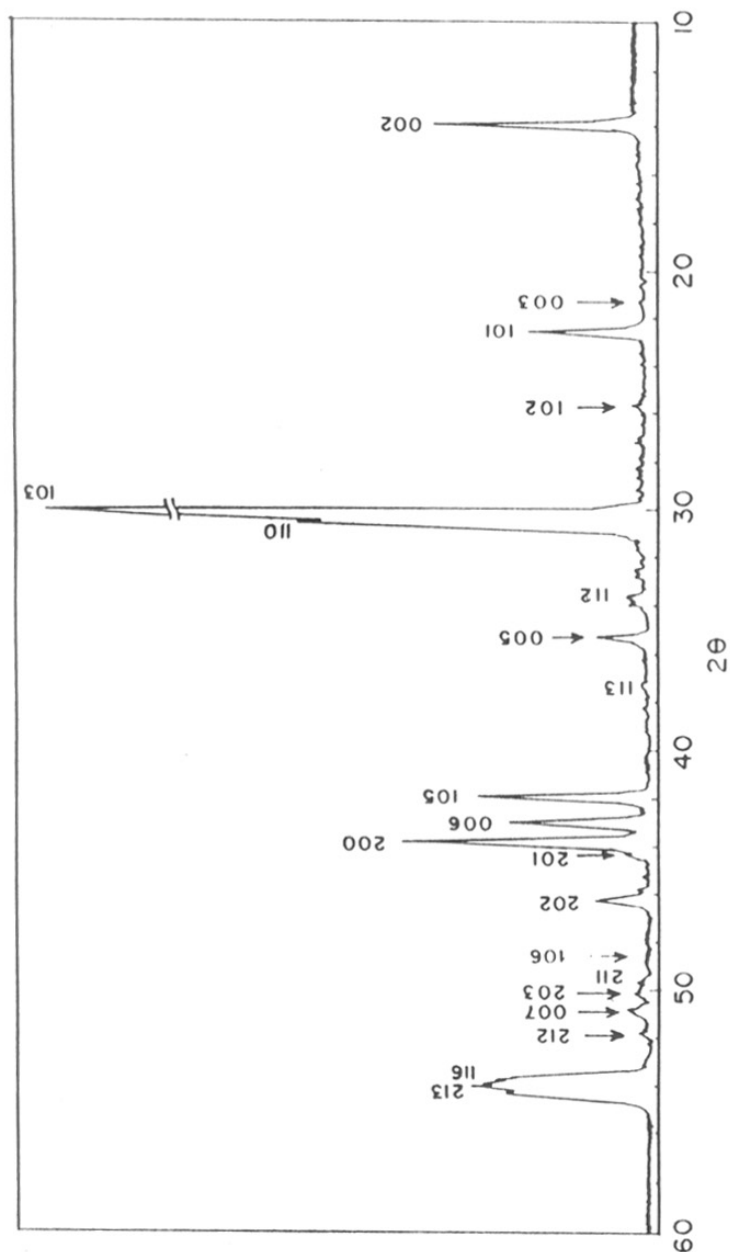


Fig. 5.4. Powder XRD pattern of tetragonal $\text{Sr}_7\text{Sn}_{0.45}\text{Pb}_{0.55}\text{O}_4$, with lattice parameters $a = 4.121 \text{ \AA}$, $c = 12.587 \text{ \AA}$, reflections marked by \downarrow are due to $P4/mmm$ symmetry.

structure, the c parameter is most significantly affected by substitution at A-site and a parameter is affected by substitution at B-site.

The important result in these studies is the absence of the orthorhombically distorted K_2NiF_4 structure as found, for example, in La_2CuO_4 or La_2NiO_4 . As discussed in the introduction earlier, such orthorhombically distorted structures are found in A_2BO_4 compound when B is a transition metal ion in the limit $0.86 < t < 0.90$. This aspect is discussed in more detail in Section 5.5.

5.4.1.3. The $Sr_{1.5}M_xPbO_{3.5+x}$ system, ($M = Cu, Zn, Cd$ and $0.05 < x < 0.5$).

Kim *et al* [7] first reported single phase structures in the Sr-Pb-Cu-O system at compositions corresponding to $Sr_{1.5}PbCu_{0.2}O_{3.50}$ and $Sr_{1.33}PbCu_{0.33}O_{3.60}$. The oxygen content in the latter compound is consistent with the existence of divalent Sr and Cu ions and tetravalent Pb ions, whereas the former compound is slightly oxygen deficient if these oxidation states are considered. $Sr_{1.33}PbCu_{0.33}O_{3.60}$ may be considered to be obtained from $Sr_{1.5}PbCu_{0.2}O_{3.50}$ by substituting some of the Sr atoms by Cu. In this case it may be considered that the Cu, Zn and Cd to be substituting only at the Sr sites. After several trial and errors it was found that single-phase compositions are obtained mainly when the Sr:Pb ratio is close to 3:2 and Pb:M ratio is greater than 2.0 which is also observed in neutron diffraction study by Babu *et al* [18].

For small Cu or Zn concentrations, $0.05 < x < 0.17$, powder XRD patterns show that the compound is biphasic with an Sr_2PbO_4 -related phase appearing along with the main hexagonal phase. For higher M concentration, $x > 0.45$, impurity peaks due to unreacted PbO_2 , CuO and ZnO are observed. The $x = 0.5$ composition, for

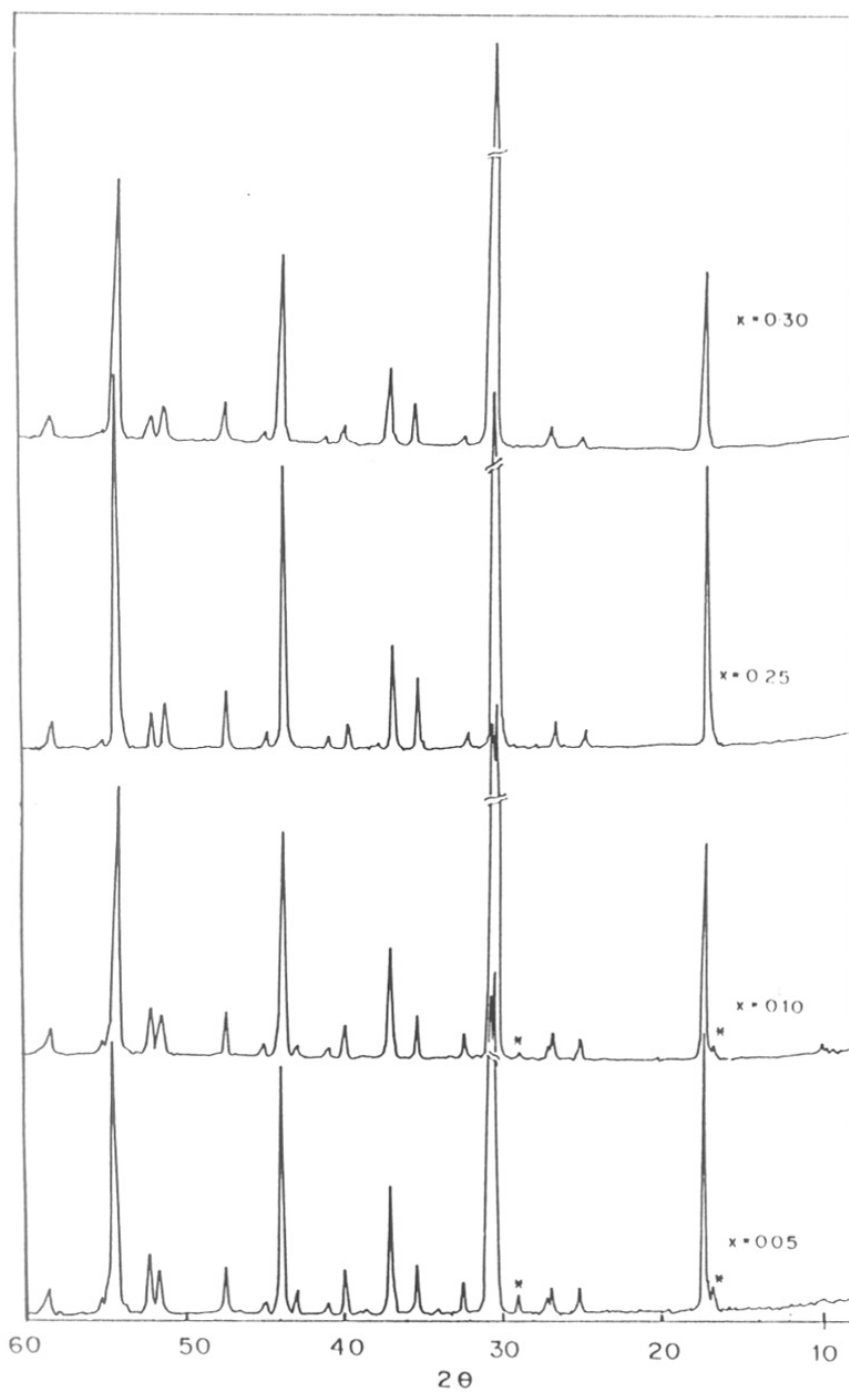


Fig. 5.5a. Powder XRD pattern of hexagonal $\text{Sr}_{1.5}\text{PbCu}_4\text{O}_{3.5+x}$ in the range $0.05 < x < 0.3$. Peaks marked by * are due to Sr_2PbO_4 phase.

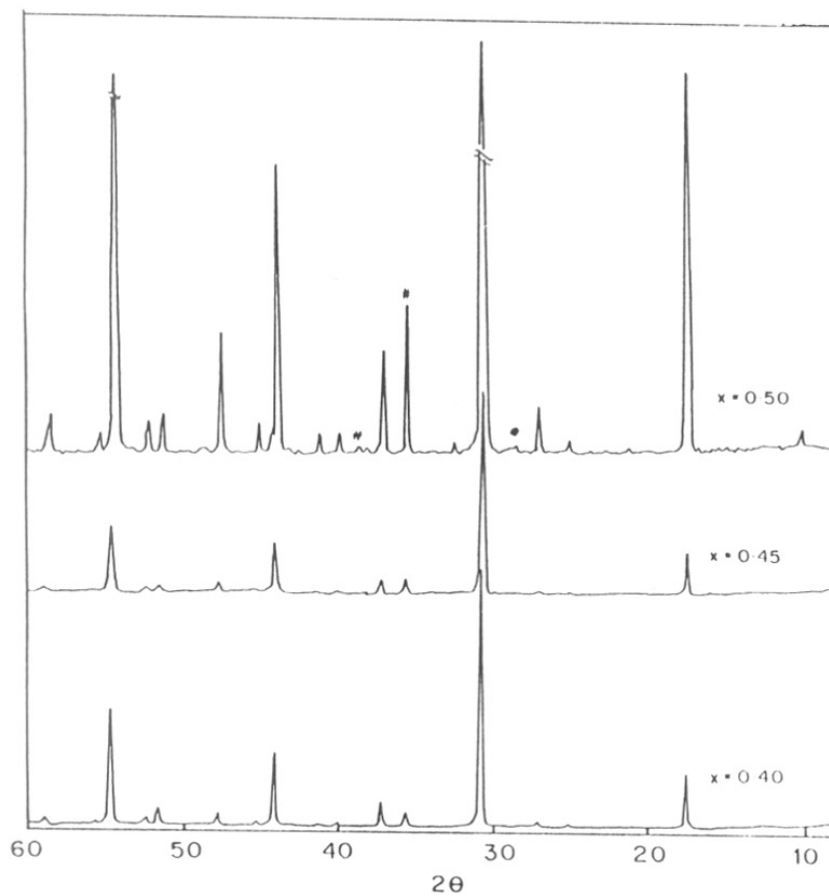


Fig. 5.5b. Powder XRD pattern of hexagonal $\text{Sr}_{1.3}\text{PbCu}_1\text{O}_{3.5+x}$ in the range $0.4 < x < 0.5$. Peaks marked by # and • are due to unreacted CuO and PbO_2 respectively.

M = Cu shows weak CuO line at $2\theta = 38.8^\circ$. There seems to be a preferred orientation of the (110) planes in the $x = 0.5$ as well as the $x = 0.45$ compositions. Similar XRD patterns due to hexagonal structures are observed for $\text{Sr}_{1.5}\text{Cd}_x\text{PbO}_{3.5+x}$ compounds in the range $0.2 < x < 0.35$.

Fig. 5.5 shows X-ray Diffraction pattern of $\text{Sr}_{1.5}\text{PbCu}_x\text{O}_{3.5+x}$ for various concentration of x . In the composition range $0.2 < x < 0.45$, $\text{Sr}_{1.5}\text{PbM}_x\text{O}_{3.5+x}$, M = Cu and Zn compounds are found to be of single phase and show X-ray Diffraction patterns typical of Ca_2IrO_4 type hexagonal structure. The XRD patterns of $\text{Sr}_{5-x}\text{Pb}_{3+x}\text{Cu}_{0.66}\text{O}_{11.76}$ could be indexed on the basis of hexagonal structure with space group $\overline{\text{P}}62\text{m}$ as reported by Kim *et al* [7]. There is little change in the lattice parameters in the $\text{Sr}_{1.5}\text{PbCu}_x\text{O}_{3.5+x}$ compositions which is given in table 5.2. The crystallographic structure of the $\text{Sr}_{1.5}\text{PbM}_{0.2}\text{O}_{3.71}$ (M = Cu, Zn, Cd) compounds has been refined using Rietveld method and the hexagonal space group $\overline{\text{P}}62\text{m}$.

The structure of $\text{Sr}_{1.5}\text{M}_x\text{PbO}_{3.5+x}$ phases at $x = 0.2$ for various M ions were refined by Rietveld method [8] using DBW 3.2S-PC-901 version of the profile refinement programme developed by Wiles *et al* [19]. Lattice parameters were obtained by least-square refinement method. Further details pertaining to data collection and refinement are summarized in table 5.3. The observed and calculated XRD profiles are shown in fig. 5.6. The final cell parameters, atomic coordinates and bond distances are given in table 5.3, 5.4. and 5.5, respectively for M = Cu, Zn, Cd.

$\text{Ca}_{5-x}\text{Ir}_3\text{O}_{12}$ [20] is reported to have the same crystal structure, as that of Ca_2IrO_4 [14] except for the occupation of Ca(1) atoms at corner position (section 5.3, fig. 5.2c). In Ca_2IrO_4 structure, a single Ca(1) atom occupies (1a) site in $0,0,0$ position of $\overline{\text{P}}62\text{m}$ space

Table. 5.2. Lattice parameters of $\text{Sr}_{1.5}\text{PbCu}_x\text{O}_{3.5+x}$

x	a (Å)	c (Å)
0.25	10.095	3.549
0.30	10.082	3.545
0.40	10.0757	3.543
0.45	10.0781	3.546

Table. 5.3. Summary of data collection and structure refinement.

Formula	$\text{Sr}_{1.5}\text{PbCu}_{0.2}\text{O}_4$	$\text{Sr}_{1.5}\text{PbZn}_{0.2}\text{O}_4$	$\text{Sr}_{1.5}\text{PbZn}_{0.2}\text{O}_4$
Formula weight	415.012	415.389	425.056
space group	hexagonal	hexagonal	hexagonal
a	10.1244 Å	10.1240 Å	10.1522 Å
c	3.5512 Å	3.5382 Å	3.5186 Å
colour	black brown	yellow	yellow brown
Diffractometer	Jeol JAD-8030	-	-
Radiation			
Wavelength	$\text{CuK}\alpha$ 1.5405 Å	-	-
Monochromator	graphite	-	-
Temperature	25°C	-	-
2 θ range	10 < 2 θ < 80	-	8 < 2 θ < 80
Scan mode	w-2 θ	-	-
Scan speed	0.05 2 θ per 10 sec.	-	-
Profile function			
used	pseudo-voigt	-	-
No. of parameters	27	26	16
No. of reflections			
measured	110	110	110
R_p	9.926	8.906	7.929
R_{wp}	12.516	13.107	11.901
$R_{exp.}$	3.179	3.36	3.591

Table. 5.4. Atomic coordinates of $\text{Sr}_{1.5}\text{PbM}_x\text{O}_{3.5+x}$.

ATOM	SITE	X	Y	Z
Pb1	3f	0.3404	0.0000	0.0000
Sr1	2d	0.3333	0.6666	0.5000
Sr2	3g	0.7012	0.0000	0.5000
Cu	2a	0.0000	0.0000	0.1282
O1	3g	0.1889	0.0000	0.5000
O2	3g	0.4718	0.0000	0.5000
O3	6j	0.2474	0.4468	0.0000



Pb1	3f	0.3388	0.0000	0.0000
Sr1	2d	0.3333	0.6666	0.5000
Sr2	3g	0.6999	0.0000	0.5000
Zn	2a	0.0000	0.0000	0.2249
O1	3g	0.1889	0.0000	0.5000
O2	3g	0.4718	0.0000	0.5000
O3	6j	0.2449	0.4467	0.0000

Table. 5.4. Contd.



Pb1	3f	0.3415	0.0000	0.0000
Sr1	2d	0.3333	0.6666	0.5000
Sr2	3g	0.7103	0.0000	0.5000
Cd1	2a	0.0000	0.0000	0.0000
O1	3g	0.1683	0.0000	0.5000
O2	3g	0.4789	0.0000	0.5000
O3	6j	0.2534	0.4644	0.0000

Table. 5.5. Bond distances for $\text{Sr}_{1.5}\text{PbM}_{0.2}\text{O}_{3.71}$.

Distance (Å)	Cu	Zn	Cd
Pb-O ₁	2.346	2.331	2.243
Pb-O ₂	2.219	2.223	2.243
Pb-O ₃	2.176	2.156	2.228
Sr(1)-O(2)	2.936	2.936	2.938
Sr(1)-O(3)	2.632	2.626	2.513
Sr(2)-O(1)	2.650	2.660	2.558
Sr(2)-O(2)	2.323	2.309	2.352
Sr(2)-O(3)	2.539	2.545	2.649
M-M	2.641	1.947	3.519
M-O	2.325	2.146	2.453

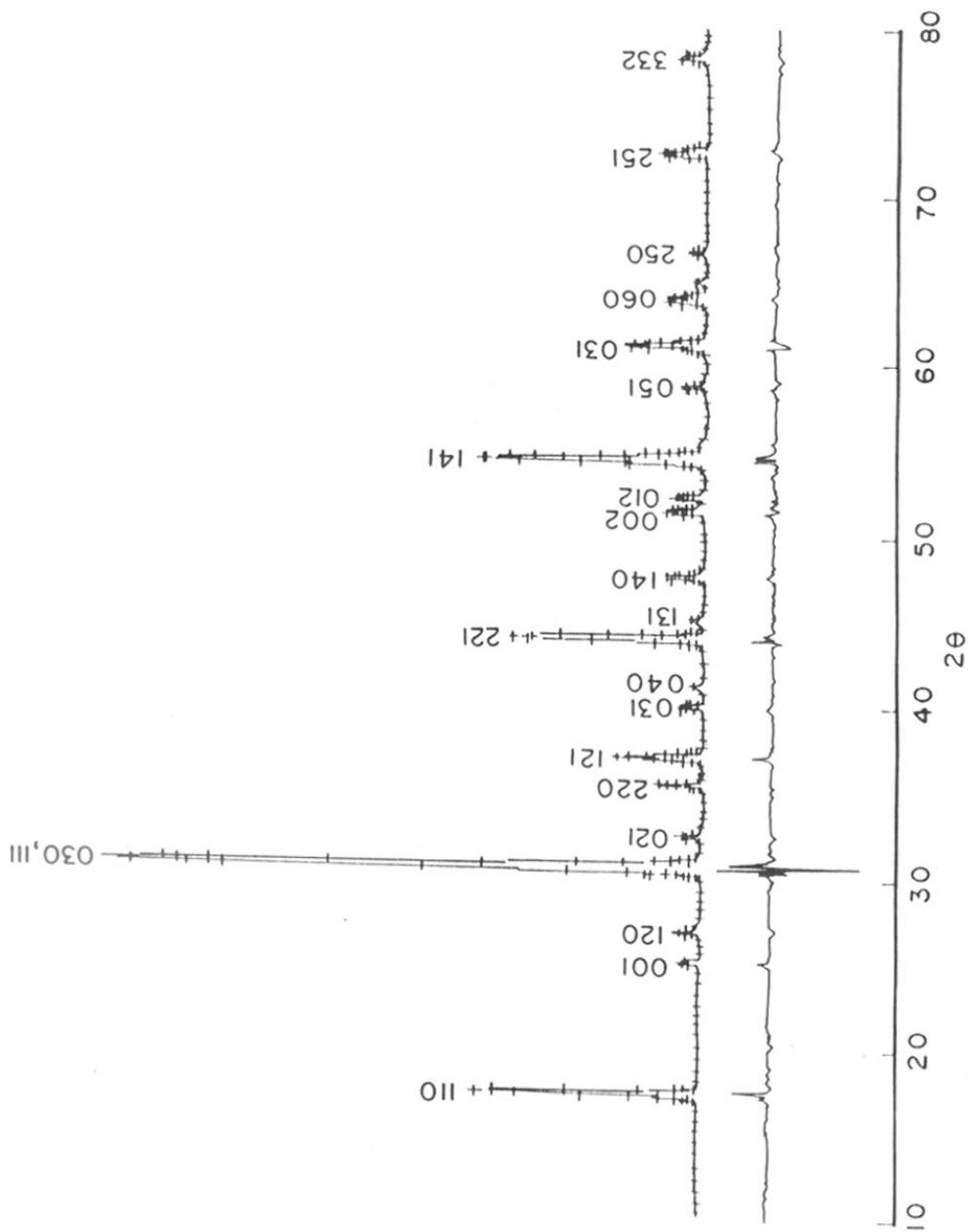


Fig. 5.6a. The observed (+) and calculated (solid line) XRD profiles of $\text{Sr}_{1.5}\text{PbCu}_{0.20}\text{O}_{3.71}$. The bottom curve is the difference spectra.

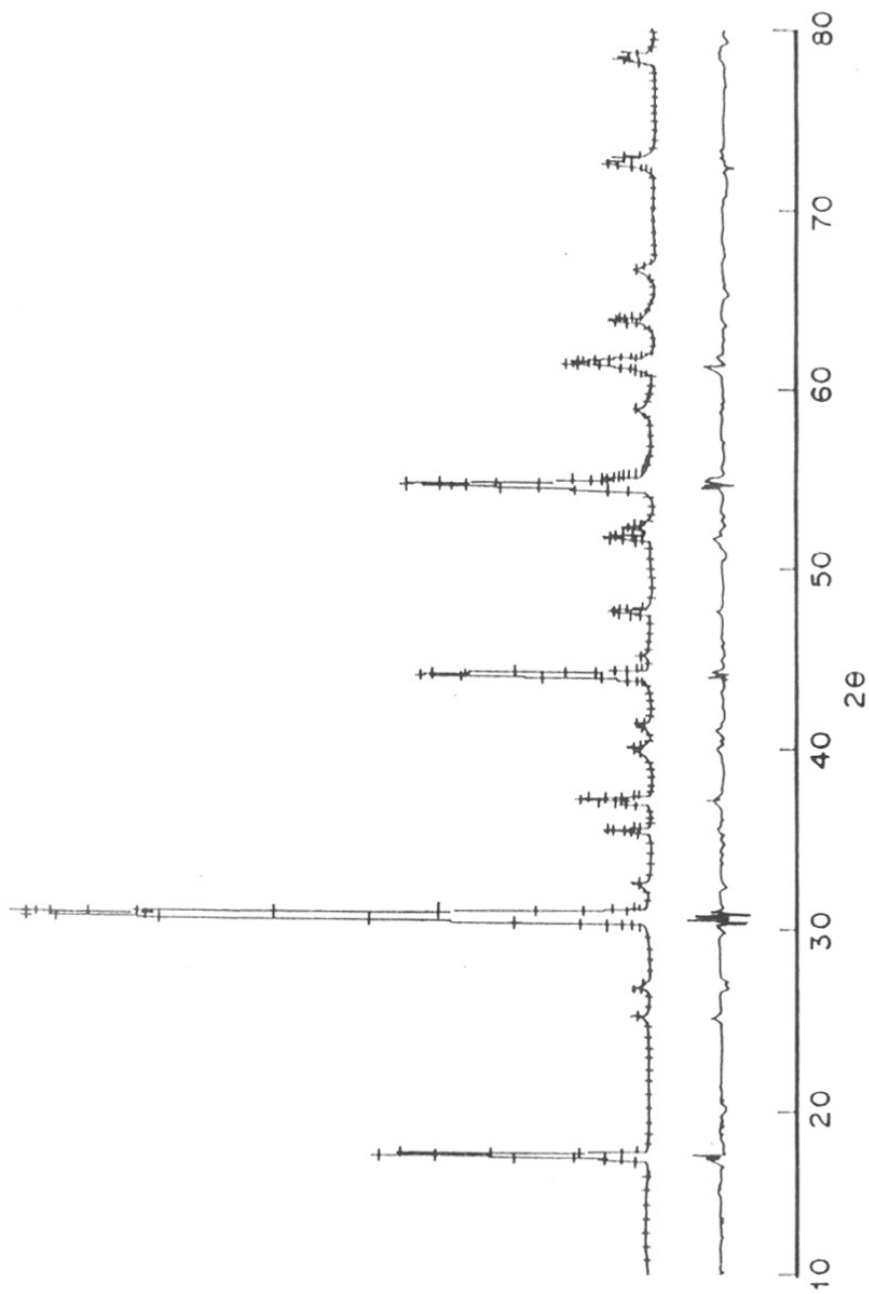


Fig. 5.6b. The observed (+) and calculated (solid line) XRD profiles of $\text{Sr}_{1.3}\text{PbZn}_{0.3}\text{O}_{3.71}$. The bottom curve is the difference spectra.

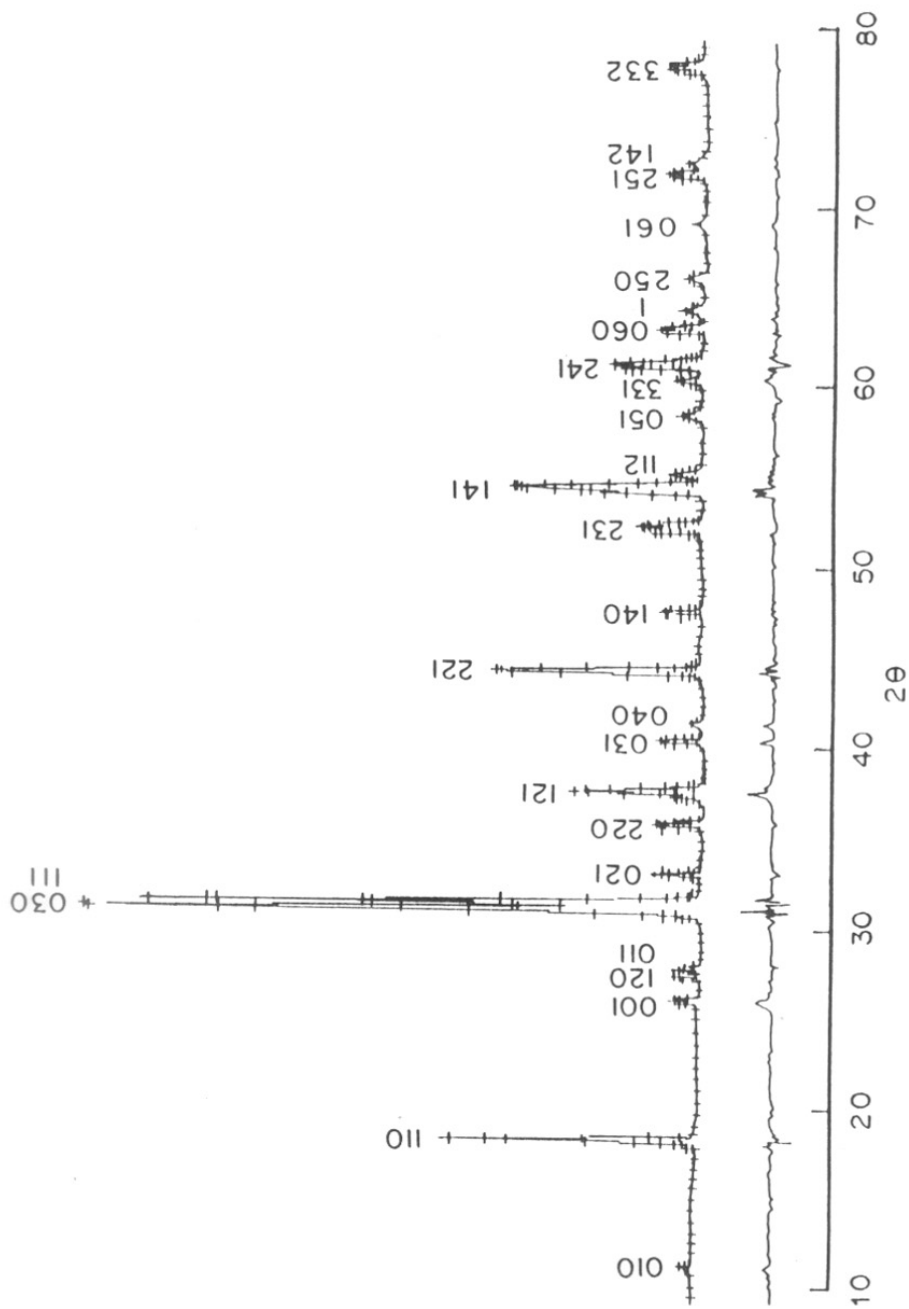


Fig. 5.6c. The observed (+) and calculated (solid line) XRD profiles of $\text{Sr}_{1.7}\text{PbCd}_{6.3}\text{O}_{9.71}$. The bottom curve is the difference spectra.

group. In this site, the Ca(1) atoms are coordinated to six oxygens. In $\text{Ca}_{5-x}\text{Ir}_3\text{O}_{12}$, this site remains vacant. Crystal structure of $\text{Ca}_{5-x}\text{Ir}_3\text{O}_{12}$ consists of rows of edge sharing IrO_6 octahedra lying parallel to the c -axis direction with Ir at $1/3, 0, 0$. Ca atoms occupy two sites in the space group and they are arranged in between rows of IrO_6 octahedra with a nine-fold coordination for Ca(2) at the (2d) site and seven-fold coordination for Ca(3) at the (3g) site. Ir occupies (3f) site in the space group. In the hexagonal structure of $\text{Sr}_{1.5}\text{M}_x\text{PbO}_{3.5+x}$, Pb occupies this (3f) site with the PbO_6 octahedra sharing edges along the c -axis. Sr(2) in nine-fold coordination and Sr(3) in seven-fold coordination are located in (2d) and (3g) sites respectively. The relative positions of the oxygen ions have been unchanged.

In $\text{Sr}_{1.5}\text{PbM}_{0.2}\text{O}_{3.7}$, Sr atoms do not occupy the Ca(1) site at $0, 0, 0$ (fig. 5.2c) as in Ca_2IrO_4 . Structure refinement shows that this position is also not occupied by Cu^{+2} ions or Zn^{+2} ions in $\text{Sr}_{1.5}\text{PbM}_x\text{O}_{3.5+x}$ compounds. A substantial increase in the R factor is observed if Cu or Zn is kept at this position. This may be due to smaller size of Cu^{+2} and Zn^{+2} (0.73 \AA and 0.74 \AA respectively, in six-fold coordination) ions compared to that of Sr^{+2} ions (1.18 \AA). Kim *et al* had also reported the Cu^{+2} is occupied at this site with two different z values. Thus the $0, 0, 0$ site remains vacant in Cu and Zn compounds and instead these atoms are found to occupy a four-coordinated site (2e) with coordinates $0, 0, z$. Kim *et al* had proposed that the Cu atoms partially occupy the $0, 0, z$ positions with $z = 0.37$ and 0.11 . The Cd^{+2} ions which are bigger in size (0.95 \AA in six-fold coordination) compared to Cu^{+2} and Zn^{+2} and are found to occupy this six-fold coordinated site at $0, 0, 0$ position. Fig. 5.7. shows a projection of the Crystal structure of $\text{Sr}_{1.5}\text{PbM}_x\text{O}_{3.5+x}$, ($M = \text{Cu}, \text{Cd}$) along c -direction, showing the CuO_4 and CdO_6 coordination polyhedra.

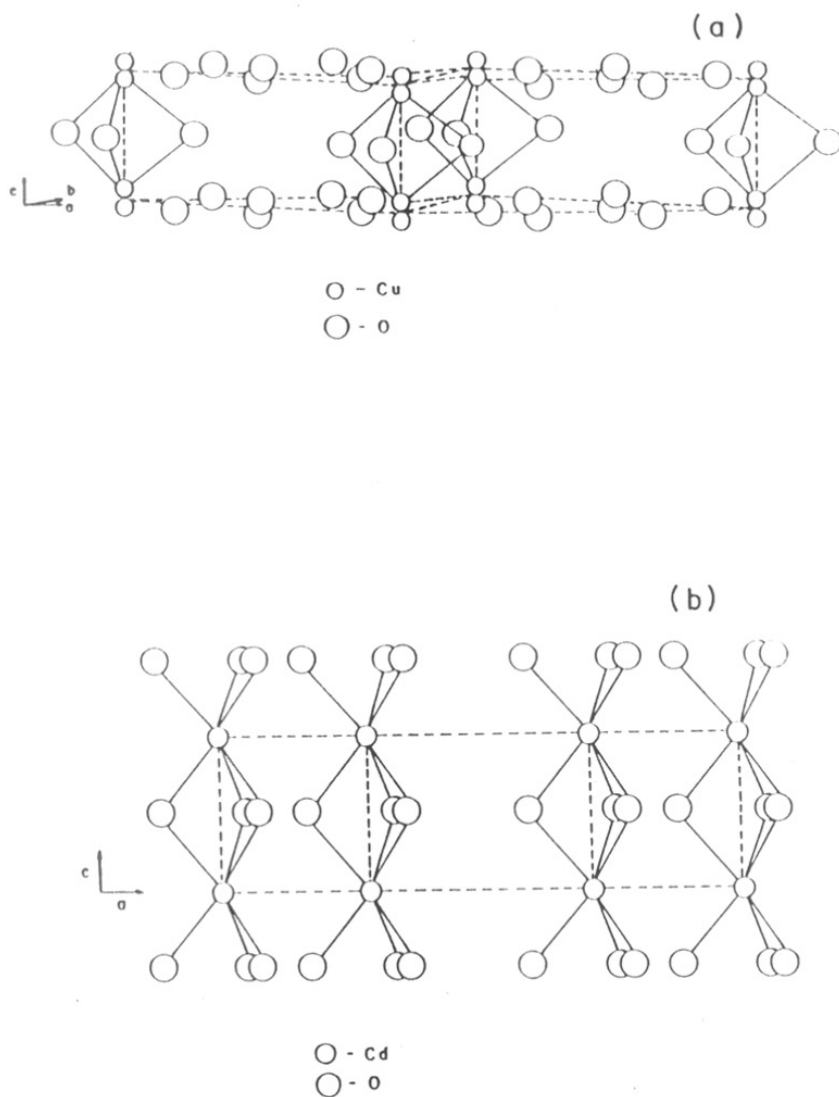


Fig. 5.7. Projection of crystal structure of $\text{Sr}_{1.5}\text{PbM}_2\text{O}_{3.5}$ along c -direction showing (a) CuO_4 (four-fold) (b) CdO_6 (six-fold) coordination polyhedra. Only Cu, Cd and O are shown for clarity.

The ideal composition of Ca_2IrO_4 when the six-fold coordinated (1a) site is unoccupied is $\text{Ca}_5\text{Ir}_3\text{O}_{12}$ [20]. The composition reported by Kim *et al* is $\text{Sr}_x\text{Pb}_{3-x}\text{Cu}_{0.66}\text{O}_{12-d}$ in which some of the Pb atoms occupy the Sr (3g) sites and Cu atoms occupy (2e) sites. Our present structure refinement essentially confirms their work. The only difference with regard to previous structure refinement lies in the position of the Cu(M) atoms. In their work, Cu (Cu1 and Cu2) atoms were found in the two positions i.e. 0,0,z site with two different z parameters. The Cu1 and Cu2 sites are each bonded to three O1 atoms at 1.77 Å and 2.20 Å distances respectively. It was proposed that a fourth O atom at 1.71 Å completes a tetrahedron around each Cu site and is situated either on a Cu1 site (to complete the Cu2 coordination) or a Cu2 site (to bond to Cu1). Such a structure involving the partial occupancy of Cu1 and Cu2 by both Cu and O seems energetically unfavorable due to electrostatic interactions. In the present study, it is found that the divalent atoms of smaller size like Cu^{12} , Zn^{12} are well localized in one position which was also observed in neutron diffraction study by Babu *et al* [18]. Based on an average unit cell, these divalent atoms appear to be 4-coordinated with a stereochemistry which may be described by flattened tetrahedron (fig.5.7). Babu *et al* [18] had reported that such a flattening which results in a change in bond angles and bond lengths, is consistent with the effect of Jahn-Teller distortion.

We find little evidence for the occupation of the Sr (2d) and (3g) sites by Pb ions. Finally it has observed that the (1a) site can be substantially more occupied by M atoms. If only the 1a site is occupied the ratio of M:Sr cannot exceed 1:5. This is to be the case when $M = \text{Cd}$. However, the ratio can be as much as 1:3 when $M = \text{Cu}$. Rietveld refinement has indicated that the R factor increases markedly when the (2d) or (3g) sites are occupied by copper in place of Sr.

The X-ray refinement does not allow us to unequivocally define the local coordination around the Pb or Cu atoms because of the known insensitivity of the X-ray intensities to the position of the oxygen atoms. Any composition with $x < 0.5$ in the $\text{Sr}_{1.5}\text{M}_x\text{PbO}_{3.5+x}$ series is bound to have oxygen vacancies. On the other hand, isolated chains of edge-shared PbO_6 octahedra require a PbO_4^{4-} composition, so that oxygen vacancies may not be stable. The possible solution to the problem when $x < 0.5$, is that chain of edge-shared PbO_6 octahedral units is not intact. Thus there could be PbO_4 tetrahedral units in the planes in which the copper atoms are located or when there is a vacancy at the Ca(1) site.

Table 5.5 lists bond distances obtained for various hexagonal compounds. Pb^{4+} is in distorted octahedral cation with O(1) and O(2) forming the basal plane and O(3) occupies axial position (fig.5.2c). Thus it can be seen from the table that Pb-O(1) and Pb-O(2) bond distances do not differ much but Pb-O(3) distance is significantly large.

The Sr atoms are situated on trigonal prismatic site. The Sr(1) site is fully occupied and its coordination polyhedron consists of tricapped trigonal prism. The Sr(2) site is not fully occupied and is bonded to seven oxygen ions. The coordination polyhedron is an incomplete tricapped trigonal prism. The four O(3) atoms constitute one square face of the trigonal prism whose edge is missing. The O(2) and two O(1) atoms are in capping positions. The Sr sites are not appropriate for the accommodation of Cu ions, since Sr-O distances are too long (table 5.5).

5.4.2. Vibrational Spectra

Vibrational spectra of a large number of ternary metal oxides of A_2BO_4 type have been reported earlier [21,22]. It provides useful information on the nature and the bonding of BO_6 polyhedron. In the A_2BO_4 type of compounds with K_2NiF_4 structure, the vibrational bands associated with B-O vibrations are of stretching type, which are observed in the high frequency region. These high frequency bands are usually attributed to in-plane and out-of-plane oxygen vibrations.

For A_2BO_4 oxides with K_2NiF_4 structure the tolerance factor is usually less than unity. As a result the B-O or O-O distances in the BO_2 plane, are usually shorter than the out-of-plane distances. The high-frequency and low-frequency IR bands are therefore attributed to the in-plane and out-of-plane O-O or O-B distances.

In this section, the Infra-red and Raman spectra of various Pb(IV)/Sn(IV) containing oxides in different structural types are examined and are compared with the vibrational modes obtained from group theory analysis.

5.4.2.1. Classification of normal modes

Using a standard group theoretical approach, it has been found that under which irreducible representations of these space groups or point groups, the atomic motions in the vibrational normal modes can be classified. The normal modes of vibrations for various structural types were obtained by "The Correlation Method" [23]. The site symmetry for each atom in the crystal lattice for different space groups has been found,

using Wyckoff's site notation [24]. The symmetry species are then identified for equivalent set of atom displacement in the site. Knowing the site species for these displacements, each species in site group is related to a species of factor group using correlation tables. This correlation explicitly identifies the species of the lattice vibrations in the crystal lattice and further allows the prediction of Infra-red and Raman active modes. In this way different vibrational modes for K_2NiF_4 , Sr_2PbO_4 and for $Sr_{1.5}PbCu_xO_{3.5+x}$ structures are predicted. The results are shown in table 5.6. The vibrations of normal modes for these three structures are compared in table 5.6d.

5.4.2.2. Compounds with K_2NiF_4 structure

As indicated in the table, for the A_2BO_4 compounds with K_2NiF_4 structure group theory predicts 7 Infra-red ($4E_u$ and $3A_{2u}$) and 4 Raman active ($2E_g$ and $2A_{1g}$) modes [25,26].

The $3A_{2u}$ modes corresponds to vertical motion of the O(II) and A atoms, with O(I) and O(II) vibrating either in phase or out of phase with each other or A. $4E_u$ modes represent the in-plane vibrations of the B atoms with the O(II) or A atoms following or not [25].

The Raman active A_{1g} modes correspond to symmetric vibration of the out-of-plane oxygen atoms O_{II} , against the B atom, with A atoms vibrating in phase (low frequency mode) and out of phase (high frequency mode) with O(II) atoms. Two E_g modes correspond to tilting of BO_6 octahedra around diagonal axes in or out of phase with A atoms [26].

Table. 5.6. Classification of normal modes :

(a). Ba_2PbO_4 (K_2NiF_4 tetragonal) structure. S.G.14/mmm

Ion	Equipoint	Site symmetry	Factor group D_{4h}^{17} species
Pb	2a	D_{4h}	$A_{2u} + E_u$
O(I)	4c	D_{2h}	$A_{2u} + B_{2u} + 2E_u$
Ba	4e	C_{4v}	$A_{2u} + E_u + A_{1g} + E_g$
O(II)	4e	C_{4v}	$A_{2u} + E_u + A_{1g} + E_g$

$$\text{Total modes } \Gamma = 5E_u + 4A_{2u} + B_{2u} + 2E_g + 2A_{1g}$$

$$\text{Acoustic modes} = E_u + 2A_{2u}$$

$$\text{IR active modes} = 3A_{2u} + 4E_u$$

$$\text{Raman active mode} = 2A_{1g} + 2E_g$$

$$\text{Inactive modes} = B_{2u}$$

Table. 5.6. Contd.

(b) Sr_2PbO_4 (orthorhombic) structure S.G. Pham

Ion	Equipoint	Site symmetry	Factor group D_{2h} species
Pb	2a	C_{2h}	$4A_u + 4B_{1u} + 8B_{2u} + 8B_{3u}$
Sr	4h	C_s	$4A_u + 4B_{1u} + B_{2u} + 8B_{3u}$ $2A_g + 2B_{1g} + B_{2g} + B_{3g}$
O(I)	4h	C_s	same as above
O(II)	4g	C_s	same as above

$$\text{Total modes } \Gamma = 4A_{2u} + 4B_{1u} + 8B_{2u} + 8B_{3u} + 6A_g + 2B_{1g} + 3B_{2g} + 3B_{3g}$$

$$\text{Acoustic modes} = B_{1u} + B_{2u} + B_{3u}$$

$$\text{IR active modes} = 3B_{1u} + 7B_{2u} + 7B_{3u}$$

$$\text{Raman active modes} = 6A_g + 6B_{1g} + 3B_{2g} + 3B_{3g}$$

$$\text{Inactive modes} = 4A_{2u}$$

Table. 5.6. Contd.

(c) $\text{Sr}_{1.5}\text{PbM}_x\text{O}_{3.5+x}$ (Ca_2IrO_4) hexagonal structure S.G. $\overline{\text{P6}}2\text{m}$.

Ion	Equipoint	Site symmetry	Factor group D_{3h} species
Sr(1)	2d	C_{3h}	$2\text{E}' + \text{A}_2'' + \text{A}_1''$
Sr(2)	3g	C_{2v}	$3\text{A}_1' + 3\text{A}_2'' + 3\text{A}_2'$
Pb	3f	C_{2v}	$3\text{A}_1' + 3\text{A}_2'' + 3\text{A}_2'$
O(I)	3g	C_{2v}	$3\text{A}_1' + 3\text{A}_2'' + 3\text{A}_2'$
O(II)	3g	C_{2v}	$3\text{A}_1' + 3\text{A}_2'' + 3\text{A}_2'$
O(III)	6j	C_3	$12\text{A}_2' + 3\text{A}_1'' + 3\text{A}_2''$
Cu	2e	C_{3v}	$\text{A}_1' + \text{A}_2'' + \text{E}' + \text{E}''$

$$\text{Total modes } \Gamma = 3\text{E}' + \text{E}'' + 13\text{A}_1' + 4\text{A}_1'' + 24\text{A}_2' + 17\text{A}_2''$$

$$\text{Acoustic modes} = 2\text{E}' + 1\text{A}_2''$$

$$\text{IR active modes} = 2\text{E}' + 16\text{A}_2''$$

$$\text{Raman active modes} = 13\text{A}_1' + 2\text{E}' + \text{E}''$$

$$\text{Inactive modes} = 4\text{A}_1'' + \text{A}_2'$$

Table. 5.6d. Comparison of normal modes of vibrations in different structures.

A_2BO_4	IR modes	Raman modes
Ba_2PbO_4	$3\text{A}_{2u} + 4\text{E}_u$	$2\text{A}_{1g} + 2\text{E}_g$
Sr_2PbO_4	$3\text{B}_{1u} + 7\text{B}_{2u} + 7\text{B}_{3u}$	$6\text{A}_g + 6\text{B}_{1g} + 3\text{B}_{2g} + 3\text{B}_{3g}$
Ca_2IrO_4	$2\text{E}' + 16\text{A}_2''$	$13\text{A}_1' + 2\text{E}' + \text{E}''$
$(\text{Sr}_{1.5}\text{PbM}_x\text{O}_{3.5+x})$		

5.4.2.2a. Infrared Spectra

The Infra-red spectra of some of the compounds with K_2NiF_4 structure is shown in fig. 5.8. It can be seen that the spectra contains one sharp band in the high frequency region at $\sim 500\text{ cm}^{-1}$ and few bands in the low frequency region which are not well resolved. Of interest to us is the high frequency bands which are usually attributed to in-plane and out-of-plane oxygen vibrations. For A_2BO_4 compounds with low tolerance factor such as those derived from Ln_2BO_4 ($Ln = \text{rare-earth ion}$, $B = \text{Cu, Co}$) compounds the B-O or O-O distances in the BO_2 plane are usually shorter than those which are out of the plane [21]. The higher frequency bands in the IR spectra of polycrystalline samples are therefore attributed to the in-plane vibrations of the oxygens [21,22,27]. For the compounds with K_2NiF_4 structure like $LaSrAlO_4$, $LaSrFeO_4$, La_2NiO_4 , $La_{2-x}Sr_xCuO_4$, the high frequency infra-red bands around 650 cm^{-1} has been assigned to an in-plane stretching E_u mode where B-O distance is shorter while the low frequency infrared bands around 500 cm^{-1} to an out-of-plane A_{2u} stretching mode.

When $A = \text{alkaline-earth ion}$ such as Sr, Ba; the tolerance factor increases (table 5.1) and the BO_6 octahedra becomes more regular so that the in-plane and out-of-plane vibrations associated with the oxygens in the BO_2 plane are expected to approach each other. Thus in Ba_2PbO_4 ($t = 0.93$; in-plane O-O distance = 3.05 \AA , Pb-O distance = 2.16 \AA compared to the expected Shannon-Prewitt distance of 2.185 \AA [9]) there is a single relatively narrow band at high frequency (518 cm^{-1}) which is consistent with the above. In $BaSrPbO_4$ ($t = 0.91$, in-plane O-O distance = 3.02 \AA , Pb-O distance = 2.13 \AA compared to the Shannon-Prewitt distance of 2.185 \AA) the single high-frequency band in Ba_2PbO_4 is shifted to

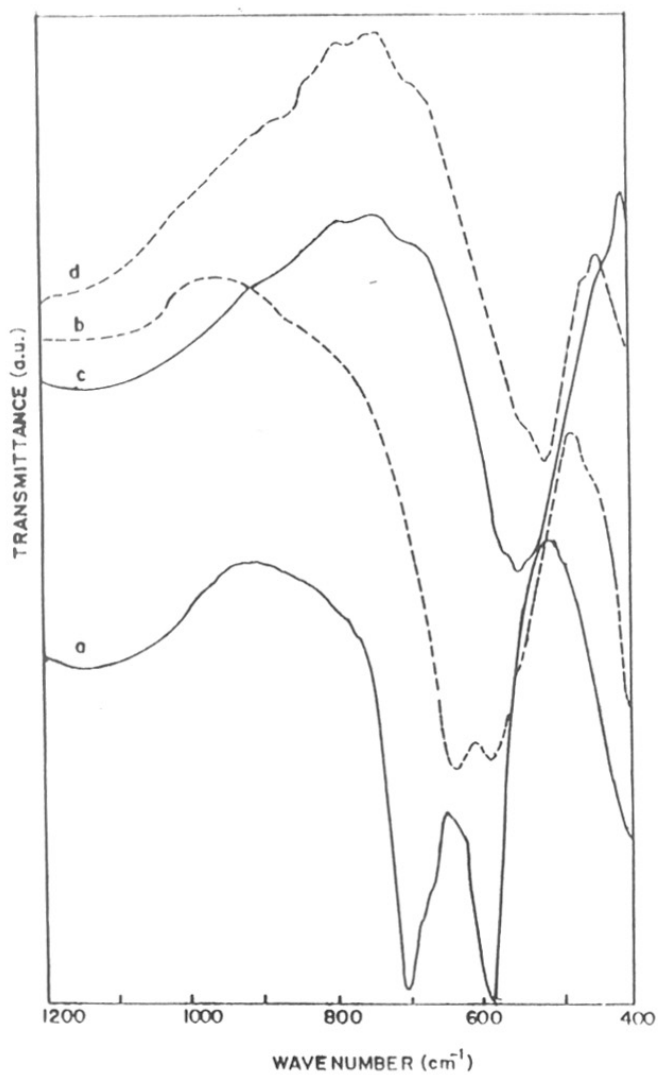


Fig. 5.8. Infra-red spectra of some of K_2NiF_4 type compounds.
(a) Sr_2SnO_4 , (b) $Sr_2Sn_{0.45}Pb_{0.55}O_4$, (c) $BaSrPbO_4$, (d) Ba_2PbO_4 .

a higher frequency (551 cm^{-1}). The band is slightly broader compared to that of Ba_2PbO_4 which could be due to the disorder that is expected from a scrambling of the Ba and Sr ions.

In $\text{Sr}_2\text{Sn}_{0.45}\text{Pb}_{0.55}\text{O}_4$, ($t = 0.89$, in-plane O-O distance = 2.91 \AA ; (Sn,Pb)-O distance = 2.06 \AA compared to expected Shannon-Prewitt (Sn,Pb)-O distance of 2.133 \AA) there is a clear splitting of the high-frequency band (644 cm^{-1}) which becomes enhanced in pure Sr_2SnO_4 (710 cm^{-1} and 685 cm^{-1}) with ($t = 0.92$) in-plane O-O distance of 2.86 \AA ; in-plane Sn-O distance of 2.02 \AA compared to the Shannon-Prewitt distance of 2.09 \AA . Thus it can be seen that for K_2NiF_4 type of A_2BO_4 (A = Sr, Ba; B = Pb, Sn) compounds, the decrease in (Pb/Sn)-O bond distance in the basal plane of (Pb,Sn)- O_6 octahedra, increases the IR stretching frequency.

In all these cases, the in-plane O-O distance is greater than the maximum Shannon-Prewitt O-O distance of 2.80 \AA . The in-plane Ba-O distance (2.897 \AA) in Ba_2PbO_4 or the (Ba,Sr)-O distance (2.827 \AA) in BaSrPbO_4 is larger than that expected from the sum of the corresponding Shannon-Prewitt radii. For example, the $\text{O}_r\text{-O}_n$ distances in Ba_2PbO_4 is 2.99 \AA and in BaSrPbO_4 it is 2.91 \AA . The layered perovskite K_2NiF_4 structure of these compounds is thus formed by corner-sharing of PbO_6 octahedra and not from a close-packing of oxygen and A atoms. In such a case the A atoms have little influence in distorting the PbO_6 octahedra. One may conclude therefore that in Ba_2PbO_4 and BaSrPbO_4 the main contributions to the high-frequency bands are from the in-plane and out-of-plane vibrations of oxygen in Pb-O bonds.

In $\text{Sr}_2\text{Sn}_{0.45}\text{Pb}_{0.55}\text{O}_4$ and Sr_2SnO_4 compounds, the $\text{O}_r\text{-O}_n$ distances are close to the Shannon-Prewitt distance of 2.80 \AA being ~ 2.82 and $\sim 2.78\text{ \AA}$, respectively. The

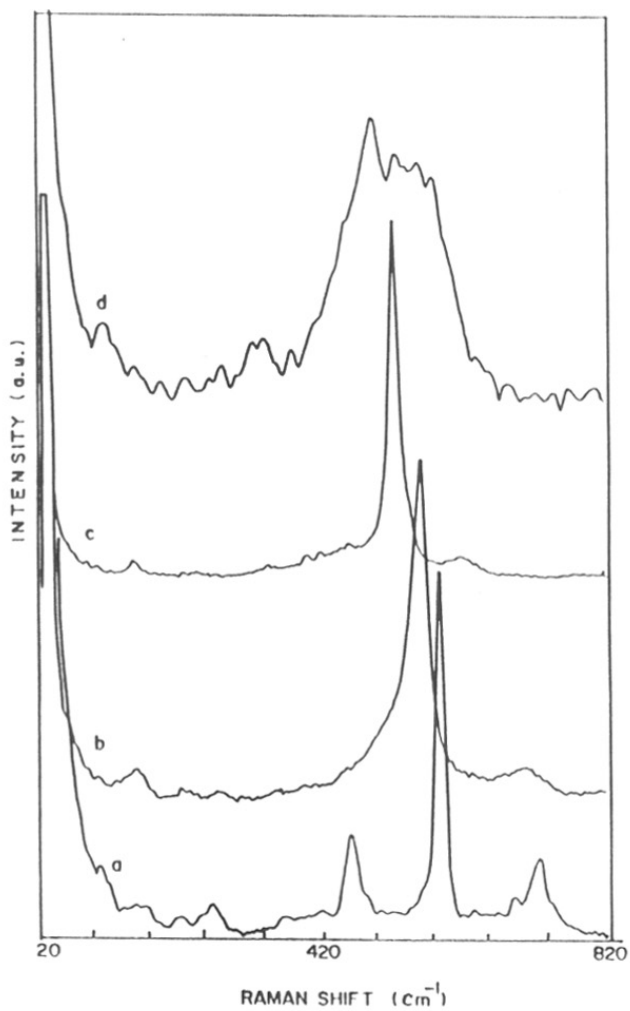


Fig. 5.9. Raman spectra of (a) Sr_2SnO_4 (b) $\text{Sr}_2\text{Sn}_{0.45}\text{Pb}_{0.55}\text{O}_4$ (c) BaSrPbO_4 (d) Ba_2PbO_4 .

in-plane O_1-O_1 distance of 2.86 \AA is greater than 2.80 \AA . The out-of-plane $\text{Sn}-O_{II}$ distance in Sr_2SnO_4 (1.914 \AA as obtained from X-ray crystal structure refinement [28]) is also considerably shorter than the in-plane $\text{Sn}-O_1$ distance (2.02 \AA). Such an anisotropy is perhaps reflected in the splitting of the high frequency band of Sr_2SnO_4 . It is, however, not clear whether the higher frequency band is to be associated with shorter axial $\text{Sn}-O_{II}$ vibration.

5.4.2.2b. Raman Spectra

The Raman spectra of A_2BO_4 compounds ($A = \text{Ba}, \text{Sr}; B = \text{Pb}, \text{Sn}$) with K_2NiF_4 structure are shown in the fig. 5.9. It can be seen that spectra contains one sharp band in the region $500-600 \text{ cm}^{-1}$ with highest Raman intensity. In addition to this, some weak bands are observed in higher as well as lower frequency side. Sr_2SnO_4 shows a sharp band at 584 cm^{-1} and weak bands at $152, 220, 260, 450, 720 \text{ cm}^{-1}$. In $\text{Sr}_2\text{Sn}_{0.45}\text{Pb}_{0.55}\text{O}_4$, a sharp band is observed at 558 cm^{-1} with weak bands at 160 and 224 cm^{-1} . The band around 700 cm^{-1} is slightly broadened. BaSrPbO_4 shows a high intensity band at 522 cm^{-1} and few very weak bands around $160, 460$ and 618 cm^{-1} . In Ba_2PbO_4 , the sharp band is shifted to still lower frequency side, it occurs at 492 cm^{-1} compared to 522 cm^{-1} in BaSrPbO_4 . It also shows some bands in $525-550 \text{ cm}^{-1}$ region with nearly same intensity as that of strong band which may be due to some hydrolysed impurity.

In the Raman spectra of La_2CuO_4 [26] which has the K_2NiF_4 related structure, a band at 140 cm^{-1} has been assigned to in-plane and the band at 412 cm^{-1} band to out-of-plane symmetric A_{1g} vibration. Two E_g modes correspond to tilting of BO_6 octahedra around diagonal axes in- or out-of-phase with La atoms. A band at 210 cm^{-1} has been assigned to E_g mode.

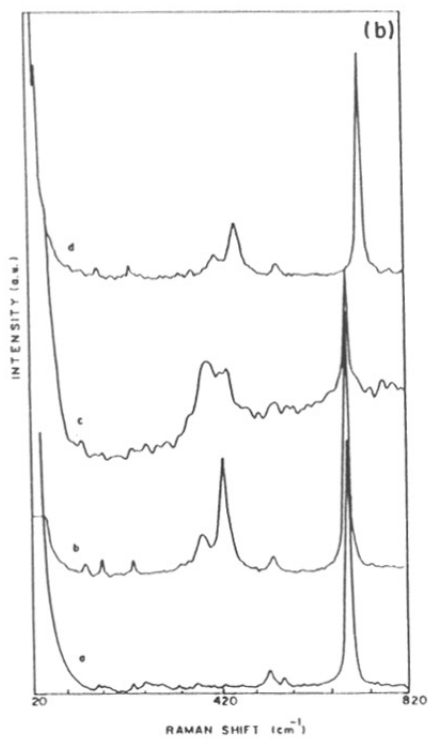
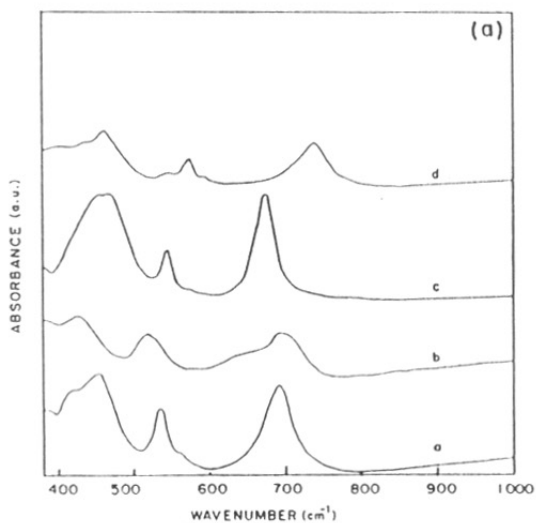


Fig. 5.10. IR (a) and Raman (b) spectra of $\text{La}_2\text{Li}_{0.5}\text{M}_{0.5}\text{O}_4$ compounds.
(a) $\text{La}_2\text{Li}_{0.5}\text{Ni}_{0.5}\text{O}_4$, (b) $\text{La}_2\text{Li}_{0.5}\text{Cu}_{0.5}\text{O}_4$, (c) $\text{La}_2\text{Li}_{0.5}\text{Co}_{0.5}\text{O}_4$,
(d) $\text{Nd}_2\text{Li}_{0.5}\text{Ni}_{0.5}\text{O}_4$.

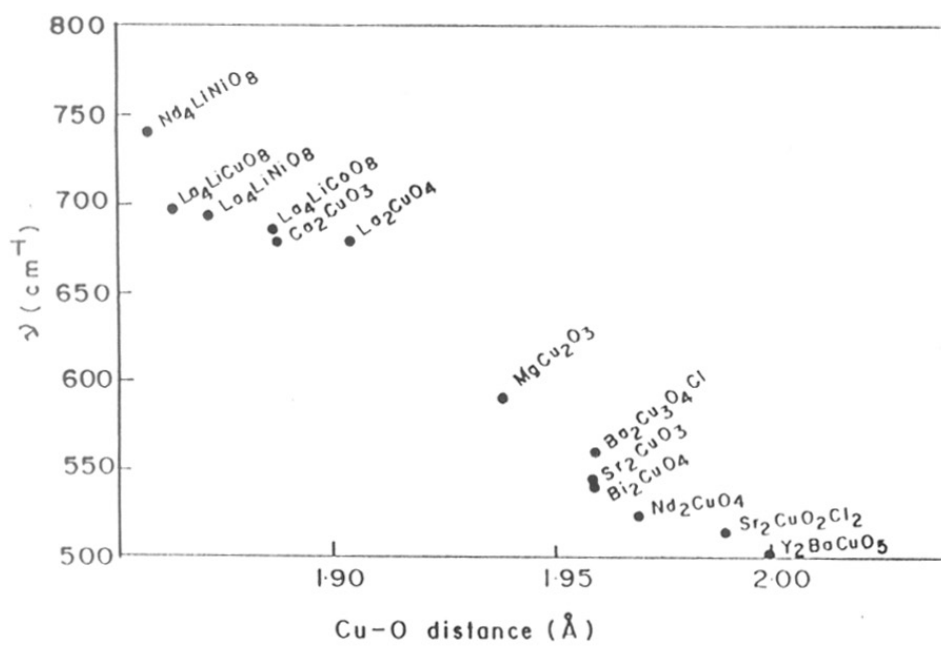


Fig. 5.11. Titration curve of ν_{max} of ternary copper oxide compounds Vs the shortest Cu-O distance.

The Raman and Infra-red spectra of some $\text{Ln}_2\text{Li}_{0.5}\text{M}_{0.5}\text{O}_4$ compounds ($\text{Ln} = \text{La}, \text{Nd}$; $\text{M} = \text{Co}, \text{Ni}, \text{Cu}$) which have K_2NiF_4 type tetragonal structure are examined and are shown in fig. 5.10. It can be seen that all the infra-red bands are Raman active without a significant change in the frequency of the bands. This would be consistent with the absence of an inversion symmetry of these compounds. Such an absence of inversion symmetry may arise simply from the absence of a three-dimensional ordering of the Li and M ions even if they are ordered in the $(\text{Li}, \text{M})\text{O}_2$ plane. Such an inter-layer ordering of different species (in an "antiferromagnetic" sense) are known to be frustrated in the body-centered symmetry of the tetragonal K_2NiF_4 structure.

The IR stretching frequencies, ν_{max} of the in-plane bands fall well on the "titration" curve in fig. 5.11, which correlates the ν_{max} of ternary copper oxides with the shortest Cu-O distance [27]. The intensities of the in-plane Raman bands (at the highest frequency) are considerably higher than that of the out-of-plane bands in the $\text{Ln}_2\text{Li}_{0.5}\text{M}_{0.5}\text{O}_4$ compounds.

Unlike the other A_2BO_4 compounds ($\text{A} = \text{La}, \text{Nd}, \text{Sr}$; $\text{B} = \text{Li}, \text{Ti}, \text{Co}, \text{Ni}, \text{Cu}$) the Raman bands with the highest frequency in the A_2BO_4 compounds with $\text{A} = \text{Sr}, \text{Ba}$; $\text{B} = \text{Pb}, \text{Sn}$ and with K_2NiF_4 structure do not have the highest intensity (fig. 5.9). We are mainly interested in the band at $\sim 500 \text{ cm}^{-1}$ which is shifted to high frequency region as observed in going from Ba_2PbO_4 to Sr_2SnO_4 compounds.

The plot (fig. 5.12a) of the frequency of the bands with highest Raman intensity as a function of the in-plane B-O ($\text{B} = \text{Pb}, \text{Sn}$) falls on the same line as that of ν_{max} of $\text{Ln}_2\text{Li}_{0.5}\text{M}_{0.5}\text{O}_4$ compounds. In the latter series of compounds, the in-plane O-O distance is less than the Shannon-Prewitt distance of 2.80 \AA . When $\text{B} = \text{Pb}$ or Sn , the O-O

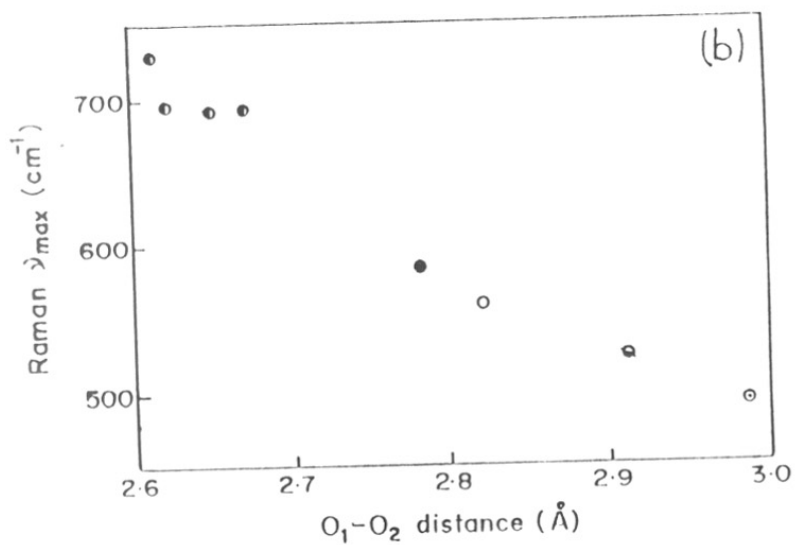
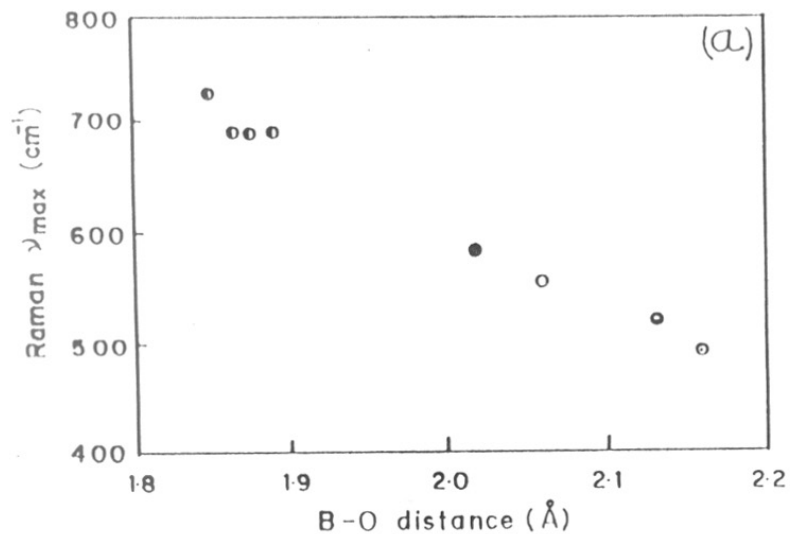


Fig. 5.12. Plot of ν_{\max} (Raman) Vs B-O distance (a) and $\text{O}_1\text{-O}_2$ distance (b) in various K_2NiF_4 type of compounds. \bullet $\text{Ln}_2\text{Li}_{0.5}\text{M}_{0.5}\text{O}_4$ (Ln = La, Nd; M = Cu, Ni, Co), \blacklozenge Sr_2SnO_4 , \circ $\text{Sr}_2\text{Sn}_{0.45}\text{Pb}_{0.55}\text{O}_4$, \blacklozenge BaSrPbO_4 , \circ Ba_2PbO_4 .

distance in the BO_6 octahedra involving the axial and basal oxygen (the $\text{O}_1\text{-O}_n$ distance) are shorter than 2.80 \AA . The plot (fig. 5.12b) of the frequency of the bands with highest Raman intensity as a function of the out-of-plane $\text{O}_1\text{-O}_n$ distance ($B = \text{Pb, Sn}$) falls on the same line as that plot of ν_{max} of $\text{La}_2\text{Li}_{0.5}\text{M}_{0.5}\text{O}_4$ compounds. The more non-polar O-O vibration is expected to show a higher Raman intensity in both these series of compounds. One may thus expect the high-intensity Raman bands as well as the infra-red bands to be associated with the O-O vibrations and their frequency correlated to the O-O distance. This is supported by the good fit of the titration curve to the $\text{O}_1\text{-O}_n$ distance.

5.4.2.3. Compounds with Sr_2PbO_4 and Ca_2IrO_4 structure

As indicated in the table 5.7b for compounds with Sr_2PbO_4 structure, group theory predicts 17 infra-red active ($3\text{B}_{1u} + 7\text{B}_{2u} + 7\text{B}_{3u}$) and 18 Raman active modes ($6\text{A}_g + 6\text{B}_{1g} + 3\text{B}_{2g} + 3\text{B}_{3g}$) [29] and for the compounds with Ca_2IrO_4 structure ($\text{Sr}_{1.5}\text{PbCu}_x\text{O}_{3.5+x}$), there should be 17 infra-red modes ($1\text{E}' + 16\text{A}''_2$) and 15 Raman modes ($13\text{A}'_1 + \text{E}' + \text{E}''$). The symmetry assignment of the infra-red and Raman bands in Sr_2PbO_4 and in hexagonal compounds with Ca_2IrO_4 -related structures have not been made as yet.

The infra-red spectra of Sr_2PbO_4 and $\text{Sr}_{1.5}\text{PbM}_{0.2}\text{O}_{3.71}$ ($M = \text{Cu, Zn, Cd}$) are shown in fig. 5.13. The spectra show one sharp band in $450\text{-}500 \text{ cm}^{-1}$ region and few weak bands in the low frequency region. Thus actually only 3 to 4 vibrations are observed in the measured frequency range for both the structures, which could be due to overlapping of close lying bands at lower frequency region and occurrence of bands at still lower frequency.

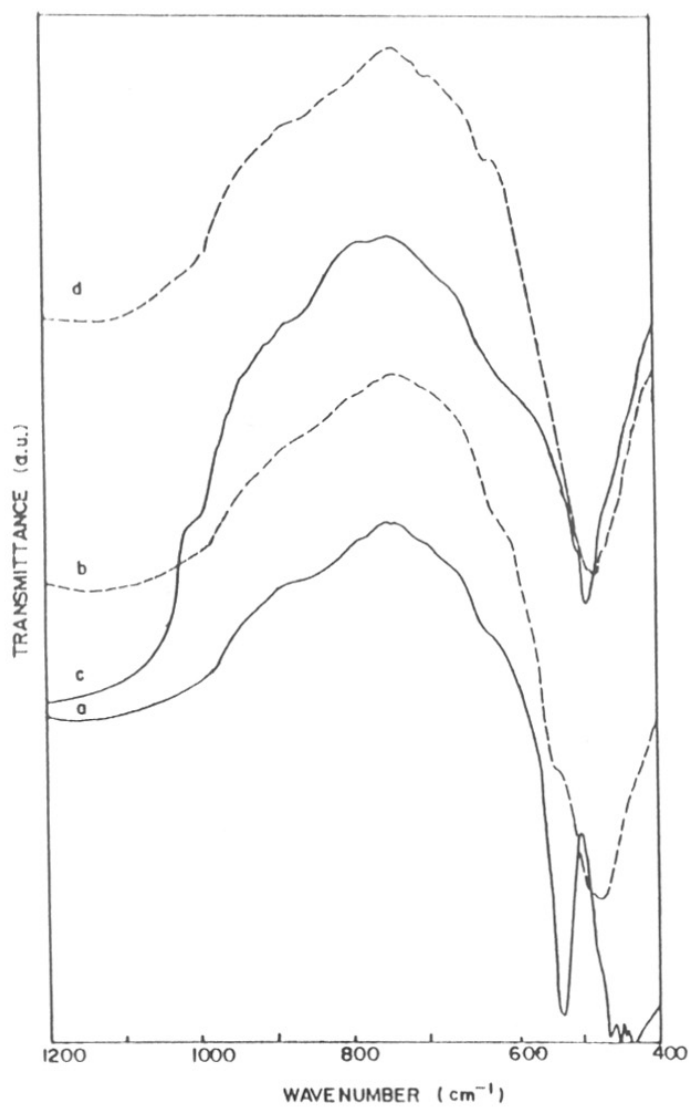


Fig. 5.13. IR spectra of (a) Sr_2PbO_4 , (b) $\text{Sr}_{1.5}\text{PbCu}_{0.20}\text{O}_{3.71}$, (c) $\text{Sr}_{1.5}\text{PbZn}_{0.20}\text{O}_{3.71}$, (d) $\text{Sr}_{1.5}\text{PbCd}_{0.20}\text{O}_{3.71}$.

For compounds having Sr_2PbO_4 structure, (Sr_2PbO_4 , Ca_2PbO_4 , Cd_2PbO_4 , Ca_2SnO_4 , Ca_2PtO_4) the predicted Raman modes are (A_g , B_{1g} , B_{2g} , B_{3g}) due to vibrations of O(I) and O(II) with A atoms. These modes are the species of the polarization tensor elements along different x, y, z directions. So it can be assigned that for Sr_2PbO_4 structure in general, Raman bands are associated with O(I)-A and O(II)-A vibrations.

Raman spectra of Sr_2PbO_4 and $\text{Sr}_{1.5}\text{PbM}_x\text{O}_{3.5+x}$ compounds are shown in fig. 5.14. It is observed that for Sr_2PbO_4 , the high frequency sharp band at 524 cm^{-1} occurs both in Raman as well as in infra-red spectra. For non-centrosymmetric space groups the infra-red and Raman bands coincide according to mutual exclusion principle. Sr_2PbO_4 crystallizes in Pbam space group which is centrosymmetric but as reported by [29] it can also crystallize in Pba2 space group which is non-centrosymmetric. Since calculated X-ray Diffraction patterns cannot differentiate these space groups, from above observation it can be concluded that Sr_2PbO_4 has non-centrosymmetric Pba2 space group.

In all these compounds (Sr_2PbO_4 and $\text{Sr}_{1.5}\text{PbM}_x\text{O}_{3.5+x}$), except for the band at high frequency ($450\text{-}500\text{ cm}^{-1}$ region), the other bands are not well resolved. For Sr_2PbO_4 this band occurs at 524 cm^{-1} which is observed in both infra-red and Raman spectra. Further this band is shifted to low frequency region ($\sim 480\text{ cm}^{-1}$) for $\text{Sr}_{1.5}\text{PbM}_x\text{O}_{3.5+x}$ compounds.

In Sr_2PbO_4 the average Pb-O distance is 2.185 \AA , which is obtained from crystal structure refinement. This observed Pb-O distance is consistent with those observed for other Pb(IV)-oxides like the metallic PbO_2 (2.18 \AA) and Pb_3O_4 (2.15 \AA) [11]. PbO_2 has rutile structure and Pb_3O_4 contains edge-shared octahedra. Both these structures are closely related to Sr_2PbO_4 structure [11]. For Pb_3O_4 ν_{max} occurs at 530 cm^{-1} and for Sr_2PbO_4 at 524 cm^{-1} . Thus the frequency

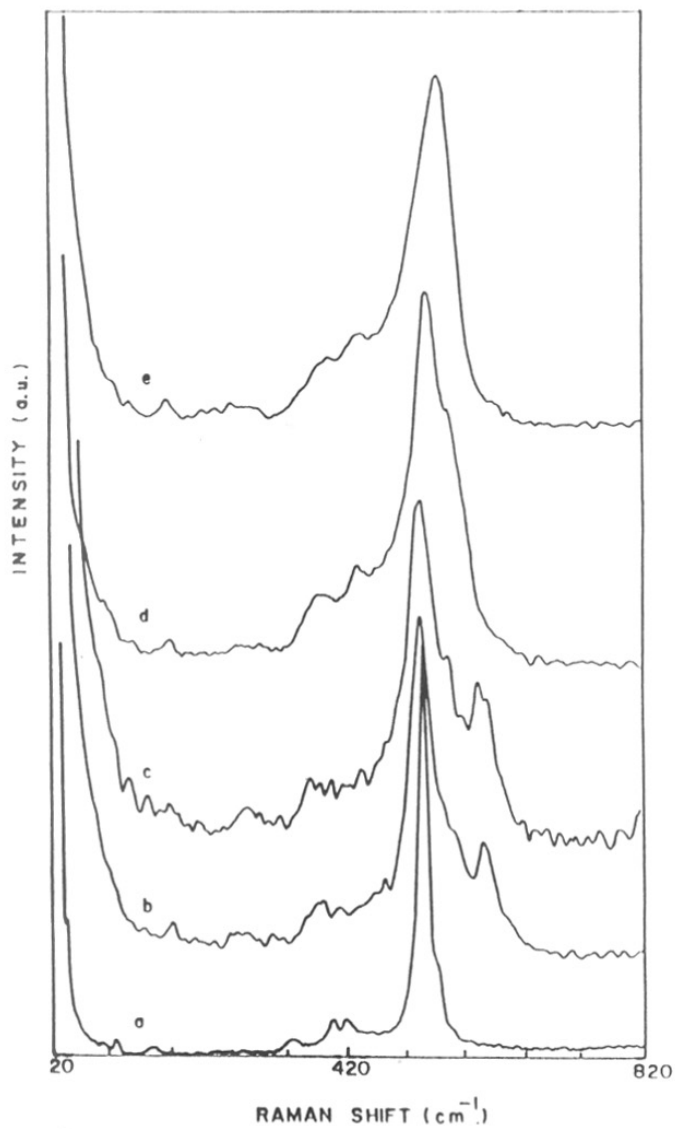


Fig. 5.14. Raman spectra of (a) Sr_2PbO_4 , (b) $\text{Sr}_{1.5}\text{PbCu}_{0.20}\text{O}_{3.71}$, (c) $\text{Sr}_{1.5}\text{PbCu}_{0.45}\text{O}_{3.9}$, (d) $\text{Sr}_{1.5}\text{PbZn}_{0.20}\text{O}_{3.71}$, (e) $\text{Sr}_{1.5}\text{PbCd}_{0.20}\text{O}_{3.71}$.

of the band is consistent with a large Pb-O distance of 2.185 Å (fig. 5.12) and is not sensitive to the details of the crystal structure as a first approximation.

In $\text{Sr}_{1.5}\text{PbM}_x\text{O}_{3.5+x}$ compounds, (derived from Sr_2PbO_4), unlike Sr_2PbO_4 , the frequencies and the intensities of the infra-red bands (fig. 5.13) are observed to be very different from that of the Raman bands (fig. 5.14).

A new feature in the Raman spectra of $\text{Sr}_{1.5}\text{PbCu}_x\text{O}_{3.5+x}$ ($x = 0.25$ and 0.45) compounds as distinct from the other $\text{Sr}_{1.5}\text{PbM}_x\text{O}_{3.5+x}$, ($M = \text{Zn}, \text{Cd}$) compounds is the appearance of a band at $\sim 600 \text{ cm}^{-1}$. For $\text{Sr}_{1.5}\text{PbCu}_x\text{O}_{3.5+x}$ compound, predicted Raman modes are $(13A_1' + 2E' + E'')$, in which E'' mode corresponds to vibrations associated with Cu atoms. This may be associated with O vibrations in O-Cu linkages. Thus the band at $\sim 600 \text{ cm}^{-1}$ corresponds to E'' mode which is attributed to vibrations of O-Cu band. This band at 600 cm^{-1} is consistent with those observed for other copper-oxide compounds [22,27].

A "titration" curve (fig. 5.11) of the vibration frequency, ν_{CuO} , of such linkages in perovskite-related structures Vs the Cu-O distance, yields a Cu-O distance of $\sim 1.94 \text{ \AA}$. Such a distance is too small for the copper ions to occupy the six-coordinated Sr site in the Ca_2IrO_4 related structures which have Cu-O distances greater than 2.2 \AA . The X-ray refinement studies shows that the Cu ion is shifted from the ideal position of Sr at 0,0,0.

Fig. 5.15 shows that the plot of IR stretching frequency ν_{max} (of Sr_2PbO_4 and $\text{Sr}_{1.5}\text{PbM}_x\text{O}_{3.5+x}$ compounds) versus the Pb-O distance falls on the same line as that obtained for the compounds with K_2NiF_4 structure. ν_{max} is thus due to vibrations associated with Pb-O linkages.

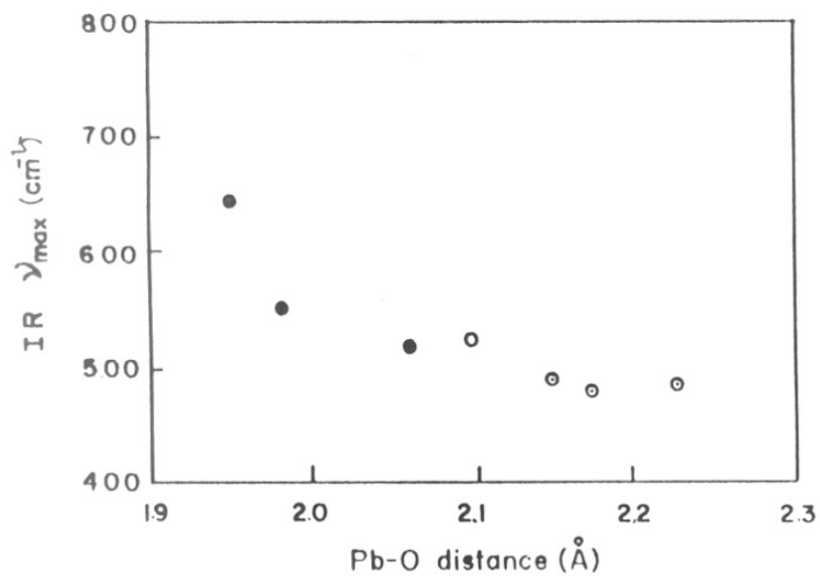


Fig. 5.15. Plot of IR stretching freq. ν_{\max} Vs Pb-O distance in various Pb(IV) Oxides. ● K_2NiF_4 , ○ Sr_2PbO_4 , ⊙ $\text{Sr}_{1.3}\text{PbM}_{0.20}\text{O}_{3.71}$ (M = Cu, Zn, Cd).

5.4.3. Electron spin resonance studies

The ESR spectra of some of the copper-containing compounds have been studied (fig. 5.16). The intensity of the ESR signal from the $\text{Sr}_{1.5}\text{Pb}(\text{Zn}_{1-y}\text{Cu}_y)_x\text{O}_{3.5+0.5x}$ compounds are always weak being at least an order of magnitude less than that expected. This is the case even when y is small. The weak signal is typical of Cu^{2+} ions in elongated octahedra or square-planar geometry. On the other hand, the ESR signal from $\text{Sr}_2\text{Pb}_{1-x}\text{Cu}_x\text{O}_4$ ($x < 0.05$) is very strong, the intensity of the signal being comparable with that obtained from corresponding amount of $\text{CuSO}_4 \cdot 5\text{H}_2\text{O}$. The absence of a strong ESR signal from the hexagonal structures therefore indicates that the copper ions are not in isolated square-planar or octahedral coordination. The ESR spectra of divalent copper ions in tetrahedral coordination in oxide matrices have not been extensively studied, so that it is not clear whether the ESR signal is consistent with tetrahedral coordination.

5.5. Description of various A_2BX_4 structures on the basis of hexagonal packing of A atoms.

The Sr_2PbO_4 structure is obtained from the K_2NiF_4 structure of Ba_2PbO_4 by a decrease of the tolerance factor involving the substitution of Ba ions by Sr ions; it is also obtained on decreasing the tolerance factor in $\text{Sr}_2\text{Sn}_{1-x}\text{Pb}_x\text{O}_4$ by substituting Sn by the larger Pb ions. The unit cell volume of the $\text{Ba}_{2-x}\text{Sr}_x\text{PbO}_4$ compounds at $x = 1$, is 234 \AA^3 . For $x > 1$, both the K_2NiF_4 and Sr_2PbO_4 structure is unstable. The unit cell volume of Ba_2PbO_4 is $\sim 245 \text{ \AA}^3$. The unit cell volume of Sr_2PbO_4 is $\sim 217 \text{ \AA}^3$ which is less than the value predicted for Sr_2PbO_4 having K_2NiF_4 structure ($\sim 224 \text{ \AA}^3$ obtained from an extrapolation of the unit cell volume of the K_2NiF_4 structures of $\text{Ba}_{2-x}\text{Sr}_x\text{PbO}_4$ to $x = 2$ [16]). In the $\text{Sr}_2\text{Sn}_{1-x}\text{Pb}_x\text{O}_4$ system, the compositions with x less than 0.75 are

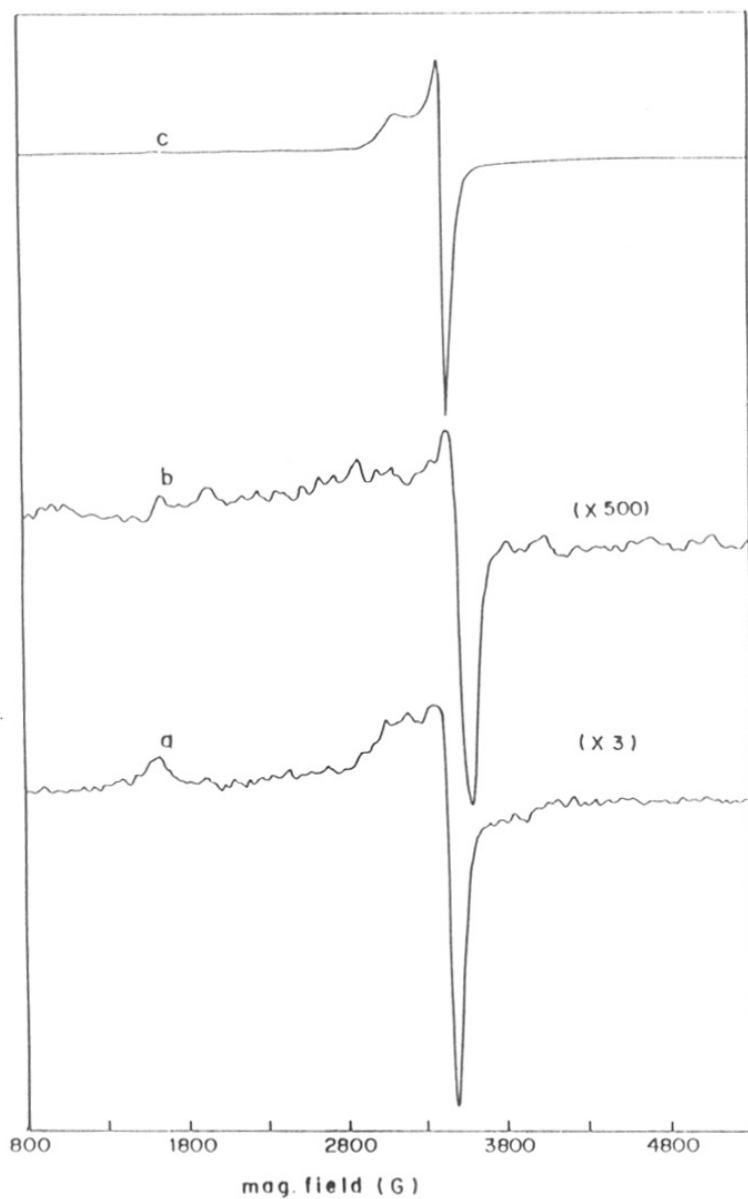


Fig. 5.16. Electron spin resonance spectra of (a) $\text{Sr}_{1.5}\text{PbZn}_{0.15}\text{Cu}_{0.06}\text{O}_{3.71}$, (b) $\text{Sr}_{1.5}\text{PbZn}_{0.15}\text{Cu}_{0.01}\text{O}_{3.71}$, (c) $\text{Sr}_2\text{Pb}_{1-x}\text{Cu}_x\text{O}_4$.

tetragonal with the compositions in the range $0.75 < x < 1.00$, being biphasic. The unit cell volume at $x = 0.75$ is $\sim 219 \text{ \AA}^3$ which is only slightly larger than that of Sr_2PbO_4 . From these considerations one may conclude that the Sr_2PbO_4 structure is an alternative structure which becomes favored because of its lower volume.

The layered perovskites and perovskite structures have been described in terms of AX_3 close-packing scheme. Other packing schemes are also possible to explain these structures. An interesting variation would be one based on close-packing of cationic or more electropositive species. For example, the fluorite (CaF_2) structure may be described by a close-packing of Ca atoms with the fluorine atoms occupying the two tetrahedral sites. The (110) plane of A_2BX_4 compounds with the K_2NiF_4 structure may be described in terms of an hexagonal packing of A ions in a honeycomb type of lattice. Although the nearest-neighbor A-A distance in these compounds is considerably larger than the expected cationic separation for the appropriate Shannon-Prewitt radii for the given co-ordination number, they are nevertheless less than the A-A distance in the corresponding elements. The Ba-Ba distance parallel to the c -axis in Ba_2PbO_4 is 3.72 \AA while the Ba-Ba distance in the Ba_2O_2 layer parallel to the ab plane is 4.22 \AA compared to the Ba-Ba distance of $\sim 4.35 \text{ \AA}$ in metallic Ba [30]. In Sr_2SnO_4 and Sr_2TiO_4 , the Sr-Sr distance along the c -axis are 3.50 and 3.53 \AA , respectively, while in the Sr_2O_2 layer parallel to the ab plane the distances are, respectively 3.96 \AA and 3.81 \AA , compared to the Sr-Sr distance of $\sim 4.30 \text{ \AA}$ in Sr metal [30]. Such short distances could form the basis for a description of the structure on the basis of a packing of A atoms alone.

In Ba_2PbO_4 , (fig. 5.17a) the hexagons of Ba atoms are stacked one on top of the other. The chains of edge-shared PbO_6 octahedra are then threaded through these hexagons. The axial O_{\parallel} (trans) oxygens are in the plane of these hexagons and the longer

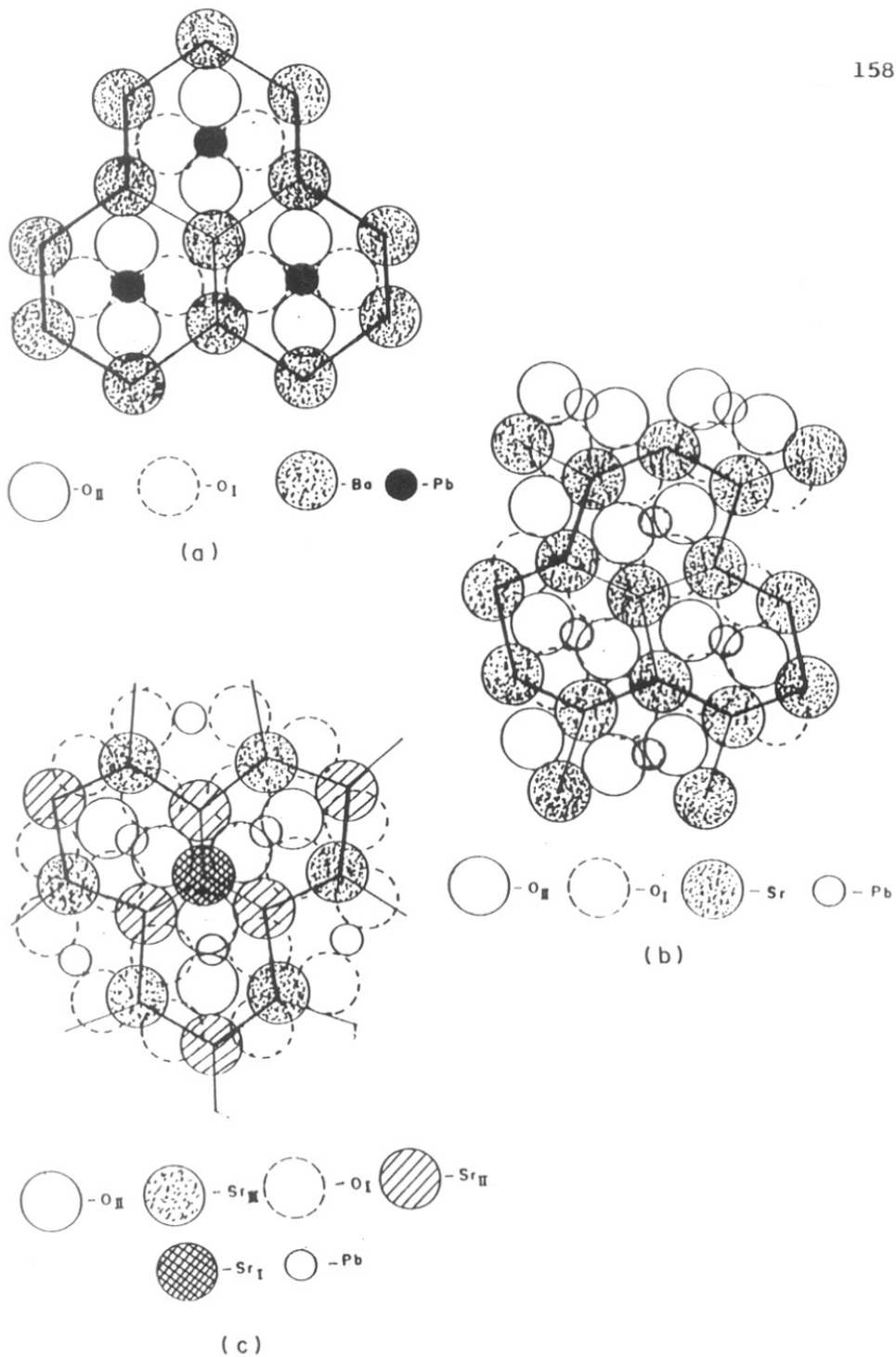


Fig. 5.17. Projection of crystal structure along (110) plane
 (a) Ba_2PbO_4 , (b) Sr_2PbO_4 , (c) $Sr_{1.5}PbM_xO_{3.5+x}$.

O_{II} -Pb- O_{II} distance is accommodated within the hexagon of Ba atoms. The threading of the chain of edge-shared PbO_6 octahedra leads to a distortion of the hexagons. In Ba_2PbO_4 the distortions of the hexagons in the honeycomb lattice of Ba atoms are in the same direction. The size of the A atoms are reduced by the substitution of large Ba ions (1.47 Å) by the small Sr ions (1.31 Å), for example, the size of the hexagons of the A atoms become too small to accommodate the O_{II} -Pb- O_{II} linkages. As a result, the hexagons of A atoms become more distorted to accommodate the chains of edge-shared PbO_6 octahedra. In addition, the positioning of the PbO_6 octahedra may be changed so that the Pb atoms are not in the same plane as the hexagons. Instead, two oxygens adjacent (cis) to each other in the PbO_6 octahedra, are in the same plane as the plane of the honeycomb hexagonal lattice of the A atoms. This is the situation in Sr_2PbO_4 (fig. 5.17b). There are two distinct directions (axes) of distortion of the hexagons in this structure. The (cis) oxygen atoms in the plane of the distorted hexagons are in close contact with each other. Because of this further contraction of the hexagons of A atoms could be resisted. A further reduction in the size of the A atoms causes displacement of an A atom (fig. 5.17c of $Sr_{1.5}PbM_xO_{3.5+x}$ having Ca_2IrO_4 structure) out of the plane of the hexagon (as to the Ca(1) position at 0,0,0 in Ca_2IrO_4) or a loss of an A atom in $Ca_{5-x}Ir_3O_{12-d}$). In this way the distortions of the hexagons take on a symmetric three-fold geometry and the packing motive is composed of these units.

One may therefore visualize the transition of Sr_2PbO_4 to the Ca_2IrO_4 structure of $Sr_{1.5}PbM_xO_{3.5+x}$, when $M = Cu, Zn$ or Cd to be due to an effective reduction in the size of the Sr atom by the substitution of the M atoms at the Sr sites. For the case when the site at 0,0,0 in the hexagonal structure, is completely vacant the ideal composition would be $Sr_{5-x}Pb_3MO_{12-x}$. When the Sr:Pb ratio is 3:2, the maximum value of x is required to be 0.5 or it is $Sr_{1.5}PbCu_{0.17}O_{3.5+x}$. In such a case the Cu atoms

substitute at the Sr (2d) or (3g) site. It is interesting to note that for a given Sr:Pb ratio of 1.5:1, a single hexagonal phase is obtained only when $x > 0.17$ in the $\text{Sr}_{1.5}\text{PbCu}_x\text{O}_{3.5+x}$ system. The single-phase hexagonal structure for the $\text{Sr}_4\text{Pb}_3\text{CuO}_6$ reported by Kim *et al* is also consistent with an ideal $(\text{Sr,Cu})_3\text{Pb}_3\text{O}_{12-d}$ composition based on a complete non-occupancy of the 0,0,0 site.

The most important feature is the observation that the orthorhombically distorted K_2NiF_4 structure is formed when the tolerance factor t is less than ~ 0.90 . The reluctance of Sr_2PbO_4 to form the orthorhombically distorted K_2NiF_4 structure requires to be understood. The main reason seems to be the reluctance of PbO_6 (or SnO_6) octahedra to be distorted, say, to the elongated configuration that is required when the tolerance factor is small. Such a preference for regular octahedral geometry could also be responsible for the segregation of Sn and Pb atoms into various layers in $\text{Sr}_2\text{Sn}_{0.45}\text{Pb}_{0.55}\text{O}_4$ [14]. The compounds of the transition metal atoms in compounds such as La_2CuO_4 , La_2NiO_4 , $(\text{La,Y})\text{CaCrO}_4$ adopt the orthorhombically distorted K_2NiF_4 structure perhaps because of the presence of unoccupied d orbitals which introduces a flexibility in the local coordination geometry.

The reluctance of closed-shell atoms such as tetravalent Pb to occupy sites with elongated octahedral geometry is perhaps important in understanding why the A_R atoms in the rock-salt layer (see Chapter 3) such as Pb^{4+} , Bi^{5+} , Tl^{3+} do not occupy the copper sites in many of the superconductors such as $\text{Bi}_2\text{Sr}_2\text{CaCu}_2\text{O}_8$ or $\text{Tl}_2\text{Ba}_2\text{CaCu}_2\text{O}_{10}$. These compounds have a tolerance factor, $t < 0.90$ just as in Sr_2PbO_4 . It would seem that the A_R atoms do not prefer an elongated octahedral geometry and instead occupies the rock-salt layers.

References

1. O. Muller and R. Roy in 'The Major Ternary Structural families', Chapter II, Springer-Verlag, Berlin-Heidelberg-New York, (1974).
2. D. Ganguli, *J. Solid State Chem.*, **30**, 353 (1979).
3. G.P. Glasser and L. S. Dent Glasser, *J. Amer. Chem. Soc.*, **46**, 377 (1963); G. Gattow, *Z. Anorg. Allg. Chem.*, **333**, 134 (1964).
4. J.B. Torrance, Y. Tokura, A. Nazzari, A. Beziere, T. Huang and S.S.P. Parkin, *Phys. Rev.*, **B61**, 1127 (1988).
5. R. Berjoan and J.P. Coutures, *J. Solid State Chem.*, **42**, 75 (1982).
6. J.D. Axe, A.H. Moudein, D. Houlouin, D.E. Cou, K.M. Mohanty and A.R. Moodenbaugh, *Phys. Rev. Lett.*, **62**, 2751 (1989).
7. J.S. Kim, X.X. Tang, A. Manthiram, J.S. Swinnea and, H. Steinfink, *J. Solid State Chem.*, **85**, 44 (1990).
8. H.M. Rietveld, *J. Appl. Cryst.*, **2**, 65 (1969).
9. R.D. Shannon, *Acta Cryst.*, **A32**, 751 (1976).
10. F. Galasso, 'Structure, Properties and preparation of perovskite-type compounds, Pergamon Press, Oxford (1969).
11. A.F. Wells, "Structural Inorganic Chemistry", Fifth Edn., Clarendon Press (1984).
12. R. Weiss, *Compton Rendus*, **106**, 248 (1959); V.M. Tromel, *Z. Anorg. Allg. Chem.*, **371**, 12 (1959).
13. M. Tromel, *Naturewissenschaften*, **52**, 492 (1965).
14. R. Babel, W. Rüdorff and R. Tschäpp, *Z. Anorg. Allg. Chem.* **347**, 282 (1966).
15. K. Vidyasagar, J. Gopalkrishnan and C. N. R. Rao, *J. Solid State Chem.* **58**, 29 (1985).

16. Bai-Hao Chen and B.W. Eichhorn, *J. Solid State Chem.*, **97**, 340 (1992).
17. S.Nomoria "Landolt-Bornstein" Group III/ 12a, p.425, Springer-Verlag, Berlin, (1978); J.B. Goodenough and J.M. Longo, 'Landolt-Bornstein" Group III/4a, p.126, Springer-Verlag, Berlin (1970).
18. G.N. Babu and C. Greaves, *J. Solid State Chem.*, **95**, 417 (1991).
19. D.B. Wiles, A. Shaktivel and R.A. Young, School of Physics, Georgia Institute of Technology, Atlanta, G. A. 30332 (1990).
20. F.J.J. Dijksma, J.F. Vente, E. Frikee and DJW Ijdo, *Mater. Res. Bull.*, **28**, 1145 (1993).
21. P. Ganguly and C.N.R. Rao, *J. Solid State Chem.*, **53**, 193 (1984); G. Burns, F.H. Dacol and M.W. Schafer, *Solid State Comm.*, **62**, 687 (1987).
22. P. Ganguly, C. Infante, S.A. Siddiqui and K. Sreedhar, *Z. Phys. B-Condensed matter.*, **83**, 23 (1991).
23. 'Infra-red and Raman rules for molecular and lattice vibrations -The Correlation method'- by F.G. Fateley, F.R. Dollish, N.T. Mcdevitt and F.F. Bertley, John Wiley & sons. Inc. (1972).
24. 'International tables for X-ray Crystallography', **1**, Symmetry Groups, edited by N.F.M. Henry and K. Landsale, The Kynoch Press, Birmingham, England, (1952).
25. G. Burns, F.H. Dacol, G. Kliche, W. Honig and M. W. Shafer, *Phys. Rev.*, **B37**, 3381 (1988).
26. M. Copic, D. Mihailovoic, M. Prester, K. Biljakovic, B. Orel and Brnicevic, *Solid State Commun.*, **64**, 297 (1987).
27. K. Sreedhar and P. Ganguly, *Phys. Rev.*, **B 41**, 371 (1990).
28. A.J.H. Macke and G. Blasse, *Inorg. Nucl. Chem.*, **38**, 1407 (1976).
29. K.L. Keester and W.M. White, *J. Solid State Chem.*, **2**, 68 (1970).

30. The bond distances for the homopolar elements have been obtained from : CRC Handbook of Physics and Chemistry, 61st Edn. Weast, R. C. Ed. CRC Press, Boca Raton, F156-F157 (1981).

CHAPTER 6

THE LAYERED CUPROCARBONATE, $\text{Ba}_3\text{SrCu}_2\text{O}_6\text{CO}_2$:

CHARACTERISATION AND PROPERTIES

6.1. Introduction

The recent discovery of novel layered copper superconductors containing carbonates was quickly followed by the synthesis of a great variety of oxycarbonates superconductor though their transition temperatures are relatively low (20-78 K) [1-7]. The structure of the growing family of cuprocarbonates is based on the interleaving of CuO_2 planes with chemically distinct charge reservoir layers in perovskite derived atomic arrays. The parent compound $\text{A}_2\text{CuO}_2\cdot\text{CO}_3$ ($\text{A} = \text{Ba}$ or Sr) may be regarded as being derived from the infinite layer ACuO_2 compounds [2,8,9] with an alternation of CuO_2 layers and CO_3 layers and with A ions being sandwiched in between these layers as shown in fig. 6.1. The CuO_6 octahedra are connected along the c -axis by the oxygen atoms of the triangular CO_3 groups which adopt a flag-like configuration. Alkaline-earth ions (Ba , Sr , Ca) plays essential part of these charge reservoir layers because of their affinity towards the carbonate groups.

The structure of $\text{Sr}_2\text{CuO}_2\cdot\text{CO}_3$ is tetragonal with a lattice parameter nearly equal to a_p of the perovskite unit cell and $c \approx 2a_p$. It is becoming apparent that an essential ingredient for the high-temperature superconductivity is the magnitude of the inter- CuO_2 -planar transfer integral [10]. In order that the carbonate layer acts as a charge reservoir or introduces interlayer exchange coupling, it is necessary that a soft, polarisable or multivalent ion is to be incorporated in this layer. The carbonate ions by themselves do not fit to such a description. Izumi *et al* [2] found evidence from neutron diffraction studies that nearly ten percent of the C sites in the carbonate layer are occupied by copper ions. These copper ions could then serve as the medium through which inter- CuO_2 -plane exchange or hole transport could take place.

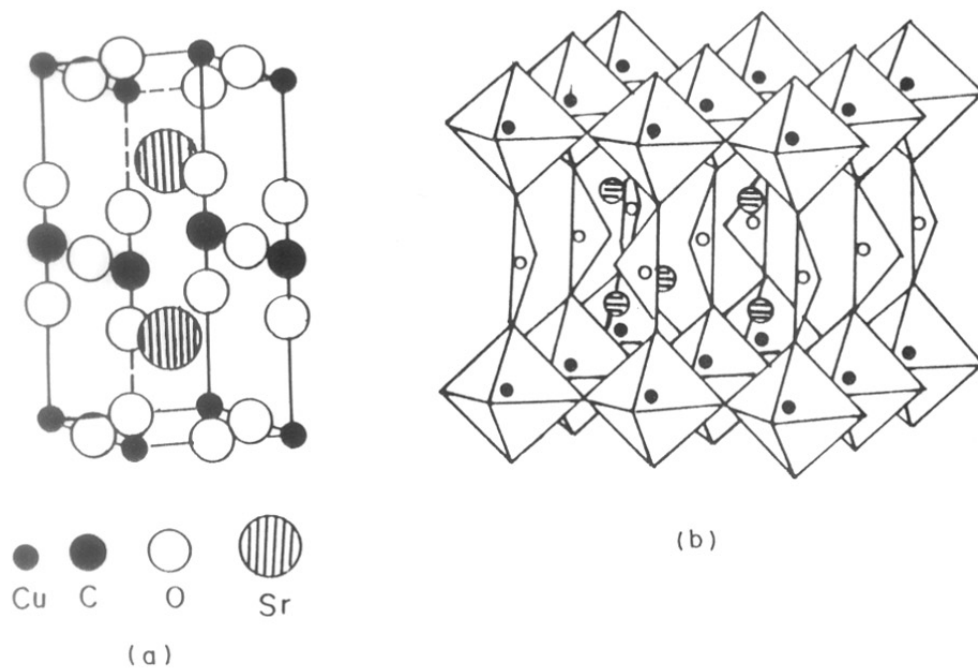


Fig. 6.1. Crystal structure of $\text{Sr}_2\text{CuO}_2\cdot\text{CO}_3$. (a) the tetragonal unit cell, (b) stacking of the layers of the CuO_6 octahedra in the c -direction.

Another important feature of these compounds is the potential of exploiting the high reactivity of the carbonate group to make new layered compounds. Matacotta *et al* [3] have given evidence to suggest that the carbonate ion may be replaced by the formate ion by reaction with formic acid. When there are Cu^{2+} ions in the carbonate layer, they are expected to be isolated and have a well defined ESR signal corresponding to its local environment. Advantage is taken of the fact that the carbonates react in a facile manner with salts of weak bases and strong acids, such as the ammonium salts. In this manner the carbonate group may be replaced by other anionic groups. Thus the environment of the copper ions can be controlled which would be reflected in the ESR signals. The systematics of the changes in the ESR signals on the substitution in the carbonate layers then gives an idea of the nature of the local distortion and hence of the orientation of the e_g orbitals of the copper ions.

In this chapter, the discussion on AX_3 close-packing (chapter 3) is extended to the carbonates by relating the packing of pure and ACO_3 carbonates to those of the ABX_3 perovskites in order to understand the crystal structure of the cuprocarbonates. The results of Electron Spin Resonance and Infra-red studies on compounds with the nominal composition $\text{Ba}_3\text{SrCu}_2\text{O}_6 \cdot 2\text{CO}_2$ are then presented.

6.2. Close-packing description of carbonates

The layered cuprocarbonates of alkaline-earth elements add a new dimension to the description of polytypism in crystal structures based on an AX_3 packing model. The AX_3 packing model has been used early by Katz and Ward [11] to describe the polytypism in the perovskite, ABX_3 , structure involving the hexagonal and cubic perovskite structures (as described in chapter 3).

The hexagonal packing has the alternating occupancy, ...abababab..., of these sites, while the cubic close-packing sequence is ...abcabcabcabc.... A mixture of such stacking sequences gives rise to the classical polytypism. This can be called *interlayer polytypism*.

A different origin for polytypism occurs in the binary intermetallic alloys of the general formula, AX_3 . Compounds such as Cu_3Au , with the face-centered cubic $L1_2$ structure are usually described by interpenetrating square-planar sublattice of A and X to give planes of AX which alternate with planes of X_2 (as shown in fig. 3.2a of chapter 3)

An alternate way of describing the structure of the AX_3 binary alloys is obtained in the AX_3 packing scheme. Such a packing may be described in terms of alternating AX and XX rows parallel to at least one of the hexagonal axis. For a given arrangement of A and X atoms in a particular row (say, AX) the arrangements in neighboring rows could be either AX or XA. There are now two limiting descriptions for such a packing. These two limiting descriptions for the AX_3 layers are,

....AX.XX.XA.XX.AX.XX.XA.XX.AX.XX.XA.XX.....(I)

or

....AX.XX.AX.XX.AX.XX.AX.XX.AX.XX.AX.XX.AX....(II)

When the AX_3 layers, described by sequence (I) are stacked in a cubic-close-packed sequence, the Cu_3Au ($L1_2$) structure is obtained while a similar stacking of the AX_3 layers described by sequence (II) gives the Ni_3Ti (DO_{22}) structure. Such a polytypism in the AX_3 compounds can be called as *intralayer polytypism*.

6.2.1. Close-packing in perovskites

The three-dimensional ABX_3 structures may be considered to be derived from the AX_3 close-packing given the close-packing intralayer sequence **(I)** which may be termed as $\langle \infty(\mathbf{I}) \rangle$ sequence. Close-packing of such layers, with the constraint that the A ions are always located on X_3 sites, yield one X_6 octahedra per A atom. Occupation of these X_6 octahedral sites by B ions yield the ABX_3 perovskite structure. The hexagonal close-packing of the $\langle \infty(\mathbf{I}) \rangle$ layers, written as $\langle \infty(\mathbf{I}), 1 \rangle$. The typical examples of the hexagonal perovskite structures are compounds such as $CsNiCl_3$, $BaNiO_3$, $BaRuO_3$, $BaMnO_3$ etc. [12]. One of the important factors for stabilizing the hexagonal perovskite structure is the relative size of the A and X atoms. In general, this is related to the tolerance factor, t , which is usually greater than unity. In hexagonal perovskite structures, the A ions such as Ba, K, Cs have small charge/radius ratio, while the B ions seems to be required to be tetravalent which may be imposed by the constraint on the charge of the A ion.

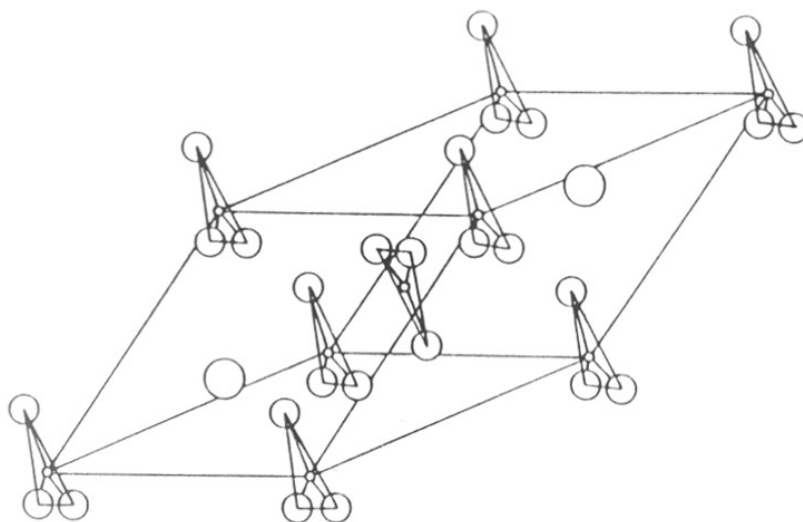
6.2.2. Carbonates: Aragonite and Calcite

The alkaline earth carbonates crystallize either in aragonite or calcite structure [12,13]. The aragonite structure (fig. 6.2) of alkaline earth carbonates ($CaCO_3$, $SrCO_3$ and $BaCO_3$) is pseudo-hexagonal. The structure can be described as hexagonal close-packing of AX_3 layers with the intralayer polytypism being that given by **(I)** so that the structure may be represented as $\langle \infty(\mathbf{I}), 1 \rangle$ (notations $\infty(\mathbf{I})$ and 1 correspond to intralayer and interlayer packing sequence respectively). This notation is similar to the hexagonal structure, in terms of the AX_3 close-packing. As in all hexagonal structures, there are rows of carbonate groups stacked in a staggered manner parallel to the AX_3

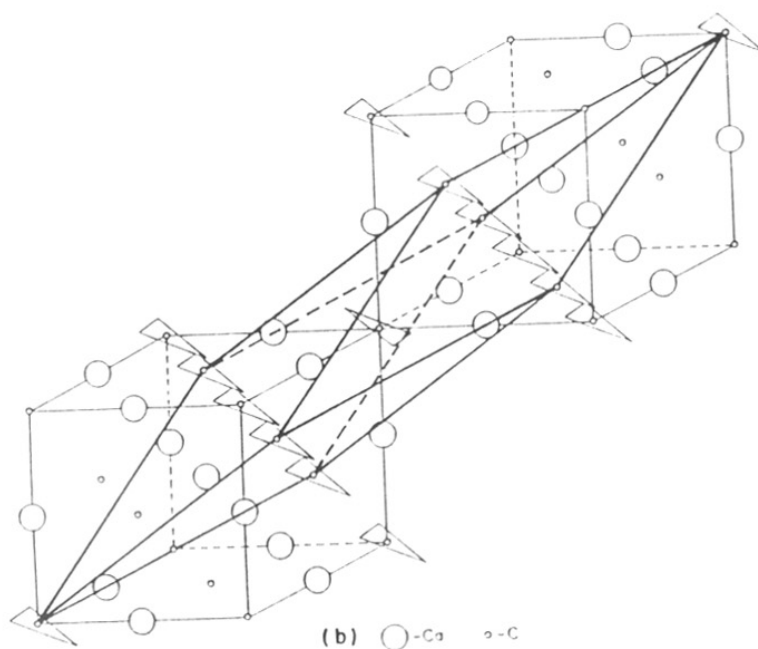
plane (the ac plane) just as there are face-shared rows of BX_6 octahedra in the hexagonal perovskites. The major difference is that the interlayer spacing in $BaCO_3$ is 3.25 \AA compared to the interlayer spacing of $2.4 - 2.6 \text{ \AA}$ in the hexagonal perovskites. The C atoms in the aragonite structure are located at the centre X_3 triangles which constitute the faces of X_6 octahedra in the AX_3 structure. These C atoms are, however, displaced from the AO_3 plane towards the position of the B sites in the hexagonal perovskite structure. Because of the strong C-O sp^2 bonding the plane of the O_3 unit is also displaced from the original AO_3 plane. The Ba sites are created by the oxygen of three different CO_3 groups above and below the plane (fig. 6.2a). Any displacement of the Ba ions by a displacement of the carbonate oxygens in a particular direction requires to be balanced by an equal and opposite displacement of an equal number of carbonate oxygens. The repulsion between C atoms at the opposite faces of the octahedra could lead to the observed increase in the interlayer spacing.

The calcite structure ($CaCO_3$) is rhombohedrally distorted hexagonal structure with two formula unit per unit cell [13,14]. The arrangements of the atoms in terms of the elongated rhombohedral unit is shown in fig. 6.3a. The carbonate ion is a planar equilateral triangle with carbon at the centre.

Alternatively, the calcite crystal structure can also be described by that of rock-salt structure. Bragg [15] pointed out that if $-(CO_3)^{2-}$ ion (groups) is treated as a rigid unit disregard of its shape, the structure of calcite formally resembles that of rock-salt ($NaCl$) structure. Rhombohedral Calcites show a very pronounced and perfect rhombohedral cleavage. The axes of the cleavage rhombohedra thus formed are those of a tetramolecular pseudo-unit which has its ions distributed as are the atoms in rock-salt structure. Fig. 6.3b. illustrates the relation between rhombohedral unit cell of $CaCO_3$ to



(a) \bigcirc -Ca, \bigcirc -O, \circ -C



(b) \bigcirc -Ca, \triangle -C

Fig. 6.3.(a) Calcite structure of CaCO_3 . The rhombohedral unit cell is shown
(b) Relation between the rock-salt and the calcite structure. The triangles correspond to O_3 unit with C at the centre.

that of NaCl cubic structure. The triangles in the figure correspond to O_3 unit with C atom at the centre (fig. 6.3). It can be seen that the carbonate triangles in the adjacent layers of the rhombohedral unit cell are oriented in opposite directions.

The AO_3 layers in the calcite structure (fig. 6.4) have the stacking sequence as described by (II). The layers are also cubic close-packed so that the notation may be used as $\langle 1, \infty(\text{II}) \rangle$. In this type of packing there are two A_2X_4 and two AX_3 octahedra per AX_3 formula unit. Only one O_3 face of the two AO_3 octahedra constitute the carbonate group in the calcite structure. There is therefore little repulsion between the carbonate groups. On the other hand, there is likely to be a repulsion between the carbonate groups and Ca ions. The repulsion is minimized by the monoclinic distortion of the calcite cell which increases the distance between the A ions and the carbon atoms. The AO_3 layers in the calcite structure corresponds to that of Ni_3Ti (DO_{22}) kind, which can also be described as $\langle 1, \infty(\text{II}) \rangle$ (intra. inter.) The layers are stacked in ccp manner. The exact location of carbonates is shown in the fig. 6.4. One may choose a stacking of the AX_3 layers such that the A ions are always located on X_3 sites.

6.2.3. Relation between close-packing of Cuprocarbonates and Perovskites

The structure of the Cuprocarbonates, $(A_2CuO_2.CO_3)$ (i.e. layered cuprate perovskites containing carbonates) can be described by the alternation of $ACuO_3$ perovskite layers with ACO_3 carbonate layers. The perovskite ABX_3 structure as well as that of the carbonates are reasonably well described by the AX_3 close-packing model. The common features are, (i) The "ferromagnetic" (hexagonal-close-packing, e.g. aragonite structure of $BaCO_3$ and hexagonal perovskite, $CsNiCl_3$) and the antiferromagnetic interlayer polytypism (cubic-close-packing descriptions of cubic

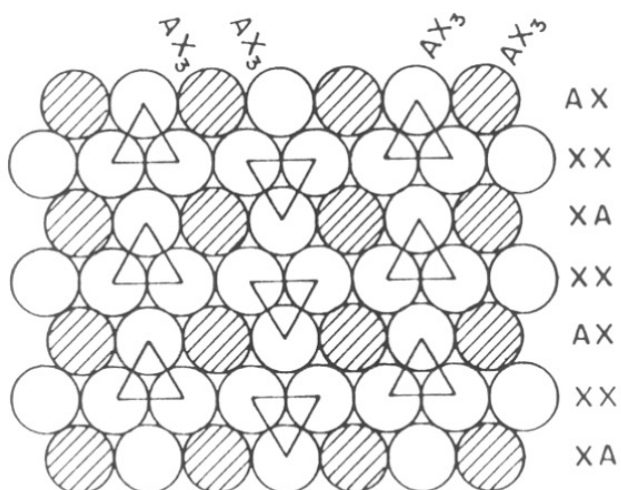


Fig. 6.4. AX_3 close-packing in the calcite structure. The triangles represent the CO_3 unit with C at the centre of the triangle.

perovskite or layered perovskites, calcite structure of CaCO_3) are valid for both the systems (as explained in chapter 3).

(ii) Larger A cations (such as Ba) favor interlayer "ferromagnetism" (hexagonal close-packing) while smaller A cations (such as Ca) favor interlayer "antiferromagnetism" (cubic-close-packing) in perovskites or formation of calcite structure. It is perhaps important to note that the 3d transition metal carbonates or CdCO_3 have the calcite structure. The cuprocarbonates would therefore favor the "antiferromagnetic" kind of stacking of the AX_3 layers.

(iii) Barium carbonate is known to transform to the Calcite structure at 850°C and to a cubic sodium chloride structure at 1050°C [12,13]. The transformation from the $\langle \infty, 1 \rangle$ structure of the hexagonal aragonite structure to the $\langle 1, \infty \rangle$ sequence of the calcite structure is most likely to involve other intermediate polytypic phases. This intermediate phase may resemble that of cubic perovskite packing $\langle \infty, \infty \rangle$. This aspect has not been studied in the literature.

(iv) As far as the AX_3 packing is concerned, the aragonite $\langle \infty, 1 \rangle$ packing to cubic-perovskite $\langle \infty, \infty \rangle$ packing transition is similar to the hexagonal to cubic perovskite transition. It involves a change in the sequence of stacking of the layers keeping the relative intralayer orientation of the AX rows the same ("ferromagnetic"). The aragonite $\langle \infty, 1 \rangle$ to calcite $\langle 1, \infty \rangle$ transition involves not only changes in the interlayer stacking but also the relative orientation of the intralayer AX_3 rows. In the $\langle \infty, \infty \rangle$ structure for the ACO_3 carbonates, the sequence is, $\dots\text{CO}_3\text{-A-CO}_3\text{-CO}_3\text{-A-CO}_3\text{-CO}_3\dots$. The C-C repulsion between the carbon atoms in the carbonate groups as well as the Ba-C repulsion becomes important. This could render

the $\langle \infty, \infty \rangle$ structure unstable relative to, say, the $\langle 1, \infty \rangle$ calcite structure. It is for this reason perhaps that there is a first-order aragonite to calcite transition in BaCO_3 .

(v) When there are B ions such as Cu to occupy the octahedral sites, it can be imagined that there is a perovskite forming (hexagonal or cubic) field. It is now conceivable that in the cuprocarbonates the perovskite structure is an intermediate or an alternate path in the transformation sequence of the aragonite structure. The stacking sequence along the body diagonal of the cubic ABX_3 perovskite, $\langle \infty, \infty \rangle$ structure involves, $\dots X_{3(\text{oct})} - X_{3(\text{oct})} - \text{A} - X_{3(\text{oct})} - X_{3(\text{oct})} - \text{A} - \dots$ where $X_{3(\text{oct})}$ corresponds to the X_3 faces of the X_6 octahedra obtained in the cubic close-packing of the AX_3 layers. The repulsive C-C or A- CO_3 interaction is not present in this case. In the above argument, the perovskite structure may be stabilized by the occupation of X_6 octahedral sites by B cations. The interlayer $\langle \infty \rangle$ stacking of the intralayer $\langle 1 \rangle \text{AX}_3$ layers in the alternating layer cuprocarbonates such as $\text{Sr}_2\text{CuO}_2 \cdot \text{CO}_3$ would lead to the sequence $\dots X_{3(\text{oct})} - \text{B} - X_{3(\text{oct})} - \text{A} - \text{CO}_{3(\text{oct})} - \text{A} - X_{3(\text{oct})} - \dots$ etc. in the ideal case. There is no C-C repulsion in the structure and is therefore more stable relative to the calcite $\langle 1, \infty \rangle$ structure. Incorporation of B cations such as copper in some of the X_6 octahedra, may therefore stabilize the perovskite structure relative to the calcite structure. There will therefore be a tendency to order alternately Cu and C at the B sites in the $\langle 111 \rangle$ direction of the primitive perovskite cell. This is the case in the layered cuprocarbonates and also the case in the Cd or Ca substituted cuprocarbonates.

(vi) In such a description one should have ideally a CO_6 unit, with the ACO_3 plane being parallel to the (111) plane of the ideal cubic perovskite cell. The location of the C atom at the B sites seems to be preferred, and as mentioned earlier, it is the electronic constraints of an sp^2 hybridization on the carbon that shifts the O_3 unit to a (111) plane

containing the B ion. In $\langle \infty \rangle$ stacking of the AX rows in an AX₃ layer one could then expect the "interlayer" carbonate plane to be parallel to an (111) plane. It is likely to be displaced from the ideal AX₃ plane, especially when the AX₃ composition is fixed as in the alkaline-earth carbonates. However, in the presence of oxygen deficiency, oxygen atoms from different planes are required to be involved in the formation of the carbonate group. Such an "interlayer" carbonate could then have the "flag"-like configuration reported for the cuprocarbonates. It is interesting to note, however, that in the (Ba,Sr)₂MCuO₂.(CO₃) (M = Li, Na etc.) the carbonate groups have an orientation parallel to the (111) plane of the pseudocubic perovskite cell (as shown in fig. 7.1 of Chapter 7).

(vii) As mentioned earlier, the C-C repulsion in the aragonite structure, is a likely mechanism for the considerably expanded volume of BaCO₃ which is more than 25% larger than hexagonal perovskites such as BaMnO₃ or BaNiO₃ nearly. On the other hand the unit cell volume of CaCO₃ and the perovskite CaTiO₃ are nearly equal to each other. The calcite structure of CaCO₃ is transformed to the aragonite structure with an increase in volume. As discussed earlier in relation to the hexagonal to cubic perovskite transition, for a given B ion, a decrease in the size of the A ion favors the $\langle \infty \rangle$ interlayer packing. On the other hand, for a given A ion, an increase in the size of the B ion in the perovskites, favors the cubic perovskite structure. It is as if a large B atom exerts an internal pressure on the close-packed AX₃ layers which is equivalent to reducing the size of the A atom. The occupation of the B sites by large cations such as Ca or Cd would stabilize the perovskite structure. This is what has been observed by Calestani *et al* [16].

From the above discussions it can be concluded that; (i) the perovskite are intermediate in the transformation of the aragonite structure to the calcite structure in the cuprocarbonates; (ii) from a consideration of the C-C repulsion in carbonate groups as well as the A-C repulsion between A ions and the C atoms in the CO_3 group, it may be concluded that there is a minimum requirement of alternating C and Cu at the B sites in the (111) diagonal of the primitive perovskite cell. This is the sequence most often observed; (iii) The possibility of an intralayer polytypism of the type $\langle 2, 1 \rangle$ may account for the particular ordering of Ca and Cd. From radius ratio considerations, one can try to show why the Cd containing compounds favor more carbonate in the AX_3 layers while the Ca containing compounds could be less "carbonated"; (iv) the description of the cuprocarbonates in terms of the polytypism found in intermetallic alloys, for example, accounts for the sensitivity of the structure that are obtained to the conditions of preparation. In the case of the carbonates, the important ambient conditions could include the partial pressure of oxygen or carbondioxide.

6.3. Experimental

Appropriate molar ratios of BaCO_3 or BaO_2 , SrCO_3 and CuO were mixed for the nominal composition $\text{Ba}_3\text{SrCu}_2\text{O}_6 \cdot 2\text{CO}_2$ and calcined first at 820°C and then at 860°C in air with intermediate grindings. Finally the samples were pelletized and annealed at $890\text{-}910^\circ\text{C}$ in air for 48 hrs.

Solid state reactions of the oxycarbonates have been carried out with ammonium salts, $(\text{NH}_4)_n\text{X}^n$, of various acids ($\text{X} = \text{F}, (\text{NO}_3)^-, (\text{VO}_3)^-, (\text{HPO}_4)^{2-}, (\text{S}_2\text{O}_8)^-, \text{Cl}^-$) which incorporates X^n anions in the structure with the liberation of ammonia. This has been done by simple grinding of the cuprocarbonate with ammonium salts in a pestle and

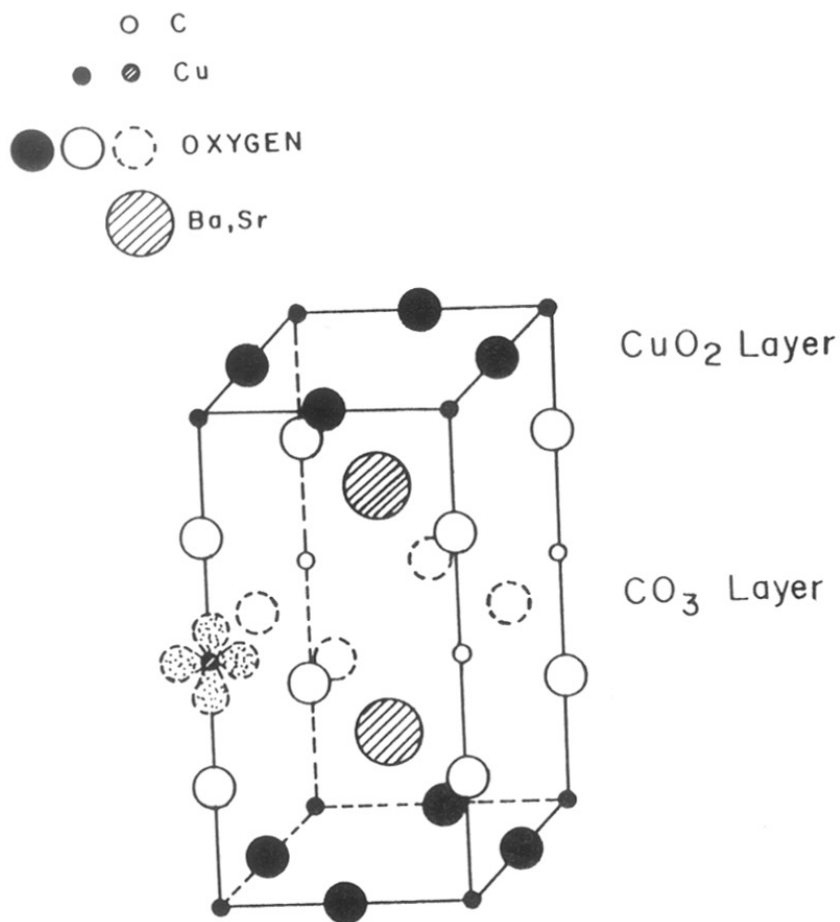


Fig. 6.5. Crystal structure of $\text{Ba}_3\text{SrCu}_2\text{O}_6 \cdot 2\text{CO}_2$. The CuO_2 and the carbonate layers are shown. The dashed circle corresponds to oxygen sites which are fifty percent occupied. The orientation of the half filled e_g orbital of the copper ions in the carbonate layer is shown.

mortar for a prolonged period (1 hour) at room temperature and if necessary keeping the ground mixture at 100 °C for a few hours. An 1:2 starting mixture of $\text{Ba}_3\text{SrCu}_2\text{O}_6 \cdot 2\text{CO}_2$: ammonium salt was taken for monovalent anions such as $\text{X} = [\text{VO}_3]$, $[\text{NO}_3]$, Cl and F; while the 1:1 molar mixture was taken for the divalent anions such as $\text{X} = \text{H}(\text{PO}_4)^{2-}$ and $(\text{S}_2\text{O}_8)^{2-}$. The extent of the reaction has been followed by noting the difference in weight before and after the grinding. Considerable reactivity have been found in this case with retention of the basic structure. Purity of all the samples were checked by powder X-ray diffraction. The polycrystalline reaction products are further examined by electron spin resonance and IR studies.

6.4. Results and discussion

6.4.1. X-ray diffraction studies

The layered copper oxycarbonates can be easily prepared in air for annealing temperatures $T < 910^\circ\text{C}$ [3], as a single phase. When BaCO_3 is used as starting material the compound seems to form as long as BaCO_3 is slowly decomposed, where as by using BaO_2 the same compound forms fast by taking CO_2 from the air. The final product has a composition corresponding closely to $\text{Ba}_3\text{SrCu}_2\text{O}_6 \cdot 2\text{CO}_2$ with an idealized structure similar to that shown in fig. 6.5. The powder XRD pattern of this compound is shown in fig. 6.6a which could be indexed on the tetragonal unit cell. The refined lattice parameters are given in table 6.1. The lattice parameters are comparable to those reported by Izumi *et al* [2]. However, it may be noted that the dimensions of the a parameter is comparable, but c parameter is significantly smaller in the present case. Maticotta *et al* [3] have reported that the orthorhombic 213 phase [5] (containing Cu-O-Cu chains) in the Ba-Sr-Cu-O system become tetragonal when the Ba:Sr ratio is close to

Table. 6.1. Weight loss on grinding and the lattice parameters of the reaction products of $\text{Ba}_3\text{SrCu}_2\text{O}_6 \cdot 2\text{CO}_2$ and $(\text{NH}_4)_n\text{X}^n$.

X^n	% weight loss# (obsd).	lattice parameters ($\pm 0.005 \text{ \AA}$)	
		a	c
-		3.997*	7.908
$(\text{VO}_3)^-$	7	4.006	7.914
$(\text{S}_2\text{O}_8)^{2-}$	9	3.974	7.954
Cl^-	1	3.984	7.934
$\text{H}(\text{PO}_4)^{2-}$	5	4.003	7.978
$(\text{NO}_3)^-$	4	3.991	7.937
F^-	10	4.005	7.911

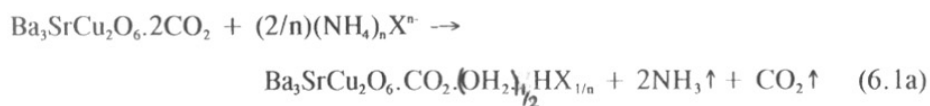
* The lattice parameters were orthorhombic with $a = 4.004 \text{ \AA}$ and $b = 3.990 \text{ \AA}$.

The percent weight loss as expected from Eqn. (6.1) is given.

3. At this Ba:Sr ratio the system becomes nearly tetragonal with the basal a parameter being nearly equal to 4.00 Å. This seems to be the reason for the facile formation of the layered copper oxycarbonates with CuO_2 planes, at the composition used in the present investigation.

These structures are important, from the viewpoint of chemical reactivity. The alkali or alkaline earth-metal carbonates are known to react readily with ammonium salts of several strong acids to liberate carbon-dioxide and ammonia to form the corresponding metal salts. The question that can be asked is whether the layered carbonates are equally reactive in a topotactical sense so that there is only a two-dimensional reaction involving only the carbonate layer with the positions of the A or CuO_2 layer being relatively unchanged. This is an important aspect. When there is such a two-dimensional reaction, there is a new design route for crystal engineering in which the carbonate layer may be replaced by another anionic layer such as nitrate, sulphate, chlorate, phosphate etc.

The parent phase has been reacted with various ammonium salts, $(\text{NH}_4)_n\text{X}^n$. The reaction is expected to proceed as follows :



The reaction mixture of $\text{Ba}_3\text{SrCu}_2\text{O}_6 \cdot 2\text{CO}_2$ and $(\text{NH}_4)_n\text{X}^n$ were taken in the ratio of 1:(2/n). The extent of the reaction as calculated from the weight loss is given in table 6.1.

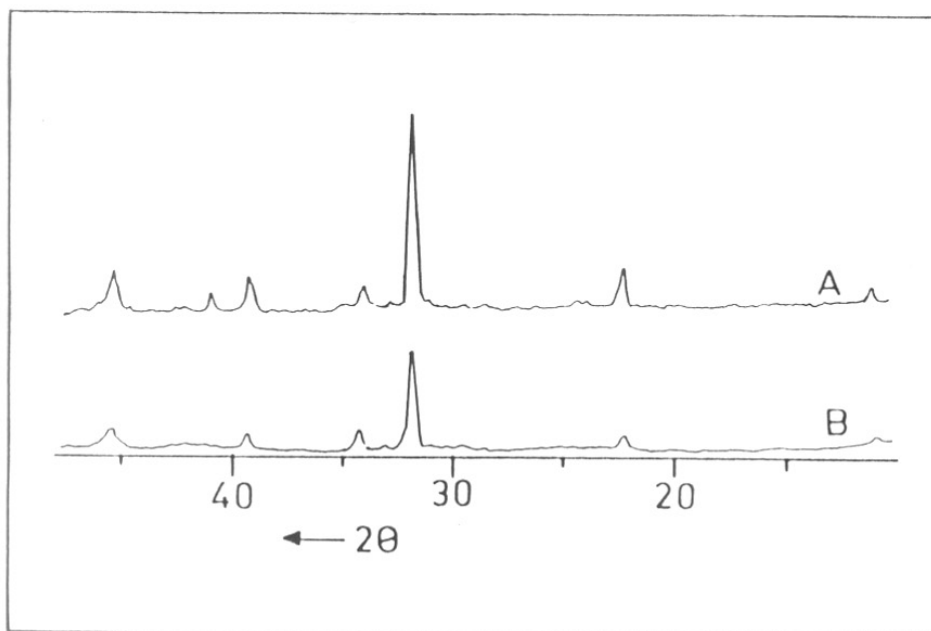


Fig. 6.6. X-ray diffraction pattern of (A) $\text{Ba}_3\text{SrCu}_2\text{O}_{6.2}\text{O}_2$ and (B) its reaction product after grinding with ammonium fluoride.

The reactivity of the cuprocarbonates to $(\text{NH}_4)_n\text{X}^{n-}$ depends on the nature of the X anion as well as the A atom. The reactions were carried out by grinding with the desired $(\text{NH}_4)_n\text{X}^{n-}$ compounds, taken in a ratio such that only half of the carbonate groups can take part in the reaction. The progress of the reaction was monitored periodically by weighing the mixture. There was little weight change after about fifteen minutes of grinding. The grinding process was continued for about one hour.

More than 90% reaction was observed for $\text{X} = \text{F}^- (\text{VO}_3)^-$ and $(\text{S}_2\text{O}_8)^{2-}$. When $\text{X} = (\text{NO}_3)^-$ there is clear evidence for a phase separation with the XRD pattern showing clear evidence for the formation of $\text{Ba}(\text{NO}_3)_2$, whereas with $\text{X} = \text{Cl}^-$ there is very little reaction. Typical XRD pattern of the reaction mixture after grinding with ammonium fluoride and that of the starting $\text{Ba}_3\text{SrCu}_2\text{O}_6 \cdot 2\text{CO}_2$ is shown in fig. 6.6b. Although there is a slight deterioration in the quality of the X-ray pattern of the cuprocarbonate phase with some peaks becoming broad, there is little evidence for the presence of other unreacted phases for other X^{n-} anions. The calculated X-ray diffraction pattern in which three of the oxygen positions of the carbonate group is replaced at random by an OH⁻ and F⁻ group is close to that of the pure $\text{Ba}_3\text{SrCu}_2\text{O}_6 \cdot 2\text{CO}_2$ phase. The changes in the lattice parameters of the $\text{Ba}_3\text{SrCu}_2\text{O}_6 \cdot \text{CO}_2 \cdot (\text{X})^{n-}$ phases are given in table 6.1.

6.4.2. Infra-red spectra

The changes in the infra-red spectra of $\text{Ba}_3\text{SrCu}_2\text{O}_6 \cdot 2\text{CO}_2$ before and after grinding with 1:2 molar mixture of $\text{Ba}_3\text{SrCu}_2\text{O}_6 \cdot 2\text{CO}_2 : \text{NH}_4\text{F}$ are shown in fig. 6.7. IR spectra shows the bands which are characteristic of $(\text{CO}_3)^{2-}$ groups in the higher frequency region (702 cm^{-1} , 850 cm^{-1} and at 1450 cm^{-1}) and three bands at 335 cm^{-1} , 380 cm^{-1} and 476 cm^{-1} in the low frequency region which are due to internal vibrations of Cu-O bond [17].

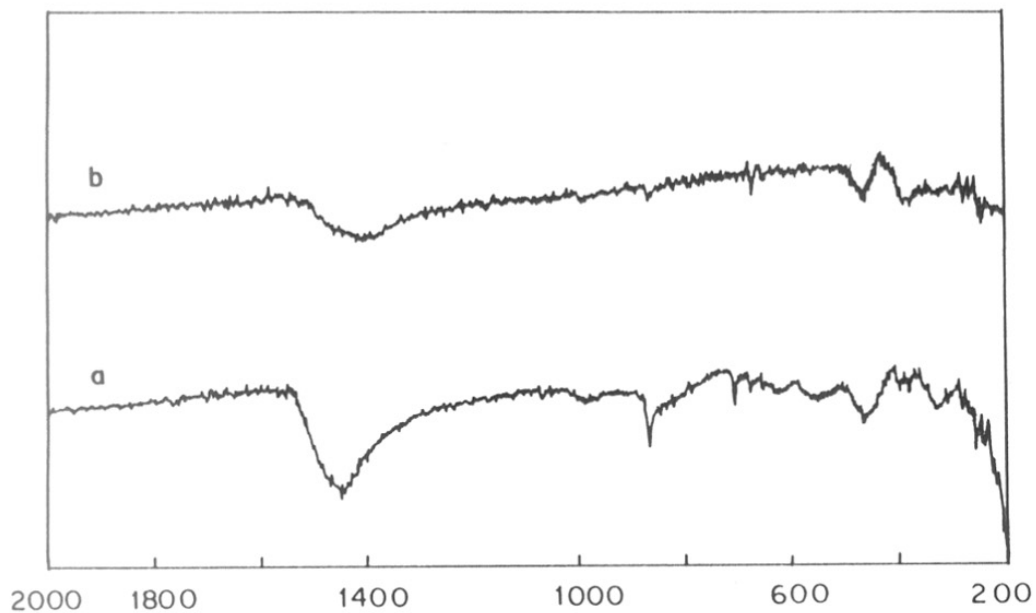


Fig. 6.7. IR spectra of $\text{Ba}_3\text{SrCu}_2\text{O}_6 \cdot 2\text{CO}_2$ (a) before and (b) after grinding with NH_4F .

BaCO₃ and SrCO₃ show characteristic IR bands due to internal vibrations of the (CO₃)²⁻ at around 700, 860, 1068, and 1460 cm⁻¹ [18]. The cuprocarbonate IR bands in the region 690-2000 cm⁻¹ are at slightly shifted position compared to that of pure Ba and Sr carbonates. There is a large diminution in the relative intensities of the bands associated with carbonate ions after the reaction with ammonium salt (fig 6.7b). The positions of the bands associated with Cu-O vibrations are also changed after reaction, with no features characteristic of the sample before reaction. The formation of the layered oxycarbonates may thus be regarded as an intercalation of CO₂ molecules between (Ba,Sr)₂CuO₃ layers. This last feature strongly suggests that there is a genuine 2D reaction of the carbonate layers with the rest of the structure being intact.

When there is an anion vacancy, as in the cuprocarbonates, there could also be a motion of anionic species such as VO₃⁻ or NO₃⁻ ions. The mobility of divalent anionic species, such as SO₄²⁻ or HPO₄²⁻, is expected to be less than that of the monovalent ions because of the stronger Coulomb interaction of such ions with the lattice. The low mobility of such species could account for the lower reaction rate. The blocking of some reaction channels (due to, say, the formation of sulphates or persulphates) may be responsible for the lower yield with the corresponding ammonium salts. The present study therefore shows that there are several novel features involved in understanding the chemical reactivity of the layered cuprocarbonates. Further detailed investigations are required for a clear understanding of their features.

6.4.3. Electron spin resonance studies

The room temperature ESR spectra of Ba₃SrCu₂O₆.2CO₂ and its reaction products are shown in fig. 6.8. There is a marked change in the nature of the ESR signal after

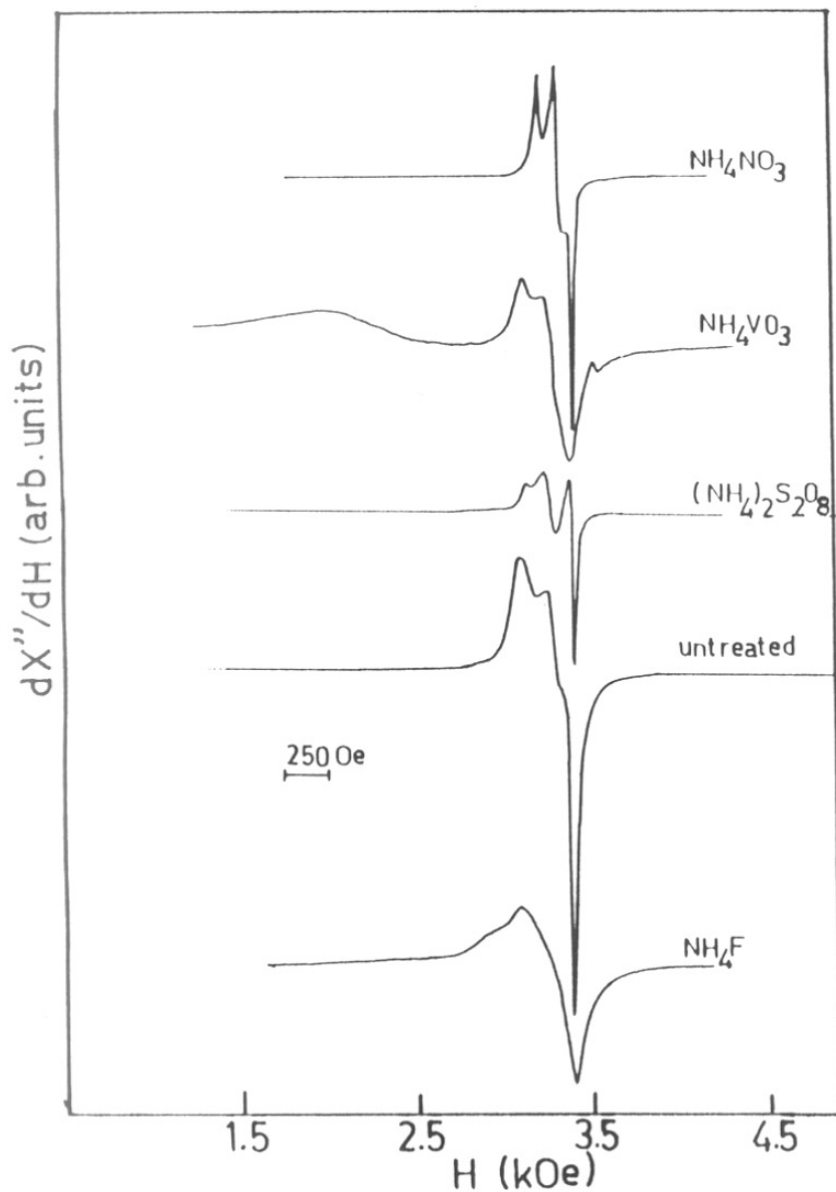


Fig. 6.8. Electron spin resonance spectra of $Ba_3SrCu_2O_{6.2}CO_2$ and its reaction products after grinding with various ammonium salts as indicated.

Table. 6.2. g values of ESR lines of $\text{Ba}_3\text{SrCu}_2\text{O}_6 \cdot 2\text{CO}_2$ and the reaction products with $(\text{NH}_4)_n\text{X}^n$.

X^n	g values		
	g_3	g_2	g_1
-	2.24	2.10	2.045
$[\text{NO}_3]^-$	2.18	2.09	2.046
$[\text{S}_2\text{O}_8]^{2-}$	2.22	2.09	2.050
$[\text{VO}_3]^-$	2.23	2.12	2.054
F^-	2.31	2.13	2.053

reaction with the ammonium salts. The spectra in all cases are characteristic of Cu^{+2} in orthorhombic symmetry. The observed g values are given in table 6.2. The parent compound is closest to tetragonal symmetry. The average g values in these compounds are close to 2.1 which is the typical value found in copper oxides [19]. In more ionic complexes, the average g value is ≥ 2.2 . Only in the case of $\text{X}^{\ominus} = \text{F}^{-}$ is there a marked increase in the g_z value which is again consistent with the more ionic nature of the Cu-O linkage. The observed changes thus cannot be attributed to a simple reaction of the parent layered cuprocarbonate to give different impurity phases of the copper salts. The facile reaction seen in this study opens up an entirely new aspect of solid state reactivity of low-dimensional systems in which one layer is reacted while the other is left intact.

In most cases the spectra are completely changed with little or no contribution from the original unreacted compound. Since the reaction is not complete, (eqn.(6.1)), this would indicate that the regions which react most strongly with the ammonium salts are those that are associated with the copper ions responsible for the ESR signal. The ESR lines are unlikely to be associated with impurity phases [20] such as unreacted CuO or BaCuO_2 . The antiferromagnetically coupled copper ions in the CuO_2 planes are not likely to give rise to an ESR signal as experiments with model systems [17] have shown. The g values of the ESR lines as well as the line shape are somewhat similar to the weak signal obtained [20,21] with the 213 phases such as Sr_2CuO_3 . Signals observed in the present case are too strong to be attributed to such phases.

The changes in the ESR spectra attest to the presence of some copper ions in the carbonate layers as first proposed by Izumi *et al* [2]. The intensity of the ESR peaks has been compared with that from $\text{CuSO}_4 \cdot 5\text{H}_2\text{O}$. In all cases the ESR intensity corresponds to a contribution from about 6 to 10 percent of all the copper ions present. The changes

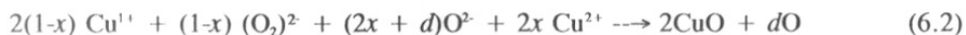
in the g values of the lines reflect the changes in the environment of these copper ions when the carbonate anionic group is replaced by the new anionic group X^n . The most considerable changes are found in the value of g_3 . The local coordination axis of the copper-oxygen pseudo-octahedron is taken as the axis parallel to the g_3 axis which is in the a - b plane or carbonate layer. The basal square-planar CuO_4 unit of the elongated pseudo-octahedron of the isolated copper ion in the carbonate plane is thus oriented [22,23] perpendicular to this layer (to the a - b -plane). The filled e_g orbitals (d_z^2 orbitals) of the Cu^{2+} ion are therefore oriented parallel to the plane. The plane of the half-filled e_g orbitals of the Cu^{2+} ions transforming as $d_{x^2-y^2}$ is therefore oriented perpendicular to the a - b plane. In this case the CuO_2 layers would be coupled through the half-filled orbitals of the isolated Cu^{2+} ions incorporated in the carbonate layer. This provides the mechanism for the interlayer coupling which is now expected to be magnetic in origin [10].

6.5. Conclusions

The presence of some Cu^{2+} ions in the carbonate layer would require the presence of extra copper ions as proposed by Izumi *et al* [2]. On the other hand the pseudo-cubic nature of the structure for the composition $\text{Ba}_3\text{SrCu}_2\text{O}_6 \cdot 2\text{CO}_2$ suggests that its origin is a cubic perovskite. In this case there is likely to be a scrambling between the copper and carbon atoms. Some carbonate groups may thus also be incorporated in the CuO_2 layer. These carbonate groups may be less reactive. Such a scrambling would also explain the infra-red spectra of Matacotta *et al* [3] which show the persistence of the carbonate group even after the reaction is complete. Preliminary infra-red data also supports this conclusion.

The compounds prepared in the present investigation are not superconducting, having a resistivity nearly two orders of magnitude higher at room temperature compared to other superconducting compounds. The magnitude of the resistivity at the onset of superconductivity is not only a good indicator of the quality of the specimen but also gives an indication of whether the T_c may be increased or not. It has been pointed out [10] that, in single phase layered cuprate oxides, superconductivity appears when the resistivity of polycrystalline samples is less than 10-20 m Ω .cm while T_c in a given family is a maximum when the onset resistivity in polycrystalline samples is close to 500 $\mu\Omega$. cm. The sample measured by Kinoshita and Yamada [8] has a resistivity less than 15 m Ω .cm at room temperature and a resistivity of \sim 8 m Ω .cm at the onset T_c . The high value of the resistivity in the present case would indicate that there could be some CuO₂ layers which have carbonate ions incorporated in them. In the present composition, the nearly cubic nature of the unit cell leads to an increased scrambling which besides increasing the unit cell c parameters (which reduces the interlayer coupling), also reduces the conductivity in the plane so as to destroy superconductivity. The possibility of incorporating novel Xⁿ⁻ anions by reaction now highlights the exciting possibility of introducing a reducing or electron donating charge reservoir in the layers proximate to the CuO₂ layers. This would serve the dual purpose of increasing the interlayer coupling and increasing the conductivity.

Another point is that the basal lattice parameters are too large for hole superconductors [8]. Instead n-type conductivity as in the electron-doped Nd_{2-x}Ce_xCuO_{4-d} compounds, is expected. The presence of excess oxygen is not necessary to be identified with hole conduction since there may be an equilibrium of the kind.



The mixed valence of the copper ions may now yield n-type conductivity. Thermopower measurements on these samples [24] of $\text{Ba}_3\text{SrCu}_2\text{O}_{6+d}\cdot 2\text{CO}_2$ show a negative sign for the Seebeck coefficient at room temperature which supports the above conclusion.

References

1. A.R. Armstrong and P.P. Edwards, *J. Solid State Chem.*, **98**, 432 (1992); Y. Miyazaki, H. Yamane, T. Kajitani, T. Oku, K. Hiraga, Y. Morii, K. Fuchizaki, S. Funahashi and T. Hirai, *Physica C* **191**, 434 (1992).
2. F. Izumi, K. Kinoshita, Y. Matsui, K. Yanagisawa, T. Ishigaki, T. Kamiyama, T. Yamada and H. Asano, *Physica C* **196**, 227 (1992).
3. F.C. Maticcotta, D. Pal, T. Mertelj, P. Stastny, P. Nozar, D. Mateev and P. Ganguly, *Solid State Commun.*, **84**, 781 (1992).
4. M. Huvé, C. Michel, A. Maignan, H. Hervieu, C. Martin and B. Raveau, *Physica C* **205**, 219 (1993).
5. M. Vehara, S. Sahoda, H. Nakata, J. Akimatsu and Y. Matsui, *Physica C* **222**, 27 (1994).
6. T. Kawashiura, Y. Matsui, E. Takamaya-Muromachi, *Physica C* **224**, 69 (1994).
7. A. Maignan, D. Pelloguin, S. Malo, C. Michel and B. Raveau, *Physica C* **249**, 220 (1995).
8. K. Kinoshita and T. Yamada, *Nature* **357**, 313 (1992).
9. T. Siegrist, S.M. Zahurak, D.W. Murphy and R.S. Roth, *Nature* **334**, 231 (1988).
10. P.W. Anderson, in 'High-Temperature superconductivity', chapter 3 (1992); J.M. Wheatley, T.C. Hsu and P.W. Anderson, *Phys. Rev.*, **B37**, 5897 (1988).
11. L. Katz and R. Ward, *Inorg. Chem.*, **3**, 205 (1964).

12. A. F. Wells, 'Structural Inorganic Chemistry', 5th edition, Clarendon Press, Oxford, (1984).
13. H.D. Megaw, 'Crystal Structures: A Working Approach', Chapter 11, W.B. Saunders Company, Philadelphia, London (1973).
14. R.W.G. Wyckoff, 'Crystal Structures', Chapter VII, Interscience Publishers, New York, London (1948).
15. W.L. Bragg, Proc. Roy. Soc. London, **89**, 248 (1914).
16. G. Calestani, P. Ganguly, F.C. Maticcotta, P. Nozar, A. Migliori, K.A. Thomas and A. Tomasi, Physica C **247**, 359 (1995).
17. P. Ganguly, C. Inafante, S. A. Siddiqui and K. Sreedhar, Z. Phys. B: Condensed Matter, **83**, 23 (1991).
18. T. Mertlj, F.C. Maticcotta, D. Pal, S. Stasny, P. Nozar, Q. Jiang, D. Mihailovic and P. Ganguly, Solid State Chem., **84**, 1115 (1992).
19. P. Ganguly, K. Sreedhar, A.R. Raju, G. Demazeau and P. Hagemuller, J. Phys. Condens. Matt. **1**, 213, 1989.
20. A.R. Armstrong, R. Janes, K.K. Singh and P.P. Edwards, Bull. Mater. Sci., **14**, 641 (1991).
21. A. Abraham and B. Bleaney, 'Electron Paramagnetic Resonance of Transition Ions', Clarendon Press, Oxford, p.455 (1970).
22. B.W. Moores and R.L. Belford, 'Electron Spin Resonance of Metal Complexes', p.13 (1969); D. Reinen and C. Friebel, 'Structure and Bonding' **1**, 37 (1979).
23. P. Ganguly and K.R. Nair, Physica C **191**, 171 (1992) and references therein.
24. F.C. Maticcotta, unpublished results.

CHAPTER 7

SYNTHESIS AND CHARACTERISATION OF NEW CUPROCARBONATES
CONTAINING Li AND TRANSITION METAL IONS

7.1. Introduction

In the recently discovered layered oxycarbonates, $\text{Sr}_4\text{LiCuO}_4(\text{CO}_3)_2$, and $\text{Ba}_4\text{LiCuO}_4(\text{CO}_3)_2$, the Li^{+1} in LiO_6 octahedra and Cu^{+2} ions in CuO_4 square-planar units alternate in the $\text{Li}_{0.5}\text{Cu}_{0.5}\text{O}_2$ plane [1]. The unit cell is tetragonal with $I4/mmm$ symmetry. The $(\text{Li,Cu})\text{O}_2$ layer in this compound is reminiscent of that in $\text{La}_4\text{LiCuO}_8$ with the tetragonal K_2NiF_4 ($I4/mmm$) structure in which Li^{+1} and Cu^{+2} ions in octahedral coordination are ordered in the $\text{Li}_{0.5}\text{Cu}_{0.5}\text{O}_2$ plane [2,3] (fig. 7.1). Other compounds like $\text{La}_4\text{LiNiO}_8$ and $\text{La}_4\text{NiCoO}_8$ are also known to have this ordered structure. It was therefore considered worthwhile investigating whether the corresponding $\text{Sr}_2\text{Li}_{0.5}\text{M}_{0.5}\text{O}_2\cdot\text{CO}_3$ compounds with $\text{M} = \text{Ni}$ and Co could also be prepared. In this chapter, physico-chemical properties of $(\text{BaSr})_2\text{Li}_{0.5}\text{M}_{0.5}\text{O}_2\cdot\text{CO}_3$ ($\text{M} = \text{Cu, Ni, Co, Fe}$) compounds are presented. These compounds are characterised by several techniques including XRD, magnetic susceptibility, electron spin resonance, Infra-red and Solid State ^7Li NMR techniques.

7.2. Experimental

The compounds with nominal composition $\text{A}_2\text{Li}_{0.5}\text{M}_{0.5}\text{O}_2\cdot(\text{CO}_3)$ ($\text{A} = \text{Sr, Ba}$; $\text{M} = \text{Cu, Ni, Co, Fe}$) for a pure and mixed range of alkaline-earth stoichiometry were synthesised using SrCO_3 , BaCO_3 , $\text{Sr}(\text{NO}_3)_2$, Li_2CO_3 and oxides (or nitrates) of Cu , Ni , Co and Fe as starting materials. Samples were fired at $800\text{-}850^\circ\text{C}$ with reaction time governed by the sample volume. Phase purity were checked by XRD.

Materials of the type $\text{Sr}_{2-x}\text{Ba}_x\text{Li}_{0.5}\text{Cu}_{0.5}\text{O}_2\cdot\text{CO}_3$ in the range $0 \leq x \leq 2$, were prepared varying x independently by balancing the components with $\text{Sr}(\text{NO}_3)_2$ partially in

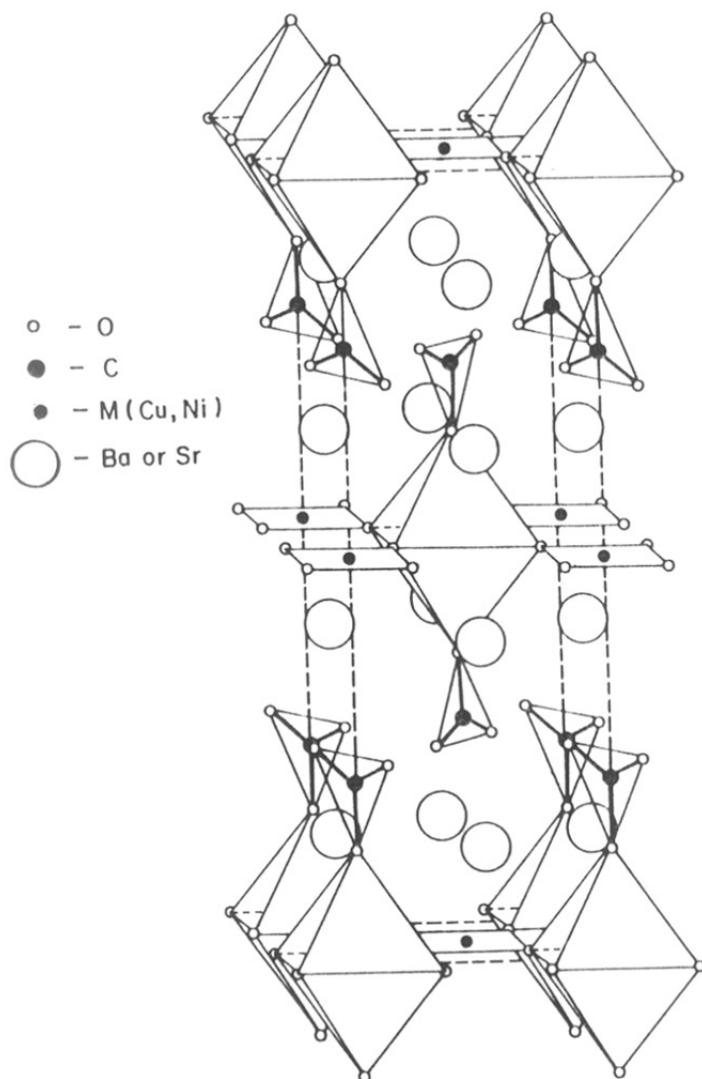


Fig. 7.1. Crystal structure of $A_4LiMO_4 \cdot (CO_3)_2$, showing the Li cation in octahedral co-ordination and M cation in square planar MO_4 units; open large circles represent Sr or Ba atoms. The triangles represent CO_3 unit.

place of SrCO_3 . Solid solution in the composition range $0 \leq x \leq 2$ could be prepared but the compounds always contain some unreacted carbonate impurity when $x < 1.25$. Thus best single phase materials were obtained with $\text{Sr}_{0.75}\text{Ba}_{1.25}\text{Li}_{0.5}\text{Cu}_{0.5}\text{CO}_3$.

All the samples contained a small quantity of $(\text{BaSr})\text{CO}_3$ as impurity. XRD patterns are calculated using computer programme PDP11 package which has the facility to calculate the reflections for mixed phases (as described in chapter 2.)

7.3. Results and discussions

The results obtained by various characterization techniques such as X-ray diffraction, dc susceptibility, Electron Spin Resonance, infra-red spectra, Nuclear Magnetic Resonance measurement for these compounds are discussed in the following section.

7.3.1. X-ray Diffraction Studies

Phase purity of the compounds were checked by powder XRD studies. All the samples show a small quantity of $(\text{Sr,Ba})\text{CO}_3$ as an impurity. Fig. 7.2 shows the observed and calculated XRD patterns of $\text{Sr}_2\text{Li}_{0.5}\text{Cu}_{0.5}\text{O}_2\text{CO}_3$. It is observed that the calculated XRD pattern (calculated by taking $\text{Sr}_2\text{Li}_{0.5}\text{Cu}_{0.5}\text{O}_2\text{CO}_3$ phase : SrCO_3 phase in 90:10 ratio) matches well with the observed pattern. Similar XRD pattern is observed for $\text{Sr}_{0.75}\text{Ba}_{1.25}\text{Li}_{0.5}\text{Cu}_{0.5}\text{O}_2\text{CO}_3$ compound which is shown in fig. 7.3. The XRD pattern of these compounds could be indexed on the basis of a tetragonal cell with $a \sim 2a_p$ and $c \sim 4a_p$, where a_p represents a basic cubic perovskite cell parameter. These compounds show a remarkable compressive distortion on the c -axis, $c \sim 0.9 \times 4a_p$. The refined lattice parameters, the observed and calculated d values and reflection intensities

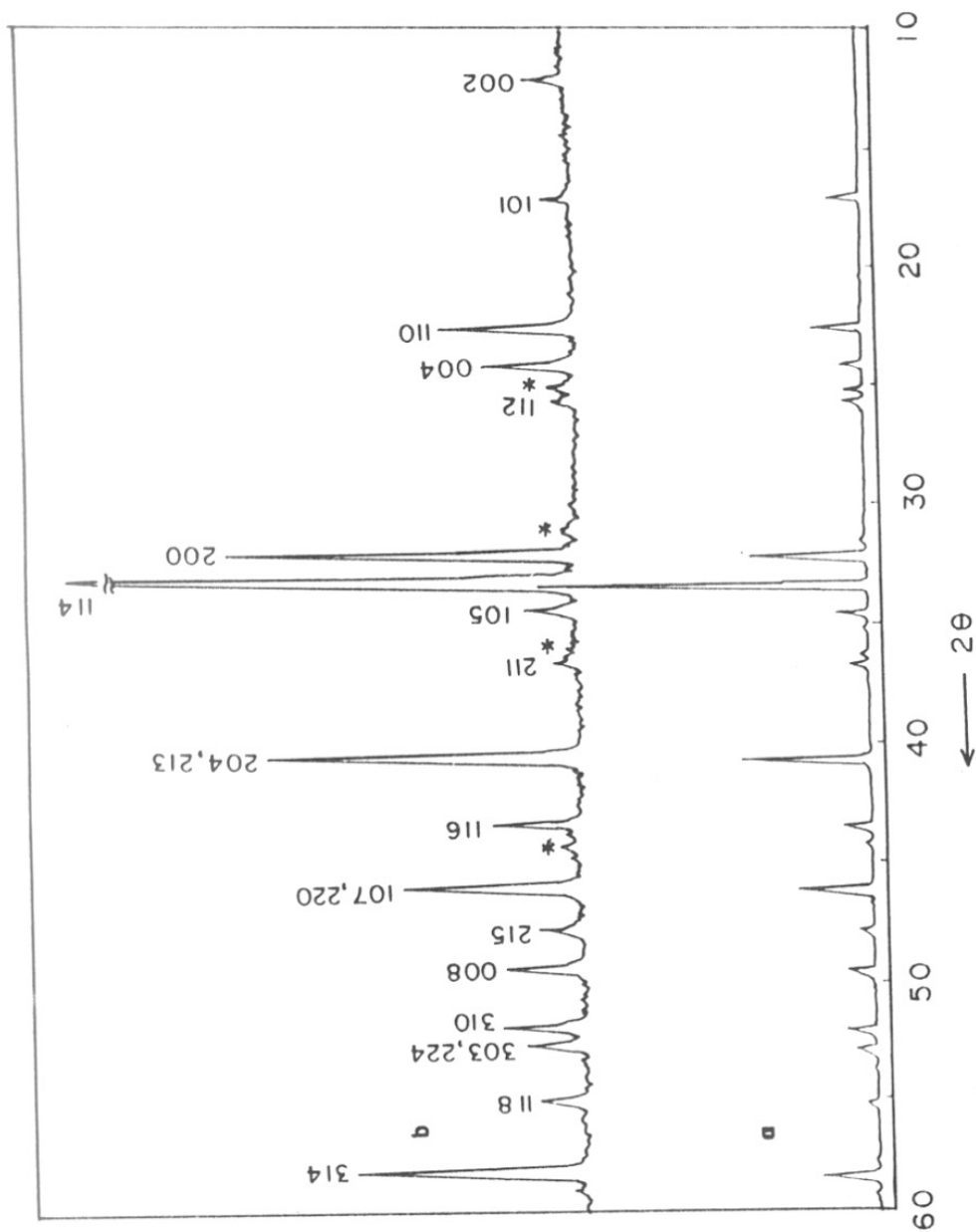


Fig. 7.2. Powder X-ray diffraction pattern of $\text{Sr}_2\text{Li}_{0.5}\text{Cu}_{0.5}\text{O}_2\text{CO}_3$.
 (a) calculated for mixed phases of the compound with 10% SrCO_3 . (b) observed pattern. Peaks marked by * are due to SrCO_3 .

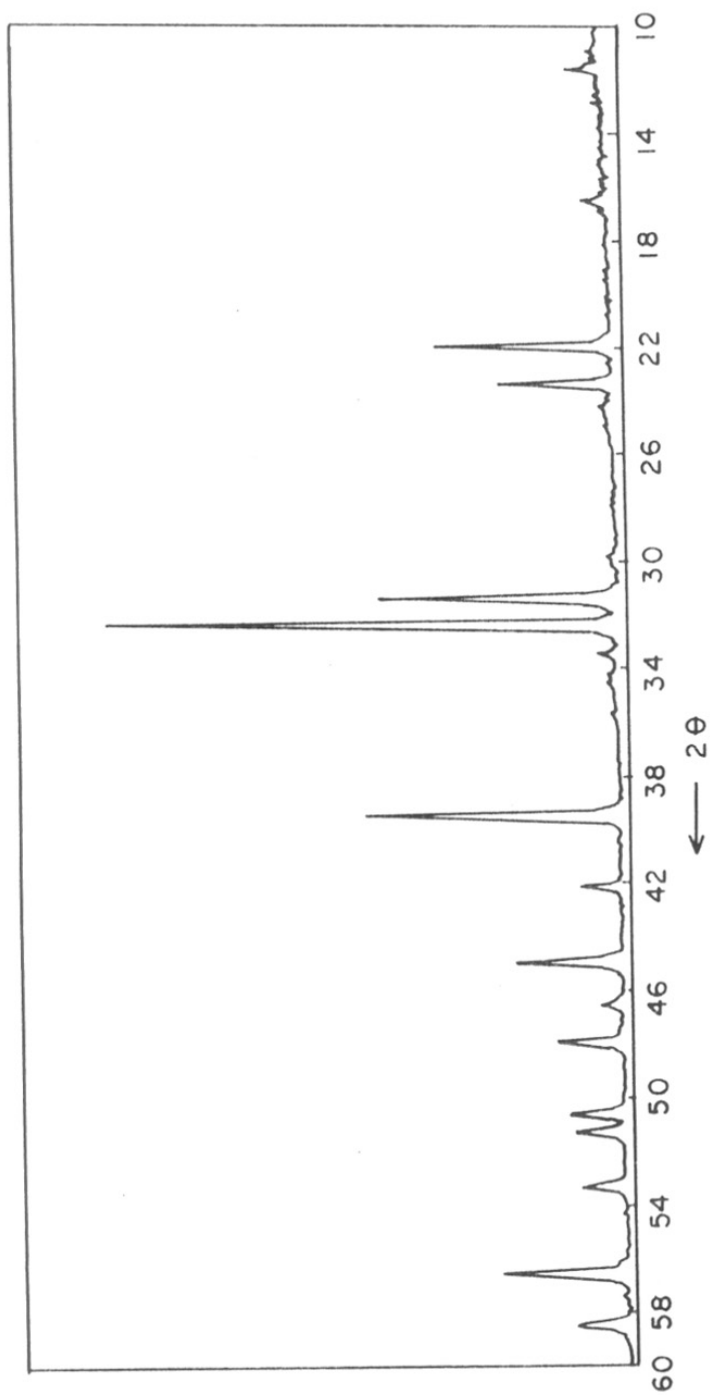


Fig. 7.3. Powder X-ray diffraction pattern of $\text{Sr}_{0.75}\text{Ba}_{1.25}\text{Li}_{0.5}\text{Cu}_{0.5}\text{O}_2 \cdot \text{CO}_3$.

refined lattice parameters, the observed and calculated d values and reflection intensities of these compounds are given in table 7.1. The lattice parameters are comparable to that reported for $\text{Sr}_4\text{LiCuO}_4\cdot(\text{CO}_3)_2$ by Calestani *et al* [1].

Fig. 7.4 shows XRD pattern of the nickel compound, $\text{Sr}_2\text{Li}_{0.5}\text{Ni}_{0.5}\text{O}_2\cdot\text{CO}_3$ compound. It can be seen that the pattern is identical to that of $\text{Sr}_2\text{Li}_{0.5}\text{Cu}_{0.5}\text{O}_2\cdot\text{CO}_3$ suggesting that both these compounds are isostructural. The $\text{Sr}_2\text{Li}_{0.5}\text{Ni}_{0.5}\text{O}_2\cdot\text{CO}_3$ compound also shows peaks due to SrCO_3 as impurity which is present only in minute amount as observed in the case of the corresponding Cu compound.

The X-ray diffraction pattern from the composition for the corresponding cobalt and iron compounds is shown in fig. 7.5. Although the pattern shows significant amount of known and unknown impurity there is a strong indication for the formation of the corresponding cobalt phase also. XRD pattern of the corresponding iron compound does not indicate the formation of this phase under present preparation conditions.

From the present studies it is seen that the range of stability of the compounds with the composition $\text{Sr}_2\text{Li}_{0.5}\text{M}_{0.5}\text{O}_2\cdot\text{CO}_3$, ($\text{M} = \text{Cu}, \text{Ni}, \text{Co}, \text{Fe}$) decreases in the order $\text{Cu} > \text{Ni} > \text{Co} > \text{Fe}$. This is roughly the decreasing order of occurrence of square-planar complexes of these elements. In the structure reported for $\text{Sr}_2\text{Li}_{0.5}\text{Cu}_{0.5}\text{O}_2\cdot\text{CO}_3$ [1] the copper ions are in predominantly square-planar coordination which is consistent with the known coordination chemistry of divalent or trivalent low-spin copper atoms in oxide matrices [4]. The Li ions in $\text{Sr}_2\text{Li}_{0.5}\text{M}_{0.5}\text{O}_2\cdot\text{CO}_3$ are in octahedral coordination.

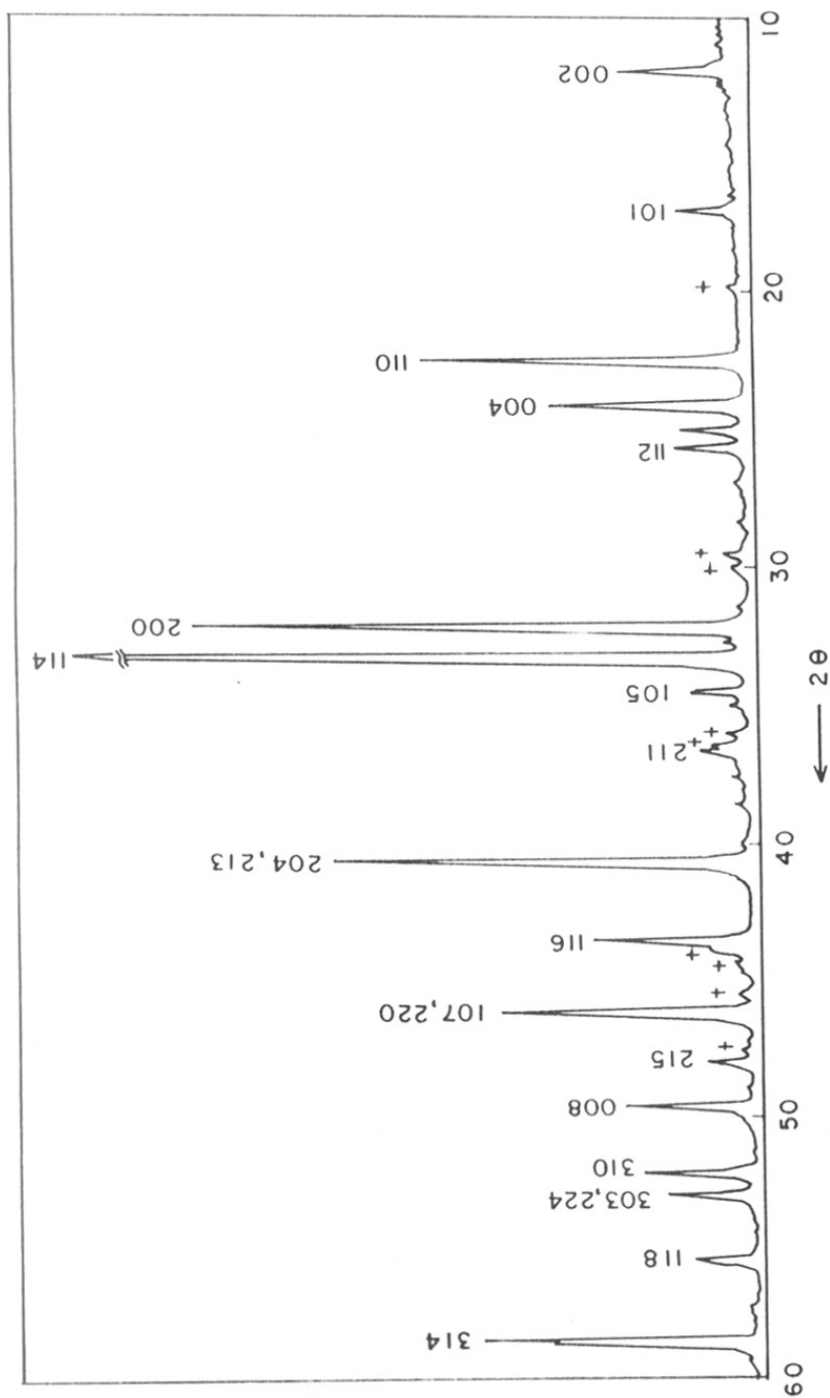


Fig. 7.4. powder X-ray diffraction pattern of $\text{Sr}_{1.5}\text{Li}_{0.5}\text{Ni}_{0.5}\text{O}_2 \cdot \text{CO}_3$. Peaks marked by + are due to SrCO_3 .

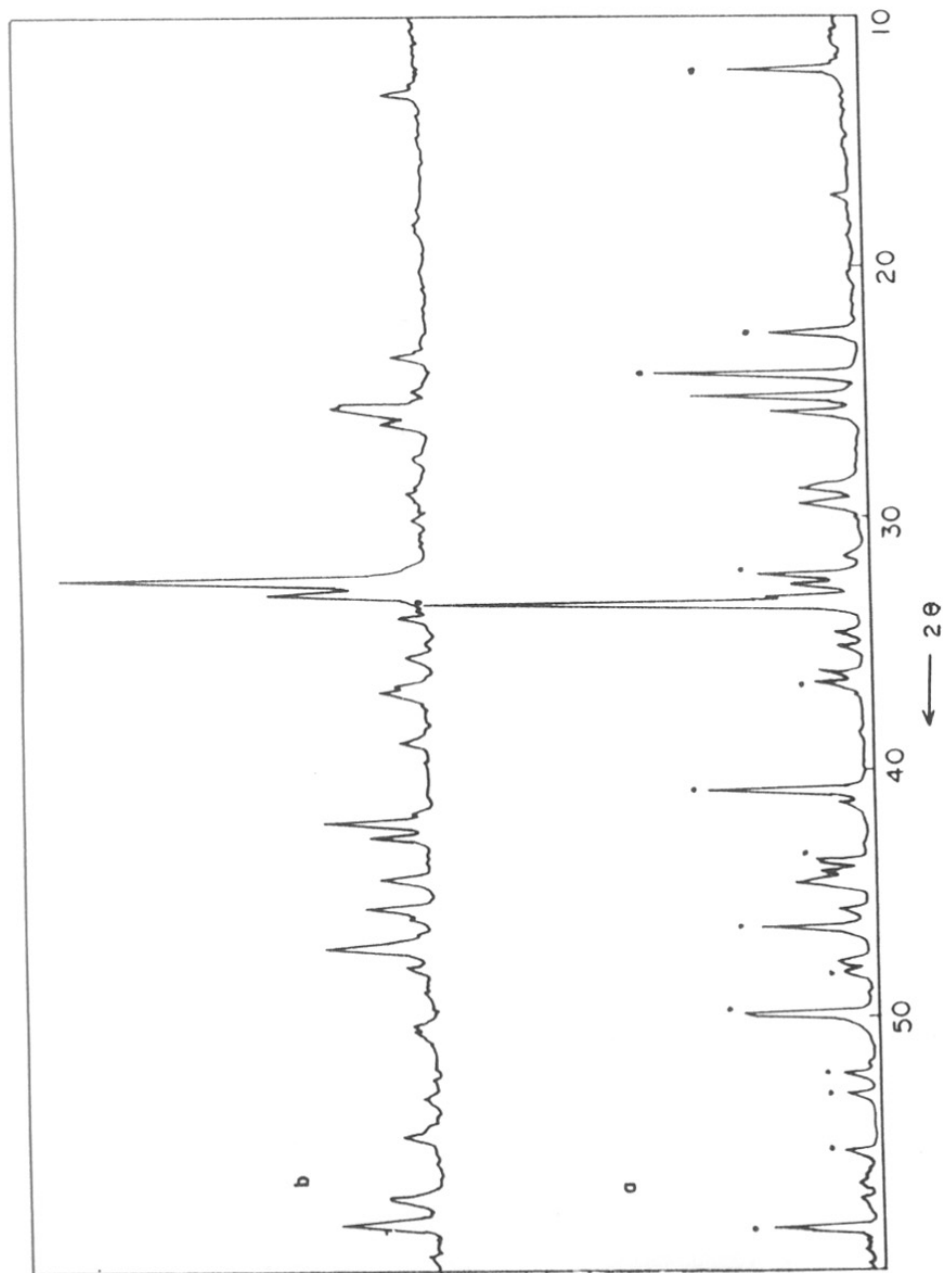


Fig. 7.5. Powder X-ray diffraction pattern of $\text{Sr}_2\text{Li}_{0.3}\text{M}_{0.5}\text{O}_2\cdot\text{CO}_3$. (a) $M = \text{Co}$, showing partial formation of the phase (marked by filled circles) (b) The compound obtained when $M = \text{Fe}$.

The electronic configuration of divalent low-spin Ni is the same as that of trivalent low-spin copper. There is therefore a possibility of the nickel atoms being in the divalent low-spin state in the square-planar coordination. The electronic configuration of low-spin trivalent nickel is that of an electron in degenerate e_g orbital in an octahedral crystal field in contrast to that of divalent copper which has a single hole in degenerate e_g orbitals. The Jahn-Teller distortion lifts the degeneracy. In the case of the well studied divalent copper, the Jahn-Teller distortion usually leads to an elongation of the octahedra because of the increased ligand-metal hybridisation when the hole is in the $d_{x^2-y^2}$ orbitals [4]. By the same argument one would anticipate that in the case of trivalent low-spin nickel atom the Jahn-Teller distortion would lead to a compressed octahedra. This is not the case at the lowest temperatures as seen from the characteristic ESR spectra of isolated low-spin trivalent nickel ions in elongated octahedra in 3D perovskite oxides such as LaAlO_3 or YAlO_3 [5]. Structural constraints could also be important. However, at higher temperatures the ESR spectra of low-spin trivalent Ni in these 3D oxide matrices show evidence for a dynamic Jahn-Teller effect reflecting thereby the proximity of the distorted compressed octahedral state. Unlike the copper atoms, the trivalent low-spin nickel atoms may thus also occupy the octahedral sites that are occupied by Li in $\text{Sr}_2\text{Li}_{0.5}\text{M}_{0.5}\text{O}_2\cdot\text{CO}_3$. As a result there could be a scrambling of the Li and Ni in the octahedral and square-planar sites. The existence of the divalent Ni atoms would be inconsistent with the $\text{Sr}_2\text{Li}_{0.5}\text{Ni}_{0.5}\text{O}_2\cdot\text{CO}_3$ stoichiometry unless some of the oxygen atoms have a hole on them or are present as spin-paired "peroxide"-like species.

The trivalent diamagnetic low-spin Co atom is an $L = 0$ species and hence prefers a regular octahedra just as the trivalent Fe atoms. This would account for the low stability or instability of the $\text{Sr}_2\text{Li}_{0.5}\text{Co}_{0.5}\text{O}_2\cdot\text{CO}_3$ or $\text{Sr}_2\text{Li}_{0.5}\text{Fe}_{0.5}\text{O}_2\cdot\text{CO}_3$ compounds.

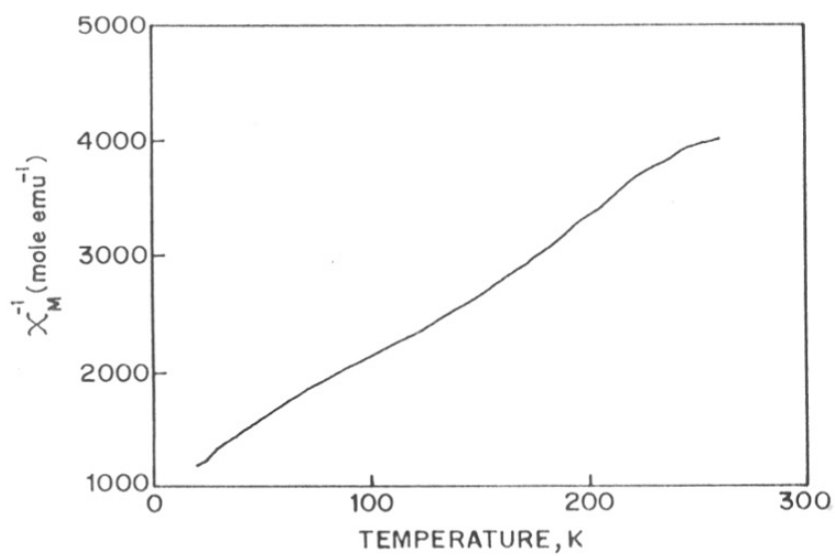


Fig. 7.6. Plot of the inverse of the dc magnetic susceptibility Vs temperature of $\text{Sr}_2\text{Li}_{0.5}\text{Ni}_{0.5}\text{O}_4 \cdot \text{CO}_3$.

7.3.2. Magnetic Susceptibility

The dc magnetic susceptibility studies on $\text{Sr}_2\text{Li}_{0.5}\text{Ni}_{0.5}\text{O}_2\cdot\text{CO}_3$ have been carried out as a function of temperature between 12 - 300 K. The inverse susceptibility Vs temperature plot shows a Curie-like behaviour (fig. 7.6). The value of the Curie constant is close to 0.20 (emu/mole)K which is nearly half the value of the expected Curie constant for the $S = 1$ low-spin state of trivalent Ni [4,6]. The low value of the Curie constant is consistent with our earlier discussion on the possible existence of diamagnetic low-spin divalent nickel species.

7.3.3. Electron Spin Resonance Studies

The electron spin resonance spectra of $\text{Sr}_2\text{Li}_{0.5}\text{Ni}_{0.5}\text{O}_2\cdot\text{CO}_3$ at 300 K and 77 K are shown in fig. 7.7. The spectra are compared with that from $\text{La}_2\text{Li}_{0.5}\text{Ni}_{0.5}\text{O}_4$ [6,7] as well as that from $\text{Sr}_2\text{Li}_{0.5}\text{Cu}_{0.5}\text{O}_2\cdot\text{CO}_3$. At 77 K, the ESR spectra from the nickelocarbonate is similar to that from $\text{La}_2\text{Li}_{0.5}\text{Ni}_{0.5}\text{O}_4$ with a characteristic splitting of the g_{\perp} and g_{\parallel} lines with $g_{\perp} > g_{\parallel}$ (2.28 and 1.88 respectively) that is characteristic of the ESR spectra of low-spin Ni^{3+} ions in elongated octahedra arising from a static Jahn-Teller distortion [6]. At room temperature, the splitting between g_{\perp} and g_{\parallel} becomes much reduced, indicative of a dynamic Jahn-Teller effect. The change from static to dynamic Jahn-Teller effect in $\text{Sr}_2\text{Li}_{0.5}\text{Ni}_{0.5}\text{O}_2\cdot\text{CO}_3$ would indicate a more compressed octahedral surrounding for the Ni atoms as compared to that in $\text{La}_2\text{Li}_{0.5}\text{Ni}_{0.5}\text{O}_4$. This supports the case put forward earlier for the low-spin trivalent nickel atoms occupying the octahedral sites. The intensity of the ESR lines are comparable with that from $\text{La}_2\text{Li}_{0.5}\text{Ni}_{0.5}\text{O}_4$ which has an ESR spectra characteristic of a static Jahn-Teller distortion at all temperatures [7,8a].

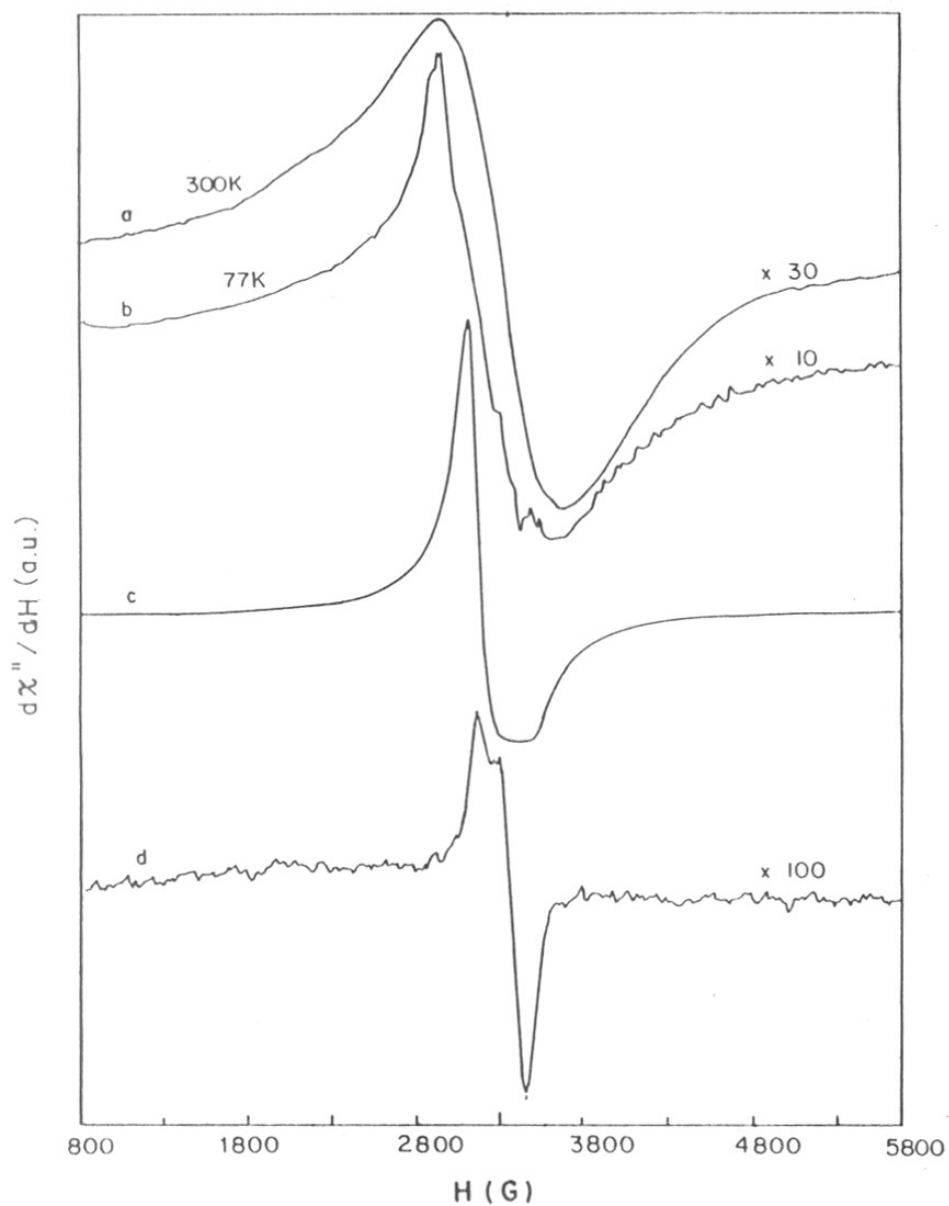


Fig. 7.7. The ESR spectra of (a) $\text{Sr}_2\text{Li}_{0.5}\text{Ni}_{0.5}\text{O}_2\cdot\text{CO}_3$ at 300 K and (b) at 77 K, (c) $\text{La}_2\text{Li}_{0.5}\text{Ni}_{0.5}\text{O}_4$ at 300 K, (d) $\text{Sr}_2\text{Li}_{0.5}\text{Cu}_{0.5}\text{O}_2\cdot\text{CO}_3$ at 300 K.

The ESR spectra of $\text{Sr}_2\text{Li}_{0.5}\text{Cu}_{0.5}\text{O}_2\cdot\text{CO}_3$ is characteristic of Cu^{2+} ions in elongated octahedra. The intensity of the ESR signal is, however, very small being less than 2% of the required intensity, showing that most of the copper atoms are in an ESR silent state, which is characteristic of low-spin trivalent copper as in $\text{La}_2\text{Li}_{0.5}\text{Cu}_{0.5}\text{O}_4$ [5].

7.3.4. IR and Raman Spectra

Infra-red spectra of these compounds are shown in the 400-4000 cm^{-1} region, in fig. 7.8. The expanded low frequency region is shown in fig. 7.9. Several phonon absorption bands are observed in low frequency region. These are located around 425, 600, 700, 865, 1070 and 1425 cm^{-1} . There are in addition some high frequency bands at 3300, 3500 cm^{-1} which may be due to O-H vibrations of hydrolysed impurities.

The IR and Raman spectra show bands which are characteristic for the internal vibration of the $-\text{CO}_3$ ions implying the presence of carbonate molecular species in agreement with that reported earlier for the other cuprocarbonates [9]. In fig. 7.8, the carbonate bands of cuprocarbonates, are compared with that of pure carbonates ($\text{Ba,Sr}\text{CO}_3$ (curve d)). It can be seen that the pure Ba and Sr carbonates show characteristic IR bands due to internal vibrations of $-\text{CO}_3$ ion at 860, 1065 and 1423 cm^{-1} .

The IR bands in the region 690-2000 cm^{-1} are at slightly shifted position in the cuprocarbonates compared to the pure carbonates. Broadening of some carbonate bands suggest the presence of disorder in the carbon containing layer or an extra mobility of the carbonate groups due to constraints imposed by the lattice.

The two lower frequency cuprocarbonate IR bands around ~ 400 and 600 cm^{-1} are intrinsic to the cuprocarbonate phase and do not appear in pure carbonates. It may be

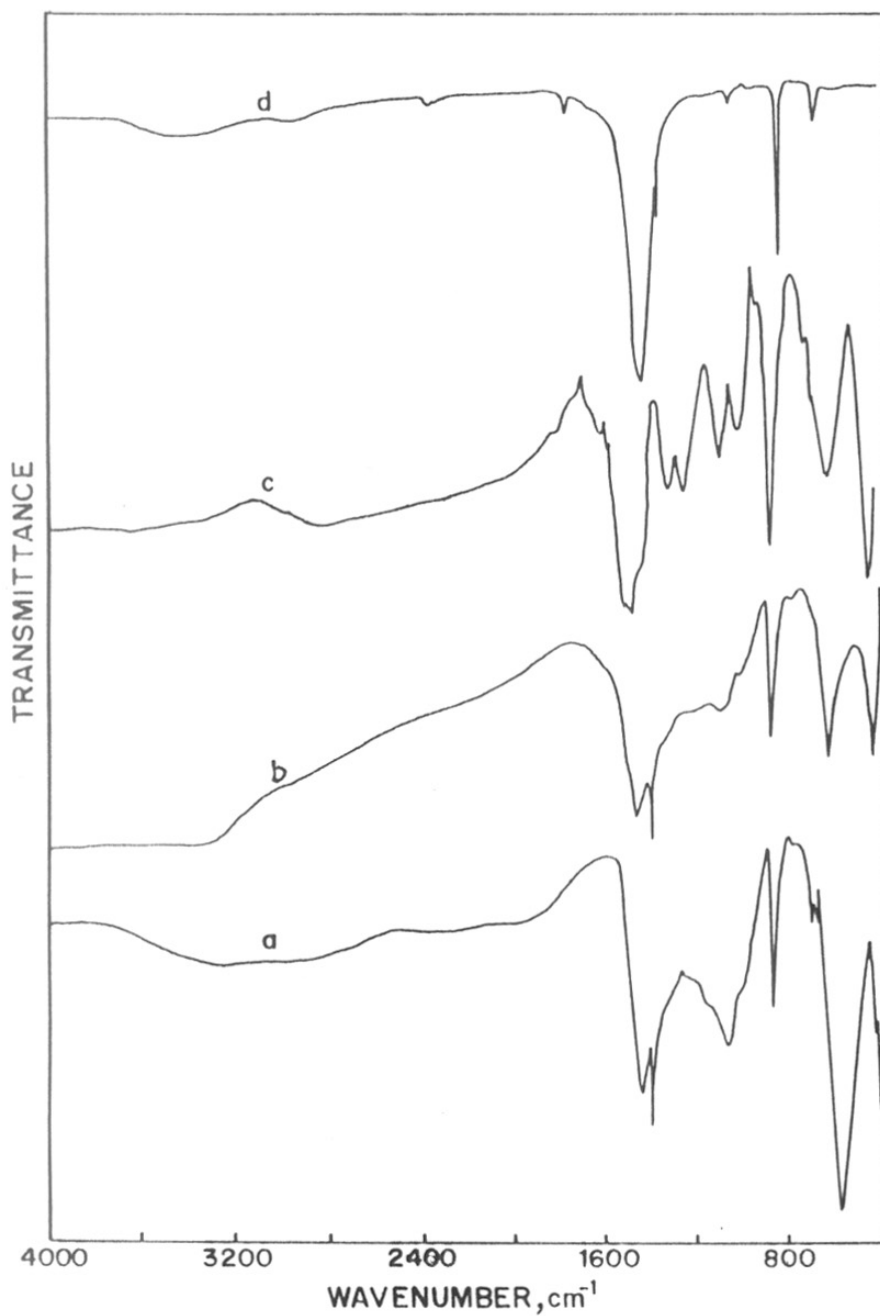


Fig. 7.8. Infra-red spectra of (a) $\text{Ba}_{1.25}\text{Sr}_{0.75}\text{Li}_{0.5}\text{Cu}_{0.5}\text{O}_2\cdot\text{CO}_3$, (b) $\text{Sr}_2\text{Li}_{0.5}\text{Cu}_{0.5}\text{O}_2\cdot\text{CO}_3$, (c) $\text{Sr}_2\text{Li}_{0.5}\text{Ni}_{0.5}\text{O}_2\cdot\text{CO}_3$, (d) SrCO_3 , in the 400-4000 cm^{-1} region.

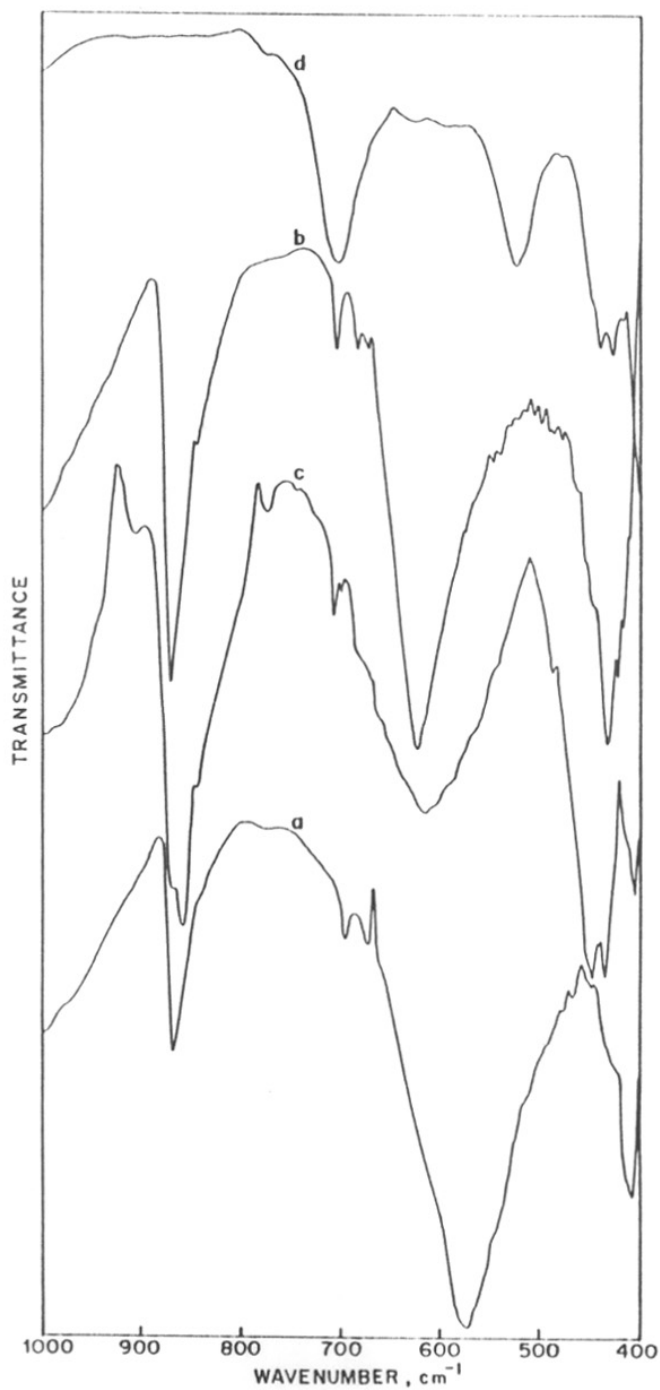


Fig. 7.9. Infra-red spectra in the low frequency region of (a) $\text{Ba}_{1.25}\text{Sr}_{0.75}\text{Li}_0.5\text{Cu}_0.5\text{O}_2\cdot\text{CO}_3$, (b) $\text{Sr}_2\text{Li}_3\text{Cu}_3\text{O}_2\text{CO}_3$, (c) $\text{Sr}_2\text{Li}_0.5\text{Ni}_0.5\text{O}_2\cdot\text{CO}_3$, (d) $\text{La}_2\text{Li}_0.5\text{Cu}_0.5\text{O}_4$.

noted that the frequency of these bands varies from sample to sample which is possibly related to different oxygen-oxygen or M-O distances.

Since $\text{La}_2\text{Li}_{0.5}\text{Cu}_{0.5}\text{O}_4$ and the cuprocarbonates $\text{A}_2\text{Li}_{0.5}\text{Cu}_{0.5}\text{O}_2\cdot\text{CO}_3$ have similar structure, the vibrational modes of these compounds can be compared. In fig. 7.9, the IR spectra of these compounds are compared with that of $\text{La}_2\text{Li}_{0.5}\text{Cu}_{0.5}\text{O}_4$ in the lower frequency region. It can be seen that $\text{La}_2\text{Li}_{0.5}\text{Cu}_{0.5}\text{O}_4$ contains three bands at 425, 500 and 700 cm^{-1} [8]. In La_2BO_4 compounds with K_2NiF_4 structure the highest frequency bands are usually associated with in-plane vibrations (E_u mode) of the oxygen atoms; the band at $\sim 500\text{ cm}^{-1}$ is believed to be an A_{2u} mode which is associated with the vibrations of the axial oxygen atom perpendicular to the ab (CuO_2) plane [10,11]. The band around $400\text{-}450\text{ cm}^{-1}$ may be associated with an in-plane vibration of the O-Cu bond in La_2CuO_4 . Comparing the spectra of La_2MO_4 compounds with that of $\text{La}_2\text{Li}_{0.5}\text{M}_{0.5}\text{O}_4$ (fig. 5.11 (M = Co, Ni, Cu) in chapter 5) it can be seen that the band around $400\text{-}450\text{ cm}^{-1}$ is shifted to higher frequency when the M atom is replaced by the lighter Li atom. Ganguly and co-workers [12] had noted earlier that in $\text{LaSrAl}_{1-x}\text{Fe}_x\text{O}_4$ the band at $400\text{-}450\text{ cm}^{-1}$ behave as independent modes corresponding to Al and Fe with their relative intensities being governed by their relative ratios. Therefore it may be assigned that the band around 400 cm^{-1} in $\text{La}_2\text{Li}_{0.5}\text{M}_{0.5}\text{O}_4$ to the in-plane vibrations of the M atom. The band $\sim 425\text{ cm}^{-1}$ in the cuprocarbonates is thus due to Cu-O vibrations.

Comparing the IR spectra of the $\text{La}_2\text{Li}_{0.5}\text{M}_{0.5}\text{O}_4$ compounds with that of the corresponding $\text{Sr}_2\text{Li}_{0.5}\text{M}_{0.5}\text{O}_2\cdot\text{CO}_3$ compounds it has been found that the most important qualitative difference at low wavenumbers is the complete absence of the band around 500 cm^{-1} in the latter series of compounds. This band is associated with the out-of-plane vibrations of the axial oxygens in $\text{La}_2\text{Li}_{0.5}\text{M}_{0.5}\text{O}_4$. The absence of such a vibration is

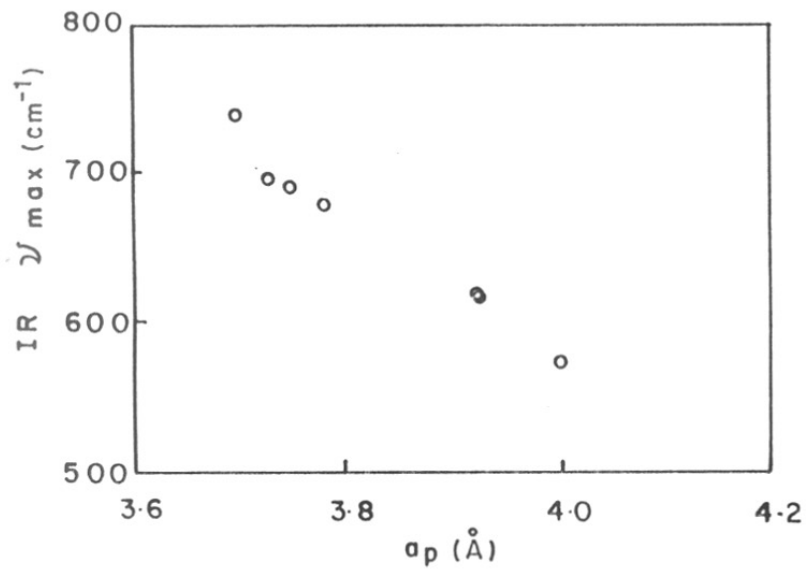


Fig. 7.10. Plot of ν_{\max} Vs basal plane quasi-perovskite a_p parameter.

a vibration is understandable since there are no axial M-O linkage in the $\text{Sr}_2\text{Li}_{0.5}\text{M}_{0.5}\text{O}_2\cdot\text{CO}_3$ compounds.

The quantitative changes in the frequency may be examined in the context of the "titration" curve given by Ganguly *et al* [8a,8b] correlating the highest vibration frequency, ν_{max} , with the Cu-O bond distance. Fig. 7.10 shows the plot of ν_{max} Vs the basal plane quasi-perovskite a_p parameter for the $(\text{Ln})_2\text{Li}_{0.5}\text{M}_{0.5}\text{O}_4$ ($\text{Ln} = \text{La, Nd}$; $\text{M} = \text{Cu, Ni, Co}$) and $(\text{Ba,Sr})_2\text{Li}_{0.5}\text{M}_{0.5}\text{O}_2\cdot\text{CO}_3$ ($\text{M} = \text{Cu, Ni}$) compounds. It can be seen that ν_{max} correlates fairly well with the a_p lattice parameter. Since for K_2NiF_4 type tetragonal compounds the in plane M-O distance is usually determined as half of the lattice a parameter, from this plot it can be concluded that the frequency (ν_{max}) varies linearly with M-O distance. The strong band around 600 cm^{-1} in these compounds, may thus be assigned to the in-plane vibrations of the oxygen atoms in the $(\text{Li,M})\text{O}_2$ plane.

7.3.5. ^7Li Nuclear Magnetic Resonance

The nuclear spin $I = 3/2$ of the ^7Li nucleus has a large nuclear quadrupole moment which makes it a sensitive probe of the structural distortion in its environment. The static ^7Li NMR spectra from $\text{La}_2\text{Li}_{0.5}\text{Cu}_{0.5}\text{O}_4$ with that from $\text{Sr}_2\text{Li}_{0.5}\text{Cu}_{0.5}\text{O}_2\text{CO}_3$ and $\text{Ba}_{1.25}\text{Sr}_{0.75}\text{Li}_{0.5}\text{Cu}_{0.5}\text{O}_2\cdot\text{CO}_3$ for the usual single pulse (SP) (fig. 7.11) and quadrupolar echo pulse sequence (QEP) [13] (fig. 7.12) modes of acquisition are compared. The features due to the central and satellite transitions are clearly seen. The relative intensity of the central transition to that of the satellite transition decreases in the QEP mode of acquisition which refocuses the decay due to the quadrupolar interactions.

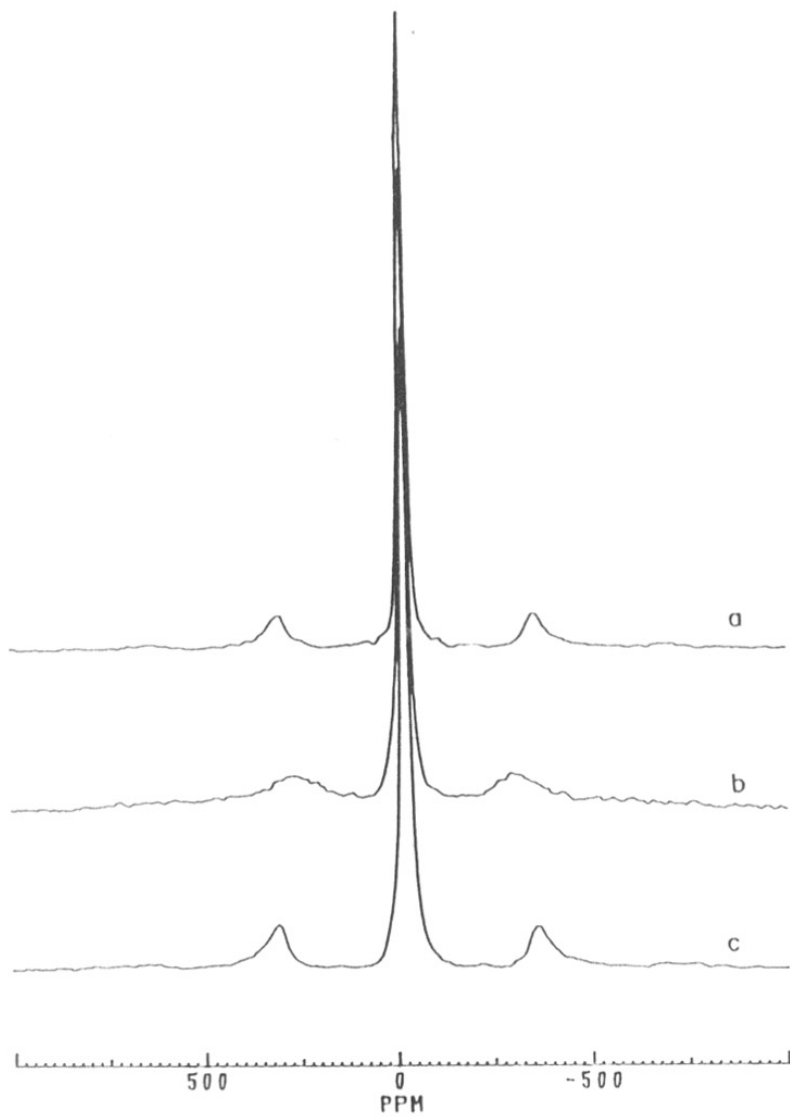


Fig. 7.11. ${}^7\text{Li}$ NMR spectra of (a) $\text{La}_2\text{Li}_{0.5}\text{Cu}_{0.5}\text{O}_4$, (b) $\text{Sr}_2\text{Li}_{0.5}\text{Cu}_{0.5}\text{O}_2\cdot\text{CO}_3$, (c) $\text{Ba}_{1.25}\text{Sr}_{0.75}\text{Li}_{0.5}\text{Cu}_{0.5}\text{O}_2\cdot\text{CO}_3$, using SP sequence.

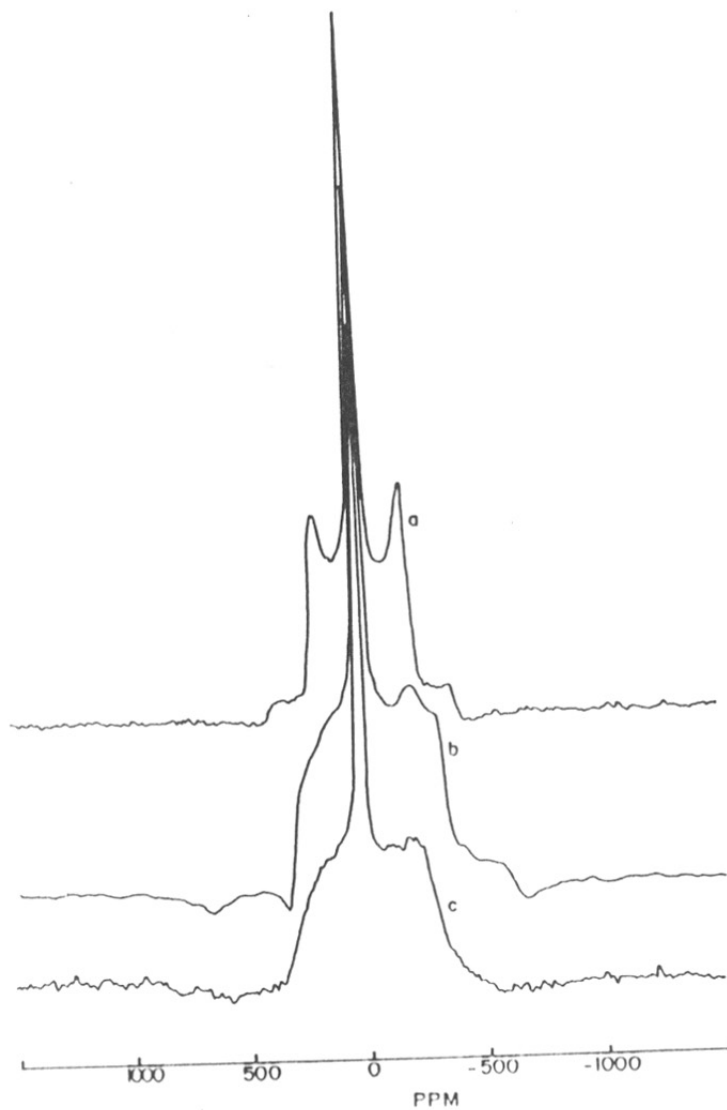


Fig. 7.12. ${}^7\text{Li}$ NMR spectra of (a) $\text{La}_2\text{Li}_{0.5}\text{Cu}_{0.5}\text{O}_4$ (b) $\text{Sr}_2\text{Li}_{0.5}\text{Cu}_{0.5}\text{O}_2\cdot\text{CO}_3$ (c) $\text{Ba}_{1.25}\text{Sr}_{0.75}\text{Li}_{0.5}\text{Cu}_{0.5}\text{O}_2\cdot\text{CO}_3$, using QEP sequence.

The magnitude of the quadrupolar splitting ν_Q in the SP sequence for $\text{Sr}_2\text{Li}_{0.5}\text{Cu}_{0.5}\text{O}_2\cdot\text{CO}_3$ is comparable to that for $\text{La}_2\text{Li}_{0.5}\text{Cu}_{0.5}\text{O}_4$ showing a nearly similar Li environment in the two cases. The value of ν_Q decreases in the $(\text{Ba},\text{Sr})_2\text{Li}_{0.5}\text{Cu}_{0.5}\text{O}_2\cdot\text{CO}_3$ compound. There is no shift in the central transition for the cuprocarbonates relative to that of $\text{La}_2\text{Li}_{0.5}\text{Cu}_{0.5}\text{O}_4$. This is consistent with a diamagnetic low-spin configuration of the copper atoms in the cuprocarbonates.

One unusual feature that requires further investigation is the decrease in ν_Q when the QEP sequence is used for the $(\text{Ba},\text{Sr})_2\text{Li}_{0.5}\text{Cu}_{0.5}\text{O}_2\text{CO}_3$ compounds. Such a change is not seen for $\text{La}_2\text{Li}_{0.5}\text{Cu}_{0.5}\text{O}_4$. Since the QEP sequence refocuses the fast-decaying quadrupolar interactions it is likely that there are two different Li environments corresponding to say Li_I and Li_{II} with, say, Li_{II} being associated with the faster decay of the quadrupolar interactions and requiring the QEP sequence for refocusing these decays. Since the refocused satellite transition have a smaller value of the quadrupolar splitting, ν_Q , it is apparent that the EFG gradient is smaller in the Li_{II} environment compared to that of Li_I . It has to be examined whether the different environments are due to the presence or absence of axial carbonate groups. Preliminary studies do not show large temperature dependence in the relative intensities or the magnitudes of the quadrupolar splitting for the satellite transition.

7.3.6. Reactivity with NH_4F

Solid state reactions of these carbocuprates have been carried out with ammonium fluoride NH_4F which is expected to incorporate F^- ions in the structure with liberation of ammonia. The reaction is expected to follow the equation 6.1 as described in chapter 6.

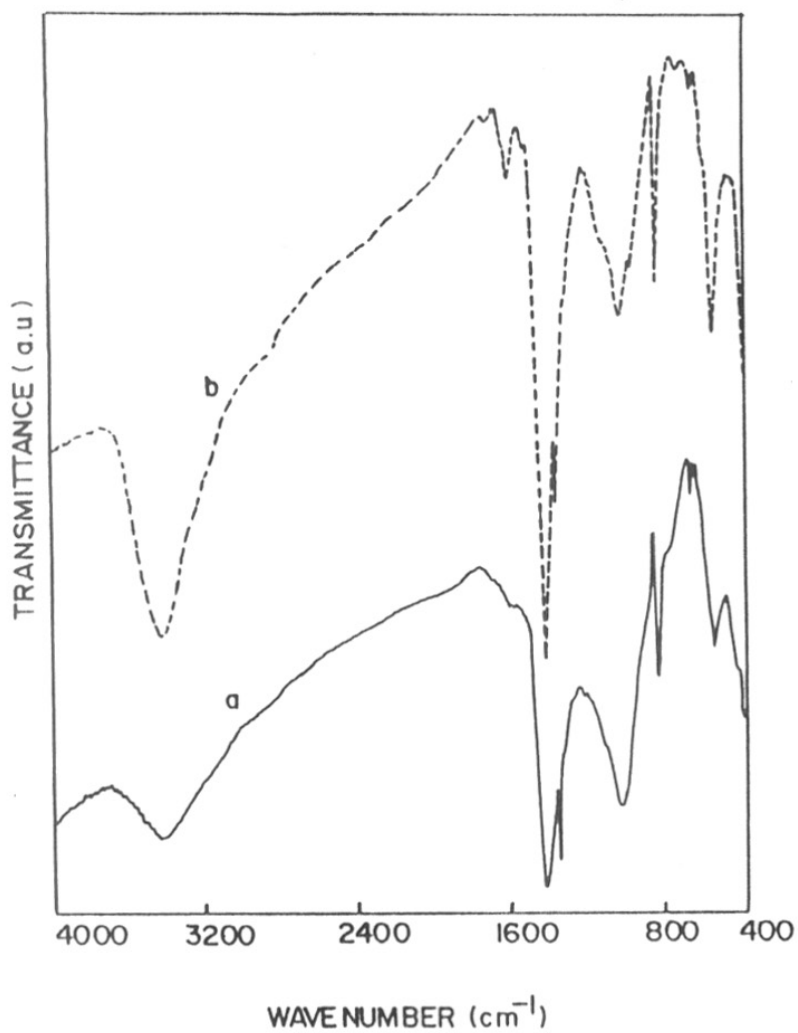


Fig. 7.13. IR spectra of $\text{Ba}_{1.25}\text{Sr}_{0.75}\text{Li}_{0.5}\text{Cu}_{0.5}\text{O}_2\cdot\text{CO}_3$ (a) before and (b) after grinding with NH_4F .

There is very little reaction of $\text{Sr}_2\text{Li}_{0.5}\text{Cu}_{0.5}\text{O}_2\cdot\text{CO}_3$ with ammonium fluoride even on grinding over protracted periods or on grinding at slightly elevated ($\sim 60^\circ\text{C}$) temperatures under an infra-red lamp. There is, however, ready reaction with $\text{Sr}_{0.75}\text{Ba}_{1.25}\text{Li}_{0.5}\text{Cu}_{0.5}\text{O}_2\cdot\text{CO}_3$. The change in weight after grinding a 1:0.5 mixture of $\text{Sr}_{0.75}\text{Ba}_{1.25}\text{Li}_{0.5}\text{Cu}_{0.5}\text{O}_2\cdot\text{CO}_3\cdot\text{NH}_4\text{F}$ corresponds to a reaction of less than 50% of the carbonate groups. The changes in the infra-red spectra before and after the reaction is shown in fig. 7.13. It can be seen that the basic nature of the infra-red spectra remains same after the grinding with ammonium fluoride except that the relative ratio of carbonate band intensity, is changed. It can be seen that the carbonate band $\sim 1425\text{ cm}^{-1}$ becomes more intense after the reaction while there is no significant change in other two carbonate bands (860 and 1065 cm^{-1}).

The reactivity of the carbonate groups towards $(\text{NH}_4)_n\text{X}^n$ in $\text{Ba}_3\text{SrCu}_2\text{O}_6\cdot 2\text{CO}_2$ and $\text{Sr}_{0.75}\text{Ba}_{1.25}\text{Li}_{0.5}\text{Cu}_{0.5}\text{O}_2\cdot\text{CO}_3$ (or $\text{Ba}_{2.5}\text{Sr}_{1.5}\text{LiCuO}_4\cdot 2\text{CO}_3$) and the lack of such a reactivity in $\text{Sr}_2\text{Li}_{0.5}\text{Cu}_{0.5}\text{O}_2\cdot\text{CO}_3$ could be of importance. The separation between the oxygen atoms could be of significance. The basal-plane lattice parameters of both $\text{Ba}_3\text{SrCu}_2\text{O}_6\cdot 2\text{CO}_2$ and $\text{Sr}_{0.75}\text{Ba}_{1.25}\text{Li}_{0.5}\text{Cu}_{0.5}\text{O}_2\cdot\text{CO}_3$ are greater than 4.00 \AA ($\sim \sqrt{2} \times 2.80\text{ \AA}$ where 2.80 \AA is the Shannon-Prewitt diameter of the O^{2-} ion) while in $\text{Sr}_2\text{Li}_{0.5}\text{Cu}_{0.5}\text{O}_2\cdot\text{CO}_3$ it is less than this value (3.923 \AA). When the basal plane parameter is greater than 4.0 \AA , it may be assumed that the separation between the oxygen atoms is greater than the sum of their van der Waals radii. The oxygen atoms are not in close contact in the same manner as in $\text{Ba}_{2-x}\text{Sr}_x\text{PbO}_4$ system. The effective diameter of the cylinder occupied by the O-O AO₃ layers of the perovskite-like (Cu_3Au) or rock-salt like (Ni_3Ti) packing is now greater than the van der Waals diameter of the oxygen ion. Free movement of fluoride ions (with van der Waals radius less than or close to that of oxygen), within the carbonate layer, is now possible. The low reactivity with ammonium chloride is consistent with the larger diameter

of the chloride ions ($\sim 3.6 \text{ \AA}$) [13] relative to that of the oxide ion. Mobility of Cl⁻ ions in the OO channel is expected to be restricted.

References

1. G. Calestani, P. Ganguly, F.C. Maticotta, P. Nozar, A. Migliori, K.A. Thomas, and A. Tomasi, *Physica C* **247**, 359 (1995).
2. G. Demazeau, B. Buffat, M. Pouchard and P. Hagenmuller, *J. Solid State Chem*, **54**, 389 (1984);
3. P. Ganguly and C.N.R. Rao, *J. Solid State Chem*, **53**, 193 (1984).
4. A. Abragham and B. Bleaney, 'Electron Paramagnetic Resonance of Transition Ions' Clarendon press, Oxford, p.455 (1970).
5. P. Ganguly and C.N.R. Rao, *Bull. Mater. Science.*, **2**, 193 (1980).
6. R. Englman, 'Jahn-Teller Effect in Molecules and Crystals' (1972).
7. G. Villeneuve, T. Rojo, G. Demazeau and P. Hagenmuller, *Mat. Res. Bull.* **23**, 1787 (1988).
8. K. Sreedhar, Ph.D. Thesis, IISc., Bangalore (1989).
9. T. Mertelj, D. Mateev, F.C. Maticotta, D. Pal, P. Stasny, P. Nozar, Q. Jiang, D. Mihailoivic and P. Ganguly, *Solid State Commun.*, **84**, 1115 (1992).
10. G. Burns, F.H. Dacol, G. Kliche, W. Honig and M.W. Shafer, *Phys. Rev.*, **B37**, 3381 (1988).
11. M. Copic, D. Mihailoivic, M. Prester, K. Biljakovic, B. Orel and N. Brnicevic, *Solid State Commun.*, **44**, 297 (1987).
12. G. Demazeau, J.M. Dance and P. Hagenmuller, *Solid State Commun.*, **73**, 617 (1990).
13. J.H. Davis, K.R. Jeffery, N. Bloom, H.I. Valic and J.P. Higgs, *Chem. Phys. Lett.*, **42**, 390 (1976).
14. R.D. Shannon, *Acta Cryst.* **A32**, 751 (1976).

List of Publications

1. Deviation from Vegard's Law: in the c -axis parameter in $\text{La}_{2-x}\text{Sr}_x\text{CuO}_{4-d}$ in relation to the insulator-superconductor-metal transition.
P. Ganguly, **N. Shah**, M. Phadke, V. Ramaswamy and I. S. Mulla.
Phys. Rev **B47**, 991 (1993).
2. Use of AX_3 close-packing description of layered perovskites in understanding the role of various A ions in cuprate superconductors.
P. Ganguly and **N. Shah**
Physica C **208**, 307 (1993).
3. Electron spin resonance evidence for the role of the copper ions in interlayer coupling in layered oxycarbonates.
P. Ganguly, **N. Shah** and F.C. Maticotta
Physica C, **206**, 70 (1993).
4. Simultaneous Determinations of mineral nutrients in different varieties of wheat and bengal gram in India by Instrumental Neutron Activation Analysis
N.S. Rajurkar, **Neepa Shah**, J. Purushottam
Appl. Radiat. Isot., **41**, 579 (1990).
5. Synthesis and characterization of hexagonal phases $\text{Sr}_{1.5}\text{PbM}_x\text{O}_{3.5+x}$ ($M = \text{Cd}, \text{Zn}$).
N. Shah, P.A. Joy, K. Sreedhar and P. Ganguly,
communicated to J. Solid State Chem. (1995).
6. Preparation and characterization of new oxycarbonate of nickel: $\text{Sr}_4\text{LiNiO}_4(\text{CO}_3)_2$.
P. Ganguly, **N. Shah**, N.V.K. Prakash and N.Y. Vasanthacharya, to be published.